People's Democratic Republic of Algeria
Ministry of Higher Education and Scientific Research
University of 8 Mai 1945 Guelma

Faculty of Sciences and Technology
Department of Process Engineering
Laboratory of Industrial Analysis and Materials Engineering (LAIGM)

Thesis

Submitted in Candidacy for the Degree of *Doctorate in Third Cycle*

Field: Sciences and Technology Stream: Process Engineering

Speciality: Process Engineering of Materials

Presented by:

MAKHLOUF Fatima Zahra

Title

Development of a screen-printed sensor decorated with Pt-Ni microstructures for the detection of Zn(II), ascorbic acid, and paracetamol

Defended on: 01/07/2025 Before the jury composed of:

Full name	Rank	University	
AMIRA-GUEBAILIA Habiba	Professor	Univ. of 8 mai 1945 Guelma	President
CHELAGHMIA Mohamed Lyamine	Professor	Univ. of 8 mai 1945 Guelma	Supervisor
NACEF Mouna	Professor	Univ. of 8 mai 1945 Guelma	Co- supervisor
HAMLAOUI Youcef	Professor	Univ. of M.C.M. Souk Ahras	Examiner
CHOUARFA Fella	MCA	Univ. of 8 mai 1945 Guelma	Examiner

Academic year: 2024-2025

République Algérienne Démocratique et Populaire
Ministère de l'Enseignement Supérieur et de la Recherche Scientifique
Université 8 Mai 1945 Guelma

Faculté des Sciences et de la Technologie
Département de Génie des procédés
Laboratoire d'Analyses Industrielles et Génie des Matériaux (LAIGM)

THÈSE

En Vue de l'Obtention du Diplôme de Doctorat en Troisième Cycle

Domaine : Sciences et Technologie Filière : Génie des procédés

Spécialité : Génie des procédés des matériaux

Présentée par

MAKHLOUF Fatima Zahra

Intitulée

Développement d'un capteur sérigraphié décoré de microstructures de Pt-Ni pour la détection de Zn(II), d'acide ascorbique et de paracétamol

Soutenue le : 01/07/2025 Devant le Jury composé de :

Nom et Prénom	Grade		
AMIRA-GUEBAILIA Habiba	Professeur	Univ. de 8 mai 1945 Guelma	Présidente
CHELAGHMIA Mohamed Lyamine	Professeur	Univ. de 8 mai 1945 Guelma	Encadreur
NACEF Mouna	Professeur	Univ. de 8 mai 1945 Guelma	Co-encadreur
HAMLAOUI Youcef	Professeur	Univ. de M.C.M. Souk Ahras	Examinateur
CHOUARFA Fella	MCA	Univ. de 8 mai 1945 Guelma	Examinatrice

Année Universitaire : 2024-2025

Dedication

I dedicate this modest thesis manuscript to my grandfather, **Salah Makhlouf** (1936-2012), and to the entire **MAKHLOUF family**, the family of chemists…

Acknowledgements

Ah, thesis, what an incredible journey that comes to an end! What a joy it has been to advance knowledge, bit by bit, uncovering a little more each day, beyond what is visible. But also, what determination and perseverance it takes to move forward, step by step, through the unknown paths of science, without seeing the end of the road.

For these four years, every morning, I came with the same enthusiasm, driven by the desire to learn, to discover, and to create. And this would not have been possible without the support and encouragement of certain people. This was the case for me, and the chemistry worked wonderfully. Thank you to everyone who contributed to this great adventure. Saying goodbye to all of this will certainly be difficult.

First and foremost, I would like to thank Allah, my Almighty God, for granting me the patience and strength to reach where I am today.

A huge thank you to my thesis supervisor, **Professor Chelaghmia Mohamed Lyamine**, for trusting me from the very beginning. The start was not easy, but you have been there to support me every step of the way. Always available to discuss measurements or experimental tests, never hesitating to spend hours helping me work through problems, even during holidays, rain or shine. And, of course, working under 47°C in Guelma was no easy feat, but with you, we got used to it! I am also deeply grateful for the freedom you gave me in conducting my research and managing my work in a way that suited my interests and inclinations.

I would also like to thank my thesis co-supervisor, **Professor Nacef Mouna**, for her exceptional guidance throughout my research journey.

This research was carried out at the Laboratory of Industrial Analysis and Materials Engineering (LAIGM) at the University of 8 Mai 1945, Guelma. I would like to express my thanks to **Professor Benhamza Mohamed El Hocine** (former director) and **Professor Affoune Abed Mohamed** (new director) for welcoming me into the laboratory during these four years.

A special thanks to the people with whom I had the chance to collaborate and who contributed to this work. In particular, I would like to thank **Professor Maxime Pontié**, head of the Analysis and Processes group, and Romain Mallet, a microscopy engineer at the University of Angers, for their invaluable help with the structural and microstructural characterization of the developed electrodes. I also thank Professor Pontié for welcoming me into his laboratory, for his kindness, motivation, and the advice he gave me, which were crucial in the writing of this thesis.

I would also like to express my deep gratitude to **Professor AMIRA-GUEBAILIA Habiba** for agreeing to chair my thesis jury. A big thank you also to **Professor Hamlaoui Youcef** and **Chouarfa Fella** for accepting to examine this manuscript and for offering their valuable advice and feedback on my work.

What would this thesis be without my colleagues, my fellow PhD students? (Some of them are now a PhD, I will likely forget some names, but you will recognize yourselves!): Sarra Abdi for always helping me without hesitation, Drissi Widad, Kadri Nahla, Makhlouf Mohamed Rabah, Saad Guermeche Rania, Boukour Mouni, Houam Sabrina... Thank you all for your precious help, your advice, and our many discussions (not always scientific, by the way!).

I am extremely grateful to Mrs. Houda Boukhdenna, Dr. Tahar Derabla, and Mrs. Nadia Chiheb for their constant support and exceptional kindness. I also want to thank Dr. Aissat Fares, my office mate, for putting up with my questionable sense of humor and my loud entrances into the office during the article-writing period.

I would also like to thank all the members of the LAIGM laboratory for their support and good humor. I felt so welcome there, and it made all the difference.

Finally, as I reach the end of this long journey, I want to express my deep gratitude to those who sparked my love for science and research: my parents, Azzedine Makhlouf and Keltoum Cherifi, and all my teachers for inspiring me.

A thesis is not solely the result of work done in the laboratory. It is the product of unwavering support, love, and encouragement from those around me. First and foremost, I want to express my deepest gratitude to my entire family, especially my sisters, Taqwa and Sadjida. And of course, I must not forget my little brother, Houdaifa, who will always hold a special place in my heart. Without them, I would not be where I am today—and more importantly, I would not be the person I am. Their support has been an invaluable source of strength throughout these past four years, which, as many know, have not always been easy.

Before I conclude this section of acknowledgments, I must also extend a heartfelt thank you to my husband, Mohamed El Amine. Though you entered my life towards the final stages of this thesis, your presence has been invaluable. Your emotional support and encouragement have been pivotal in helping me push through and complete what I set out to achieve.

Abstract

Self-medication with over-the-counter (OTC) analgesics like paracetamol (PA) and its toxic byproduct, 4-aminophenol (4-AP), is on the rise. While OTC analgesics are generally safe at recommended doses, overuse can lead to liver and kidney damage. Ascorbic acid (AA) and zinc ion (Zn(II)) are often combined with PA, but excessive intake can cause gastrointestinal, kidney, and neurological issues. The unmonitored use of these substances individually or in combination raises concerns about potential overdoses and adverse reactions, highlighting the need for reliable, sensitive detection methods to ensure patient safety. Due to the electroactive nature of PA, 4-AP, AA, and Zn(II), electrochemical sensors, particularly screen-printed electrodes (SPEs), have emerged as a promising tool. SPEs, typically consisting of a working electrode, counter electrode, and reference electrode on a single substrate, have gained widespread popularity in electroanalysis over the past few decades for offering advantageous material properties, including disposability, fast response times, compact size, low cost, and ease of portability.

This thesis presents the development of two electrochemical sensors based on screen-printed electrodes modified with Pt–Ni bimetallic nanoparticles for detecting paracetamol, 4-aminophenol, ascorbic acid, and zinc. The sensors, differing in their working electrodes (graphite vs graphene), utilize Pt–Ni nanoparticles for enhanced electro-catalytic performance, enabling both individual and simultaneous detection in pharmaceutical and biological samples.

The first sensor, a Pt–Ni-modified graphite-based SPE, enabled the simultaneous detection of 4-AP, PA, AA, and Zn(II). The Pt–Ni/SPE electrode was characterized by field emission scanning electron microscope (FE–SEM), transmission electron microscope (TEM), energy dispersive X–ray spectroscopy (EDX), X–ray diffractometry (XRD), and atomic force microscopy (AFM), and its electrochemical performance was assessed using cyclic voltammetry (CV) and electrochemical impedance spectroscopy (EIS). Under optimum conditions, the content of 4-AP, PA, AA and Zn(II) was quantified using cyclic voltammetry (CV), differential pulse voltammetry (DPV) and square-wave voltammetry (SWV) techniques. The sensor demonstrated a linear DPV response for 4-AP and PA (0.5 to 200 µM) with detection limits (LODs) of 0.33 µM and 0.23 µM (*S/N* = 3), and sensitivities of $0.768 \pm 0.01\ \mu A\ \mu M^{-1}\ cm^{-2}$ and $1.289 \pm 0.01\ \mu A\ \mu M^{-1}\ cm^{-2}$, respectively. For PA, AA, and Zn(II), the sensor exhibited linear responses ranging from 0.01 to 0.8 µM for Zn(II), 10 to 1800 µM for AA, and 0.5 to 200 µM for PA, with detection limits of 0.004 µM, 9.0 µM, and 0.15 µM for Zn(II), AA, and PA, respectively. The sensor demonstrated excellent reproducibility, stability, and anti-interference performance, successfully detecting 4-AP, PA, AA, and Zn(II) in pharmaceutical formulations and human plasma samples.

The second sensor, a Pt–Ni-modified graphene-based SPE (Pt–Ni/SPGE), was developed for individual and simultaneous detection of 4-AP, AA, and PA. It showed excellent performance, exhibiting linear CV ranges from 1.0 to 1000 µM, with LOD (*S/N* = 3) value of 2.0 µM for both 4-AP and PA, alongside sensitivities of $2.8 \pm 0.01\ \mu A\ \mu M^{-1}\ cm^{-2}$ for 4-AP and $1.4 \pm 0.01\ \mu A\ \mu M^{-1}\ cm^{-2}$for PA. Additionally, it demonstrated linearity from 10 µM to 2400 µM for AA and 1.0 µM to 800 µM for PA, with LODs of 30 µM and 5.0 µM, respectively.

These findings demonstrate the potential of Pt–Ni-modified SPEs for sensitive, simultaneous detection of pharmaceuticals, offering a cost-effective, rapid tool for monitoring self-medication and preventing drug interactions.

Keywords: Electrochemical sensors, Platinum-Nickel nanoparticles, Screen-printed electrodes, Paracetamol, 4-aminophenol, Ascorbic acid, Zinc, Simultaneous detection, Self-medication.

Résumé

L'automédication avec des analgésiques en vente libre tels que le paracétamol (PA) et son sous-produit toxique, le 4-aminophénol (4-AP), est en augmentation. Bien que les analgésiques en vente libre soient généralement sûrs aux doses recommandées, une surconsommation peut entraîner des dommages au foie et aux reins. L'acide ascorbique (AA) et l'ion zinc (Zn(II)) sont souvent associés au PA, mais une ingestion excessive peut causer des problèmes gastro-intestinaux, rénaux et neurologiques. L'utilisation non contrôlée de ces substances, individuellement ou en combinaison, soulève des inquiétudes concernant les risques de surdoses et de réactions indésirables, ce qui met en évidence la nécessité de méthodes de détection fiables et sensibles pour garantir la sécurité des patients. En raison de la nature électroactive du PA, du 4-AP, de l'AA et du Zn(II), les capteurs électrochimiques, en particulier les électrodes sérigraphiées (SPE), ont émergé comme un outil prometteur. Les SPE, qui se composent généralement d'une électrode de travail, d'une contre électrode et d'une électrode de référence sur un seul substrat, ont gagné une grande popularité dans le domaine de l'électroanalyse au cours des dernières décennies en raison de leurs propriétés matérielles avantageuses, telles que la jetabilité, des temps de réponse rapides, une taille compacte, un faible coût et une grande portabilité.

Cette thèse présente le développement de deux capteurs électrochimiques basés sur des électrodes sérigraphiées modifiées avec des nanoparticules bimétalliques Pt-Ni pour détecter le paracétamol, le 4-aminophénol, l'acide ascorbique et le zinc. Les capteurs, qui diffèrent par leurs électrodes de travail (graphite contre graphène), utilisent des nanoparticules de Pt-Ni pour améliorer les performances électro-catalytiques, ce qui permet une détection individuelle et simultanée dans des échantillons pharmaceutiques et biologiques.

Le premier capteur, une SPE à base de graphite modifié par du Pt-Ni, a permis la détection simultanée de 4-AP, PA, AA et Zn(II). L'électrode Pt-Ni/SPE a été caractérisée par microscope électronique à balayage à émission de champ (FE-SEM), microscope électronique à transmission (TEM), spectroscopie à rayons X à dispersion d'énergie (EDX), diffractométrie à rayons X (XRD) et microscopie à force atomique (AFM), et ses performances électrochimiques ont été évaluées par voltampérométrie cyclique (CV) et spectroscopie d'impédance électrochimique (EIS). Dans des conditions optimales, la teneur en 4-AP, PA, AA et Zn(II) a été quantifiée par voltampérométrie cyclique (CV), voltampérométrie différentielle (DPV) et voltampérométrie à ondes carrées (SWV). Le capteur a démontré une réponse DPV linéaire pour le 4-AP et le PA (0,5 à 200 µM) avec des limites de détection (LOD) de 0,33 µM et 0,23 µM (*S/N* = 3) et des sensibilités de $0{,}768 \pm 0{,}01\ \mu A\ \mu M^{-1}\ cm^{-2}$ et $1{,}289 \pm 0{,}01\ \mu A\ \mu M^{-1}\ cm^{-2}$, respectivement. Pour le PA, l'AA et le Zn(II), le capteur a présenté des réponses linéaires allant de 0,01 à 0,8 µM pour le Zn(II), de 10 à 1800 µM pour l'AA et de 0,5 à 200 µM pour le PA, avec des limites de détection de 0,004 µM, 9,0 µM et 0,15 µM pour le Zn(II), l'AA et le PA, respectivement. Le capteur a démontré une excellente reproductibilité, stabilité et performance anti-interférence, détectant avec succès le 4-AP, le PA, l'AA et le Zn(II) dans les formulations pharmaceutiques et les échantillons de plasma humain.

Le deuxième capteur, une SPE à base de graphène modifiée par du Pt–Ni (Pt–Ni/SPGE), a été développé pour la détection individuelle et simultanée de 4-AP, AA et PA. Il a montré d'excellentes performances, avec des gammes linéaires de CV allant de 1,0 à 1000 µM, avec une LOD (*S/N* = 3) de 2,0 µM pour les deux 4-AP et PA, ainsi que des sensibilités de $2{,}8 \pm 0{,}01\ \mu A\ \mu M^{-1}\ cm^{-2}$ pour 4-AP et $1{,}4 \pm 0{,}01\ \mu A\ \mu M^{-1}\ cm^{-2}$ pour PA. De plus, il a démontré une linéarité de 10 µM à 2400 µM pour l'AA et de 1,0 µM à 800 µM pour le PA, avec des LOD de 30 µM et 5,0 µM, respectivement.

Ces résultats démontrent le potentiel des SPE modifiées par le Pt-Ni pour la détection sensible et simultanée de produits pharmaceutiques, offrant ainsi un outil rapide et rentable pour le contrôle de l'automédication et la prévention des interactions médicamenteuses.

Mots-clés: Capteurs électrochimiques, nanoparticules de platine-nickel, électrodes sérigraphiées, paracétamol, 4-aminophénol, acide ascorbique, zinc, détection simultanée, automédication.

ملخص

إن استخدام الأدوية المسكنة التي تُصرف دون وصفة طبية مثل الباراسيتامول (PA) ومنتجه السام 4-أمينوفينول (4-AP)في تزايد. بينما تكون الأدوية المسكنة التي تُصرف دون وصفة طبية عادةً آمنة عند استخدامها بالجرعات الموصى بها، فإن الإفراط في استخدامها يمكن أن يؤدي إلى تلف الكبد والكلى. يتم دمج حمض الأسكوربيك (AA) وأيون الزنك (Zn(II))غالبًا مع الباراسيتامول، ولكن الاستهلاك المفرط يمكن أن يسبب مشاكل في الجهاز الهضمي والكلى والجهاز العصبي. إن الاستخدام غير المراقب لهذه المواد سواء بشكل فردي أو معًا يثير القلق بشأن احتمال حدوث جرعات زائدة وردود فعل سلبية، مما يسلط الضوء على الحاجة إلى طرق كشف موثوقة وحساسة لضمان سلامة المرضى. نظرًا للطبيعة الكهروكيميائية للباراسيتامول و4-أمينوفينول وحمض الأسكوربيك والزنك، فقد ظهرت المستشعرات الكهروكيميائية، وخاصةً الأقطاب الكهربائية المطبوعة على الشاشة (SPE) ، كأداة واعدة. تعتبر الأقطاب الكهربائية المطبوعة على الشاشة، التي تتكون عادة من قطب عمل، وقطب ضد، وقطب مرجعي على ركيزة واحدة، قد اكتسبت شهرة واسعة في التحليل الكهروكيميائي في العقود الأخيرة بسبب خصائص المواد المميزة لها، بما في ذلك القابلية للتخلص منها، وأوقات الاستجابة السريعة، والحجم المدمج، والتكلفة المنخفضة، وسهولة حملها.

تستعرض هذه الأطروحة تطوير جهازين استشعار كيميائي كهربائي معتمدان على أقطاب كهربائية مطبوعة بالشاشة تم تعديلها بجزيئات نانو ثنائية المعدن من البلاتين-النيكل للكشف عن الباراسيتامول، 4-أمينوفينول، حمض الأسكوربيك، والزنك. تختلف المستشعرات في أقطابها العاملة (غرافيت مقابل جرافين)، وتستخدم جزيئات نانو البلاتين-النيكل لتحسين الأداء الكهرو-تحفيزي، مما يسمح بالكشف الفردي والمتزامن في العينات الصيدلانية والبيولوجية.

المستشعر الأول، الذي يعتمد على قطب كهربائي من الغرافيت المعدل بالبلاتين-النيكل، مكّن من الكشف المتزامن عن 4-أمينوفينول، الباراسيتامول، حمض الأسكوربيك، والزنك .تم تمييز قطب Pt–Ni/SPE باستخدام المجهر الإلكتروني الماسح بالإصدار الميداني(FE–SEM) ، والمجهر الإلكتروني الناقل (TEM) ، والتحليل الطيفي للأشعة السينية المشتتة للطاقة (EDX) ، والحيود بالأشعة السينية (XRD) ، والمجهر القوي الذري (AFM) ، وتم تقييم أدائه الكهروكيميائي باستخدام الفولتمترية الدورية (CV) وتحليل مقاومة الأقطاب الكهروكيميائية (EIS). في ظل الظروف المثلى، تم تحديد محتوى 4-أمينوفينول، الباراسيتامول، حمض الأسكوربيك، والزنك باستخدام تقنيات الفولتمترية الدورية(CV) ، والفولتمترية بالنبض التفاضلي(DPV) ، والفولتمترية بالموجات المربعة (SWV). أظهر المستشعر استجابة خطية باستخدام الفولتمترية بالنبض التفاضلي (DPV) للـ 4-أمينوفينول والباراسيتامول (من 0.5 إلى 200 ميكرومتر) مع حدود الكشف (LOD) بلغت 0.33 ميكرومتر و0.23 ميكرومتر(S/N = 3) ، وحساسية بلغت 0.768 ±0.01 و1.289 ±0.01 $\mu A\ \mu M^{-1}\ cm^{-2}$ على التوالي. بالنسبة للباراسيتامول، حمض الأسكوربيك والزنك، أظهر المستشعر استجابات خطية تتراوح من 0.01 إلى 0.8 ميكرومتر للزنك، ومن 10 إلى 1800 ميكرومتر لحمض الأسكوربيك، ومن 0.5 إلى 200 ميكرومتر للباراسيتامول، مع حدود كشف بلغت 0.004 ميكرومتر، 9.0 ميكرومتر، و0.15 ميكرومتر للزنك ، حمض الأسكوربيك، والباراسيتامول على التوالي. أظهر المستشعر تكرارية ممتازة، استقرارًا وأداءً مقاومًا للتداخل، مما مكّنه من الكشف بنجاح عن 4-أمينوفينول، الباراسيتامول، حمض الأسكوربيك والزنك في التركيبات الصيدلانية وعينات البلازما البشرية.

تم تطوير المستشعر الثاني، وهو جهاز SPE قائم على الجرافين المعدل بـ Pt–Ni (Pt–Ni/SPGE) ، للكشف الفردي والمتزامن عن4-AP و AA وPA . أظهر أداء ممتازًا، حيث عرض نطاقات CV خطية من 1.0 إلى 1000 ميكرومتر، مع قيمة LOD (S/N = 3) تبلغ 2.0 ميكرومتر لكل من 4-AP وPA ، إلى جانب حساسيات قدرها $\pm$ 2.8 $\mu A\ \mu M^{-1}\ cm^{-2}$ 0.01 لـ 4-AP و $\pm$ 0.01 $\mu A\ \mu M^{-1}\ cm^{-2}$ 1.4 لـ PA .بالإضافة إلى ذلك، أظهر خطية من 10 ميكرومتر إلى 2400 ميكرومتر لـ AA ومن 1.0 ميكرومتر إلى 800 ميكرومتر لـPA ، مع قيم LOD تبلغ 30 ميكرومتر و 5.0 ميكرومتر على التوالي.

تُظهر هذه النتائج إمكانية استخدام الأقطاب الكهربائية المطبوعة بالشاشة المعدلة بالبلاتين-النيكل للكشف الحساس والمتزامن عن الأدوية، مما يوفر أداة فعالة من حيث التكلفة وسريعة لمراقبة استخدام الأدوية الذاتية ومنع التفاعلات الدوائية.

الكلمات المفتاحية :أجهزة استشعار كيميائية كهربائية، جزيئات نانو البلاتين-النيكل، أقطاب كهربائية مطبوعة بالشاشة، باراسيتامول، 4-أمينوفينول، حمض الأسكوربيك، زنك، الكشف المتزامن، الاستخدام الذاتي للأدوية.

Table of contents

List of figures

Chapter I

Chapter II

Chapter III

Chapter IV

Part A

Part B

List of tables

List of abbreviations and symbols

Abbreviations

Abbreviation	Significance
PA	Paracetamol
4-AP	4-aminophenol
AA	Ascorbic acid
Zn(II)	Zinc ion
SPEs	Screen-printed electrodes
PtNPs	Platinum nanoparticles
AuNPs	Gold nanoparticles
AgNPs	Silver nanoparticles
CNTs	Carbon nanotubes
MWCNTs	Multiwall carbon nanotubes
SWCNT	Single-walled carbon nanotube
Ni	Nickel
Pt–Ni	Platinum-nickel
CP	Conducting polymer
PPy	Polypyrrole
PANI	Polyaniline
PTs	Polythiophene
PEDOT	Poly(3,4-ethylenedioxythiophene)
MIPs	Molecularly imprinted polymers
OTC	Over-the-counter
COVID-19	Coronavirus disease 2019
HPLC	High-performance liquid chromatography
FE-SEM	Field-emission scanning electron microscopy
TEM	Transmission electron microscopy
XRD	X-ray diffraction
AFM	Atomic force microscopy
EIS	Electrochemical impedance spectroscopy
CV	Cyclic voltammetry
SWV	Square wave voltammetry
DPV	Differential pulse voltammetry
DPASV	Differential pulse anodic stripping voltammetry
UV	Ultraviolet
AAS	Atomic absorption spectrometry

Amp	Amperometry
CA	Chronoamperometry
INN	International non-proprietary name
WHO	World health organization
NAPQI	N-acetyl-p-benzo-quinone imine
MA	Marketing authorization
NB	Note well
SVCT1	Sodium-dependent vitamin C transporter 1
SVCT2	Sodium-dependent vitamin C transporter 2
LOD	Limits of detection
CE	Counter electrode
WE	Working electrode
PRE	Pseudo-reference electrode
PBS	Phosphate buffer solution
ABS	Acetate buffer solution
Caf	Caffeine
Glu	Glucose
Fru	Fructose
Gal	Galactose
Cit	Citric acid

Symbols

Symbol	**Significance**
α	Transfer coefficient
ΔE_p	Potential peak separation
λ	X-ray wavelength
ψ	Kinetic parameter
θ	Bragg angle
υ	Voltammetric scanning rate
A	Electroactive area of working electrode
C	Bulk concentration
C_{dl}	Double-layer capacitor
CPE	Constant phase element
D	Diffusion coefficient
d	Interplanar distance

E	Potential
E_{pa}	Oxidation peak potential
E_{pc}	Reduction peak potential
F	Faraday constant
I	Current
I_C	Capacitive current
I_F	Faradic current
I_{pa}	Anodic peak current
I_{pc}	Cathodic peak current
k°	Heterogeneous electron transfer rate constant
n	Number of electrons
R	Universal gas constant
R_{ct}	Charge transfer resistance
R_s	Solution resistance
t	Time
T	Temperature
Z	Impedance
Z_w	*Warburg* impedance
W	Warburg element

General introduction

General introduction

In recent years, there has been an increasing demand from patients for access to medications without the need for a medical consultation or prescription. This shift in consumer behavior has had significant economic implications for manufacturers, prompting a change in the status of various pharmaceutical products. Many drugs have transitioned from being prescription-only to being available over-the-counter (OTC); with pain relievers (analgesics) among the most commonly used medications globally, whether dispensed with or without a prescription. OTC analgesics are generally well tolerated when used in short-term treatments at recommended doses. However, their misuse can pose significant health risks, of which patients are often unaware.

Paracetamol (PA), also known as acetaminophen, is one of the most commonly used OTC analgesics. It is effective in treating mild to moderate pain, such as headaches, back pain, and arthritis, and is also used to reduce fever **[1, 2]**. At standard therapeutic doses, PA is considered safe, but overuse can lead to the accumulation of toxic metabolites, causing severe liver and kidney damage, as well as other complications like pancreatitis and skin rashes. In some cases, these side effects can result in fatal outcomes **[3]**. The degradation product 4-Aminophenol (4-AP), which is formed when PA breaks down in the body, is known for its nephrotoxic and teratogenic effects. To prevent potential harm, its concentration in pharmaceutical formulations is strictly regulated **[4]**.

Ascorbic acid (AA), or vitamin C, is another essential compound widely used as a dietary supplement and for treating various conditions, such as scurvy, cardiovascular disease, and oxidative stress **[5]**. While AA is crucial for human health, excessive intake can lead to adverse effects like abdominal cramps and diarrhea **[6]**. Similarly, zinc ion (Zn(II)) is an essential mineral involved in numerous biological processes, including immune function and enzyme catalysis. Both a deficiency and an excess of zinc can cause serious health issues, such as gastrointestinal disturbances, kidney damage, and neurological problems **[7]**.

Self-medication, particularly through the use of OTC medications and dietary supplements, has become increasingly common. This trend is particularly evident during health crises, such as the COVID-19 pandemic, when individuals turned to unregulated drug combinations in an attempt to manage symptoms. This unmonitored use of medications raises concerns about potential overdose and adverse reactions, which may lead to life-threatening complications. Therefore, the need for sensitive and reliable methods to detect and quantify these substances has become more urgent.

While traditional analytical methods, such as high-performance liquid chromatography (HPLC) and capillary electrophoresis, are effective for detecting paracetamol, 4-aminophenol, ascorbic acid, and zinc, they are often impractical for routine analysis due to their complexity, cost, and the need for skilled operators **[8]**. Due to the electroactive nature of PA, 4-AP, AA and Zn(II) compounds, elctrochemical sensors, particularly those based on voltammetric techniques, offer a promising alternative. These sensors are cost-effective, easy to use, and capable of providing rapid, on-site measurements **[9]**.

Among the most promising technologies are screen-printed electrodes (SPEs), which offer significant advantages such as disposability, fast response times, low cost, and ease of portability **[10]**. SPEs are typically configured with a working electrode, a counter electrode, and a reference electrode. These electrodes can be modified with nanomaterials **[11, 12]**, such as noble metals, to enhance their electrochemical properties via electrochemical deposition technique. Platinum nanoparticles (PtNPs), in particular, have been widely studied for their excellent electro-catalytic properties **[13]**. However, platinum's tendency to become poisoned by adsorbed intermediates can limit its efficiency **[14]**. This issue can be addressed by creating bimetallic systems, such as platinum-nickel (Pt–Ni), which combine the advantages of both metals. The incorporation of Pt with another transition metal enhances both the synergistic and electronic properties. In the synergistic process, the secondary metal plays a pivotal role in facilitating the oxidative removal of blocking residues at the Pt active sites **[15]**, improving the overall electrochemical performance of the system. Nickel (Ni), a widely researched transition metal, is known for its stability, cost-effectiveness, environmental friendliness, and abundant availability **[16]**. These features make it an ideal candidate for combination with platinum to form Pt–Ni bimetallic systems. These Pt–Ni bimetallic materials have been extensively studied and applied in various fields due to their superior catalytic and electronic properties, making them highly effective for electrochemical sensing applications.

This thesis introduces a novel electrochemical sensor based on screen-printed electrodes, featuring two types of working electrodes, either graphite or graphene, modified with Pt–Ni bimetallic nanoparticles via a facile and effective electrodeposition technique. The sensor is designed for the individual or simultaneous detection of paracetamol, 4-aminophenol, ascorbic acid, and zinc in pharmaceutical and biological samples. This configuration offers a simple, rapid, and cost-effective tool for monitoring self-medication practices.

This thesis is organized into four main chapters:

Chapter one provides a detailed introduction to the target pharmaceutical molecules, highlighting their toxicity when misused, and discusses various detection methods used for these compounds.

Chapter two starts with an overview of the fundamentals of electrochemical sensors, focusing on key features like sensitivity, selectivity, and stability. It then reviews the literature on screen-printed electrodes, covering their configuration, fabrication, and the use of various nanomaterial modifiers, including polymers, carbon-based materials, and special emphasis is placed on metallic nanoparticles for enhancing sensor performance. The chapter concludes with a discussion on the application of modified SPEs for detecting target analytes in clinical and environmental settings.

Chapter three describes the experimental study, presenting the methods used for developing and characterizing the new electrochemical sensors. This chapter covers the preparation and functionalization of screen-printed electrodes, as well as the characterization of the Pt–Ni nanoparticles using field-emission scanning electron microscopy (FE-SEM), transmission electron microscopy (TEM), energy-dispersive X-ray spectroscopy (EDX), X-ray diffraction (XRD), and atomic force microscopy (AFM) techniques. Electrochemical techniques such as electrochemical impedance spectroscopy (EIS), cyclic voltammetry (CV), square wave voltammetry (SWV), and differential pulse voltammetry (DPV) are used to assess the sensor performance.

Chapter four is divided into two parts:

Part A focuses on the development, as well as the physical and electrochemical characterization, of the Pt–Ni/SPE sensor featuring a graphite working electrode, designed for the detection of paracetamol, 4-aminophenol, ascorbic acid, and zinc.

Part B further investigates the use of Pt–Ni bimetallic nanoparticles on a graphene-based screen-printed electrode (Pt–Ni/SPGE). Following the physical characterization of the sensor, it was employed for the individual and simultaneous detection of paracetamol, 4-aminophenol, and ascorbic acid, while investigating the electrochemical behavior of these compounds.

The thesis concludes by summarizing the findings and discussing the implications of the research, with suggestions for future work in the field of electrochemical sensor development.

References

[1] H. Wang, S. Zhang, S. Li, J. Qu, Electrochemical sensor based on palladium reduced graphene oxide modified with gold nanoparticles for simultaneous determination of acetaminophen and 4-aminophenol, Talanta 178 (2018) 188–194.
[2] N. Dou, J. Qu, Rapid synthesis of a hybrid of rGO/AuNPs/MWCNTs for sensitive sensing of 4-aminophenol and acetaminophen simultaneously, Anal. Bioanal. Chem. 413 (2021) 813–820.
[3] M. Kenarkob, Z. Pourghobadi, Electrochemical sensor for acetaminophen based on a glassy carbon electrode modified with ZnO/Au nanoparticles on functionalized multi-walled carbon nano-tubes, Microchem. J. 146 (2019) 1019–1025.
[4] T.T. Calam, A modified pencil graphite electrode with 2-thiobarbituric acid for the efficient and cheap voltammetric sensing of 4-aminophenol in water samples and child syrup sample, J. Food Compos. Anal. 98 (2021) 103809.
[5] L. Suntornsuk, W. Gritsanapun, S. Nilkamhank, A. Paochom, Quantitation of vitamin C content in herbal juice using direct titration, J. Pharm. Biomed. Anal. 28 (2002) 849–855.
[6] Y. Ma, Y. Zhang, L. Wang, An electrochemical sensor based on the modification of platinum nanoparticles and ZIF-8 membrane for the detection of ascorbic acid, Talanta 226 (2021) 122105.
[7] Y. Shao, Y. Dong, L. Bin, L. Fan, L. Wang, X. Yuan, D. Li, X. Liu, S. Zhao, Application of gold nanoparticles/polyaniline-multi-walled carbon nanotubes modified screen-printed carbon electrode for electrochemical sensing of zinc, lead, and copper, Microchem. J. 170 (2021) 106726.
[8] M.Nemakal, S. Aralekallu, I. Mohammed, M. Pari, K.R.V. Reddy, L.K. Sannegowda, Nanomolar detection of 4-aminophenol using amperometric sensor based on a novel phthalocyanine, Electrochim. Acta 318 (2019) 342–353.
[9] R.M. Hanabaratti, S.M. Tuwar, S.T. Nandibewoor, J.I. Gowda, Fabrication and characterization of zinc oxide nanoparticles modified glassy carbon electrode for sensitive determination of paracetamol, Chem. Data Coll. 30 (2020) 100540.
[10] B. Thakur, E. Bernalte, J.P. Smith, C.W. Foster, P.E. Linton, S.N. Sawant, C. E. Banks, Utilising copper screen-printed electrodes (CuSPE) for the electroanalytical sensing of sulfide, Analyst 141 (2016) 1233.
[11] P.M. Jahani, S.Z. Mohammadi, A. Khodabakhshzadeh, J.H. Cha, M.S. Asl, M. Shokouhimehr, K. Zhang, Q.V. Le, W. Peng, Simultaneous detection of morphine and diclofenac using graphene nanoribbon modified screen-printed electrode, Int. J. Electrochem. Sci. 15 (2020) 9037–9048.
[12] H. Beitollahi, M. Shahsavari, I. Sheikhshoaie, S. Tajik, P.M. Jahani, S. Z. Mohammadi, A.A. Afshar, Amplified electrochemical sensor employing screen printed electrode modified with Ni–ZIF–67 nanocomposite for high sensitive analysis of sudan I in present bisphenol A, Food Chem. Toxicol. 161 (2022) 112824.
[13] B. Patella, A. Sortino, F. Mazzara, G. Aiello, G. Drago, C. Torino, A. Vilasi, A. O'Riordan, R. Inguanta, Electrochemical detection of dopamine with negligible interference from ascorbic and uric acid by means of reduced graphene oxide and metals-NPs based electrodes, Anal. Chim. Acta 1187 (2021) 339124.
[14] M. Nacef, M.L. Chelaghmia, O. Khelifi, M. Ponti´ e, M. Djelaibia, R. Guerfa, V. Bertagna, C. Vautrin-Ul, A. Fares, A.M. Affoune, Electrodeposited Ni on pencil graphite electrode for glycerol electrooxidation in alkaline media, Int. J. Hydrogen Energ. 46 (2021) 37670–37678.
[15] M.L. Chelaghmia, M. Nacef, H. Fisli, A.M. Affoune, M. Ponti´ e, A. Makhlouf, T. Derabla, O. Khelifi, F. Aissat, Electrocatalytic performance of Pt–Ni nanoparticles supported on an activated graphite electrode for ethanol and 2–propanol oxidation, RSC Adv. 10 (2020) 36941–36948.
[16] M.L. Chelaghmia, H. Fisli, M. Nacef, D.A.C. Brownson, A.M. Affoune, H. Satha, C. E. Banks, Disposable non-enzymatic electrochemical glucose sensors based on screen-printed graphite macroelectrodes modified via a facile methodology with Ni, Cu, and Ni/Cu hydroxides are shown to accurately determine glucose in real human serum blood samples, Anal. Methods 25 (2021) 2812–2822.

Chapter I

Paracetamol, 4-aminophenol, ascorbic acid, zinc-analytes of interest

I.1. Introduction

In recent years, there has been an increasing demand for patients to access medications without a prescription. Analgesics, especially paracetamol, are widely used, either with medical guidance or in self-medication. However, their use carries risks, particularly in older individuals or those on multiple medications, due to potential drug interactions and toxicity. Paracetamol's primary risk is liver toxicity, linked to the formation of its toxic metabolite, 4-aminophenol, which becomes hazardous in overdose situations.

Additionally, many patients combine paracetamol with supplements like vitamin C and zinc to boost immunity, which can increase the risk of overdose if not monitored properly. This chapter reviews paracetamol, its toxic metabolite, 4-aminophenol, as well as ascorbic acid and zinc, and discusses various methods for detecting these substances. It covers both traditional analytical techniques, highlighting their limitations, and electroanalytical methods, which offer more sensitive and efficient detection. Understanding these detection approaches is crucial for monitoring patient safety and managing the risks associated with drug-supplement interactions.

I.2. Target analytes: Background

I.2.1. Paracetamol

I.2.1.1. History

At the beginning of the 19th century, numerous experiments were carried out with an organic compound, aniline, a raw material for the dye industry. The antipyretic and later analgesic properties of a derivative, acetanilide, were discovered by chance in 1886. *Arnold Cahn* and *Paul Hepp*, two researchers at the University of Strasbourg working on the antiparasitic effect of naphthalene, received acetanilide after a delivery error. It was only when they resumed their experiments and obtained unusual antipyretic effects that they realized the confusion. The antipyretic properties of acetanilide were discovered and Antifébrine® was marketed. Unfortunately, this drug was responsible for numerous adverse effects, including methemoglobinemia **[1, 2]**.

Cinchona bark was once widely used for its antipyretic properties, but as it became scarce and expensive, a substitute had to be found, and thus acetaminophen was born. Paracetamol was first synthesized in 1878 by *Harmon Northrop Morse* under the name acetylaminophenol **[3, 4]**.

In 1893, a German doctor, *J. Von Mering*, discovered the antipyretic and analgesic properties of acetylaminophenol, and recognized it as a medicine **[5]**. Nevertheless, it wasn't until 1948 that three American researchers, *Brodie*, *Flinn* and *Axelrod*, succeeded in obtaining

a pure form of paracetamol. Subsequently, *Bernard Brodie* and *Julius Axelrod* discovered that the body breaks down acetanilide and phenacetin into various metabolites. Their experiments showed that paracetamol was the metabolite responsible for the analgesic and antipyretic activity, while the others were responsible for the various adverse effects observed **[6]**. Paracetamol was first launched on the American market in 1955 by McNeil Consumer Healthcare under the name Tylenol Children's Elixir®, an over-the-counter syrup for fever and pain in children (Figure I.1). It was later introduced in the United Kingdom in 1956 under the brand name Panadol® by Sterling Drug Inc. [7].

In France, it appeared in 1957 under the name Algotropyl® for children and in 1961 under the name Doliprane®, and paracetamol gradually filled pharmacy counters. By 2011, in many forms and under many names, it had become the most widely used over-the-counter medicine in the world **[8]**.

Figure I.1. Tylenol® packaging.

I.2.1.2. Denomination and chemical structure

The paracetamol (PA) molecule (Figure I.2) belongs to the anilide group, sharing a common core with several compounds with antipyretic and analgesic properties. The molecule consists of a benzene ring, substituted with a hydroxyl group and an amide group in the para position. Paracetamol has no asymmetric carbon and no stereoisomer. One of the two free doublets of the oxygen atom of the hydroxyl group, the benzene ring, the free doublet of the nitrogen atom and the p-orbital of the carbonyl carbon form a conjugated system (possible mesomerism). This conjugation reduces the basicity of the oxygens and nitrogen and makes the hydroxyl group more acidic (as in phenols), since charge delocalization occurs on a phenolate ion. The two activating groups make the ring highly reactive and thus facilitate possible electrophilic aromatic substitutions in the ortho or para positions. However, all positions in the

ring (ortho, meta, para) are equally activated, so there is no preferred site for electrophilic substitution **[9]**.

There are many different names for paracetamol, the most common of which are:

-The international non-proprietary name (INN) recommended by the World Health Organization (WHO) is Paracetamol.

-The name recommended by the US pharmacopeial convention is Acetaminophen.

In the literature, it is also known as acetamidophenol, acetyl-aminophenol, 4-hydroxyacetanilide, parahydroxy-acetanilide, or N-acetyl-paraaminophenol **[10, 11]**.

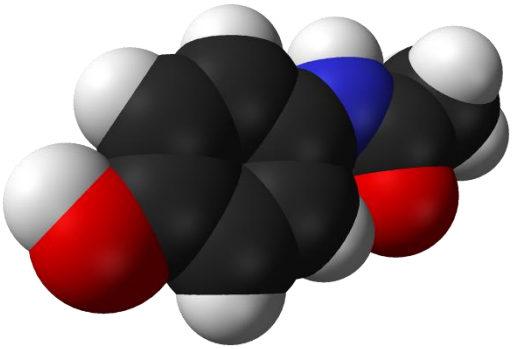

Figure I.2. Chemical structure of paracetamol.

I.2.1.3. Physicochemical properties

The principal physicochemical properties of paracetamol are listed in the following table:

Table I.1. Physicochemical properties of paracetamol **[12]**.

Molecular formula	$C_8H_9NO_2$
Molar mass	151.2 g/mol
Melting point	168-172°C
Dissociation constant	pKa = 9.5 at 25°C
Density	1.263 g/cm^3
Ultraviolet (UV) absorption	An absorption maximum at 240 nm (in ethanol)
Solubility	Water: quite soluble Alcohol: easily soluble Methylene chloride, Ether and Chloroform: very slightly soluble
Aspects	white, odorless, crystalline powder with a bitter taste

I.2.1.4. Pharmacokinetics and pharmacodynamics

I.2.1.4.1. Pharmacokinetics

Pharmacokinetics is the quantitative relationship between an administered dose of a pharmaceutical product and changes in plasma and tissue concentrations over time **[13]**.

a) Absorption

Absorption of paracetamol follows 1st-order kinetics by passive diffusion **[14]**. The good absorption of paracetamol is explained by its pKa close to 9.5, with a non-ionized form in the lumen of the digestive tract, which facilitates its assimilation. It is also possible to use the rectal route, with an absorption rate almost similar to that of the oral route. This route offers advantages for children and comatose patients who may have difficulty with oral treatment **[15]**.

Following oral administration, paracetamol is almost completely absorbed, primarily in the intestine. The rate of absorption is rapid and independent of the dose ingested. Absorption is influenced by gastric emptying. In patients with slow gastric emptying, absorption from the small intestine is delayed **[16]**. Peak plasma levels in adults vary between 30 and 60 minutes for the fastest cases, and between 2 and 3 hours for the slowest. Variations in peak plasma levels depend on the route of administration and dosage form used. The time required to halve the plasma concentration of paracetamol (plasma half-life) is 1 to 3 hours in children. In adults, it is 2 to 3 hours, while in the elderly, the half-life is 3 to 5 hours **[17, 18]**.

b) Distribution

At standard therapeutic doses, paracetamol exhibits minimal plasma protein binding (less than 20%), while at acutely toxic concentrations, only 20-50% binding is possible. The distribution of paracetamol is relatively uniform across all tissues, with the exception of adipose tissue, due to its low lipid solubility. The volume of distribution is approximately 1 L/kg, and the concentrations in blood, saliva, and plasma are comparable. Due to its low molecular weight, paracetamol is able to cross the foeto-placental barrier and enter milk. However, the amount excreted in milk is less than 2% of the amount ingested, which is why acetaminophen is not inadvisable during lactation **[19-21]**. It is also found in saliva at a fraction of 1.21 compared to plasma levels **[22]**.

c) Metabolism

At usual therapeutic doses, 95% of paracetamol is hepatically metabolized in the cytosol of hepatocytes. This conjugation takes place at the phenolic OH group, mobilizing glucuronic acid or sulfuric acid. Paracetamol is thus transformed into non-toxic glucuro- or sulfoconjugated derivatives, which are eliminated in the urine. The remaining 5% is metabolized by cytochromes P450 (CYP2E1 and CYP3A4) to a highly reactive electrophilic intermediate, N-acetyl-p-benzo-quinone imine (NAPQI). The latter is neutralized by conjugation with glutathione and rapidly inactivated into non-toxic cysteine and the mercapturic acid metabolite (Figure I.3) **[23]**.

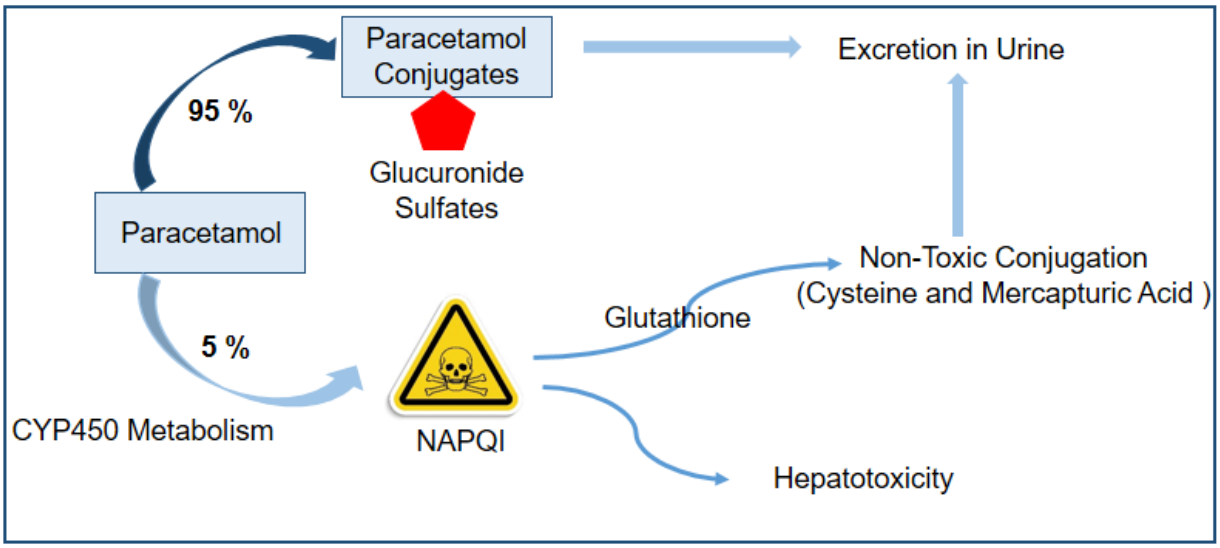

Figure I.3. Paracetamol metabolism in healthy individuals **[24]**.

d) Elimination

Metabolites of paracetamol are primarily excreted in the urine. Approximately 90% of the administered dose is excreted in the urine within 24 hours, mainly in glucuroconjugated and sulfoconjugated forms. Less than 5% is excreted unchanged. The elimination half-life is 1.5 to 3 hours, but may be prolonged in cases of severe hepatic impairment or overdose **[25, 26]**.

I.2.1.4.2. Pharmacodynamics

Paracetamol belongs to the pharmacological class of tier I analgesics, with a rapid onset of action and analgesia comparable to that of aspirin. It has two main actions :

a) Analgesic action

Paracetamol is a simple analgesic capable of reducing the perception of painful sensations (toothache, headache, arthritis, menstruation, colds, sore throat, backache, reactions to vaccinations). The analgesic effect appears 30 minutes after absorption, peaks in 2 hours and 30 minutes and disappears in 4 hours. Paracetamol exerts its analgesic action by reducing the level of prostaglandin metabolites in the urine, but does not reduce prostaglandin synthesis. Paracetamol is well tolerated, making it the reference analgesic for children and pregnant women. It is widely used for self-medication **[27, 28]**.

b) Antipyretic action

Paracetamol is a drug with only a symptomatic effect. It lowers body temperature when fever occurs (most commonly in children). It has little effect on normal body temperature, but reduces abnormally high temperatures. This effect is due to an increase in hypothalamic

thermolysis, which cools the body. The analgesic and antipyretic effects of paracetamol are predominant, while its anti-inflammatory effect is very weak **[29, 30]**.

I.2.1.5. Mechanism of action

Although more than a century has passed since its synthesis, the mechanism of action of paracetamol remains poorly defined and the subject of much debate. Numerous studies have been carried out and as illustrated in the diagram below (Figure I.4), several hypotheses have been put forward **[31-35]**:

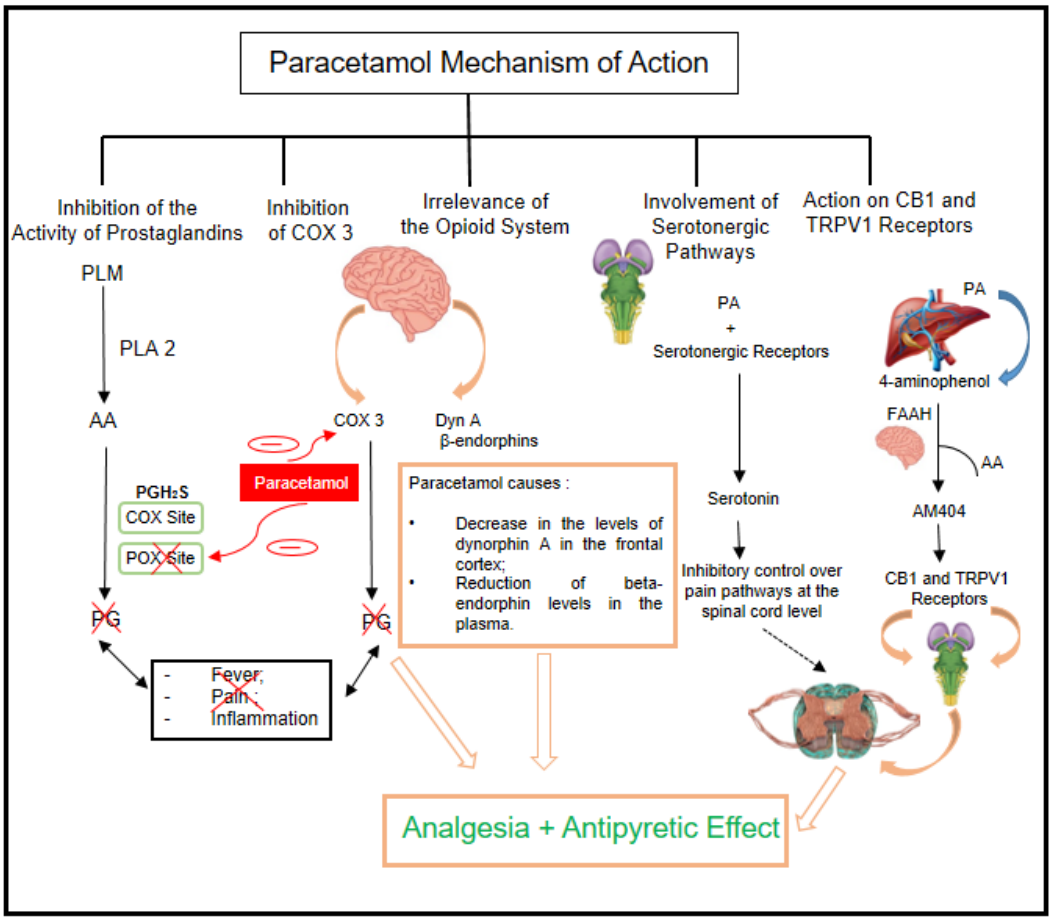

Figure I.4. Hypotheses on the mechanism of action of paracetamol.

Key:

PLM: Membrane phospholipases, **PLA 2:** Phospholipase A2, **AA:** Arachidonic acid, **PGH2S:** Prostaglandin H2 synthetase enzyme of which there are two types: 1 and 2, commonly known as COX 1 and COX 2, **COX site**: Cyclooxygenase site, **POX site :** Peroxidase site, **PG :** Prostaglandins, **COX 3:** Cyclooxygenase type 3; a new variant of COX 1, **Dyn A:** Dynorphin A, **CB1 receptors:** Cannabinoid type 1 receptors, **TRPV1 receptors:** Type 1 vanilloid

receptors, **FAAH:** Fatty acid amido-hydrolase enzyme; conjugates 4-aminophenol to arachidonic acid in the brain.

All these hypotheses have been demonstrated and verified under specific conditions, and may correspond to the true mechanism of action of paracetamol. However, the mystery of this mechanism remains to be unraveled in terms of the initiating site, the neuronal sequence involved and the extrapolation of its antipyretic effect.

I.2.1.6. Pharmacology

I.2.1.6.1. Indications

The marketing authorization (MA) for paracetamol lists the indications for which it is indicated, which depend mainly on the route of administration. Oral and rectal forms are indicated for the "symptomatic treatment of mild to moderate pain and/or febrile conditions" **[36, 37]**. As for injectable forms, the indications are more precise and concern the “short-term treatment of pain of moderate intensity, particularly in the post-operative period, and in the short-term treatment of fever, when the intravenous route of administration is clinically justified by the urgency of treating pain or hyperthermia and/or when other routes of administration are not possible” **[38]**.

Thanks to its two pharmacological actions (analgesic and antipyretic), paracetamol can be used in a number of treatments in various medical disciplines: pneumology, rheumatology, gastroenterology, surgery, etc. **[39]**.

I.2.1.6.2. Contraindications

Absolute contraindications are **[40]**:

-Known hypersensitivity to paracetamol or to any of the product's constituents;

-Severe hepatic insufficiency responsible for a decrease in NAPQI neutralization by glutathione.

-porphyria

NB: paracetamol must be taken at least eight hours apart in cases of renal insufficiency with creatinine clearance of less than 10 ml/min **[41]**.

I.2.1.6.3. Posology

The usual recommended dosage of a drug is the dose and frequency of drug to be administered to obtain the desired therapeutic effect. The resulting plasma concentration lies

within the so-called therapeutic range. It enables the expected physiological effect to be achieved with a minimum risk of side effects and adverse reactions **[42]**.

The recommended therapeutic dose of paracetamol (oral, rectal or parenteral) every 24 hours is based on the patient's weight (Table I.2) **[43]**.

Table I.2. Average paracetamol dosage as a function of weight.

Patient	Therapeutic dose per 24 hours	Maximum recommended dose per 24 hours
Children and infants (≤ 38kg)	60 mg/kg/day in 4 doses	80 mg/kg
Between 38 and 50kg	3g spaced 6 hours apart	3g
Adults and children (≥ 50kg)	3 g spaced 4 hours apart	4g in 4 doses spaced 6 hours apart

I.2.1.6.4. Drug interactions

Paracetamol drug interactions include those summarized in the table below:

Table I.3. Paracetamol drug interactions **[44-47]**.

Medicines	Consequences of interaction	Interaction mechanism
Oral anticoagulants (Warfarin and other VKAs)	Potentiation of anticoagulant effect and bleeding risk if paracetamol is taken at maximum doses (4 g/d) for at least 4 days.	The metabolite of paracetamol (NAPQI) exerts an oxidative effect on several stages of the vitamin k cycle, while warfarin inhibits vitamin k epoxide reductase. The combination of these effects results in profound depletion of activated vitamin k-dependent coagulation factors.
Flucloxacillin	Risk of metabolic acidosis with long-term concomitant use of both molecules.	NAPQI and flucloxacillin interfere with the gamma-glutamyl cycle, leading to an accumulation of 5-oxoproline (pyroglutamic acid), resulting in severe metabolic acidosis with a high anion gap.

Table I.3. Cont.

Medicines	Consequences of interaction	Interaction mechanism
Chelating resins such as cholestyramine and activated charcoal	Reduced paracetamol absorption and efficacy.	Intraluminal complexation.
Cytochrome P450 inducers such as anti-epileptics and rifampicin	Potentiation of paracetamol liver toxicity.	Induction of metabolism may result in the production of hepatotoxic paracetamol metabolites in quantities exceeding the reduction capacity of glutathione.

I.2.1.6.5. Use precautions

It has been reported that paracetamol may exceptionally, and even at therapeutic doses, cause liver toxicity after short-term treatment in patients with no history of liver disorders. It is also recommended not to exceed 3 g/day in the following situations:

- Weight under 50 kg;
- Mild to moderate hepatic impairment;
- Severe renal insufficiency;
- Chronic alcoholism;
- Dehydration ;
- Low glutathione reserves, e.g. chronic malnutrition, fasting, recent weight loss, over 75 or over 65 years of age and polypathology, chronic viral hepatitis and human immunodeficiency virus infection, cystic fibrosis **[48, 49]**.

I.2.1.6.6. Side effects

Although considered safe, paracetamol, like any other drug, has a number of adverse effects **[50-52]**:

- Asthma;
- Rarely observed hypersensitivity reactions such as anaphylactic shock and angioedema;
- Erythema, urticaria, skin rash, and very rare severe skin disorders (Stevens-Johnson syndrome and epidermal necrolysis) have been reported;
- Thrombocytopenia, leukopenia and neutropenia (exceptional);

- Cytolytic liver disease ;
- Rhabdomyolysis;
- Upper gastrointestinal bleeding, nausea, vomiting and epigastric pain, which occur more frequently with chronic use;
- Increased risk of cardiovascular diseases such as myocardial infarction and stroke.

I.2.1.7. Toxicity

Paracetamol has been extensively studied and is known to be safe to use at the usual recommended doses. In the event of overdose, in addition to well-documented liver toxicity and less commonly renal damage, cardiac toxicity has also been reported **[53, 54]**.

Paracetamol is mainly metabolized by the liver, with rapid elimination of metabolites under normal circumstances. In the event of overdose, NAPQI, a highly reactive electrophilic metabolite of the minor metabolic pathway, accumulates, saturating the major pathways and exceeding glutathione reduction capacity. In the kidneys, paracetamol can be metabolized to NAPQI by prostaglandin H synthetase, via a free radical (N-acetyl-para-benzosemiquinone-imine: NAPSQI). This can have a direct toxic effect on the kidney **[55]**.

In light of the impact paracetamol can have on health, it is essential to develop analytical methods to monitor and control the use of this drug.

I.2.2. 4-aminophenol

I.2.2.1. Denomination and chemical structure

4-aminophenol (4-AP) is an aromatic organic compound. It consists of a benzene ring substituted by a hydroxyl group (phenol) and an amine group (aniline) in positions 1 and 4 (Figure I.5). It is therefore one of three possible isomers of aminophenol, the *para* compound, the other two being 2-aminophenol (*ortho*) and 3-aminophenol (*meta*). In literature it is also known as 4-hydroxyaniline, 4-amino-1-hydroxybenzene, *para*-aminophenol, *p*-aminophenol, phenol, 4-Aminobenzenol, citol, azol, and paranol.

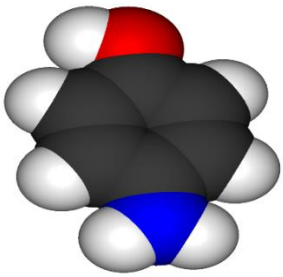

Figure I.5. Chemical structure of 4-aminophenol **[56]**.

I.2.2.2. Physicochemical properties

The table below lists the main physicochemical characteristics of 4-aminophenol **[57]**:

Table I.4. Physicochemical properties of 4-aminophenol.

Molecular formula	C_6H_7NO
Molar mass	109.13 g/mol
Melting point	189-190°C
Dissociation constant	pK_1 5.50 at 21°C, 4.86 at 30°C, 5.48 at 25°C pK_2 10.30 at 22°C, 10.60 at 30°C
Density	1.29 g/cm^3
Boiling point	284°C at 101.3 kPa
Flash point	195°C
Aspects	Light brown powder or white or reddish-yellow crystals that turn violet when exposed to light

The solubility of 4-aminophenol in common solvents is given in table I.5.

Table I.5. 4-aminophenol's solubility in standard solvents.

Solvents	**4-aminophenol solubility**
Acetone	soluble
Acetonitrile	soluble
Benzene	insoluble
Chloroform	insoluble
Diethyl ether	slightly soluble
Dimethylsulfoxide	very soluble
Ethanol	slightly soluble
Ethyl acetate	soluble
Toluene	slightly soluble
Water	
Hot	soluble
Cold	slightly soluble

I.2.2.3. Synthesis

I.2.2.3.1. Synthesis of 4-aminophenol and paracetamol from phenol or chlorobenzene precursors

a) Synthesis of 4-aminophenol and paracetamol by coupling

Couplings are reactions enabling the formation of C-C, C-O, C-N **[58]** or even C-S and C-P bonds. Generally catalyzed by transition metals such as palladium, copper, nickel or, more recently, iron; couplings have become widely used reactions in organic synthesis. For example, *Ullmann-Golberg* couplings with copper or *Buchwald-Hartwig* couplings with palladium enable the synthesis of arylamines and arylamides, and are potentially applicable to the synthesis of 4-aminophenol and paracetamol (Figure I.6) **[59]**.

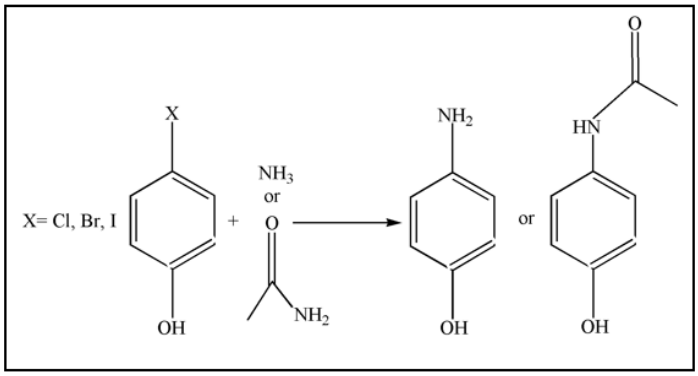

Figure I.6. General diagram of the coupling reaction for the synthesis of 4-aminophenol and paracetamol.

b) Synthesis of 4-aminophenol from 4-nitrophenol

Since coupling reactions cannot be used to introduce acetamide, other methods are employed. Of these, the predominant route uses 4-nitrophenol as an intermediate (Figure I.7). 4-aminophenol can thus be easily obtained by reduction of 4-nitrophenol **[60]**. The difficulty then lies in accessing the latter compound.

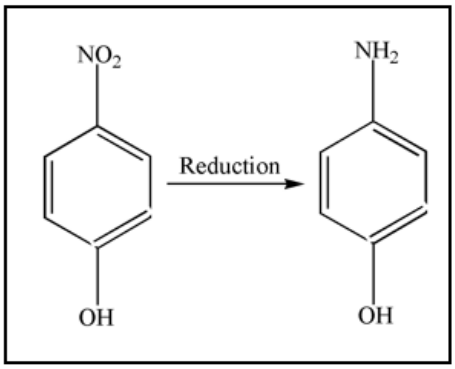

Figure I.7. Synthesis of 4-aminophenol by reduction of 4-nitrophenol.

c) Synthesis of 4-aminophenol by nucleophilic substitution on hydroquinone

Phenols have been shown to undergo aromatic nucleophilic substitution reactions in ipso. For example, phenol can be converted to aniline by the action of ammonia in the gas phase at 400°C, in the presence of alumina, with conversions greater than 99% and selectivities of 99% **[61]**. Similarly, the substitution of a hydroquinone hydroxyl with an ammonia/ammonium mixture is possible at temperatures lower than 200°C **[62]**. This reaction gives yields of 60% after 12 hours of reaction (Figure I.8). The synthesis of 4-aminophenol by aromatic nucleophilic substitution on hydroquinone has the advantage of producing only water as a by-product.

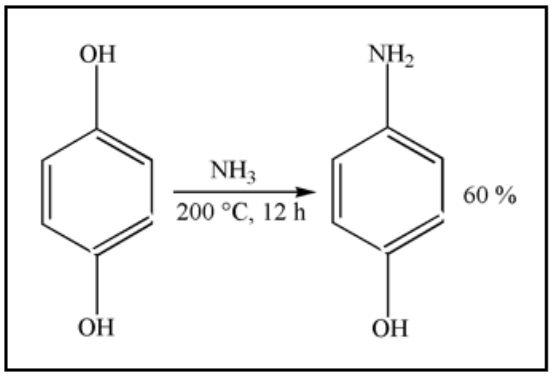

Figure I.8. Synthesis of 4-aminophenol by amination of hydroquinone.

I.2.2.3.2. Synthesis of paracetamol from 4-aminophenol

Paracetamol was first synthesized in 1878 by *Harmon Northrop Morse*. The first step was the reduction of 4-nitrophenol to 4-aminophenol in the presence of tin in glacial acetic acid. The resulting product was then acylated with acetic acid (ethanoic acid) to give paracetamol. *Vignolo* simplified this synthesis by using 4-aminophenol as the starting material. Only one acylation step is needed to obtain the desired product, which shortens the synthesis (Figure I.9).

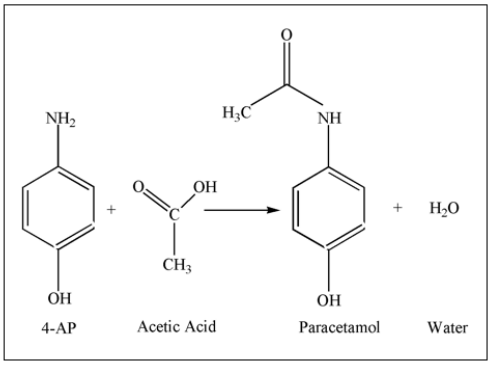

Figure I.9. Schematic diagram of 4-AP acylation with acetic acid.

Later, *Friedlander* modified the synthesis by acylating 4-aminophenol with acetic anhydride (ethanoic anhydride) instead of acetic acid, giving a higher yield (Figure I.10) **[63, 64]**.

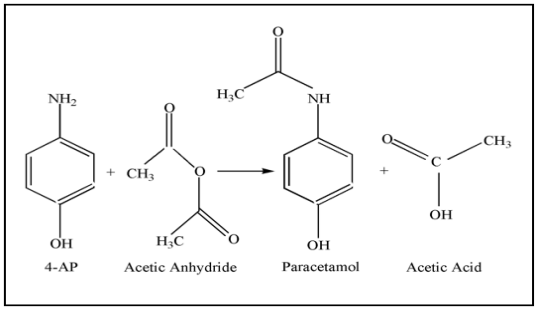

Figure I.10. Schematic diagram of 4-AP acylation with acetic anhydride.

I.2.2.4. Storage and degradation conditions

When exposed to air and light, 4-aminophenol, which is unstable in atmospheric conditions, can degrade and generate quinone-imine (Figure I.11) **[65]**. This is the reason why 4-aminophenol is stored in brown glass containers and kept out of the light and air, preferably in a nitrogen-rich atmosphere, to prevent any interaction with ambient air humidity. 4-Aminophenol discoloration can be prevented by using activated iron oxide in a different cellophane bag within the storage container **[66]**.

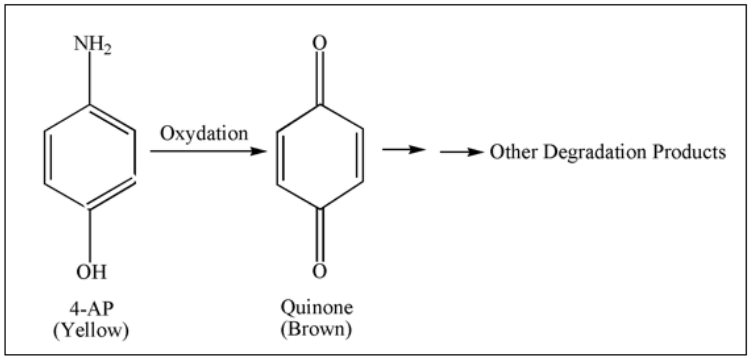

Figure I.11. 4-aminophenol degradation in an atmospheric setting.

I.2.2.5. Use and toxicity

Broadly speaking, 4-aminophenol compound is recognized as a raw material with numerous and diverse uses in the production of pharmaceuticals (including paracetamol and other medications), thermal dyes, black and white developer (sold under the name Rodinal), antioxidants, polymer stabilizers, petroleum additives, fungicides, herbicides, and insecticides **[67–69]**.

Due to the widespread use of 4-AP, high concentrations of the chemical have unavoidably been released into the environment, especially into water sources, where it might have harmful consequences because it contains structural phenol and aniline. Serious health effects as dermatitis, eczema, pancreatitis, nephrotoxicity, and teratogenic problems might result from 4-AP's entry into the human body **[70, 71]**. The kidney and blood are the two organs that 4-AP targets in the body. The pharmacopoeia in Europe, USA, UK, Germany and China have set a maximum level of 50 ppm (0.005%, w/w) for 4-AP in pharmaceuticals due to its severe toxicity **[72]**. In this approach, 4-AP, which is ecologically and biochemically harmful, can easily penetrate plant membranes and epidermis, contaminating and endangering both living beings and natural resources. Therefore, it's crucial to develop a simple and reliable analytical technique to determine low concentrations of 4AP.

I.2.3. Ascorbic acid (Vitamin C)

I.2.3.1. History

Vitamin C was first discovered in the 18th century during an ocean trip. Sailors were suffering from a very serious disease: scurvy, characterized by bone pain, gum bleeding, and severe anemia. An English naval physician, *James Lind*, demonstrated the effectiveness of a few drops of lemon or orange juice in the prevention and treatment of scurvy, which is caused by a prolonged vitamin C deficiency **[73]**.

In 1927, *Szent-Györgyi*, a Hungarian chemist, isolated vitamin C by chance. He found an unknown substance in large quantities in the adrenal glands, but also in cabbage and oranges **[74]**. *Szent-Györgyi* named it "ignose", in reference to the sugar terminology "ose" and the fact that this compound was still unknown. When he discovered that it was an acid with 6 carbon atoms, he preferred the name hexuronic acid. In 1932, *Szent-Györgyi* and *King* discovered that hexuronic acid prevented scurvy in guinea pigs. Thanks to this discovery, the molecule was renamed "ascorbic acid" in 1933 **[75]**. It was an English biochemist, *Norman Haworth*, who first synthesized D- and L-ascorbic acid. The industrial production of vitamin C began in 1936 **[76]**.

I.2.3.2. Denomination and chemical structure

The chemical structure of ascorbic acid (AA) was determined by the English chemist *Walter Norman Haworth* in 1932. It has one enediol function (HO-C=C-OH), two alcohol functions, and a lactone function linking carbons C1 and C4 (Figure I.12). Its oxidized form is dehydroascorbic acid (DHA), chemical formula $C_6H_6O_6$.

Other names for ascorbic acid include vitamin C, L-threo-hex-2-enoiquegamma-lactone, and L-xyloascorbic acid; the latter refers to its antiscorbutic properties **[77]**.

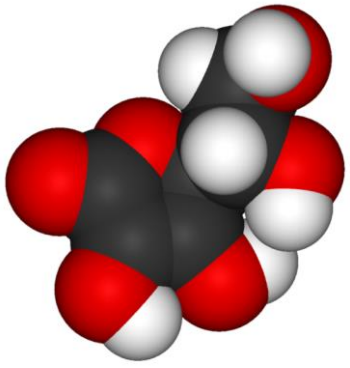

Figure I.12. Chemical structure of ascorbic acid.

I.2.3.3. Physicochemical properties

Ascorbic acid is stable in the anhydrous state (reduced form), protected from humidity and light, and gradually darkens when exposed to light. Table I.6 shows the physicochemical properties of this substance.

Table I.6. Physicochemical properties of ascorbic acid **[78]**.

Molecular formula	$C_6H_8O_6$
Molar mass	176.12 g/mol
Melting point	190-192°C
Dissociation constant	pK_1 4.2 pK_2 11.6 at 25°C
Density	1.65 g/cm^3
Solubility	Water: very soluble 333 g/L at 25°C Alcohol and polyols: slightly soluble Ether and Chloroform: insoluble
Aspects	white, or slightly yellow, odorless, crystalline powder with a strong acid taste

I.2.3.4. Pharmacokinetics

Compared to a typical low-molecular-weight oral drug, vitamin C has several differences in terms of pharmacokinetic properties **[79]**.

a) Absorption

The total amount of ascorbic acid in the body is estimated to be between 1.5 and 3 g. Ascorbic acid is mainly absorbed from the ileum via an active Na-dependent transport mechanism **[80]**. Optimal absorption occurs in a neutral environment where ascorbate, the ionized form of ascorbic acid, is transported by the protein essential for vitamin C absorption in cells, SVCT1 (sodium-dependent vitamin C transporter 1). Once in the bloodstream, ascorbic acid is absorbed into cells by the sodium-dependent vitamin C transporter 2 (SVCT2) **[81]**.

b) Distribution and metabolism

Ascorbic acid is rapidly absorbed into the bloodstream and penetrates all tissues. Most of the ascorbic acid in the blood is in its reduced form (about 85%). At physiological pH, the predominant form is the ascorbate anion AH^- (85%). The oxidized form (DHA) is only 15%. The concentration of ascorbic acid in plasma is low (5 to 15 mg. L^{-1}), whereas it is 10 to 30 times higher in leukocytes and platelets. The leukocyte concentration reflects the tissue concentration. The adrenal and pituitary glands have the highest tissue concentrations (30-50 µg per g). However, the kidneys, brain, and spleen together contain the majority of ascorbic acid. Ascorbic acid is metabolized in the liver and kidneys, resulting in several reactions **[82]**.

c) Elimination

The main routes of elimination for vitamin C are urine, faeces and sweat. Urinary elimination dominates, while faecal elimination is of little importance, except during diarrhoea.

For vitamin C intakes of 100 mg/day, 25% is excreted. For doses above 0.5 g, only a portion is ingested, and almost the entire absorbed dose is excreted. Elimination takes place in native form or as metabolites. When plasma concentration exceeds 79 µmol.L^{-1}, ascorbic acid is eliminated unchanged in the urine. The main metabolite of ascorbic acid is oxalic acid **[83]**.

I.2.3.5. Sources

Vitamin C is a water-soluble vitamin with two isomers: L-ascorbic acid and D-ascorbic acid. Only the L form is effectively metabolized in humans, whereas the D form is synthesized and utilized by lower eukaryotes such as fungi. Like other primates and guinea pigs, humans are unable to synthesize vitamin C due to a mutation in the gene encoding L-gulonolactone oxidase. Additionally, the human body lacks storage capacity for vitamin C, making a daily intake from dietary sources or supplements essential **[84, 85]**. The half-life of vitamin C in humans is between 14 and 40 days after normal intake, and a deficiency can lead to scurvy within approximately 3 to 4 months of a diet lacking this vitamin **[86]**.

The primary sources of ascorbic acid are fresh fruits and vegetables (Figure I.13). Fruits such as oranges, kiwis, mangoes, guavas, grapefruits, mandarins, lemons, limes, papayas, strawberries, pineapples, and cantaloupes are known for their high vitamin C content (ranging from 10 to 100 mg per 100 g). Many vegetables are also rich in vitamin C, including tomatoes, broccoli, green and red bell peppers (raw or cooked), raw lettuce, and other leafy green vegetables **[87, 88]**.

Figure I.13. Vitamin C-rich foods.

I.2.3.6. Physiological role

Ascorbic acid performs multiple functions in the body, largely due to its antioxidant and hydroxylating properties. It plays a crucial role in the synthesis of collagen, tyrosine, carnitine, cholesterol, and bile acids. It also contributes to iron metabolism and helps in the elimination of carcinogens and cancer-causing nitrosamines **[89]**. The redox pair formed by ascorbic acid and dehydroascorbic acid appears to be fundamental to its physiological activities:

- As an electron donor, ascorbic acid is a powerful water-soluble antioxidant:

  -It protects the skin from oxidative stress **[90]**.

  -It is capable of reacting directly with reactive oxygen and nitrogen species, reducing superoxide anion in acid or basic form:

  $$\mathbf{AH^-} + \mathbf{HO_2} \rightarrow \mathbf{A^-} + \mathbf{H_2O_2} \qquad \text{Eq.I.1}$$

  -It limits lipid peroxidation by reacting with peroxyl radicals and oxoferryl complexes:

  $$\mathbf{AH^-} + \mathbf{ROO} \rightarrow \mathbf{A^-} + \mathbf{ROOH} \qquad \text{Eq.I.2}$$

  $$\mathbf{AH^-} + [(\mathbf{IV}) = \mathbf{O}] \rightarrow \mathbf{A^-} + (\mathbf{III}) + \mathbf{OH} \qquad \text{Eq.I.3}$$

  -It is involved in many iron-dependent enzymatic reactions as an electron transmitter **[91]**.

- Thanks to its hydroxylating properties, it plays an important role in maintaining mature, normal collagen, by preventing the auto-inactivation of lysyl and prolyl hydroxylase, considered key enzymes in collagen biosynthesis **[92]**.
- Numerous epidemiological studies have established a correlation between high consumption of vitamin C-rich foods and low rates of cancer and cardiovascular disease.

  -With regard to stomach cancer, vitamin C inhibits the damaging action of Helicobacter Pilori bacteria on the mucosa.

  -Vitamin C mitigates the side effects of chemotherapy and radiotherapy, while also helping to destroy malignant cells and prevent them from multiplying.

  -Vitamin C directly fights certain cancer cells without harming healthy tissue **[93]**.

I.2.3.7. Deficiency and toxicity

Since humans cannot synthesize ascorbic acid on their own, it must be obtained through dietary sources or supplements. However, excessive intake of AA can lead to adverse effects, including early symptoms of scurvy, stomach cramps, gastric irritation, diarrhea, decreased

fertility in women, and potential impacts on embryo development **[94, 95]**. The optimal amount of AA in the human body is generally between 70 mg and 90 mg **[96]**. A deficiency in vitamin C can result in anemia, scurvy; bleeding gums, premature aging, skin hemorrhages, weakened immune response, and fatigue due to oxidative stress **[97-101]**. Given these concerns, it is crucial to develop practical and effective methods for monitoring AA content in food and pharmaceuticals.

I.2.4. Zinc

I.2.4.1. Basics

Zinc, together with cadmium and mercury, belongs to group IIB of the periodic table of the elements (Mendeleyev's classification); it has an atomic number of 30 and a molecular weight of 65.37 g/mol. In some aspects it is similar to magnesium in that its common oxidation state is +2, yielding a cation (Zn^{2+}) comparable in size to Mg^{2+}.

Zinc is an essential trace element for life. The term trace elements refers to elements found consistently in the chemical analysis of living organisms, but in very small quantities (in the milligram or microgram range). The main trace elements are zinc, copper, manganese, selenium, silicon, cobalt, chromium and others. Despite their low dosage, trace elements play an important role in metabolism; deficiency or excess of these essential trace elements is the cause of many diseases and abnormalities. Deficiency disorders can be prevented or corrected by the intake of this single element **[102-104]**.

Metallic elements have the ability to bind to proteins, modifying their molecular structure and mode of action. These structural modifications may be essential to the proper functioning of certain proteins, or on the contrary, may induce a toxic effect by inactivating them. Organisms are capable, to a certain extent, of using and regulating the concentrations of metals that are essential to them. Toxic effects occur when this regulation can no longer take place.

I.2.4.2. Antioxidant properties

Zinc exerts an antioxidant effect indirectly by stabilizing Cu-Zn SOD **[105]**. However, the role of zinc appears to be much less important than that of the other cofactor, copper. Beyond this function, zinc possesses other antioxidant properties for which the precise mechanism remains incompletely understood **[106,107]**:

- Zinc inhibits the production of radical oxygen species by transition metals, competing with them in the Fenton reaction. It also competes with iron and copper, reducing both

their intestinal absorption and their chelation by cysteine. Iron bound to cysteine can transfer electrons to oxygen, enabling the production of superoxide anions.

- Zinc protects protein thiol groups from oxidation by iron or oxygen radicals, preventing the formation of intramolecular disulfide bridges **[108]**.
- Zinc inhibits lipid peroxidation induced by $FeSO_4$/ascorbic acid in liposomes and lipid micelles.
- Zinc plays an important role in membrane stabilization. Zinc is an inhibitor of the NADPH oxidase enzyme, which catalyzes the production of $O_2^{\bullet}$ from O_2 **[109]**.
- Zinc induces the production of cysteine-rich metallothioneins, which can trap hydroxyl radicals. This leads to the formation of disulfide bridges and, consequently, the release of zinc, which can then be captured by membranes **[110]**.

I.2.4.3. Biological role

Zinc biology is an emerging and exciting field that scientists are increasingly recognizing as crucial, given zinc's involvement in most biological activities and processes within the human body. Intestinal absorption of zinc is a key step in its metabolism, playing a major role in regulating the body's zinc levels **[111]**. This essential element is the second most abundant metal in the human body, with a concentration ranging from 1.5 to 3 g, following iron, which ranges from 2 to 4 g **[112, 113]**. Zinc functions as a cofactor for over 1000 enzymatic reactions and is involved in the regulation of more than 2000 transcription factors **[114, 115]**.

Zinc is sometimes referred to as the intelligence mineral, because it is involved in the immune system and is essential for the development and functioning of the nervous system **[116]**. This antioxidant with purifying properties therefore plays an important role in our body's essential functions, as it fights free radicals, prevents blindness and the degenerative effects of aging, and plays a part in the synthesis of proteins and nucleic acids, the basic materials of DNA **[117, 118]**. It is also known to play a part in the glycemic control mechanism and protects against diabetes, since it is used in the synthesis of insulin, whose receptors on cell membranes it protects **[119]**.

I.2.4.4. Sources

Zinc bioavailability varies according to physiological situations. For example, intestinal absorption capacity decreases with age, whereas it increases in the last trimester of pregnancy

and during lactation **[120]**. Zinc supplementation may therefore be recommended for the very elderly, who are often at risk of deficiency, as well as for vegetarians and alcohol abusers.

Zinc is mainly found in foods of animal origin, such as seafood, innards, meat, fish, egg yolks, and unpasteurized dairy products (Figure I.14). Zinc from animal sources is better absorbed by the body **[121]**. However, certain fruits, such as pomegranate, provide a zinc-rich vegetarian option. Zinc is also found in smaller amounts in other plant foods, such as whole grains, legumes, and seeds. However, zinc from these plant sources is less well absorbed, largely due to antinutrients such as phytates. These inhibit intestinal absorption of zinc and can lead to deficiencies. For this reason, we recommend soaking these foods before consumption to reduce phytate content **[122]**.

Figure I.14. Zinc-rich foods.

I.2.4.5. Deficiency and toxicity

Zinc deficiency is linked to a higher susceptibility to bacterial, fungal, and viral infections. It also impairs the incorporation of dietary nitrogen and can lead to various health issues, including gastrointestinal disorders, altered taste and smell (such as dysgeusia and dysosmia), delayed wound healing, reduced insulin production, and diarrhea **[123-125]**. The human body contains approximately 2.5 g of zinc, with about 30% stored in bones and 60% in muscles, reflecting the large mass of these tissues. Notably, the highest concentrations of zinc are found in the prostate, hair, and eyes. In healthy individuals, zinc levels typically range between 6000 and 9000 µg L^{-1} **[126]**. Zinc absorption is influenced by the size of zinc particles, the solubility of zinc-containing compounds, and its speciation **[127]**.

The effects of zinc deficiency have been well-known and studied for years. However, less attention has been paid to the potential consequences of excessive zinc intake. Many studies suggest that zinc is relatively non-toxic, and mammals, including humans, have a high tolerance for elevated zinc levels. While it is true that significant amounts of zinc are required to cause

acute toxicity symptoms, even relatively low levels of excess zinc intake can, in some cases, lead to adverse effects **[128]**. Overconsumption of Zn(II) may lead to issues such as epilepsy, headaches, anemia, apoptosis, nausea, and neurotoxicological effects, including Alzheimer's and Parkinson's diseases **[129-132]**. Consequently, there is an urgent need for a sensitive and straightforward analytical method to monitor Zn(II) concentrations in human fluids and pharmaceutical products.

I.3. Target analytes: Detection methods

I.3.1. Analytical methods

Various analytical methods have been developed to detect paracetamol, 4-aminophenol, ascorbic acid, and Zn(II) in different matrices. The main analytical methods routinely used in laboratories include spectrophotometry, high-performance liquid chromatography, and atomic absorption spectrometry.

I.3.1.1. UV-visible spectrophotometry

UV and visible absorption spectrophotometry is a non-destructive physical method used in analytical laboratories, based on the property of molecules to absorb light radiation of specific wavelengths. It has long been widely used in quantitative analysis in the visible range. Measurements are based on *Beer* and *Lambert*'s law, which relates, under certain conditions, the absorption of light to the concentration of a compound in solution **[133]**.

Target analytes have been determined by several forms of spectrophotometry for many years **[134-139]**. Glavanović et al. **[135]** developed novel UV spectrophotometric methods based on multivariate chemometric techniques for quantitative data analysis. These techniques were effectively used to determine the active pharmacological components in paracetamol and tramadol pills simultaneously. The proposed techniques are both simple and accurate, providing a reliable approach for the simultaneous quantification of tramadol and paracetamol in tablet formulations, making them highly suitable for routine laboratory analysis. Another spectrophotometric method has been introduced for the straightforward and sensitive detection of paracetamol and 4-aminophenol. This approach relies on the hydrolysis of paracetamol into 4-aminophenol, utilizing dissolved oxygen as an oxidizing agent in an alkaline environment. The proposed method is effective for analyzing and ensuring the quality control of paracetamol in commercial formulations, with minimal interference from common excipients found in pharmaceuticals **[136]**.

Also, ascorbic acid was determined in pharmaceutical preparations and food products using a sensitive spectrophotometric method developed by Zarei et al. **[137]**. This method is based on the reduction of Ag^+ ions to silver nanoparticles by ascorbic acid, with polyvinylpyrrolidone serving as a stabilizing agent. This reaction produces a highly intense surface plasmon resonance peak characteristic of silver nanoparticles.

I.3.1.2. High-performance liquid chromatography

High-Performance Liquid Chromatography (HPLC) is a widely used technique in analytical laboratories. It enables the separation of compounds in a solution, among other things, to determine their concentrations. HPLC relies on the differential migration of the components of a mixture, achieved by transporting them using a mobile phase and passing them through a stationary phase, which exhibits different affinities for each compound to be separated. Depending on the nature of the interactions between these two phases and the sample being analyzed, various separation mechanisms can be distinguished: adsorption chromatography, partition chromatography, ion-exchange chromatography, and ion-pair chromatography **[140,141]**.

High-performance liquid chromatographic methods with lower detection limits have been validated for the determination of PA, 4-AP, and AA **[142-149]**. Abdel Rahman et al. **[143]** investigated, for the first time, the separation of etoricoxib, paracetamol, and its two toxic impurities, 4-aminophenol and 4-hydroxyacetophenone, using a selective HPLC method. The limits of detection (LODs) were found to be 1.5-30.0 µg/mL for etoricoxib and paracetamol, and 0.5-10.0 µg/mL for 4-aminophenol and 4-hydroxyacetophenone. Two simple, validated methods, TLC-densitometry and HPLC, were described for the simultaneous determination of caffeine, codeine, paracetamol, and 4-aminophenol in their quaternary mixture. These chromatographic methods are suitable for quality control and routine analysis **[144]**. Szultka et al. **[145]** conducted the first study employing HPLC coupled with triple quadrupole mass spectrometry to investigate the degradation products of ascorbic acid. The study's findings indicate that AA can degrade under exposure to sunlight or room temperature, and this degradation can also be accelerated by hydrogen peroxide.

I.3.1.3. Atomic absorption spectrometry

Atomic Absorption Spectrometry (AAS), since its advent as an essential analytical technique for the determination of metallic species, has continued to evolve in the direction of increased sensitivity, reliability and reproducibility.

Atomic absorption is a process that occurs when an atom in its ground state changes to an excited state through the absorption of energy, in the form of electromagnetic radiation, corresponding to a specific wavelength. The atomic absorption spectrum of an element is made up of a series of resonance lines; all originating in the fundamental electronic state and ending in different excited states. In general, the line at the transition between the ground state and the first excited state defines the highest absorption capacity, and is the line usually used. Transitions between ground and excited states only occur when the incident radiation from a light source is exactly equal to the frequency of a specific transition **[150, 151]**.

R. Manjusha et al. **[152]** developed a noval ultrasound-assisted extraction method for the determination of Pb, Cd, Cr, Mn, Fe, Cu, and Zn in edible oils extracted from multiple seeds (such as mustard, sunflower, sesame, groundnut, coconut, rice bran, and corn oils). This method involves the use of tetramethylammonium hydroxide and EDTA at pH 12, followed by analysis with a graphite furnace atomic absorption spectrometer. The procedure was validated against a microwave digestion method.

I.3.2. Analytical methods: Drawbacks

Laboratory analytical methods are relatively complex systems, combining mechanical, chemical and electrical elements, and require experienced operators. Response times are long, from a few minutes to several hours, and equipment is often expensive, bulky and energy-consuming. The major drawback of all the above-mentioned analysis techniques is the difficulty of sample preparation. The sample must be in a form compatible with the technique. Nevertheless, they have the advantage of enabling complete (virtually all elements) and precise analysis of the medium, with detection limits ranging from ppm (mg. L^{-1}) to ppt (ng. L^{-1}**) [153-155]**.

I.3.3. Electroanalytical methods

Electroanalytical methods focus on the interaction between electricity and chemistry, specifically the measurement of electrical quantities and their correlation with chemical parameters. This approach has a broad range of applications, including clinical diagnostics, environmental monitoring, industrial quality control, and biomedical analysis. Disposable electrochemical sensors, utilized as electroanalytical tools in conjunction with voltammetric techniques, offer significant advantages over traditional analytical methods. Notable features of these sensors include their ease of use, low cost, on-site monitoring capabilities, and suitability for miniaturization **[156-158]**.

Various electrochemical sensors combined with voltammetric methods have been widely employed for the determination of PA, 4-AP, AA, and Zn(II) **[159-165]**. Zhang et al. **[160]** reported the development of an electrochemical sensor based on a novel composite material, Ti_3C_2 QDs/Fe-NC, for the simultaneous detection of paracetamol and 4-aminophenol using the differential pulse voltammetry (DPV) method. The sensor demonstrated excellent analytical performance, including lower detection limits and broader linear ranges. It was successfully applied for the simultaneous detection of 4-AP and PA in river water samples and paracetamol tablets. An electrochemical sensor for the concurrent detection of paracetamol and 4-aminophenol using a carbon paste electrode modified with MoO_3 nanobelt-graphene oxide was also developed by Vazan et al. **[161]**. The electro-oxidation behavior of these two phenolic compounds was investigated using CV, EIS, and DPV techniques. The sensor demonstrated effective performance for detecting PA and 4-AP in urine samples, yielding satisfactory results.

Mohammadnezhad et al. **[162]** developed a new electrochemical sensor for the direct oxidation of ascorbic acid using CV and DPV methods. This sensor was fabricated by decorating palladium nanoparticles onto a nitrogen-doped graphene quantum dot-modified glassy carbon electrode. The sensor's validity and efficiency were successfully verified by measuring ascorbic acid in real samples, including chewing tablets and fruit juice. Gutiérrez et al. **[163]** also reported the electrochemical quantification of ascorbic acid in the presence of paracetamol, and vice versa, in pharmaceutical samples using CV and DPV methods. This was achieved with a glassy carbon electrode modified with multi-walled carbon nanotubes and polyarginine. The proposed sensor demonstrated excellent specificity, sensitivity, stability, and reproducibility, outperforming previously reported sensors for the detection of these target analytes.

Karazan et al. **[164]** successfully developed a selective and rapid electrochemical sensor using a glassy carbon electrode modified with a covalent organic framework and carbon black. The fabricated sensor demonstrated acceptable electrocatalytic activity for the simultaneous and individual detection of Zn^{2+}, Cd^{2+}, Pb^{2+}, and Hg^{2+} metal ions, utilizing differential pulse anodic stripping voltammetry (DPASV). The proposed sensor showed reliability for routine analysis in the quantification of these target metal ions in food samples, exhibiting good recovery rates. Additionally, atomic absorption spectrometry was employed as a standard validation method to quantify the metal ions in the food samples, further confirming the accuracy of the electrochemical sensor. Graphite screen-printed electrodes modified with tin nanoparticles via a “green,” rapid, and highly efficient sparking process were utilized for the anodic stripping voltammetric detection of trace amounts of cadmium (Cd) and zinc (Zn) in

both tap and bottled water samples. The findings indicate that SnNPs/GSPEs produced through this sparking technique offer a promising, environmentally friendly sensor solution. These sensors outperform those reported in the literature regarding simplicity, cost-effectiveness, time efficiency, labor intensity, waste generation during the modification process, and the overall affordability of the final sensor **[165]**.

I.4. Conclusion

This chapter has highlighted the physicochemical, pharmacokinetic, and pharmacodynamic properties of paracetamol, 4-aminophenol, ascorbic acid, and zinc, as well as their chemical structures and synthesis. It has also addressed the natural sources of vitamin C and zinc, alongside the potential toxicity of these target analytes when overdosed, emphasizing the risks associated with both under- and overdosing.

Given these concerns, it is crucial to develop analytical approaches that are simple, cost-effective, sensitive, and accurate for the individual or simultaneous detection of these analytes in pharmaceutical samples or biological fluids. To this end, a review of conventional detection methods for paracetamol, 4-aminophenol, ascorbic acid, and zinc has been presented, illustrating the limitations of traditional techniques. Disposable electrochemical sensors, particularly when paired with voltammetric techniques, offer significant advantages in terms of sensitivity, cost, and ease of use. A detailed review of screen-printed sensors, the electrochemical tool used in this study, will be presented in the next chapter.

References

[1] A. Cahn, P. Hepp, Sur l'action de l'antifébrine (acétanilide) et de quelques corps analogues, Prog. Méd. J. Médecine Chir. Pharm. 5 (1887) 43–6.
[2] A. Bertolini, A. Ferrari, A. Ottani, S. Guerzoni, R. Tacchi, S. Leone, Paracetamol: new vistas of an old drug, CNS Drug Rev. 12 (2006) 250–75.
[3] U. Freo, C. Ruocco, A. Valerio, I. Scagnol, E. Nisoli, Paracetamol: a review of guideline recommendations, J. Clin. Med. 10 (2021) 3420.
[4] Y. Driad, Stabilité du paracétamol : application à un sachet produit en industrie pharmaceutique, PhD thesis in pharmacy, University of HENRI POINCARE, NANCY 1, 2009.
[5] F. Nicoulaud, Aspirine –Paracétamol : des faux jumeaux ?, PhD thesis in pharmacy, University of LIMOGES, 1997.
[6] P. Queneau, La saga du paracétamol, Thérapeutiques, 2 (2006) 158–159.
[7] C. Le Marec, Histoire du paracétamol, Prat. Anesth. Reanim. 9 (2005) 321–328.
[8] P.Y. Tremblay, Mécanismes d'action et de toxicité de l'acétaminophène, BIT. 27 (2011).
[9] R.C. Craig, R. Stitzel, Modern pharmacology, Chap.39: Opiod and nonopioid analgesics, 4th ed. (1994) 431–437.
[10] European Pharmacopoeia 7th ed. (2010).
[11] S. Behera, S. Ghanty, F. Ahmad, S. Santra, S. Banerjee, UV-visible spectrophotometric method development and validation of assay of paracetamol tablet formulation, J. Anal. Bioanal. Techniques, 3 (2012) 151–157.
[12] F. Medjdoub, Adsorption du paracétamol par l'utilisation des différents types d'adsorbants naturels, PhD thesis in environmental engineering, University of MHAMED BOUGARA, BOUMERDES, 2018.
[13] X. Wittebole, P. Hantson, Influence des relations toxicocinétiques-toxicodynamiques sur la prise en charge des patients intoxiqués, Réanimation, 11 (2002) 533–539.
[14] T. Gramatte, K. Richter, Paracetamol absorption from different sites in the human small intestine, Br. J. Clin. Pharmacol. 37 (1994) 608–11.
[15] IA. Gibb, B.J. Anderson, Paracetamol (acetaminophen) pharmacodynamics: interpreting the plasma concentration, Arch. Dis. Child. 93 (2008) 241–7.
[16] M. Ramlawi, C. Marti, F. Sarasin, Intoxication aiguë au paracétamol, Rev. Med. Suisse, 9 (2013) 1478–1482.
[17] L.J. Roberts, J.D. Marrow, J.G. Hardman, L.E. Limbird, Analgesics-antipyretic and anti-inflammatory agents and drugs employed in the treatment of gout. Goodman and Gilman's The Pharmacological basis of therapeutics, Mc Graw-Hill: NewYork, 10th ed. (2001) 687–732.
[18] W. Aouacheri, Le rôle du système enzymatique du glutathion dans la détoxication du paracétamol : effets hépatotoxiques et anatomopathologiques, PhD thesis in Applied Biochemistry, University of BADJI MOKHTAR, ANNABA, 2010.
[19] M. Bidault, Prise en charge des intoxications au paracétamol : étude rétrospective sur trois ans dans le service des urgences adultes du CHU de LIMOGES, PhD thesis in medicine, University of LIMOGES, 2011.
[20] R.G. Peterson, B.H. Rumack, Pharmacokinetics of acetaminophen in children. Pediatrics, 62 (1978) 877–9.
[21] J. Dangoumau, N. Moore, M. Molimard, A. Fourrier-Reglat, K. Latry, F. Haramburu, G. Miremont-Salme, K. Titier, Pharmacologie générale, University of VICTOR SEGALEN, BORDEAUX 2, 2006.
[22] J.M. Cardot, J.M. Aiache, R. Renoux, J.P. Kantelip, Correlation entre les taux salivaires et les taux plasmatiques de paracetamol ; interet pour les études de biodisponibilité. S.T.P. Pharm.1 (1985) 114–120.
[23] D.M. Aronoff, J.A. Oates, O. Boutaud, New insights into the mechanism of action of acetaminophen: Its clinical pharmacologic characteristics reflect its inhibition of the two prostaglandin H_2 synthases. Clin. Pharmacol. Ther. 79 (2006) 9–19.
[24] J.S. Lubel, P.W. Angus, P.J. Gow, Accidental paracetamol poisoning, Med. J. Aust. 186 (2007) 371–2.
[25] N. Kerckhove, Implication des canaux Cav3. 2 dans l'effet antalgique du paracétamol et dans la douleur inflammatoire, PhD thesis in neuropharmacology, University of AUVERGNE, 2013.

[26] P. Marzuillo, S. Guarino, E. Barbi, Paracetamol: a focus for the general pediatrician, Eur. J. Pediatr. 173 (2014) 415–25.
[27] American Society of Health-System Pharmacists (ASHP), Acetaminophen, Med master patient drug information, 2007.
[28] G.D. Benson, R.S. Koff, K.G. Tolman, The therapeutic use of acetaminophen in patients with liver desease, Am. J. Ther. 12 (2005) 133–41.
[29] B. Bannwarth, F. Péhourcq, Pharmacologic basis for using paracetamol: pharmacokinetic and pharmacodynamic issues, Drugs 63 (2003) 5–13.
[30] VIDAL, The dictionary of medicines, 2011.
[31] B.J. Anderson, Paracetamol (Acetaminophen): mechanisms of action, Paediatr. Anaesth. 18 (2008) 915–21.
[32] S.S. Ayoub, R.J. Flower, Loss of hypothermic and anti-pyretic action of paracetamol in cyclooxygenase-1 knockout mice is indicative of inhibition of cyclooxygenase-1 variant enzymes, Eur. J. pharmacol. 861 (2019) 172609.
[33] D. Barriere, A. Eschalier, C. Mallet, Le paracétamol, de nouvelles cibles pour un vieux médicament, The UPSA pain institute newsletter 33 (2010) 88.
[34] C.V. Sharma, V. Mehta, Paracetamol: Mechanisms and updates, Contin. Educ. Anaesth, Crit. Care &Pain 14 (2014) 153–158.
[35] D.A. Barriere, C. Mallet, A. Blomgren, C. Simonsen, L. Daulhac, F. Libert, et al., Fatty acid amide hydrolase-dependent generation of antinociceptive drug metabolites acting on TRPV1 in the brain, Plos One 8 (2013) 70690.
[36] European Pharmacopoeia 5th ed. (2004).
[37] L.F. Prescott, Paracetamol: past, present, and future, Am. J. Ther. 7 (2000) 143–147.
[38] X. Oudinot, Amélioration de l'usage du paracétamol au CHU de Rouen, PhD thesis in pharmacy, University of ROUEN, 2016.
[39] G. Geraud, N. Fabre, Guide pratique des migraines et céphalées, Elsevier Masson, 1st Ed. Paris (2001).
[40] G. Dutau, F. Rancé, S. Fejji, A. Juchet, F. Brémont, P. Nouilhan, Intolérance aux additifs alimentaires chez l'enfant : mythe ou réalité, Rev FR Allergol. 36 (1996) 129–42.
[41] VIDAL, The dictionary of medicines, 2018.
[42] I. Claverie, H. Hedde, Pharmacologie générale toxicologie: Mécanismes fondamentaux, Rueil Malmaison: Porphyre, 2nd Ed. (2008).
[43] C. Penhoat, Rôle des acides gras dans l'induction du cytochrome P450 2E1 (CYP2E1) hépatique: implication dans la stéatohépatite non alcoolique (NASH) et dans l'hépatotoxicité du paracétamol, PhD thesis, University of RENNES, 2023.
[44] L.R. van den Bersselaar, J.M.D. van den Brule, J.G. van der Hoeven, Acetaminophen use concomitant with long-lasting flucloxacillin therapy: a dangerous combination, Eur. J. Case Rep. Intern. Med. 7 (2020).
[45] Z. Bouzerouata, Les antalgiques utilisés dans la prise en charge de la douleur aigue postopératoire au sein du service de chirurgie générale B CHU Tlemcen, PhD thesis in pharmacy, University of ABOU BEKR BELKAÎD, TLEMCEN, 2019.
[46] G.M. Pinson, J.W. Beall, J.A. Kyle, A review of warfarin dosing with concurrent acetaminophen therapy, J. Pharm. Pract. 26 (2013) 518–21.
[47] D. Leong, P.E. Wu, Warfarin and acetaminophen interaction in a 47-year-old woman, CMAJ. 192 (2020) 506–8.
[48] G. Olive, Traitement analgésique/antipyrétique: ibuprofène ou paracétamol? Mise au point, Therapies 61 (2006) 151–60.
[49] D.D. Vital, C. Le jeune, Ph. Dorosz, Guide pratique des médicaments, Maloine, 33rd Ed. Paris (2013).
[50] J. Laëtitia, Toxicité du paracétamol : résultats d'une étude multicentrique relative aux intoxications volontaires au paracétamol dans les SAU adultes français, PhD thesis in pharmacy, University of ANGERS, 2014.
[51] J. Buxeraud, Le paracétamol: ami ou ennemi?, Actualités pharmaceutiques 546 (2015).
[52] J. McCrae, E. Morrison, I. MacIntyre, J. Dear, D. Webb, Long-term adverse effects of paracetamol–a review, Br. J. Clin. Pharmacol. 84 (2018) 2218–30.

[53] F. KhabazianZadeh, T. Kazemi, S. Nakhaee, et al., Acetaminophen poisoning-induced heart injury: a case-based review, DARU J. Pharm. Sci. 27 (2019) 839–51.
[54] R. Tittarelli, M. Pellegrini, M. Scarpellini, E. Marinelli, V. Bruti, N. Di Luca, et al., Hepatotoxicity of paracetamol and related fatalities, Eur. Rev. Med. Pharmacol. Sci. 21 (2017) 95–101.
[55] F. Michel, Pratiques de l'automédication par le paracétamol en population générale: étude quantitative sur les connaissances des patients à propos du paracétamol en automédication dans le département de la Seine-Maritime, PhD thesis in medicine, University of ROUEN, 2016.
[56] Z. Lu, H. Guo, X. Wei, L. Sun, Z. Pan, B. Liu, Y. Liu, J. Xu, J. Tian, W. Yang, A novel electrochemical sensing platform based on covalent organic frameworks/WC/NH_2-MWCNT for highly selective determination of acetaminophen and 4-aminophenol, Microchem. J. 193 (2023) 109075.
[57] S.C. Mitchell, R.H. Waring, Aminophenols, Ullmann's Encycl. Ind. Chem. 3 (2000) 59–77.
[58] F. Monnier, M. Taillefer, Catalytic C-C, C-N, and C-O Ullmann-type coupling reactions, Angew. Chem. Int. Ed. 48 (2009) 6954–6971.
[59] J. Hassan, M. Sévignon, C. Gozzi, E. Schulz, M. Lemaire, Aryl–Aryl bond formation one century after the discovery of the Ullmann reaction, Chem. Rev. 102 (2002) 1359–1469.
[60] R.M.N. Kalla, T. Kaliraja, S.K. Lakkaboyana, S.C. Kim, I. Kim, Hierarchically porous polyaromatic carbon spheres decorated $NiMn_2O_4$ nanocomposite: efficient selective azo dye degradation from aqueous water and reduction of p-nitrophenol to p-aminophenol, Carbon Lett. 34 (2024) 1229–1237.
[61] M. Yasuhara, F. Matsunaga, European patent, EP 0.321.275, for Mitsui Petrochemical Ind. (1989).
[62] F.R. Bean, T.S. Donovan, U.S. patent, US 2.376.112, for Eastman Kodak Co. (1945).
[63] J. Dehostingue, La consommation de Paracétamol chez l'adulte et ses consequences, PhD thesis in pharmacy, University of PICARDIE JULES VERNE, 2019.
[64] A.A.E. Prisca, Evaluation de la qualité des médicaments à base de paracetamol commercialises en côte d'ivoire par une étude de stabilité accélérée, PhD thesis in pharmacy, University of FELIX HOUPHOUET-BOIGNY, ABIDJAN, 2016.
[65] J.E. Fairbrother, Acetaminophen, Anal. Profiles Drug Subst. 3 (1974) 1–109.
[66] Mitsui Toatsu Chem. Inc., JP Kokai 8081843, (1980).
[67] H. Zhang, Z. Xing, M. Pan, H.B. Wang, Y.M. Liu, Highly sensitive and selective electrochemical determination of 4-aminophenol based on flower-like Ag-Au nanocomposites modified glassy carbon electrode, J. Electrochem. Soc. 167 (2020) 126504.
[68] L. Sun, M. Yang, H. Guo, T. Zhang, N. Wu, M. Wang, W. Yang, COOH-MWCNT connected COF and chemical activated CTF as a novel electrochemical sensing platform for simultaneous detection of acetaminophen and p-aminophenol, Colloids Surf. A Physicochem. Eng. Asp. 647 (2022) 129092.
[69] X. Wei, H. Guo, M. Wang, Z. Lu, Z. Yang, L. Sun, Z. Yu, Y. Liu, W. Yang, MoS_2 embedded triangular silver nanosheets modified MOF-808 as electrochemical sensing platform for highly sensitive simultaneous detection of ACOP and 4-AP, Colloids Surf. A Physicochem. Eng. Asp. 676 (2023) 132264.
[70] M.M. Rahman, Selective and sensitive 4-aminophenol chemical sensor development based on low-dimensional Ge-doped ZnO nanocomposites by electrochemical method, Microchem. J. 157 (2020) 104945.
[71] S. Chen, R. Huang, J. Zou, D. Liao, J. Yu, X. Jiang, A sensitive sensor based on MOFs derived nanoporous carbons for electrochemical detection of 4-aminophenol, Ecotoxicol. Environ. Saf. 191 (2020) 110194.
[72] Y. Fan, J.H. Liu, C.P. Yang, M. Yu, P. Liu, Graphene–polyaniline composite film modified electrode for voltammetric determination of 4-aminophenol, Sens. Actuators B 157 (2011) 669–674.
[73] E. Schwartz, La vitamine C, monography, University of QUEBEC, CHICOUTIMI, 2016.
[74] A. Szent Györgyi, Observation on the function of peroxidase systems and the chemistry of the adrenal cortex: Description of the new carbohydrate derivative, Biochem. J. 22 (1928) 1387–1409.
[75] L. Pimentel, Scurvy: historical review and current diagnostic approach, Am. J. Emerg. Med. 21 (2003) 328–332.
[76] W. Waugh, C. King, Isolation and identification of vitamin C, J. Biol. Chem. 97 (1932) 325–331.
[77] F. Sekli-Belaidi, Fonctionnalisation de surfaces d'électrodes par un film de poly(3,4-éthylènedioxythiophène) PEDOT pour l'élaboration de microcapteur spécifique des acides ascorbique

et urique : application à l'étude des propriétés antioxydantes du sérum sanguine, PhD thesis in Process and Environmental Engineering, University of TOULOUSE, 2011.
[78] G.R. Buettner, B.A. Jurkiewiez, Chemistry and biochemistry of ascorbic acid, In hand book of Antioxydants, M. Dekker, New York, (1996).
[79] P. Tveden-Nyborg, J. Lykkesfeldt, Does vitamin C deficiency increase lifestyle-associated vascular disease progression? Evidence based on experimental and clinical studies, Antioxid. Redox Signal. 19 (2013) 2084–2104.
[80] O. Fain, New concept in the biology and biochemistry of ascorbic acid, N. Engl. J. Med. 314 (1986) 892–902.
[81] K.M. Riepe, Optimization and validation of an HPLC method for detecting plasma vitamin C, University of ARIZONA STATE, 2021.
[82] D. Faouzi, L'effet combiné de la vitamine C (acide ascorbique) et de la vitamine E (α-tocophérol) contre la toxicité du nickel chez les souris (Mus musculus), PhD thesis in Science, University of BADJI MOKHTAR, ANNABA, 2016.
[83] O. Traxer, B. Huet, J. Poindexter, C. Pak, M. Pearle, Effect of ascorbic acid consumption on urinary stones risk factors, J. Urol 17 (2003) 397–401.
[84] P. Combris, M.J. Amiot-carlin, F. Caillavet, M. Causse, J. Dallongenville, M. Padilla, C. Renard, Les fruits et légumes dans l'alimentation. Enjeux et déterminants de la consommation, Exper. Sci. coll. Inra (2007) 3–18.
[85] S.J. Devaki, R.L. Raveendran, Vitamin C: Sources, functions, sensing and analysis, In book: Vitamin C, IntechOpen, (2017).
[86] P.A. Seib, B.M. Tolbert, Ascorbic acid: Chemistry, metabolism, and uses, ACS Publ. 27 (1983) 1028–1028.
[87] E.N. Ellong, C. Billard, S. Adenet, K. Rochefort, Polyphenols, carotenoids, vitamin C content in tropical fruits and vegetables and impact of processing methods, Food Sci. Nutr. 6 (2015) 299–313.
[88] S. Qiu, Q.D. Gao, Z.Y. Liu, B. Qiu, G.N. Chen, Electrochemical impedance spectroscopy sensor for ascorbic acid based on copper(I) catalyzed click chemistry, Biosens. Bioelectron. 26 (2011) 4326–4330. [89] M. Doseděl, E. Jirkovský, K. Macáková, L.K. Krčmová, L. Javorská, J. Pourová, et al., Vitamin C—sources, physiological role, kinetics, deficiency, use, toxicity, and determination, Nutrients 13 (2021) 615.
[90] S.J. Padayatty, A. Katz, Y. Wang, P. Eck, O. Kwon, S. Chen, C. Crop, et al., Vitamin C as an antioxidant: evaluation of its role in disease prevention, J. Amer. Coll. Nutr. 22 (2003) 18–35.
[91] A. Renaud, Fer, vitamine C et acide folique: convergence sanguine, J. Péd. Puéricul. 16 (2003) 281–283.
[92] N. Boyera, I. Galey, B.A. Bernard, Effect of vitamin C and its derivatives on collagen synthesis and cross-linking by normal human fibroblasts, Int. J. Cosmet. Sci. 20 (1998) 151–158.
[93] E. Cameron, L. Pauling, Supplemental ascorbate in the supportive treatment of cancer: reevaluation of prolongation of survival times in terminal human cancer, Proc. Natl. Acad. Sci. U. S. A. 75 (1978) 4538–4542.
[94] L.K. Massey, M. Liebman, S.A. Kynast-Gales, Ascorbate increases human oxaluria and kidney stone risk, J. Nutr. 135 (2005) 1673–1677.
[95] S.J. Padayatty, A. Katz, Y.H. Wang, P. Eck, O. Kwon, J.H. Lee, S.L. Chen, C. Corpe, A. Dutta, S.K. Dutta, M. Levine, Vitamin C as an antioxidant: evaluation of its role in disease prevention, J. Am. Coll. Nutr. 22 (2003) 18–35.
[96] X. Zuo, H. Zhang, N. Li, An electrochemical biosensor for determination of ascorbic acid by cobalt (II) phthalocyanine-multiwalled carbon nanotubes modified glassy carbon electrode, Sens. Actuators B Chem. 161 (2012) 1074–1079.
[97] A.S. Chang, A. Tahira, F. Chang, A.G. Solangi, M.A. Bhatti, B. Vigolo, A. Nafady, Z.H. Ibupoto, Highly heterogeneous morphology of cobalt oxide nanostructures for the development of sensitive and selective ascorbic acid non-enzymatic sensor, Biosensors 13 (2023) 147.
[98] B.S. He, J.X. Zhang, Electrochemical determination of vitamin C on glassy carbon electrode modified by carboxyl multi-walled carbon nanotubes, Int. J. Electrochem. Sci. 10 (2015) 9621.
[99] S. Liu, X. Jiang, M. Yang, Electrochemical sensing of L-ascorbic acid by using a glassy carbon electrode modified with a molybdophosphate film, Microchim. Acta 186 (2019) 445.

[100] A.N. Farida, E. Fitriany, A. Baktir, F. Kurniawan, M. Harsini, Voltammetric study of ascorbic acid using polymelamine/gold nanoparticle modified carbon paste electrode, Environ. Earth Sci. 217 (2019) 012004.
[101] S. Rostami, A. Mehdinia, A. Jabbari, Seed-mediated grown silver nanoparticles as a colorimetric sensor for detection of ascorbic acid, Spectrochim. Acta Part A Mol. Biomol. Spectrosc. 180 (2017) 204–210.
[102] D. Fudge, Quantification of mitochondrial zinc homeostasis and analysis of zinc and polyamine-mediated axonal trafficking, PhD thesis, University of DENVER, 2020.
[103] E.J. Underwood, Factors influencing trace element needs and tolerances in man, Mar. Pollut. Bull. 5 (1974) 86–88.
[104] B. Jacotot, B. Campillo, Nutrition humaine, Masson, Paris, (2003).
[105] H.J. Forman, I. Fridovich, On the stability of bovine superoxide dismutase. The effects of metals, J. Biol. Chem. 248 (1973) 2645–2649.
[106] S.R. Powell, The antioxidant properties of zinc, J. Nutr. 130 (2000) 1447S–1454S.
[107] A.S. Prasad, B. Bao, F.W. Beck, O. Kucuk, H. Sarkar, Antioxidant effect of zinc in humans, Free Radic. Biol. Med. 37 (2004) 1182–1190.
[108] N. Koukay, F. Laporte, A. Favier, Zinc et radicaux libres (étude in vitro), in: A. Favier, J. Arnaud, H. Faure (Eds.), Le zinc en médecine et biologie, Editions Médicales Internationales, Paris, (1987).
[109] M. Chvapil, L. Stankova, C.T. Zukoski, C. Zukoski, Inhibition of some functions of polymorphonuclear leukocytes by in vitro zinc, J. Lab. Clin. Med. 19 (1977) 186–196.
[110] W. Maret, Metallothionein/disulfide interactions, oxidative stress, and the mobilization of cellular zinc, Neurochem. Int. 27 (1995) 111–117.
[111] R.J. Cousins, Absorption, transport, and hepatic metabolism of copper and zinc: special reference to metallothionein and ceruloplasmin, Physiol. Rev. 65 (1985) 238–309.
[112] E. Mammadova-Bach, A. Braun, Zinc homeostasis in platelet-related diseases, Int. J. Mol. Sci. 20 (2019) 5258.
[113] S.S. Gropper, J.L. Smith, J.L. Groff, Advanced nutrition and human metabolism, 5th ed. Cengage Learning, (2012).
[114] C.T. Chasapis, A.C. Loutsidou, C.A. Spiliopoulou, M.E. Stefanidou, Zinc and human health: an update, Arch. Toxicol. 86 (2012) 521–534.
[115] F. Stéphan, J. Revuz, Sels de zinc en dermatologie, Ann. Dermatol. Vénéréol. 131 (2004) 455–460.
[116] D. Dréau, J.P. Lallés, Contribution to the study of gut hypersensitivity reactions to soybean proteins in preruminant calves and early-weaned piglets, Livest. Prod. Sci. 60 (1999) 209–218.
[117] J.P. Mackay, M. Crossley, Zinc fingers are sticking together, Trends Biochem. Sci. 23 (1998) 1–4.
[118] A. Ghisolfi-Marque, et al., Activité anti-oxydante, lipoperoxydation et vieillissement chez l'homme, Nutr. Clin. Métabol. 10 (1996) 151–160.
[119] M. Woods, et al., Effects of insulin on melanoma and brain metabolism, Biochim. Biophys. Acta. 12 (1953) 329–346.
[120] M. Kirchgessner, E. Weigand, Zinc absorption and excretion in relation to nutrition, Metal ions in biological systems, Marcel Dekker, 1st Ed. New York (1983).
[121] J. Olza, J. Aranceta-Bartrina, M. González-Gross, et al., Reported dietary intake and food sources of zinc, selenium, and vitamins A, E and C in the Spanish population: findings from the ANIBES study, Nutrients 9 (2017) 697.
[122] D. Oberleas, A.S. Prasad, Factors affecting zinc homeostasis, Zinc and copper, Academic Press, New York, (1976).
[123] J. Jia, H. Zhao, A multi-responsive AIE-active tetraphenylethylene-functioned salicylaldehyde-based schiff base for reversible mechanofluorochromism and Zn^{2+} and CO_3^{2-} detection, Org. Electron. 73 (2019) 55–61.
[124] C. Livingstone, Zinc: physiology, deficiency, and parenteral nutrition, Nutr. Clin. Pract. 30 (2015) 371–382.
[125] M.M. Berger, Rôle des oligo-éléments et des vitamines en nutrition périopératoire, Ann. Fr. Anesth. Réanim. 14 (1995) 82–94.

[126] G.V. Iyengar, Reference values for the concentrations of As, Cd, Co, Cr, Cu, Fe, I, Hg, Mn, Mo, Ni, Pb, Se and Zn in selected human tissue and body fluids, Biol. Trace Element Res. 12 (1987) 263–295.
[127] I. Adamson, et al., Zinc is the toxic factor in the lung response to an atmospheric particulate sample, Toxicol. Appl. Pharmacol. 166 (2000) 111–119.
[128] R. Claeyssen, Zinc et brûlure: Etude du statut en zinc et de l'influence de la supplémentation sur un modèle animal de brûlure sévère. Approche métabolique et moléculaire, PhD thesis, University of GRENOBLE–JOSEPH FOURIER, 2009.
[129] G. Wu, Q. Gao, M. Li, X. Tang, K.W.C. Lai, Q. Tong, A ratiometric probe based on coumarin-quinoline for highly selective and sensitive detection of Zn^{2+} ions in living cells, J. Photochem. Photobiol. A 355 (2018) 487–495.
[130] H. Kaur, et al., Highly selective and sensitive fluorescence sensing of nanomolar Zn^{2+} ions in aqueous medium using Calix[4]arene passivated Carbon Quantum Dots based on fluorescence enhancement: Real-time monitoring and intracellular investigation, Anal. Chim. Acta 1009 (2018) 1–11.
[131] C.T. Chasapis, P.S.A. Ntoupa, C.A. Spiliopoulou, M.E. Stefanidou, Recent aspects of the effects of zinc on human health, Arch. Toxicol. 94 (2020) 1443–1460.
[132] S. Tubek, Zinc supplementation or regulation of its homeostasis: advantages and threats, Biol. Trace Elem. Res. 119 (2007) 1.
[133] M. Logeais, Optimisation de la productivité des méthodes analytiques de contrôle d'un médicament, PhD thesis in pharmacy, University of POITIERS, 2013.
[134] F.A. Mohamed, M.A. AbdAllah, S.M. Shammat, Selective spectrophotometric determination of p-aminophenol and acetaminophen, Talanta 44 (1997) 61–68.
[135] S. Glavanović, M. Glavanović, V. Tomišić, Simultaneous quantitative determination of paracetamol and tramadol in tablet formulation using UV spectrophotometry and chemometric methods, Spectrochim. Acta Part A: Mol. Biomol. Spectrosc. 157 (2016) 258–264.
[136] S.D. Çekiç, H. Filik, R. Apak, Simultaneous spectrophotometric determination of paracetamol and p-aminophenol in pharmaceutical products with tiron using dissolved oxygen as oxidant, J. Anal. Chem. 60 (2005) 1019–1023.
[137] K. Zarei, S. Moghaddary, Sensitive spectrophotometric determination of ascorbic acid in drugs and foods using surface plasmon resonance band of silver nanoparticles, Cogent Chem. 1 (2015) 1109172.
[138] B. Morelli, Spectrophotometric determination of paracetamol in pure form and in tablets, J. Pharm. Biomed. Anal. 7 (1989) 577–584.
[139] H. Bi, A.C. Fernandes, S. Cardoso, P. Freitas, Interference-blind microfluidic sensor for ascorbic acid determination by UV/vis spectroscopy, Sens. Actuators B 224 (2016) 668–675.
[140] C. Terrai, N. Zekkari, S. Amrani, Optimisation de la méthode de dosage par HPLC du chlorhydrate d'amiodarone dans les comprimés dosés à 200 mg, PhD thesis in pharmacy, University of SAAD DAHLEB-1, BLIDA, 2019.
[141] G. Burgot, J.L. Burgot, Méthodes instrumentales d'analyse chimique et applications : méthodes chromatographiques, électrophorèses, méthodes spectrales et méthodes thermiques, Tec, 3rd Ed. Paris (2011).
[142] T. Belal, T. Awad, C.R. Clark, Determination of paracetamol and tramadol hydrochloride in pharmaceutical mixture using HPLC and GC–MS, J. Chromatogr. Sci. 47 (2009) 849–854.
[143] M.A. Abdel Rahman, M.R. Elghobashy, H.E. Zaazaa, S.A. Atty, S.S. El Mosallamy, Validated HPLC–PDA methodology utilized for simultaneous determination of Etoricoxib and Paracetamol in the presence of Paracetamol toxic impurities, BMC Chem. 16 (2022) 108.
[144] R.A. Fekry, K.M. Kelani, Y.M. Fayez, M.A. Tantawy, Comparative validated chromatographic methods for the simultaneous determination of caffeine, codeine, paracetamol along with the related compound "p-aminophenol" in tablets, J. Planar Chromatogr. Mod. TLC 35 (2022) 51–59.
[145] M. Szultka, M.B. Forajta, R. Kaliszan, B. Buszewski, Determination of ascorbic acid and its degradation products by high-performance liquid chromatography-triple quadrupole mass spectrometry, Electrophoresis 35 (2014) 585–592.

[146] M. Sadeghi, L. Fotouhi, S. Seidi, Voltage-step pulsed electromembrane extraction followed by high performance liquid chromatography analysis for simultaneous determination of paracetamol and codeine, Separ. Sci. Technol. (2021) 1–9.
[147] L. Monser, F. Darghouth, Simultaneous LC determination of paracetamol and related compounds in pharmaceutical formulations using a carbon-based column, J. Pharm. Biomed. Anal. 27 (2002) 851–860. [148] F.J. Pereira, Development and validation of an RP-HPLC-PDA method for determination of paracetamol, caffeine and tramadol hydrochloride in pharmaceutical formulations, Pharmaceuticals 14 (2021) 466.
[149] G. Vinci, F. Botre, G. Mele, Ascorbic acid in exotic fruits: a liquid chromatographic investigation, Food Chem. 53 (1995) 211–214.
[150] P. Patnaik, Dean's Analytical Chemistry Handbook, The McGraw-Hill Handbooks, 2nd Ed. (2004).
[151] J.A.C. Brokaert, Analytical atomic spectrometry with flames and plasmas, Wiley-VCH Verlag GmbH, Weinheim, 2nd Ed. Germany (2004).
[152] R. Manjusha, R. Shekhar, S.J. Kumar, Ultrasound-assisted extraction of Pb, Cd, Cr, Mn, Fe, Cu, Zn from edible oils with tetramethylammonium hydroxide and EDTA followed by determination using graphite furnace atomic absorption spectrometer, Food Chem. 294 (2019) 384–389.
[153] J.V. Piovesan, E.R. Santana, A. Spinelli, A carbon paste electrode improved with poly(ethylene glycol) for tannic acid surveillance in beer samples, Food Chem. 326 (2020) 127055.
[154] W.K. Abdulsahib, H.H. Sahib, M.A. Mahdi, L.S. Jasim, Adsorption study of cephalexin monohydrate drug in solution on poly (vinyl pyrrolidone-acrylamide) hydrogel surface, Int. J. Drug Deliv. Technol. 11 (2021) 1169–1172.
[155] M. Malakootian, S. Hamzeh, H. Mahmoudi-Moghaddam, A novel electrochemical sensor based on $FeNi_3$/CuS/BiOCl modified carbon paste electrode for determination of bisphenol A, Electroanalysis 33 (2021) 38–45.
[156] H. Yin, Q. Ma, Y. Zhou, S. Ai, L. Zhu, Electrochemical behavior and voltammetric determination of 4-aminophenol based on graphene-chitosan composite film modified glassy carbon electrode, Electrochim. Acta 55 (2010) 7102–7108.
[157] S.N. Vieira, L.F. Ferreira, D.L. Franco, A.S. Afonso, R.A. Gonçalves, A.G. Brito-Madurro, J.M. Madurro, Electrochemical modification of graphit with poly(4-aminophenol), Macromol. Symp. 245–246 (2006) 236–242.
[158] H.J. Salavagione, J. Arias, P. Garcés, E. Morallon, C. Barbero, J.L. Vázquez, Spectro-electrochemical study of the oxidation of aminophenols on platinum electrode in acid medium, J. Electroanal. Chem. 565 (2004) 375–383.
[159] Y. Li, M. Zhang, Y. Huang, P. Zhao, J. Zhao, J. Fei, Y. Xie, An ultrasensitive 4-aminophenol electrochemical sensor based on zinc and nitrogen-doped γ-cyclodextrin composites, Microchem. J. 197 (2024) 109905.
[160] J. Zhang, S. Xu, W. Liu, Q. Wang, J. Qu, Detection of acetaminophen and p-aminophenol simultaneously by an electrochemical sensor based on Fe-NC derivatives attached with Ti_3C_2 QDs, Talanta 275 (2024) 126192.
[161] M. Vazan, J. Tashkhourian, B. Haghighi, A novel electrochemical sensor based on MoO_3 nanobelt-graphene oxide composite for the simultaneous determination of paracetamol and 4-aminophenol, Diamond Relat. Mater. 140 (2023) 110549.
[162] K. Mohammadnezhad, F. Ahour, S. Keshipour, Electrochemical determination of ascorbic acid using palladium supported on N doped graphene quantum dot modified electrode, Sci. Rep. 14 (2024) 5982.
[163] A. Gutiérrez, M.G. Ramírez-Ledesma, G.A. Rivas, G. Luna-Bárcenas, R.A. Escalona-Villalpando, J. Ledesma-García, Development of an electrochemical sensor for the quantification of ascorbic acid and acetaminophen in pharmaceutical samples, J. Pharm. Biomed. Anal. 249 (2024) 116334.
[164] Z.M. Karazan, M. Roushani, S.J. Hoseini, Simultaneous electrochemical sensing of heavy metal ions (Zn^{2+}, Cd^{2+}, Pb^{2+}, and Hg^{2+}) in food samples using a covalent organic framework/carbon black modified glassy carbon electrode, Food Chem. 442 (2024) 138500.

[165] M.G. Trachioti, J. Hrbac, M.I. Prodromidis, Determination of Cd and Zn with “green” screen-printed electrodes modified with instantly prepared sparked tin nanoparticles, Sens. Actuators B 260 (2018) 1076–1083.

Chapter II

Modified screen printed sensors-literature review

II.1. Introduction

In recent decades, significant advancements in analytical techniques have greatly enhanced the precision and selectivity of detection methods. These improvements have found applications in a wide range of fields, including medicine, clinical diagnostics, food safety, and environmental monitoring. Among these innovations, electrochemical sensors stand out due to their simplicity, reliability, rapid response, and selectivity, making them a promising alternative to traditional analytical methods.

This chapter begins with a review of the fundamental principles and metrological characteristics of electrochemical sensors, including key performance parameters such as sensitivity, selectivity, stability, and reproducibility. The second part of the chapter focuses specifically on screen-printed electrochemical sensors, covering their fabrication processes, modifications, and the various materials, such as carbon-based composites, polymers, and metallic nanoparticles that are used to enhance their performance.

By highlighting recent advancements, this review underscores the potential of modified screen-printed sensors for detecting target analytes with greater accuracy and efficiency.

II.2. Electrochemical sensors

II.2.1. Definition

By definition, a sensor is a device that can transform chemical or biological information into an analytically interpretable signal. A sensor generally comprises two basic components connected in series: a receptor or recognition element, which recognizes the target analyte, and a signal transduction element (transducer), which converts the chemical response into an electrochemical signal.

Electrochemical sensors are particularly attractive because of their remarkable detectability, experimental simplicity, low cost (purchase and maintenance) and relatively short response time. They have a leading position among currently available sensors that have reached the commercial phase and found a wide range of applications in clinical and industrial analysis, environmental or medical monitoring, as well as in the control of biological processes **[1-3]**.

II.2.2. Principle

Electrochemical sensors are based on the variation of stimulated or spontaneous electrical parameters due to the presence of the analyte **[4]**. The operating principle of these analysis systems is shown below (Figure II.1):

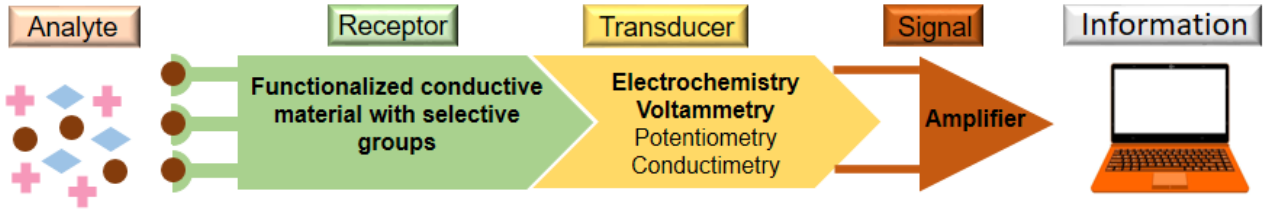

Figure II.1. Schematic representation of the general principle of an electrochemical sensor.

II.2.2.1. Receiver system

The key element of an electrochemical sensor is the receiver. In the case of electrochemical sensors, this is generally made up of an electrode material and a functional layer. The electrode material must feature high conductivity, a wide range of electro-activity, good chemical inertness and sufficient mechanical strength to maintain its integrity during prolonged immersion in the analysis medium. The choice of electrode material is therefore crucial, and the most commonly used in the literature are gold, platinum and carbon. The functional layer can be organic, inorganic, hybrid or biological. It enables pre-concentration of the species with which it interacts. If it is selective, it can also limit interference. Functional layers must also be robust and inert to the analysis media **[5, 6]**.

II.2.2.2. Transducer system

The transducer is used to transfer the response of the recognition system, mainly to the electrical signal. Transduction can be related to phenomena of different kinds: piezoelectric, optical, thermal or electrochemical **[7]**. There are several modes of transduction for electrochemical sensors :

1) Static techniques : potentiometry.

2) Potentiostatic techniques involve the use of a potentiostat instrument, such as amperometry, chronocoulometry and voltametry/polarography.

3) Impedance measurement techniques **[8]**.

II.2.2.3. Analyzer system

The signal obtained from the transducer is transformed by amplification into a signal that can be processed by the operator. The measurement, managed by microelectronics and associated software, is translated into a comprehensible message. For example, a current can be translated into a numerical concentration value, but this usually requires prior calibration of the transducer.

II.2.3. Metrological characteristics

The performance of a sensor used in a given environment is characterized by a number of parameters that constitute the effective links between the sensor and the quantity it measures:

II.2.3.1. Detection limit

The limit of detection (LOD) is the smallest detectable measurement value (activity or concentration). In the case of amperometric sensors, the electrical signal at low values is interfered with electrical noise from a variety of sources. The detection limit is generally defined as the smallest concentration value that generates an electrical signal at least three times greater than the noise amplitude. It is described mathematically by several methods, such as that corresponding to the measurement background noise. If SD and s are the standard deviation of the response and the slope, the LOD expression is determined by equation II.1 **[9]**:

$$LOD = 3.3 * SD / s \qquad \text{Eq.II.1}$$

II.2.3.2. linearity

The linear domain is the range of values where the sensor response evolves linearly between the detection limit and the maximum saturation concentration.

II.2.3.3. Sensitivity

Sensitivity is defined as the variation of the output signal (ΔS) with respect to the variation of the measurand (Δm) (slope of the linear portion of the calibration curve). The expression for sensitivity (S) is formulated by equation II.2 **[10]**:

$$S = \Delta \boldsymbol{S}/\Delta \boldsymbol{m} \qquad \text{Eq.II.2}$$

In the frequent case where the calibration curve is non-linear, this notion will itself vary depending on where you are on the calibration curve.

II.2.3.4. Repeatability and reproducibility

Repeatability is the closeness of agreement between the results of successive measurements of the same quantity carried out using the same method, by the same experimenter, with the same measuring instruments and at relatively short time intervals.

Reproducibility characterizes the closeness of agreement between the results of successive measurements of the same quantity when the measurements are carried out under different conditions **[11]**.

II.2.3.5. Stability

This is a sensor performance that ensures long-term measurement reliability, (the response is very similar in repeated applications) **[12]**.

II.2.3.6. Selectivity

The selectivity of a sensor refers to its ability to specifically detect a target chemical substance, even in the presence of other substances **[13]**.

II.2.3.7. Response time

Response time is the time required to obtain a 99% response after contact with the target species to be detected. Knowing the response time of a sensor is crucial when implementing a measurement. Sensors are more efficient when these mechanisms are faster **[14]**.

II.2.3.8. Resolution-Accuracy

The smallest measurand variation the sensor can detect.

II.2.4. Drawbacks

The advancement of robust portable electrochemical sensors has greatly enhanced living standards, as they are user-friendly and straightforward to use while also being exceptionally sensitive and providing immediate, real-time results. Nonetheless, detectors like oxygen and glucose sensors tend to be costly to manufacture. While they are relatively repeatable, these devices can be affected by numerous factors **[15]**, leading to erroneous measurements. Conditions such as variations in sensitivity, possibly caused by fluctuations in temperature or humidity, raise concerns about their consistency.

Clearly, these instruments cannot be employed by law enforcement organizations, even though they can yield dependable outcomes under optimal conditions, depending on the quality of the specific device. Another limitation of these traditional electrodes is the maintenance requirement; many electrodes, including the BODE and Glacy carbon electrode, necessitate thorough cleaning with a pad containing alumina prior to, throughout, and following testing. Moreover, these electrodes are significantly more expensive compared to the 'next generation' of electrodes discussed below.

Electrochemists are dedicated to exploring methods to enhance the electro-analytical performance of electrochemical sensors. One promising approach is the use of screen-printed electrodes, which will be assessed in the next section.

II.3. Choice of substrate: Screen-printed electrodes

A notable application of screen-printed sensors is the glucose biosensor used by individuals with diabetes, representing a billion-dollar global market **[16]**. Society is continuously evolving, and the demand for sensing devices in clinical and industrial contexts is bound to grow. To meet this demand, there is a significant need for affordable, disposable devices that are both highly accurate and rapid. Moreover, the portability of these devices is crucial. Decentralized sensing is increasingly essential, making traditional methods that rely on costly, stationary analytical instruments impractical for use beyond standard laboratories.

Scenarios where portable, cost-effective, and sensitive sensors are particularly valuable include their use in hospitals for suspected drug overdoses **[17]**, personal monitoring of conditions like diabetes **[18]**, screening drinking water from various sources **[19]**, and quickly determining biologically occurring molecules **[20]**. Screen-printed sensors not only address affordability but also meet the previously desired standards of high reproducibility and sensitivity for target species, while reaping the benefits of large-scale production.

II.3.1. History

In the initial electrochemical investigations, the use of solid metal electrodes was essential. However, as time progressed, the emphasis shifted towards lowering production expenses, as electrochemistry gained prominence in technology. Eventually, attention turned to carbon-based substances in electrochemistry, leading to the development of inexpensive and accessible methods like carbon paste electrodes. While these alternatives significantly lower costs, they may suffer from inconsistencies in reproducibility **[21]**.

Starting in the early 1990s, various printing techniques such as pad-printing, roll-to-roll, and screen-printing have been employed for the creation of electrode circuits in electrochemistry. Each of these methods presents its own unique benefits and drawbacks. For instance, pad-printing facilitates a thin-film transfer suitable for electrochemical applications; however, it is not ideal for large-scale production of electrode systems and is often regarded as a preliminary step to screen-printing technology. In contrast, the screen-printing method allows for the large-scale manufacturing of highly consistent electrode configurations **[22]**.

Given this context, screen-printed electrodes have transformed the field by connecting laboratory research with real-world applications **[23, 24]**. This impact is further enhanced by the billion-dollar annual glucose monitoring industry, which has significantly profited from the integration of screen-printed electrodes, enabling individuals to monitor their blood glucose levels at home with immediate results, eliminating the need for hospital or clinic visits **[25]**.

This technological method facilitates the large-scale production of highly consistent electrode configurations that offer excellent economies of scale. These electrode designs provide enhancements in sensitivity, signal clarity, and smaller sample volumes, creating potential alternatives to traditional (solid and reusable) electrode substrates. Additionally, the straightforward mass production of screen-printed sensors allows them to be used as single-use devices, helping to prevent contamination and eliminating the need for pre-treatment, which is often required for solid electrodes before use **[26, 27]**. Furthermore, these sensors have also been applied within electrophoretic miniaturised devices due to their benefits such as significant improvement in analysis times, lower consumption of reagents and samples, flexibility, and procedural simplicity.

In addition to the widely accessible electrochemical glucose biosensors, these screen-printed electrodes have frequently been used for various bio-sensing applications. These systems can be applied not only to biological contexts but also as analytical sensors for a range of electrochemically active contaminants, additives, and pharmaceuticals, among others. While it is true that these screen-printed electrodes may not achieve the same detection limits as much more expensive equipment, the potential for developing point-of-care sensors represents an promising and swiftly advancing field of research **[28–30]**. Moreover, screen-printed sensors have also been employed in miniaturized electrophoretic devices, thanks to their advantages, including significantly improved analysis times, reduced reagent and sample usage, adaptability, and ease of operation **[31]**.

II.3.2. Screen printing

Screen printing has been utilized for millennia to produce designs. The progression of screen printing comes from two different beginnings: the older one is about stencil fabrication, while the newer one involves ink and textile. The earliest documentation of screen printing was recorded during the medieval epoch when bitumen was applied to taut, unembellished cloth and allowed to cure, forming a negative stencil. Dye was then compelled through a rigid applicator across regions untainted by bitumen onto banners or apparel **[32, 33]**.

In the mid-nineteenth century, a more traditional phase of screen printing began. The capability to secure stencils to a stable mesh allowed for detailed designs to be accurately aligned and applied with a brush. Shortly thereafter, the squeegee was developed, allowing for a more uniform application of ink compared to the brush **[34]**. Today, screen printing is seen as one of the most straightforward techniques for creating prints. The technique employs a stencil positioned on a fabric mesh tightened over a sturdy frame. Ink poured into the frame is forced

through the open areas of the stencil using a squeegee. This creates an image when the underside of the screen touches the substrate, as illustrated in figure II.2.

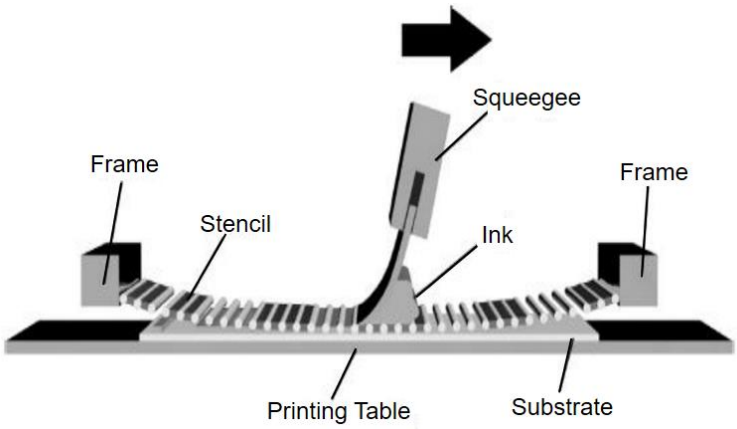

Figure II.2. Screen-printing procedure.

This technology is straightforward and allows for the large-scale fabrication of highly consistent, disposable, single-use screen-printed electrodes at a lower cost and in a minimal amount of time. The substrate used for screen printing can vary widely (such as PS plates, PVC, epoxy resin, glass, ceramics, etc.), and can be either rigid or flexible. Inks should be chosen based on the surface characteristics of the substrates. A sharp edge in the printed image necessitates inks with high viscosity. Another benefit of screen printing is that it supports a range of configurations (single working electrodes, groups of working electrodes, 3-electrode setups, etc.) with different electrode shapes and sizes. The use of these low-cost, disposable SPEs for stripping measurements offers an appealing alternative to more traditional electrode substrates **[35–37]**.

II.3.3. Configuration and production

Screen-printed electrodes represent a new generation of electrodes with diverse applications in electrochemistry, including analytical chemistry, drug monitoring, clinical, and environmental assessments, owing to their substantial advancements over recent decades **[38]**. The distinctiveness of these screen-printed electrodes lies in their typical design as three-electrode systems, where the working electrode, counter electrode, and reference electrode are all printed together.

The working electrode is the site of the electrochemical reaction, the reference electrode ensures a stable and precise potential, and the counter electrode allows for charge transfer to the working electrode. This configuration creates a complete sensor that can be printed on a single sheet, thus reducing the costs of materials for the working electrode as well as for the

reference and counter electrodes. The ink utilized to manufacture screen-printed electrodes is carbon-based (such as carbon nanotubes, nanoporous carbon, carbon fibers, graphite, graphene, etc.), which is relatively inexpensive, making the total expense of a complete screen-printed electrode quite low. The following figure II.3 displays a typical screen-printed sensor and outlines its key components **[39, 40]**.

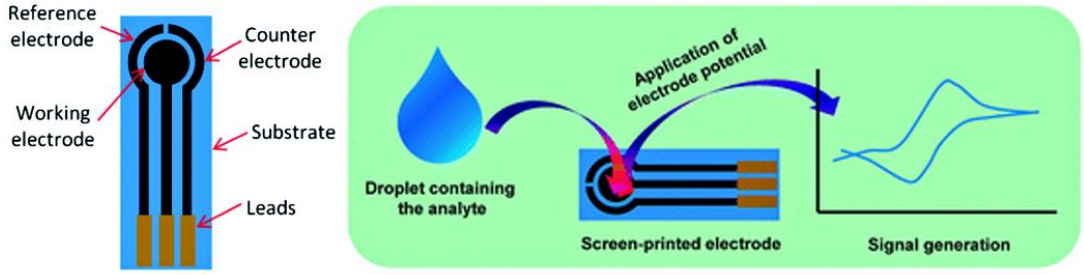

Figure II.3. Diagrammatic representation of screen-printed electrodes and their applications.

Figure II.4 illustrates a conventional laboratory-based three-electrode system alongside a system printed with conductive inks. This comparison highlights the potential to develop electrochemical configurations that are compact, cost-effective, and consistent **[41]**.

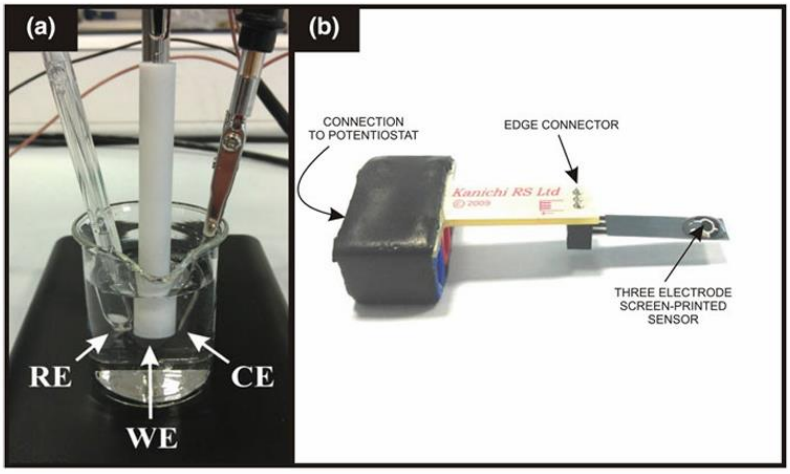

Figure II.4. (a) Comparison of size between a traditional three-electrode system (edge pyrolytic plane working electrode, saturated calomel reference electrode, and platinum counter electrode) and (b) a screen-printed electrode in an electrolyte solution.

The complete production process of screen-printed electrodes involves five steps (Figure II.5):

(i) Choosing the screen or mesh, which determines the geometry and dimensions of the SPE;

(ii) Selecting and preparing the inks;

(iii) Selecting the substrate material;

(iv) Printing;

(v) Drying and curing.

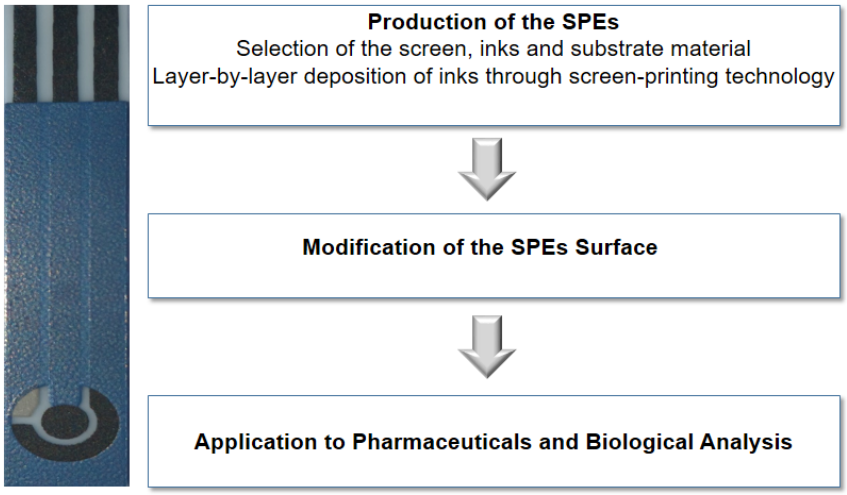

Figure II.5. Steps in the development of a screen-printed electrode.

SPEs are generally associated with electrochemical detection techniques such as amperometric techniques (measuring current), potentiometric techniques (based on potential difference) and conductimetric techniques (measuring conductivity or resistivity). These are devices that provide fast, sensitive responses, are simple to manufacture and can be single-use, i.e. disposable. This last point simplifies the in-situ measurement process, since the surface can be renewed after each use. Their cost is generally low, making them competitive with other detection systems, with the added advantage of easy packaging and undeniable portability **[42]**.

II.4. Modification of screen-printed electrodes

II.4.1. Modification purpose

Not every species can be detected by an electrode **[43]**. Nonetheless, many substances of pharmaceutical, clinical and analytical interest are generally little or not reactive at electrode level. These are often species whose oxidation or reduction potential lies outside the electroactivity window of the electrode in question. This is why, in the mid-70s, the concept and practical realization of modified electrodes **[44, 45]** emerged, aimed at increasing the electrocatalytic activity and kinetics of the electrochemical reaction taking place at the surface of this electrode by limiting overvoltage problems, and lowering the oxidation or reduction potential of the target species so that it is detectable within the electrolyte's electroactivity range.

Recently, electrode modification strategies have enabled the development of analytical procedures using immobilized reagents. The principle consists in attaching electroactive species to a metal or carbon electrode by adsorption or covalent bonding. Modified electrodes have many applications in electroanalysis and electrocatalysis **[46]**.

One of the advantages of these systems is that they require a minimum amount of reagents, often expensive, to perform the analyses. Another advantage is the selectivity of modified electrodes. Indeed, by carefully selecting the immobilized reagent, it is possible to control the selectivity of the electrode towards a given species, which is of considerable interest when measurements have to be carried out in complex media. In addition, these electrodes can be used to increase sensitivity through the deposition stage. During this accumulation stage, the target species is pre-concentrated in a small volume on the electrode surface, enabling very low concentrations to be measured. In addition, these methods are less costly and time-consuming than other conventional analytical methods.

All these reasons justify the efforts currently being made to develop new materials, as well as the interest aroused by modified electrodes in various fields such as clinical biology analysis, monitoring of agri-food processes, environmental control and so on.

II.4.2. Choice of modifier

The upcoming sections present recent advancements in electrode modifications (Figure II.6). These developments are examined from both fundamental electrochemistry and sensor development perspectives. While discussed separately, it is recognized that these materials are frequently combined in sensor development. This thesis places specific emphasis on metallic nanoparticles.

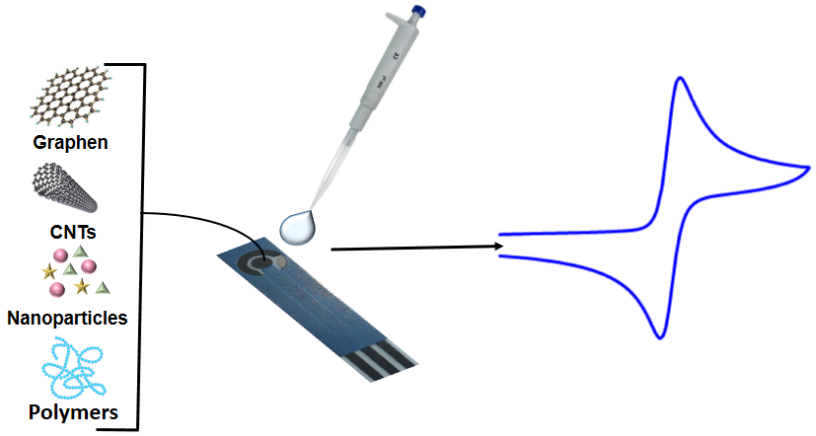

Figure II.6. Screen-printed sensor modifiers.

II.4.2.1. Nanomaterials

Recently, nanotechnology has become one of the most promising fields in analytical chemistry. As a result, a wide variety of nanomaterials have found broad application in many

types of sensor, and have demonstrated interesting analytical performance in terms of sensitivity and detection limits.

The interest in such materials stems from their potential advantages and their many excellent properties in terms of electrode/electrolyte contact area, porosity, electron transfer rate, chemical stability, mechanical strength, electrocatalytic activity, etc., thus overcoming some of the limitations of bulk materials **[47, 48]**.

Nanomaterials frequently used for the modification of electrodes applied in electroanalysis include metal nanoparticles such as gold nanoparticles (AuNPs) **[49, 50]**, platinum nanoparticles (PtNPs) **[51, 52]**, silver nanoparticles (AgNPs) **[53-55]**, cobalt nanoparticles **[56]** and others. Metal oxide nanomaterials **[57, 58]**, carbon nanotubes (CNTs), in particular multiwall carbon nanotubes (MWCNTs) **[59, 60]** and graphene **[61]**.

This section will review the literature on the different types of nanomaterials generally used for elctrode modification.

II.4.2.1.1. Carbon-based nanomaterials

Graphene is a carbon layer of monoatomic thickness, with a hexagonal structure composed of sp^2-hybridized carbon atoms (Figure II.7). The accumulation of graphene layers leads to the formation of graphite (3D). It was first studied theoretically by *P. R. Wallace* in 1947 **[62, 63]** and then obtained experimentally for the first time in 2004 by *Andre Geim* and *Konstantin Noroselov* of the University of Manchester [64-66], whose discovery was crowned with the 2010 Nobel Prize, officially "for pioneering experiments on the two-dimensional material graphene".

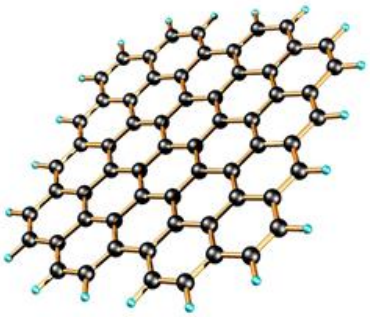

Figure II.7. Schematic of a graphene layer.

Graphene has since gained a great deal of attention from researchers, as it exhibits a unique combination of extremely interesting properties experimentally obtained far better than those of any other material: electron mobility of 3.105 $cm^2.V^{-1}s^{-1}$ at room temperature **[67]**, a

Young's modulus of 1TPa **[68]**, high thermal conductivity (over 3000 $W.mK^{-1}$ **[69]**), impermeability to gases **[70]**, and the ability to withstand very high current densities (a million times higher than copper **[71]**). This two-dimensional crystal displays fascinating electrical, mechanical and optical properties **[72]**.

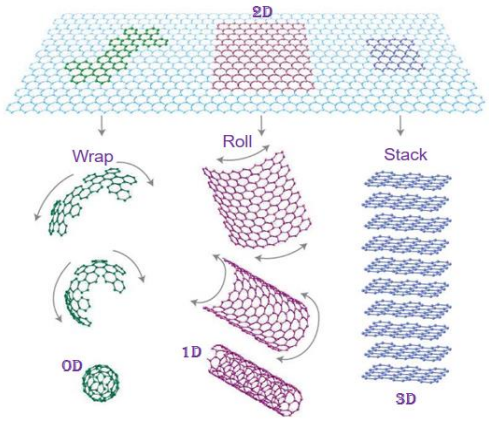

Figure II.8. The 2D structure of graphene is a basis for certain allotropic forms of carbon (graphite, nanotube, fullerene, etc.) **[73, 74]**.

There are a variety of methods for synthesizing graphene to meet the high demand for it. There are two main approaches: bottom-up and top-down. The main fabrication methods commonly used, such as mechanical exfoliation, epitaxial growth or graphene oxide reduction, each have their advantages and limitations **[75]**.

In the present environment, where technology serves as the engine of the economy and science acts as the fuel to keep this engine operating, graphene is regarded as one of the most significant scientific advancements in recent history. Following the discovery of graphene, a variety of studies were documented that demonstrated enhanced sensor performance attributed to the utilization of this material **[76]**. Zang et al. **[77]** created a noval electrochemical sensor based on a molecularly imprinted film at an NH_2–graphene modified screen-printed electrode for the electrochemical detection of the psychoactive substances methcathinone and cathinone in human serum samples. In this research, NH_2–graphene was employed as the supporting material, enhancing the conductivity of the SPE, while pyrrole served as the monomer to construct the molecularly imprinted film on the SPE's surface. These imprinted films exhibited rapid adsorption kinetics, notable selectivity, substantial binding capacity, and exceptional reuse performance. Moreover, the proposed sensors were assembled with a graphite working electrode (WE) and counter electrode (CE) and a silver/silver chloride (Ag/AgCl) pseudo-reference electrode (PRE), which were produced using screen-printing process on a polyester substrate.

Graphene's unique properties and structure make it an attractive candidate for sensing applications. However, for practical and cost reasons, it is the oxidized form of graphene, functionalized by alcohol, carboxylate and epoxide groups, that is used for such applications. This oxide also possesses conductive properties, but the groups present on its surface facilitate functionalization by coupling with a wide variety of ligands **[78]**. Thus, this material has also been utilized in the modification of screen-printed electrodes for the electrochemical determination of pharmaceuticals. In this regard, Ping et al. described the fabrication of an SPE from a graphene and ionic liquid-doped screen-printing ink for the simultaneous detection of vitamin C, dopamine, and uric acid using cyclic voltammetry and differential pulse voltammetry techniques **[79]**. The thickness of the chemically reduced graphene oxide was characterized using trapping-mode AFM, while its surface morphology was evaluated via scanning electron microscopy. It was found that the resulting graphene–ionic liquid–cellulose acetate ink SPE presented a regular surface structure, allowing for the simultaneous analysis of AA, DA, and UA in real samples. Jian et al. also nanostructured SPEs with graphene oxide and achieved a detection limit of 1 $\mu g.L^{-1}$ for Pb(II) **[80]**. In this case, it is the oxygen functions of the graphene oxide that serve to complex the Pb(II).

Carbon nanotubes are attracting considerable interest in the world of research and industry alike, due to their exceptional intrinsic properties and dimensional characteristics **[81]**. First observed in 1991, nanotubes appear as concentric hollow tubes separated by 0.34 nanometres (sometimes there is only one tube), with an internal diameter of the order of a nanometre and a length of the order of a few micrometres. These elongated structures are optionally closed at their ends by carbon pentagons characteristic of fullerenes. A filament of this type is 100 times stronger than steel, and six times lighter, with uncommon resistance to high temperatures. Their diameter is of the order of a millionth of a millimeter. Carbon nanotubes are subdivided into two types: single-walled carbon nanotubes, discovered in 1993 by Iijima (Figure II.9a), and multi-walled carbon nanotubes, discovered in 1991 (Figure II.9b) **[82, 83]**.

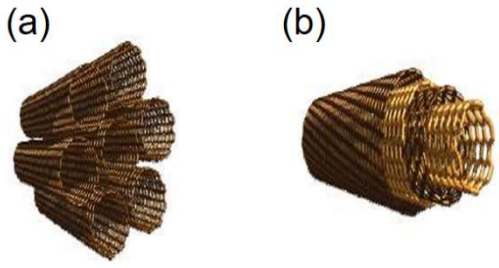

Figure II.9. Schematic representation of the two classes of single-walled carbon nanotube (SWCNT) (a) and multi-walled carbon nanotube (MWCNT) (b).

Carbon nanotubes exhibit high chemical and thermal stability, high elasticity, good tensile strength and, above all, high conductivity. This conductivity is at the origin of their electronic properties and is very important for their use in electrochemistry, notably as nanoelectrodes **[84]**. The first application of nanotubes in electrochemistry was by Britto et al. with a MWNT-functionalized carbon paste electrode for the study of dopamine oxidation **[85]**.

The nano-dimensions, surface chemistry of graphite and electronic properties of carbon nanotubes make them ideal for the detection of chemical and biochemical species. There is growing interest in the use of carbon nanotubes in the development of sensors, as they minimize the problem of diffusion, increase the contact surface area with the surrounding medium and the grafting density of molecules, while maintaining the molecule's stability and activity. In terms of improving sensor performance, carbon nanotubes make it possible to increase sensitivity and lower the detection threshold.

Numerous investigators have utilized the benefits of CNTs, merging them with the disposability of SPEs to create CNT-modified SPEs. Jiménez-Pérez et al. altered various carbon-based SPEs for electrochemical identification of hydroperoxides. The highest electrochemical efficacy was attained with MWCNTs-based screen-printed electrodes, featuring a detection limit within the range of 24–558 nM among all carbon-based composites evaluated **[86]**. Crevillén et al. **[87]** likewise documented the detection of the water-soluble vitamins pyridoxine, ascorbic acid, and folic acid in pharmaceutical formulations by employing two distinct carbon electrodes (a glassy carbon electrode and a screen-primted carbon electrode) modified with multi-walled carbon nanotubes, revealing that the optimal analytical performance was realized for the MWCNTs-SPCE. This developed electrode facilitated the precise detection of the three vitamins in four different pharmaceuticals in a brief time frame, utilizing a straightforward protocol that incorporated the use of small volumes of sample and no prior treatment.

The impetus for the utilization of both carbon nanotubes and graphene has frequently been described as providing superior electrocatalytic effects compared to traditional electrode materials such as glassy carbon and graphite. Nevertheless, there has also been an indication that the advantages of employing these materials may be somewhat exaggerated. This underscores the necessity to support any assertion of improved electroanalytical performance resulting from carbon nanostructures with suitable controls. For instance, it has been proposed that the electroactive sites of carbon nanotubes are located at the edge sites of the structure and do not deliver superior electrocatalytic activity in comparison to edge plane pyrolytic graphite

[88, 89]. Likewise, imperfections in the basal plane and edge planes have been demonstrated to be regions of electrochemical activity in graphene.

In spite of certain apprehensions, carbon nanomaterials continue to hold a prominent position in sensor development today. One rationale for this is that graphene and carbon nanotubes can now be functionalized to enable enhanced attachment of biomolecules.

II.4.2.1.2. Polymeric nanomaterials

Polymers are encouraging substances for SPE applications owing to their reduced material expenses and straightforward methods for fabrication. By modifying a solid electrode with a polymer film, it is possible to form multilayers of active species on its surface. Typically, polymers used for the chemical modification of electrodes have electrochemically or chemically active groups, such as redox or chelating sites. Compared with electrodes modified by a monolayer of adsorbed or grafted molecules, polymer films offer clear advantages, such as better manufacturing reproducibility, high stability and a much greater number of accessible active sites **[90]**.

Conducting polymer (CP) nanomaterials have discovered uses across numerous domains in recent years as a result of their enhanced chemical and physical characteristics compared to traditional metallic substances. They are distinguished by their extensive pi orbital system, which facilitates electron movement along the polymer's backbone **[91]**. Moreover, CPNPs provide inherent advantages such as ease of surface alteration, biocompatibility, and large surface areas, positioning them as excellent candidates for uses in electrical and optoelectronic detection instruments **[92, 93]**.

The use of films of electron-conducting polymers, such as polypyrrole (PPy), polyaniline (PANI), and polythiophene (PTs), is a promising way of obtaining electrode materials for electroanalytical devices. PANI offers the benefit of remarkable stability and processability; however, in contrast to PPy, it cannot be applied onto electrode surfaces using neutral pH solutions **[94]**. These materials combine the properties of organic polymers (ease of processing, good mechanical properties and high resistance to acids and bases) with semiconductor properties thanks to their electrical conductivity, which can be very high. They have demonstrated interesting analytical performance thanks to their mediator properties and, above all, their morphology, which favors the immobilization of a large number of electro-active substances **[95]**. Some conductive polymers are electro-active and have catalytic effects on certain redox reactions, for example, the oxidation of hydrazine on polyaniline **[96]**, and the oxidation of hydrazine and ascorbic acid on polypyrrole **[97, 98]**. These polymer films have

been used as sensitive layers, making direct use of their electrocatalytic properties. However, in order to further enhance this catalytic activity, different strategies have been developed by incorporating chemical species into the polymer matrix, thus facilitating the electron transfer process **[99]**.

Poly(3,4-ethylenedioxythiophene) (PEDOT) has also been widely utilized in biosensor applications **[100]**. Thivya et al. **[101]** explored the application of PEDOT coated with taurine (TA) on a SPE as an electrochemical approach for detecting cholesterol. Excellent stability and dispersibility were attained through the electrostatic interactions facilitated by TA sulfonic acid. Employing a linear response (3 µM to 1 mM) in both CV and SWV, the PEDOT/TA composite exhibited a lower detection limit of 0.95 µM.

Molecularly Imprinted Polymers (MIPs) provide biological recognition elements with exceptional stability, customization, and cost-effective production **[102]**. Utilizing a macroporous gold SPE, Tabrizi et al. created an ultrasensitive electrochemical sensor based on molecularly imprinted polymers for detecting SARS-CoV-2 RBD. Microporous gold screen-printed electrodes were employed to fabricate MIP sensors. The detection limits of the MIP sensors were 0.7 pg ml^{-1} (3-4.8 × 10^2 virus μl^{-1}) **[103]**. For more details on electrochemical sensors based on Molecularly Imprinted Polymers, see reference **[104]**.

II.4.2.1.3. Inorganic nanomaterials

Nanoparticles are typically characterized as particles ranging from 1 nm to 100 nm (Figure II.10) whose characteristics differ from those of the bulk substance **[105]**. The enhancement in the surface area to volume ratio, which occurs gradually as the particle diminishes in size, results in an increasing influence of the behavior of surface atoms compared to those within the particle's interior. This impacts both the properties of the particle when considered alone and its interactions with other substances. The surface area is a vital element in the efficiency of catalysis and in structures like electrodes, facilitating enhancements in performance **[106]**.

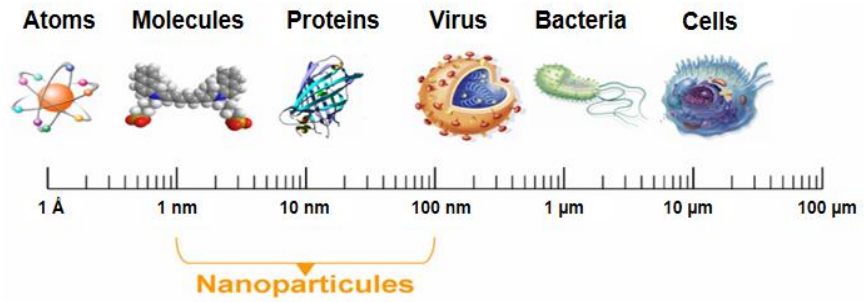

Figure II.10. Nanoparticle size compared with chemical and biological structures.

Nanoparticles are generally classified into three categories **[107]**:

-**Organic nanoparticles**: organic nanoparticles are biodegradable, non-toxic particles such as dendrimers, micelles and liposomes. They are most commonly used in the biomedical field, as drug delivery systems.

-**Inorganic nanoparticles**: inorganic nanoparticles are metal- or metal oxide-based particles.

-**Carbon-based nanoparticles**: these are nanoparticles made entirely of carbon, such as fullerenes, graphene, carbon nanotubes, carbon nanofibers and carbon black.

Lately, nanoparticles have been widely researched and utilized for the efficient alteration of an electrode surface, thereby enhancing the electrocatalytic performance of the working electrode. They have attracted considerable attention in biosensor applications because of their distinctive electronic, magnetic, optical, and electrocatalytic characteristics **[108]**.

Nanoparticles are synthesized using two main approaches, summarized in figure II.11: the "top-down" approach and the "bottom-up" approach.

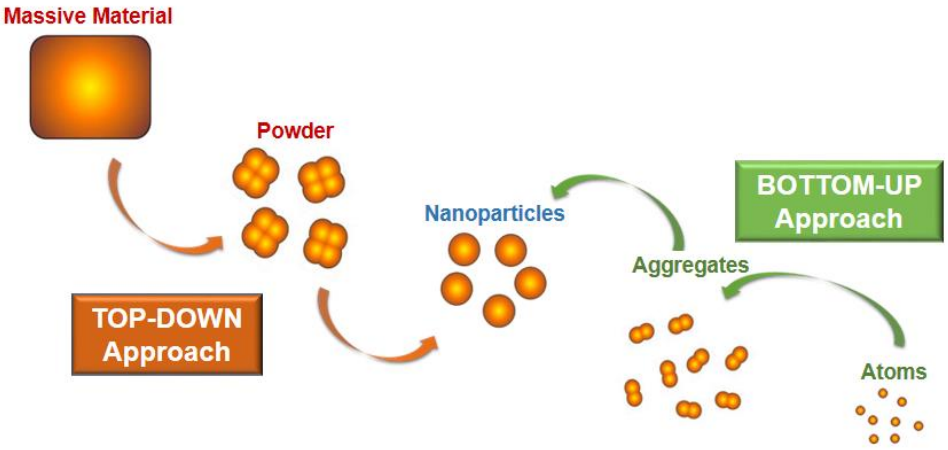

Figure II.11. Approaches to nanoparticle production.

Top-down nanoparticle synthesis starts with a bulk material and transforms it into nano-sized particles. Bottom-up nanoparticle synthesis involves nucleating and growing nanoparticles from isolated atoms. It involves the use of physico-chemical phenomena on the atomic and molecular scales to chemically transform a precursor into particles. The assembly and positioning of atoms, molecules or particles enable the creation of simple or elaborate nanostructures.

In this section of the thesis, the applications involving metallic nanoparticles will be examined, emphasizing their specific functions within sensing devices. Furthermore, various techniques employed to modify the surfaces of screen-printed electrodes with metallic nanoparticles will be addressed.

II.4.2.1.3.1. Metallic nanoparticles-Overview

Metal nanoparticles can function as catalysts in both enzymatic and non-enzymatic devices, serve as sensing components for the immediate identification of various analytes, or act as support substrates for sensing platforms. They can catalyze significant processes, such as the reduction of peroxides or the oxidation of carbohydrates, enabling the detection of enzymatic products, sugars, and amino acids in actual samples **[109-114]**.

Additionally, metal nanoparticles can monitor other analytes, paving the way for new applications (see table II.1). Platinum nanoparticles can catalyze the oxidation of minor organic compounds, including ethanol and formaldehyde, enabling the creation of alcohol sensors for wine and beer **[115]** as well as gas sensors for formaldehyde detection **[116]**. Palladium NPs can also detect formaldehyde and other analytes, including hydrazine and sulfuric acid, using the traditional method of ink mixing. Additionally, hydrogen was evaluated in a proof-of-concept assay, demonstrating the potential for palladium-based screen-printed sensors to function as gas detectors **[111]**. Iridium nanoparticles are also proficient at detecting NADH generated during the dehydrogenase oxidation of glycerol. This method led to the development of a triglyceride biosensor that exhibited a strong correlation with bovine and human serum **[117]**.

Nanoparticles of noble metals such as platinum, gold and silver are of particular interest due to their size-dependent optoelectronic, magnetic, optical and chemical properties. These nanoparticles have been extensively studied, not only from a fundamental point of view, but also with a view to numerous technological applications. Their ease of synthesis and characterization, as well as the surface functionalization possibilities they offer **[118, 119]**, open up new prospects in the analytical and bioanalytical fields. What's more, the use of colloidal suspensions of metal nanoparticles (suspensions of nanoparticles formed by chemical reduction of metal salts) makes them considerably easier to handle, with less risk of exposure than nanoparticles in powder form.

Noble metal nanoparticles were employed in enzyme-free devices due to their ability to detect peroxide at a reduced overpotential in comparison to traditional bare electrodes. Additionally, it is now feasible to synthesize noble metal nanoparticles with precise control over their size, shape, surface, charge, and physicochemical properties, allowing them to be customized for specific electrocatalytic uses **[120-122]**. Integrating these qualities with additional characteristics like low toxicity, high surface area, a diverse array of surface functionalization chemistries, and colloidal stability, these nanomaterials have been widely employed recently to create advanced biosensing platforms and devices on their own.

Platinum is the predominant noble metal used in non-enzymatic sensors. Thanks to its effective electrocatalytic activity against peroxide, platinum can be employed to identify this substance in a range of real-life samples, such as cosmetics **[123]**, household items **[124]**, and food and drinks **[125]**, with satisfactory recovery outcomes.

Similarly to platinum and its analogs, other noble metals such as gold, silver, and copper are used in sensing devices. Sensors incorporating these nanoparticles demonstrate reduced catalytic activity and are significantly influenced by particle size and fabrication techniques. Nonetheless, they offer a more cost-effective alternative compared to platinum-modified screen-printed sensors. Dominguez et al. **[126]** have optimized a new, user-friendly, and rapid approach for integrating silver nanoparticles onto the surface of screen-printed carbon electrodes. The modification of SPCEs with AgNPs enhances the well-recognized capabilities of these disposable electrodes. To showcase their practical applications, these modified electrodes were employed for the detection of Sb(III), a notable pollutant of significant concern. Burgoa et al. also developed a screen-printed carbon electrode modified with AgNPs for the detection of the antiepileptic medication lamotrigine in pharmaceuticals, utilizing DPAdSV technique **[127]**. The surface of the modified AgNPs/SPCEs was analyzed using scanning electron microscopy before being employed for the determination of lamotrigine in pharmaceutical products.

Several studies have indicated the use of screen-printed electrodes modified with gold nanoparticles (AuNPs) to improve sensitivity for detecting various toxins in different samples. For instance, gold nanoparticles combined with graphene oxide have been utilized to quantify carbofuran **[128]**, while a rGO/AuNPs/boronic acid nanocomposite modified SPE was employed to identify glycosides in food samples **[129]**. Additionally, a nanocomposite incorporating AuNPs and GO quantum dots was used as a modifier for SPEs for the electrochemical detection of Aflatoxin B1 **[130]**. Furthermore, a screen-printed electrode was utilized to detect antibiotics like tetracycline and cefixime in milk, employing a gold electrode modified with a self-assembled monolayer of cysteine on AuNPs through SWV technique **[131]**. This developped electrode was combined with chemometric techniques to quantify antibiotics in biological fluids, demonstrating its potential as a viable option for biosensing. Additionally, poly (l-lactide)-stabilized AuNPs were used to enhance a disposable screen-printed carbon electrode for detecting As(III) via differential pulse adsorptive stripping voltammetry. The sensitivity achieved was sufficient to identify As(III) at parts per billion levels, offering a straightforward and specific detection approach for As(III) in natural water sources **[132]**.

Work on modified electrodes based on metal oxides has made a major contribution to the emergence of new electrocatalytic sensors. The presence of an oxidized form on the electrode surface leads to intense electrocatalytic activity, enabling the oxidation of various organic molecules. The resulting electrodes have been used in particular for the determination of oxidizable substances such as glucose, ethanol, 1-butanol, histidine, paracetamol and other molecules. For example, graphite and glassy carbon electrodes modified by the formation of layers of nickel, cobalt, iron and mixed oxides have been used for the consecutive or simultaneous electrochemical determination of several families of oxidizable organic substances such as sugars, acids, amino acids and alcohols, and have shown very high stability at room temperature, good reproducibility and a detection limit of the order of micrograms per liter **[133]**.

Moreover, various metallic oxide elements possess the ability to catalyze the hydrolysis of carbohydrates, facilitating the identification of these analytes in actual samples. Nickel nanoparticles demonstrate commendable electrocatalytic characteristics for the oxidation of sugars. They have been employed in non-enzymatic devices for glucose detection in food **[134, 135]**, blood **[136]**, or urine **[137]** as practical samples. It is essential to highlight that an initial voltammetric or amperometric pretreatment is required for these nanoparticles to generate metal oxide species, including oxyhydroxides, which play a vital role in the catalytic oxidation of carbohydrates.

Table II.1. Applications of metallic NPs modified screen-printed electrodes.

Metallic NPs	**Analyte**	**Technique**	**Linear Range**	**Detection Limit**	**Matrix**	**Ref.**
Ag	H_2O_2	AD	0.5 µM to 12 mM	0.21 µM	Contact lens care solution	**[138]**
Ag	Sulfite	AD	1.96 to 16.66 mM	1.99 mM	Beverages	**[139]**
Ag	Metronidazole	DPV	3.1 to 310 µM	0.4 µM	Serum,Urine, and Tablets	**[140]**
Ag	Lamotrigine	DPCSV	0.3 to 1.50 µM	0.372 µM	Pharmaceuticals	**[127]**
Ag	Chloride Bromide Iodide	LSV	3 to100 µM 5 to 90 µM 5 to 80 µM	3 µM 5 µM 5 µM	Synthetic sweat	**[141]**
Au	Trazodone	OCP	10 µM to 10 mM	6.8 µM	Pharmaceuticals	**[142]**

Table II.1. Cont.

Metallic NPs	Analyte	Technique	Linear Range	Detection Limit	Matrix	Ref.
Au	Carbofuran	DPCSV	1–250 µM	0.22 µM	Food	**[128]**
Au	H_2O_2 Glucose	AD	0.2 to 4.2 mM 2 to 10 mM	- 180 µM	Blood	**[143]**
Au	Sulfite	AD	9.8 to 83.33 µM	9.79 µM	Beverages	**[139]**
Au	Ascorbic acid	DPV	1.9 to 16.6 µM	0.99 µM	Serum	**[144]**
Au	Glucose	AD	1.5 to 16 mM	25 µM	Serum	**[145]**
Au	Ciprofloxacin	CV, SWV	0.1 to 150 µM	0.001 µM	Serum, Plasma Urine	**[146]**
Au	Sulfide	DPCSV	0.05 to 1.5 µM	0,2 µM	Tap water	**[147]**
Au	Aspirin	CV, DPV	1 pg/mL to 1 µg/mL	0.03 pg/mL	Urine, Saliva, Pharmaceuticals	**[148]**
Au	Glucose	CV	0.01 to 5 mM	6 µM	Beverages	**[149]**
Cu	Ascorbic acid	CA	0.0125 to 10 mM	6 mM	Tablets, Urine	**[150]**
Cu	Glucose Fructose Arabinose Galactose Mannose Xylose	CV, CA	1 to 10000 µM	0.57 µM 0.61 µM 1.0 µM 0.89 µM 1.3 µM 1.04 µM	honey, orange juice, normal/sugar-free soft drinks	**[151]**
Ir	Triglyceride	CA	Up to 10 mM	-	Serum	**[117]**
Ir	Methimazole	CV, CA	0.01 to 0.5 µM	0.003 µM	Pharmaceuticals, Serum	**[152]**
Ir	Meclizine	DPV	6.66 to 196.08 µM	1.69 µM	Pharmaceuticals, Urine	**[153]**
Ni	Glucose	CA	0.5 µM to 4 mM	0.07 µM	Blood	**[136]**
Ni	Glucose	AD	0.2 to 9 mM	4.1 µM	Urine	**[137]**
Ni	Insulin	CV, CA, AD	20.0 to 260.0 nM	6.1 nM	-	**[116]**
Ni	Glucose Fructose	CA	25 to 1000 µM	Between 8 µM and 20 µM	Food	**[135]**
Ni	Glucose Fructose Mix 1:1	AD, FIA	0.05 to 1 mM	0.06 mM 0.04 mM 0.04 mM	Honey	**[134]**

Table II.1. Cont.

Metallic NPs	Analyte	Technique	Linear Range	Detection Limit	Matrix	Ref.
Pd	Dopamine	DPV	0.35 to 135.35 µM	0.056 µM	Injection	**[154]**
Pd	Hydrazine	AD	0.05 to 1415 µM	4 nM	Drainage water	**[155]**
Pd	Dissolved O_2	CV	Up to 250 µM	-	Ground and tap water	**[112]**
Pt	H_2O_2	AD	1 M to 10 mM	0.43 µM	Contact lens care solution	**[156]**
Pt	H_2O_2	AD	Up to 0.1 mM	6.6 µM	Whitening Strips	**[157]**
Pt	Arsenic(III)	CV	0.66 to 333 µM	5.68 µg/L	Spiked tap water	**[158]**
Pt	Ethanol	LSV	15 to 102 mM	15 mM	Beverages	**[115]**
Pt	Bisphenol-A	AD	0.01 to 1.0 µM 1.0 to 300 µM	6.63 nM	Tap water	**[159]**
Pt	Glucose	CV	0.5 to 20 mM	32.8 µM	Serum	**[160]**
Pt	H_2O_2	CA	10 to 100 µM	10 µM	Green tea	**[124]**
Pt	H_2O_2	AD	6 to 215 µM	7.6 µM	Hair lightener Antiseptic Plantextract	**[123]**
Pt	H_2O_2	AD	Up to 6.5 mM	80 µM	Hair lightener	**[161]**
Rh	H_2O_2	AD	5 to 600 µM	2 µM	Tea extracts	**[162]**
Rh	Bromide	CSV	Up to 40 mM	39 µM	Seawater Pharmaceuticals	**[163]**

AD: Amperometric detection, **CA**: Chronoamperometry, **FIA**: Flow Injection Analysis**, CSV**: Cathodic Stripping Voltammetry, **DPCSV**: Di erential-Pulse Cathodic Stripping Voltammetry, **LSV**: Linear Sweep Voltammetry.

Bimetallic materials synthesized in nanoparticle form were used to combine the catalytic properties of these metals and thus improve analytical performance (see table II.2). Bimetallic alloys made from nanoparticles that can catalyze carbohydrate oxidation have been synthesized. Cu-Ti **[164]** and Ni-Co **[165]** show an enhanced response to glucose by harnessing the properties of both metals involved. Additionally, alloys of Cu-Pd **[166]** and Au-Ag **[147]** were created to improve sensitivity for the detection of hydrazine and free sulfide in actual samples, including tap water and cigarette smoke, respectively.

Table II.2. Applications of bimetallic NPs modified screen-printed electrodes.

Bimetallic NPs	Analyte	Technique	Linear Range	Detection Limit	Matrix	Ref.
Cu-Ti	Glucose	CA	25 µM to 2 mM	7 µM	Honey Plasma	**[164]**
Cu-Pd	Hydrazine	AD, FIA	2 to 100 µM	270 nM	Cigarette tobacco	**[166]**
Pt-Ag	H_2O_2	AD	2.2 to 67 µM	0.34 µM	Antiseptic and Laundry boosters	**[124]**
Pt-Pd	H_2O_2 Glucose	AD	0.005 to 6 mM Up to 16 mM	0.87 µM 10 µM	Simulative blood	**[167]**
Au-Ag	Sulfide	LSCSV	0.5 to 12.5 µM	0.2 µM	Water	**[147]**

AD: Amperometric detection, **CA**: Chronoamperometry, **FIA**: Flow Injection Analysis, **LSCSV**: Linear-Scan Cathodic Stripping Voltammetry.

Among bimetallic systems, the Pt–Ni systems have been widely documented across various fields using different types of electrodes **[168-171]**, rather than screen-printed electrodes, as the combination of platinum with nickel enhances both their synergistic and electronic properties. In the synergistic mechanism, Ni serves an essential function in promoting the oxidative removal of obstructive residues from the active sites of Pt **[172, 173]**. While numerous applications have been reported for platinum **[123, 156-161, 174, 175]** or nickel **[176, 134-137]** nanoparticles individually as modifiers in screen-printed electrodes, primarily for the development of voltammetric sensors and biosensors due to their distinctive properties, there appears to be no existing research on utilizing them simultaneously to modify the surface of SPEs. This highlights a key aspect of novelty in the work presented in this thesis.

II.4.2.1.3.2. Methods for modifying SPEs with metallic NPs

Modification of the electrode surface in SPEs is typically accomplished through three established techniques illustrated in figure II.12: ink mixing with the modifying substance, electrochemical deposition of a metallic precursor, or drop casting of a previously formed nanoparticulate material.

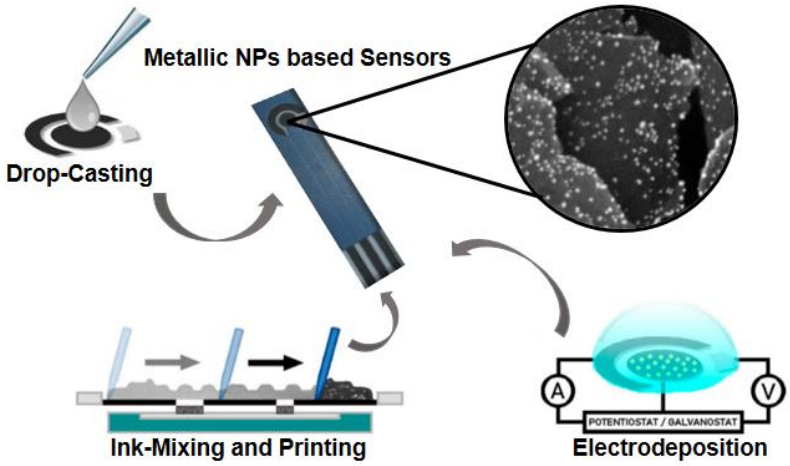

Figure II.12. Illustration of the three primary techniques commonly used for the modification of SPEs with metal nanoparticles.

II.4.2.1.3.2.1. Ink mixing

Ink mixing for screen-printed electrodes modification involves creating an ink that always includes three key components: conductive particles typically composed of carbon-based material, a solvent/binder mixture that facilitates the transfer of particulate matter onto the substrate, and the modifying agent, metal nanoparticles. Based on the intended application, the primary factors that should be optimized include the ink formulation, its rheological properties, substrate choice, and thermal curing process.

As the initial method investigated, early studies emerged in the early 1990s. These papers utilized conductive materials directly bonded to metal particles, resulting in metallized carbon with platinum **[109]**, palladium **[113]**, or iridium **[117, 177]** blended with standard inks used for screen printing to create second-generation enzymatic sensors, in which metallic particles serve as catalysts. The primary benefit of this approach lies in the straightforward mixing of commercially accessible materials with printing binders and solvents, allowing for optimization of only the mixing recipe.

Subsequently, pristine metallic particles, formerly isolated from carbon, were combined with conductive material and binder **[178]**. While the metal dispersion percentage can influence the reactivity of the supported metal substrates, the analytical response is not uniformly affected when the ink mixing method is employed. This behavior can be attributed to the characteristics of the mixing procedure. As the nanoparticulated material is blended, agglomeration takes place, reducing the level of dispersion, which ultimately results in larger particles in the micro range at the same metal concentration. This explains why only a limited number of publications **[139, 179]** focus on ink mixing with metal nanoparticles, as the primary advantage of

nanoparticles-namely, a high surface area resulting from particle spacing and their nanoscale size is compromised.

II.4.2.1.3.2.2. Drop casting

This is the simplest technique used to modify SPEs. Just a single parameter needs to be fine-tuned: the final quantity deposited onto the electrode. This can be adjusted by varying the size of the drop and the amount of the metal nanoparticles dispersed in the solution. Devices created using this technique are based on two primary strategies: direct modification of specific nanoparticles onto the working electrode or ex-situ production of composites composed from nanoparticles bonded to carbon-based nanomaterials.

The first strategy is simpler to implement, as no functionalization step is required. Consequently, various metal nanoparticle solutions have been utilized, including bismuth **[180]**, platinum **[158, 174]**, rhodium **[174]**, gold **[128]**, silver **[181]**, copper **[182]**, and nickel **[134]**. Devices created in this manner exhibit stability, even in flow injection systems, facilitating the development of more accessible and cost-effective sensors compared to those produced by the ink mixing technique. However, agglomeration remains the primary limitation encountered with these devices.

To address this drawback, the second strategy is more frequently employed, as it yields more consistent nano-sized metallic centers. Nanoparticles are synthesized onto a conductive carbon-based substrate, similar to the particulate metallized carbon materials initially used with the ink mixing technique. In contrast to the two-step process of successively casting carbon nanomaterial followed by nanoparticles **[128]**, these new composites provide not only a "real" nanoparticulate foundation but also an enhanced electroactive area due to the properties of the carbon nanomaterials utilized. Leveraging this advantage, platinum **[125]**, silver **[138]**, nickel **[183]**, and gold **[143]** have been combined with carbon nanotubes, reduced graphene oxide, and nanoporous carbon, or graphene oxide, respectively, to create innovative composite sensors with enhanced catalytic efficiency.

II.4.2.1.3.2.3. Electrochemical deposition

This represents the most widely used technique for modifying screen-printed electrodes with metal nanoparticles, as it allows for precise control over the morphology of the nanoparticles. This approach is founded on the reduction of oxidized species, commonly

metallic water-soluble salts, at a fixed potential or current to produce custom-designed metal particles that grow on conductive substrates.

The parameters that are typically optimized can be categorized into two main groups: those related to the precursor solution, which include the type and concentration of the salt, and the conditions for electrochemical deposition. A list of commonly used salts includes $AgNO_3$ **[124, 139-141]** for silver nanoparticles; $HAuCl_4$ **[139, 144, 145]** and $AuCl_3$ **[184]** for gold nanoparticles; $CuCl_2$ **[185]**, CuSO4 **[186]**, and $CuNO_3$ **[187, 188]** for copper nanoparticles; $NiCl_2$ **[136, 165]** and $NiSO_4$ **[135, 137]** for nickel nanoparticles; $PdCl_2$ **[112, 154, 155]** for palladium nanoparticles; and H_2PtCl_4 **[160]**, H_2PtCl_6 **[116, 123, 161, 167, 189]**, and $PtCl_2$ **[184]** for platinum nanoparticles, among others.

Even though higher concentrations of precursors facilitate the production of larger particles, the size and shape are typically controlled electrochemically; thus, the precursor concentration is often kept sufficiently high to ensure there is enough material available for deposition, and it is not usually optimized **[127]**. Keeping this in consideration, two parameters are essential for controlling the size and shape of the growing nanoparticles: the applied potential or current and the deposition time. The latter modulates the quantity and size of metal deposited onto the electrode, such that a longer deposition time results in a greater quantity of nanoparticles with larger particle sizes **[184]**. Regarding the first parameter, potential variations form the basis of potentiostatic techniques, while changes in current underpin galvanostatic techniques.

Potentiostatic methods rely on the application of a constant potential. When a specific potential is applied for the deposition of nanoparticles, their size and shape can be adjusted. At more negative applied potentials, the nucleation rate increases, resulting in a higher quantity of nanoparticles with smaller particle sizes, thereby enhancing the electroactive surface area.

Galvanostatic methods involve applying a constant negative current that is capable of reducing precursor metallic salts. The more negative the applied current, the greater the nucleation rate attained, analogous to potentiostatic techniques. The deposition duration is also an essential parameter. Even though this method is not widely utilized, the use of current instead of potentials is more practical when working with screen-printed electrodes **[190]**. Due to the pseudo-reference electrode, potentials can fluctuate when oxidizing media are employed in the deposition step. Since the structure of the nanoparticle surface significantly influences the overall analytical output of the sensor, small changes in the reference potential can lead to less accurate results. The implementation of a constant current reduces the impact of pseudo-referenced systems **[186]**, but careful management of the applied current remains crucial.

The large-scale production poses a significant limitation of this technique, as electrodeposition must be performed for each sensor individually, making the deposition step a time-consuming procdure when considering large batch production.

II.4.3. Modified SPEs for target analytes detection

Numerous studies have highlighted the use of screen-printed electrodes modified with various substances for the detection of paracetamol, 4-aminophenol, ascorbic acid, and zinc, both individually and in combination across different matrices **[191-198]**. For instance, Gilmartin et al. **[193]** developed a disposable amperometric sensor strip utilizing surface-modified screen-printed carbon electrodes for the selective electrochemical detection of paracetamol in urine. The SPCEs were enhanced through drop-coating with a cellulose acetate solution. The findings from paracetamol determination in urine using these modified electrodes closely aligned with the results obtained from a standard enzyme colorimetric kit. Abdi et al. **[194]** successfully modified the surface of screen-printed electrodes with chitosan-coated nickel nanoparticles to enable the individual and simultaneous detection of 4-aminophenol and paracetamol. The modified sensor demonstrated a high recovery rate and excellent selectivity, making it effective for detecting both compounds in pharmaceutical tablets. Additionally, Crevillén et al. reported the simultaneous detection of ascorbic acid and two other vitamins, pyridoxine and folic acid, in pharmaceutical formulations using two different carbon electrodes: a glassy carbon electrode and a screen-printed carbon electrode modified with multi-walled carbon nanotubes. They found that the MWCNTs-SPCE exhibited the most superior analytical performance **[196]**. In another investigation, a screen-printed carbon electrode was enhanced with a composite of poly(3,4-ethylenedioxythiophene), poly(vinyl alcohol), and silver nanoparticles to simultaneously detect Zn(II), Cd(II), and Pb(II) in a ternary mixture using the SWASV technique, yielding a strong electrochemical response **[198]**.

Despite numerous published studies on the detection of target analytes, none have successfully identified all of them in a single analytical run, highlighting another novel aspect of our work.

II.5. Conclusion

This chapter provided an overview of the fundamental concepts related to electrochemical sensors and the various modifiers used to enhance the performance of screen-printed electrodes. A particular focus was placed on metallic nanoparticles as inorganic nanomaterials for modifying SPE surfaces, with an emphasis on platinum and nickel bimetallic

nanoparticles, which are the primary modifiers used in this work. A detailed review of recent studies highlighted the unique properties of these nanoparticles as advanced materials for sensor modification.

The chapter also examined the three main methods for modifying SPEs with metallic nanoparticles: Ink mixing, electrochemical deposition of metallic precursors, and drop-casting of pre-formed nanoparticulate materials. Of these, electrochemical deposition was identified as the most effective technique for improving sensor performance and was selected for use in this work. More details on the electrochemical deposition process and its application in this study will be provided in the next chapter.

Finally, the chapter discussed the use of modified SPEs for the detection of paracetamol, 4-aminophenol, ascorbic acid, and zinc, either individually or simultaneously, in various sample matrices. The electrochemical modification of SPEs significantly enhanced their sensitivity and selectivity, making them highly suitable for the detection of these target analytes in complex biological and pharmaceutical samples.

References

[1] D.W. Kimmel, G. LeBlanc, M.E. Meschievitz, D.E. Cliffel, Electrochemical sensors and biosensors, Anal. Chem. 84 (2012) 685–707.
[2] F.X. Guillon, Biocapteurs electrochimiques de microARNs pour le diagnostic médical, PhD thesis in therapeutic chemistry, University of PARIS SCIENCES ET LETTRES, 2017.
[3] D. Udomsap, Développement de polymères à empreintes moléculaires électrochimiques pour la surveillance en micropolluants organiques des eaux dans les ouvrages du Canal de Provence, PhD thesis in chemistry, University of TOULON, 2014.
[4] P. Fabry, C. Gondran, Capteurs électrochimiques-fonctionnement, utilisation, conception, Ellipses, (2008).
[5] M. Ayat, Réalisation de capteurs chimiques et biocapteurs à base de silicium poreux et pillars de silicium pour la détection d'espèces chimiques toxiques, PhD thesis in physics, University of USTHB, ALGIERS, 2019.
[6] G. March, T.D. Nguyen, B. Piro, Modified electrodes used for electrochemical detection of metal ions in environmental analysis, Biosensors 5 (2015) 241–275.
[7] N.R. Stradiotto, H. Yamanaka, M.V.B. Zanoni, Electrochemical sensors: A powerful tool in analytical chemistry, J. Braz. Chem. Soc. 14 (2003) 159–173.
[8] B. Bansod, T. Kumar, R. Thakur, S. Rana, I. Singh, A review on various electrochemical techniques for heavy metal ions detection with different sensing platforms, Biosens. Bioelectron. 94 (2017) 443–455.
[9] S. Hadnine, Extraction et modification des substances naturelles et leur application à la détection des métaux lourds, PhD thesis, University of 20 AOUT 1955, SKIKDA, 2020.
[10] D. Lakhdari, Elaboration et caractérisation d'un matériau à base de nanoparticules magnétique NiFe-PANi par électrodéposition: application dans la détection de glucose, PhD thesis in chemistry, University of MOULOUD MAMMERI, TIZI-OUZOU, 2021.
[11] N. Zehani, Étude et développement de biocapteurs électrochimiques pour la détection de polluants dans un milieu aqueux, PhD thesis in chemistry, co-tutelle thesis between university of CLAUDE BERNARD, LYON 1, and BADJI MOKHTAR, ANNABA, 2015.
[12] I. Boubezari, Conception et développement de nouveaux capteurs chimiques et de (bio) capteurs à transduction électrochimique, PhD thesis in chemistry, co-tutelle thesis between university of CLAUDE BERNARD, LYON 1, and MOHAMED SEDDIK BENYAHIA, JIJEL, 2021.
[13] K. Duarte, C.I.L. Justino, A.C. Freitas, A.C. Duarte, T.A.P. Rocha Santos, Direct-reading methods for analysis of volatile organic compounds and nanoparticles in workplace air, Trends Anal. Chem. 53 (2014) 21–32.
[14] A. Bensana, Développement d'un Biocapteur pour la détection des polluants organiques: étude expérimentale et modélisation, PhD thesis in process engineering, University of FERHAT ABBAS, SETIF, 2021.
[15] G. Asch, B. Poussery, M. Desjardins, Les capteurs en instrumentation industrielle, Technique et ingénierie, 5th ed. Dunod, (1999).
[16] S.K. Vashist, D. Zheng, K. Al-Rubeaan, H.T. Luong, F.S. Sheu, Technology behind commercial devices for blood glucose monitoring in diabetes management: A review, Anal. Chim. Acta 703 (2011) 124–136.
[17] K. Peterson, J. Zapletalova, P. Kudlova, V. Matuskova, J. Bartek, D. Novotny, R. Chlup, Benefits of three-month continuous glucose monitoring for persons with diabetes using insulin pumps and sensors, Biomed. Pap. Med. Fac. Univ. Palacky Olomouc Czech Repub. 153 (2009) 47–52.
[18] I. Kusumi, K. Ito, K. Uemura, M. Honda, T. Hayashishita, K. Miyamato, Y. Kako, S. Tsuchida, N. Hashimoto, T. Koyama, Progress in neuro-psychopharmacology and biological psychiatry, Prog. Neuropsychopharmacol. Biol. Psychiatry 35 (2011) 1922.
[19] Z.H. Rivera, E. Oosterink, L. Rietveld, F. Schoutson, L. Stolker, Anal. Meths. Acta. 700 (2011) 114.
[20] W. Wang, W.Y. Wu, X.Q. Zhong, W. Wang, Q.A. Miao, J.J. Zhu, Biosens. Bioelectron. 26 (2011) 3110.
[21] K. Ravichandran, R.P. Baldwin, Chemically modified carbon paste electrodes, J. Electroanal. Chem. Interfacial Electrochem. 126 (1981) 293–300.

[22] L. Mooring, N.G. Karousos, C. Livingstone, J. Davis, G.G. Wildgoose, S.J. Wilkins, R.G. Compton, Evaluation of a novel pad printing technique for the fabrication of disposable electrode assemblies, Sens. Actuators B: Chem. 107 (2005) 491–496.
[23] J.P. Metters, R.O. Kadara, C.E. Banks, New directions in screen printed electroanalytical sensors: an overview of recent developments, Analyst 136 (2011) 1067–1076.
[24] K.C. Honeychurch, J.P. Hart, Screen-printed electrochemical sensors for monitoring metal pollutants, Trends Anal. Chem. 22 (2003) 456–469.
[25] A. Heller, B. Feldman, Electrochemical glucose sensors and their applications in diabetes management, Chem. Rev. 108 (2008) 2482–2505.
[26] E.P. Randviir, D.A.C. Brownson, J.P. Metters, R.O. Kadara, C.E. Banks, The fabrication, characterisation and electrochemical investigation of screen-printed graphene electrodes, Phys. Chem. Chem. Phys. 16 (2014) 4598–4611.
[27] A.V. Kolliopoulos, J.P. Metters, C.E. Banks, Screen printed graphite electrochemical sensors for the voltammetric determination of antimony(III), Anal. Methods 5 (2013) 3490–3496.
[28] A. Amine, H. Mohammadi, I. Bourais, G. Palleschi, Enzyme inhibition-based biosensors for food safety and environmental monitoring, Biosens. Bioelectron. 21 (2006) 1405–1423.
[29] Z. Nie, C.A. Nijhuis, J. Gong, X. Chen, A. Kumachev, A.W. Martinez, M. Narovlyansky, G.M. Whitesides, Electrochemical sensing in paper-based microfluidic devices, Lab Chip 10 (2010) 477–483.
[30] A.P. Ruas de Souza, C.W. Foster, A.V. Kolliopoulos, M. Bertotti, C.E. Banks, Screen-printed back-to-back electroanalytical sensors: heavy metal ion sensing, Analyst 140 (2015) 4130–4136.
[31] E.P. Randviir, C.E. Banks, Electrode substrate innovation for electrochemical detection in microchip electrophoresis, Electrophoresis 36 (2015) 1845–1853.
[32] J.F. Jing, P.F. Li, J. Wang, Appl. Mech. Mater. 29 (2010) 896.
[33] I. Locher, G. Trosler, Text. Res. J. 77 (2007) 837.
[34] M. Mikuz, S. Turk, P.F. Traveer, Coloration Technol. 126 (2010) 249.
[35] G. Hughes, K. Westmacott, K.C. Honeychurch, A. Crew, R.M. Pemberton, J.P. Hart, Recent advances in the fabrication and application of screen-printed electrochemical (bio)sensors based on carbon materials for biomedical, agri-food and environmental analyses, Biosensors 6 (2016) 50.
[36] A. Hayat, J.L. Marty, Disposable screen printed electrochemical sensors: tools for environmental monitoring, Sensors 14 (2014) 10432–10453.
[37] X. Niu, M. Lan, H. Zhao, C. Chen, Y. Li, X. Zhu, Electrochemical stripping analysis of trace heavy metals using screen-printed electrodes, Anal. Lett. 46 (2013) 2479–2502.
[38] M.A. Alonso-Lomillo, O. Domínguez-Renedo, M.J. Arcos-Martínez, Electrochemical sensors in the development of selective methods for antiepileptic drugs determination, Comb. Chem. High Throughput Screen. 13 (2010) 650–657.
[39] N. Zavanelli, W.H. Yeo, Advances in screen printing of conductive nanomaterials for stretchable electronics, ACS Omega 6 (2021) 9344.
[40] M. Li, Y. Li, D. Li, Y. Long, Recent developments and applications of screen-printed electrodes in environmental assays – A review, Anal. Chim. Acta 734 (2012) 31–44.
[41] C.W. Foster, R.O. Kadara, C.E. Banks, Introduction and current applications of screen-printed electrochemical architectures, in: Screen-Printing Electrochemical Architectures, SpringerBriefs Appl. Sci. Technol. 2016.
[42] V.M. Ekomo, Du polymère à empreintes moléculaires électrochimiques au capteur: Etude de faisabilité pour la détection du Bisphénol A, PhD thesis in chemistry, University of TOULON, 2018
[43] D.M. Radzik, S.M. Lunte, Application of liquid chromatography/electrochemistry in pharmaceutical and biochemical analysis: A critical review, CRC Crit. Rev. Anal. Chem. 20 (1989) 317–358.
[44] R.W. Murray, Polymer modification of electrodes, Annu. Rev. Mater. Res. 14 (1984) 145–169.
[45] R.F. Lane, A.T. Hubbard, Electrochemistry of chemisorbed molecules. I. Reactants connected to electrodes through olefinic substituents, J. Phys. Chem. 77 (1973) 1401–1410.
[46] M. Ozsoz et al., Clay/sol-gel-modified electrodes for the selective electrochemical monitoring of 2,4-dichlorophenol, Langmuir 19 (2003) 4728–4732.
[47] X. Luo, A. Morrin, A.J. Killard, M.R. Smyth, Application of nanoparticles in electrochemical sensors and biosensors, Electroanalysis 18 (2006) 319–326.

[48] S.R. Belding, F.W. Campbell, E.J.F. Dickinson, R.G. Compton, Nanoparticle-modified electrodes, Phys. Chem. Chem. Phys. 12 (2010) 11208–11221.
[49] A. Corma, H. Garcia, Supported gold nanoparticles as catalysts for organic reactions, Chem. Soc. Rev. 37 (2008) 2096–2126.
[50] M. Zayats, R. Baron, I. Popov, I. Willner, Biocatalytic growth of Au nanoparticles: from mechanistic aspects to biosensors design, Nano Lett. 5 (2005) 21–25.
[51] R. Polsky, R. Gill, L. Kaganovsky, I. Willner, Nucleic acid-functionalized Pt nanoparticles: Catalytic labels for the amplified electrochemical detection of biomolecules, Anal. Chem. 78 (2006) 2268–2271.
[52] R. Narayanan, M.A. El-Sayed, Shape-dependent catalytic activity of platinum nanoparticles in colloidal solution, Nano Lett. 4 (2004) 1343–1348.
[53] F.W. Campbell, S.R. Belding, R. Baron, L. Xiao, R.G. Compton, Hydrogen peroxide electroreduction at a silver-nanoparticle array: Investigating nanoparticle size and coverage effects, J. Phys. Chem. C 113 (2009) 9053–9062.
[54] C.A. de Lima, E.R. Santana, J.V. Piovesan, A. Spinelli, Silver nanoparticle-modified electrode for the determination of nitro compound-containing pesticides, Anal. Bioanal. Chem. 408 (2016) 2595–2606.
[55] K. Cui, Y. Song, Y. Yao, Z. Huang, L. Wang, A novel hydrogen peroxide sensor based on Ag nanoparticles electrodeposited on DNA-networks modified glassy carbon electrode, Electrochem. Commun. 10 (2008) 663–667.
[56] A.O. Simm, X.B. Ji, C.E. Banks, M.E. Hyde, R.G. Compton, AFM studies of metal deposition: Instantaneous nucleation and the growth of cobalt nanoparticles on boron-doped diamond electrodes, ChemPhysChem 7 (2006) 704–709.
[57] X.M. Miao, R. Yuan, Y.Q. Chai, Y.T. Shi, Y.Y. Yuan, Direct electrocatalytic reduction of hydrogen peroxide based on Nafion and copper oxide nanoparticles modified Pt electrode, J. Electroanal. Chem. 612 (2008) 157–163.
[58] S. Qu, J. Wang, J.L. Kong, P.Y. Yang, G. Chen, Magnetic loading of carbon nanotube/nano-Fe_3O_4 composite for electrochemical sensing, Talanta 71 (2007) 1096–1102.
[59] N.S. Lawrence, R.P. Deo, J. Wang, Comparison of the electrochemical reactivity of electrodes modified with carbon nanotubes from different sources, Electroanalysis 17 (2005) 65–72.
[60] F. Valentini, S. Orlanducci, M.L. Terranova, A. Amine, G. Palleschi, Carbon nanotubes as electrode materials for the assembling of new electrochemical biosensors, Sens. Actuators B 100 (2004) 117–125.
[61] Y. Wang, Y. Li, L. Tang, J. Lu, J. Li, Application of graphene-modified electrode for selective detection of dopamine, Electrochem. Commun. 11 (2009) 889–892.
[62] J.C. Slonczewski, P.R. Weiss, Band structure of graphite, Phys. Rev. 109 (1958) 272–279.
[63] P.R. Wallace, The band theory of graphite, Phys. Rev. 71 (1947) 622–634.
[64] K.S. Novoselov, A.K. Geim, S.V. Morozov, D. Jiang, Y. Zhang, S.V. Dubonos, I.V. Grigorieva, A.A. Firsov, Electric field effect in atomically thin carbon films, Science 306 (2004) 666–669.
[65] K.S. Novoselov, D. Jiang, F. Schedin, T.J. Booth, V.V. Khotkevich, S.V. Morozov, A.K. Geim, Two-dimensional atomic crystals, Proc. Natl. Acad. Sci. U. S. A. 102 (2005) 10451–10453.
[66] K.S. Novoselov, A.K. Geim, S.V. Morozov, D. Jiang, M.I. Katsnelson, I.V. Grigorieva, S.V. Dubonos, A.A. Firsov, Two-dimensional gas of massless Dirac fermions in graphene, Nature 438 (2005) 197–200.
[67] A.S. Mayorov, R.V. Gorbachev, S.V. Morozov, L. Britnell, R. Jalil, L.A. Ponomarenko, P. Blake, K.S. Novoselov, K. Watanabe, T. Taniguchi, A.K. Geim, Micrometer-scale ballistic transport in encapsulated graphene at room temperature, Nano Lett. 11 (2011) 2396–2399.
[68] C. Lee, X. Wei, J.W. Kysar, J. Hone, Measurement of the elastic properties and intrinsic strength of monolayer graphene, Science 321 (2008) 385–388.
[69] A.A. Balandin, Thermal properties of graphene and nanostructured carbon materials, Nat. Mater. 10 (2011) 569–581.
[70] J.S. Bunch, S.S. Verbridge, J.S. Alden, A.M. Van Der Zande, J.M. Parpia, H.G. Craighead, P.L. McEuen, Impermeable atomic membranes from graphene sheets, Nano Lett. 8 (2008) 2458–2462.
[71] J. Moser, A. Barreiro, A. Bachtold, Current-induced cleaning of graphene, Appl. Phys. Lett. 91 (2007) 4–6.
[72] K.S. Novoselov, et al., A roadmap for graphene, *Nature* 490 (2012) 192.

[73] F.A. Alussail, Synthesis and characterization of reduced graphene oxide films, University of WATERLOO, CANADA, 2015.
[74] S. Pei, H.M. Cheng, The reduction of graphene oxide, Carbon 50 (2012) 3210–3228.
[75] X. Wan, Y. Huang, Y. Chen, Focusing on energy and optoelectronic applications: A journey for graphene and graphene oxide at large scale, Acc. Chem. Res. 45 (2012) 598.
[76] Y. Shao, J. Wang, H. Wu, J. Liu, I.A. Aksay, Y. Lin, Graphene Based Electrochemical Sensors and Biosensors: A Review, Electroanalysis 22 (2010) 1027–1036.
[77] D. Zang, M. Yan, S. Ge, L. Ge, J. Yu, Disposable simultaneous electrochemical sensor array based on a molecularly imprinted film at a NH_2-graphene modified screen-printed electrode for determination of psychotropic drugs, Analyst 138 (2013) 2704.
[78] J. Liu, Z. Liu, C.J. Barrow, W. Yang, Molecularly engineered graphene surfaces for sensing applications: A review, Anal. Chim. Acta 859 (2015) 1–19.
[79] J. Ping, J. Wu, Y. Wang, Y. Ying, Simultaneous determination of ascorbic acid, dopamine and uric acid using high-performance screen-printed graphene electrode, Biosens. Bioelectron. 34 (2012) 70–76.
[80] J.M. Jian, Y.Y. Liu, Y.L. Zhang, X.S. Guo, Q. Cai, Fast and sensitive detection of pb^{2+} in foods using disposable screen-printed electrode modified by reduced graphene oxide, Sensors 13 (2013) 13063–13075.
[81] S. Iijima, Helical microtubules of graphitic carbon, Nature 354 (1991) 56–58.
[82] J. Wang, B. Tian, J. Lu, D. MacDonald, J. Wang, D. Luo, Renewable-reagent enzyme inhibition sensor for remote monitoring of cyanide, Electroanal. 10 (1998) 1034–1037.
[83] M.H. Smit, G.A. Rechnitz, Toxin detection using a tyrosinase-coupled oxygen electrode, Anal. Chem. 65 (1993) 380–385.
[84] Q. Zhao, Z. Gan, Q. Zhuang, Electrochemical Sensors Based on Carbon Nanotubes, Electroanalysis 14 (2002) 1609–1613.
[85] P.J. Britto, K.S.V. Santhanam, P.M. Ajayan, Carbon nanotube electrode for oxidation of dopamine, Bioelectrochem. Bioenergetics 41 (1996) 121–125.
[86] R. Jiménez-Pérez, J. Iniesta, M.T. Baeza-Romero, E. Valero, On the performance of carbon-based screen-printed electrodes for (in)organic hydroperoxides sensing in rainwater, Talanta 234 (2021) 122699. [87] A.G. Crevillén, M. Pumera, M.C. González, A. Escarpa, Carbon nanotube disposable detectors in microchip capillary electrophoresis for water-soluble vitamin determination: analytical possibilities in pharmaceutical quality control, Electrophoresis 29 (2008) 2997–3004.
[88] C.E. Banks, R.G. Compton, New electrodes for old: from carbon nanotubes to edge plane pyrolytic graphite, The Analyst 131 (2006) 15.
[89] D.A.C. Brownson, L.J. Munro, D.K. Kampouris, C.E. Banks, Electrochemistry of graphene: not such a beneficial electrode material? RSC Adv. 1 (6) (2011) 978–988.
[90] J.M. Zen, A.S. Kumar, D.M. Tsai, Recent updates of chemically modified electrodes in analytical chemistry, Electroanalysis 15 (2003) 1073–1087.
[91] Md.A. Rahman, P. Kumar, D.S. Park, Y.B. Shim, Electrochemical sensors based on organic conjugated polymers, Sensors 8 (2008) 118–141.
[92] C.S. Park, C. Lee, O.S. Kwon, Conducting polymer based nanobiosensors, Polymers 8 (2016) 249.
[93] S. Cinti, Polymeric materials for printed-based electroanalytical (bio) applications, Chemosensors 5 (2017) 31.
[94] F.R.R. Teles, L.P. Fonseca, Applications of polymers for biomolecule immobilization in electrochemical biosensors, Mater. Sci. Eng. C 28 (2008) 1530–1543.
[95] A. Ramanavicius, A. Ramanaviciene, A. Malinauskas, Electrochemical sensors based on conducting polymer—polypyrrole, Electrochim. Acta 51 (2006) 6025–6037.
[96] L. Doubova, M. Fabrizio, G. Mengoli, S. Valcher, Electrocatalytic oxidation of hydrazine in acid media on polyaniline-filmed vitreous carbon, Electrochim. Acta 35 (1990) 1425–1431.
[97] D. Oukil, L. Makhloufi, B. Saidani, Preparation of polypyrrole films containing ferrocyanide ions deposited onto thermally pre-treated and untreated iron substrate: Application in the electroanalytical determination of ascorbic acid, Sens. Actuators B 123 (2007) 1083–1089.
[98] D. Oukil, L. Benhaddad, L. Makhloufi, R. Aitout, B. Saidani, Gold nanoparticles modified polypyrrole/iron electrode used as sensor for hydrazine detection, Sens. Lett. 11 (2013) 395–404.

[99] Y. Wei, M. Li, S. Jiao, Q. Huang, G. Wang, B. Fang, Fabrication of CeO_2 nanoparticles modified glassy carbon electrode and its application for electrochemical determination of UA and AA simultaneously, Electrochim. Acta 52 (2006) 766–772.
[100] B.D. Malhotra, A. Chaubey, S.P. Singh, Prospects of conducting polymers in biosensors, Anal. Chim. Acta 578 (2006) 59–74.
[101] P. Thivya, R. Ramya, J. Wilson, Poly(3,4-thylenedioxythiophene)/taurine biocomposite on screen-printed electrode: Nonenzymatic cholesterol biosensor, Microchem. J. 157 (2020) 105037.
[102] A. Poma, A. Guerreiro, M.J. Whitcombe, E.V. Piletska, A.P.F. Turner, S.A. Piletsky, Solid-phase synthesis of molecularly imprinted polymer nanoparticles with a reusable template—"plastic antibodies," Adv. Funct. Mater. 23 (2013) 2821–2827.
[103] M. Amouzadeh Tabrizi, J.P. Fernández-Blázquez, D.M. Medina, P. Acedo, An ultrasensitive molecularly imprinted polymer-based electrochemical sensor for the determination of SARS-CoV-2-RBD by using macroporous gold screen-printed electrode, Biosens. Bioelectron. 196 (2022) 113729.
[104] R.D. Crapnell, N.C. Dempsey-Hibbert, M. Peeters, A. Tridente, C.E. Banks, Molecularly imprinted polymer-based electrochemical biosensors: Overcoming the challenges of detecting vital biomarkers and speeding up diagnosis, Talanta Open 2 (2020) 100018.
[105] M. Auffan, J. Rose, J.Y. Bottero, G.V. Lowry, J.P. Jolivet, M.R. Wiesner, Towards a definition of inorganic nanoparticles from an environmental, health and safety perspective, Nature Nanotechnol. 4 (2009) 634–641.
[106] X. Luo, A. Morrin, A.J. Killard, M.R. Smyth, Application of nanoparticles in electrochemical sensors and biosensors, Electroanalysis 18 (2006) 319–326.
[107] A.M. Ealias, A review on the classification, characterisation, synthesis of nanoparticles and their application, Mater. Sci. Eng. 263 (2017) 032019.
[108] E. Katz, I. Willner, J. Wang, Electroanalytical and bioelectroanalytical systems based on metal and semiconductor nanoparticles, Electroanalysis 16 (2004) 19–44.
[109] M.F. Cardosi, S.W. Birch, Screen printed glucose electrodes based on platinised carbon particles and glucose oxidase, Anal. Chim. Acta 276 (1993) 69–74.
[110] N.A. Choudhry, D.K. Kampouris, R.O. Kadara, N. Jenkinson, C.E. Banks, Next generation screen printed electrochemical platforms: Non-enzymatic sensing of carbohydrates using copper(II) oxide screen printed electrodes, Anal. Methods 1 (2009) 183–187.
[111] J.P. Metters, F. Tan, C.E. Banks, Screen-printed palladium electroanalytical sensors, J. Solid State Electrochem. 17 (2013) 1553–1562.
[112] C.C. Yang, A.S. Kumar, J.M. Zen, Electrocatalytic reduction and determination of dissolved oxygen at a preanodized screen-printed carbon electrode modified with palladium nanoparticles, Electroanalysis 18 (2006) 64–69.
[113] J. Wang, Q. Chen, Screen-printed glucose strip based on palladium-dispersed carbon ink, Analyst 119 (1994) 1849–1851.
[114] Y.C. Luo, J.S. Do, C.C. Liu, An amperometric uric acid biosensor based on modified Ir-C electrode, Biosens. Bioelectron. 22 (2006) 482–488.
[115] M.M. Pereira Silva Neves, M.B. González-García, P. Bobes-Limenes, A. Pérez-Junquera, D. Hernández Santos, F.J. Vidal-Iglesias, J. Solla-Gullón, P. Fanjul-Bolado, A non-enzymatic ethanol sensor based on a nanostructured catalytic disposable electrode, Anal. Methods 9 (2017) 5108–5114.
[116] C. Chou, J. Chang, J. Zen, Effective analysis of gaseous formaldehyde based on a platinum-deposited screen-printed edge band ultramicroelectrode coated with Nafion as solid polymer electrolyte, Sens. Actuators B: Chem. 147 (2010) 669–675.
[117] W.Y. Liao, C.C. Liu, T.C. Chou, Detection of triglyceride using an iridium nano-particle catalyst based amperometric biosensor, Analyst 133 (2008) 1757–1763.
[118] A. Chen, S. Chatterjee, Nanomaterials based electrochemical sensors for biomedical applications, Chem. Soc. Rev. 42 (2013) 5425–5438.
[119] I. Willner, B. Willner, R. Tel-Vered, Electroanalytical applications of metallic nanoparticles and supramolecular nanostructures, Electroanalysis 23 (2011) 13–28.
[120] L. García-Cruz, V. Montiel, J. Solla-Gullón, Shape-controlled metal nanoparticles for electrocatalytic applications, Phys. Sci. Rev. 4 (2018) 1–34.
[121] S. Cao, F.F. Tao, Y. Tang, Y. Li, J. Yu, Size- and shape-dependent catalytic performances of oxidation and reduction reactions on nanocatalysts, Chem. Soc. Rev. 45 (2016) 4747–4765.

[122] G.J. Leong, M.C. Schulze, M.B. Strand, D. Maloney, S.L. Frisco, H.N. Dinh, B. Pivovar, R.M. Richards, Shape-directed platinum nanoparticle synthesis: Nanoscale design of novel catalysts, Appl. Organomet. Chem. 28 (2014) 1–17.
[123] J. Agrisuelas, M.I. González-Sánchez, E. Valero, Hydrogen peroxide sensor based on in situ grown Pt nanoparticles from waste screen-printed electrodes, Sens. Actuators B: Chem. 249 (2017) 499–505.
[124] B. Gómez-Monedero, M.I. González-Sánchez, J. Iniesta, J. Agrisuelas, E. Valero, Design and characterization of effective Ag, Pt and AgPt nanoparticles for H_2O_2 electrosensing from scrapped printed electrodes, Sensors 19 (2019) 1685.
[125] T. Chou, K. Wu, F. Hsu, C. Lee, Pt-MWCNT modified carbon electrode strip for rapid and quantitative detection of H_2O_2 in food, J. Food Drug Anal. 26 (2017) 662–669.
[126] O. Dominguez-Renedo, M.J. Arcos Martinez, Electrochem. Commun. 9 (2007) 820.
[127] M.E. Burgoa Calvo, O. Domínguez Renedo, M.J. Arcos Martínez, Determination of lamotrigine by adsorptive stripping voltammetry using silver nanoparticle-modified carbon screen-printed electrodes, Talanta 74 (2007) 59–64.
[128] A. Jirasirichote, E. Punrat, A. Suea-Ngam, O. Chailapakul, S. Chuanuwatanakul, Voltammetric detection of carbofuran determination using screen-printed carbon electrodes modified with gold nanoparticles and graphene oxide, Talanta 175 (2017) 331–337.
[129] Z. Shi, Y. Lu, Z. Chen, C. Cheng, J. Xu, Q. Zhang, Z. Yan, Z. Luo, Q. Liu, Electrochemical non-enzymatic sensing of glycoside toxins by boronic acid functionalized nano-composites on screen-printed electrode, Sens. Actuators B: Chem. 329 (2021) 129197.
[130] A. Gevaerd, C.E. Banks, M.F. Bergamini, L.H. Marcolino-Junior, Nanomodified screen-printed electrode for direct determination of aflatoxin B1 in malted barley samples, Sens. Actuators B: Chem. 307 (2020) 1–7.
[131] M. Asadollahi-Baboli, A. Mani-Varnosfaderani, Rapid and simultaneous determination of tetracycline and cefixime antibiotics by means of gold nanoparticles-screen printed gold electrode and chemometrics tools, Measurement 47 (2014) 145–149.
[132] Y.S. Song, G. Muthuraman, Y.Z. Chen, C.C. Lin, J.M. Zen, Screen printed carbon electrode modified with poly(L-lactide) stabilized gold nanoparticles for sensitive As(III) detection, Electroanalysis 18 (2006) 1763.
[133] M.A. Benchettara, Modification d'une électrode de graphite par des oxydes de métaux de transition-Application à la detection électrochimique de substances oxydables, PhD thesis in chemistry, University of USTHB, ALGIERS, 2016.
[134] M. García, A. Escarpa, A class-selective and reliable electrochemical monosaccharide index in honeys, as determined using nickel and nickel-copper nanowires, Anal. Bioanal. Chem. 402 (2012) 945–953.
[135] B. Pérez-Fernández, D. Martín-Yerga, A. Costa-García, Electrodeposition of nickel nanoflowers on screen-printed electrodes and their application to non-enzymatic determination of sugars, RSC Adv. 6 (2016) 83748–83757.
[136] X. Niu, M. Lan, H. Zhao, C. Chen, Highly sensitive and selective nonenzymatic detection of glucose using three-dimensional porous nickel nanostructures, Anal. Chem. 85 (2013) 3561–3569.
[137] J. Yang, J.H. Yu, J. Rudi Strickler, W.J. Chang, S. Gunasekaran, Nickel nanoparticle-chitosan-reduced graphene oxide-modified screen-printed electrodes for enzyme-free glucose sensing in portable microfluidic devices, Biosens. Bioelectron. 47 (2013) 530–538.
[138] Z. Yao, X. Yang, F. Wu, W. Wu, F. Wu, Synthesis of differently sized silver nanoparticles on a screen-printed electrode sensitized with a nanocomposite consisting of reduced graphene oxide and cerium(IV) oxide for nonenzymatic sensing of hydrogen peroxide, Microchim. Acta 183 (2016) 2799–2806.
[139] B. Molinero-Abad, M.A. Alonso-Lomillo, O. Domínguez-Renedo, M.J. Arcos-Martínez, Amperometric determination of sulfite using screen-printed electrodes modified with metallic nanoparticles, Microchim. Acta 180 (2013) 1351–1355.
[140] S. Sadeghi, M. Hemmati, A. Garmroodi, Preparation of Ag-Nanoparticles/Ionic-Liquid Modified Screen-Printed Electrode and Its Application in the Determination of Metronidazole, Electroanalysis 25 (2013) 316–322.

[141] J. Bujes-Garrido, D. Izquierdo-Bote, A. Heras, A. Colina, M.J. Arcos-Martínez, Determination of halides using Ag nanoparticles-modified disposable electrodes. A first approach to a wearable sensor for quantification of chloride ions, Anal. Chim. Acta 1012 (2018) 42–48.
[142] F.M. Salama, K.A. Attia, R.A. Said, A. El-Olemy, A.M. Abdel-Raoof, Disposable gold nanoparticle functionalized and bare screen-printed electrodes for potentiometric determination of trazodone hydrochloride in pure form and pharmaceutical preparations, RSC Adv. 8 (2018) 11517–11527.
[143] C. Shan, H. Yang, D. Han, Q. Zhang, A. Ivaska, L. Niu, Graphene/AuNPs/chitosan nanocomposites film for glucose biosensing, Biosens. Bioelectron. 25 (2010) 1070–1074.
[144] M.A. Alonso-Lomillo, O. Domínguez-Renedo, A. Saldaña-Botín, M.J. Arcos-Martínez, Determination of ascorbic acid in serum samples by screen-printed carbon electrodes modified with gold nanoparticles, Talanta 174 (2017) 733–737.
[145] N.X. Viet, M. Chikae, Y. Ukita, Y. Takamura, Enzyme-free glucose sensor based on micro-nano dualporous gold-modified screen-printed carbon electrode, Int. J. Electrochem. Sci. 13 (2018) 8633–8644.
[146] K.R. Reddy, P.K. Brahman, L. Suresh, Fabrication of high performance disposable screen printed electrochemical sensor for ciprofloxacin sensing in biological samples, Measurement 127 (2018) 175–186.
[147] Y.H. Chen, R. Kirankumar, C.L. Kao, P.Y. Chen, Electrodeposited Ag, Au, and AuAg nanoparticles on graphene oxide-modified screen-printed carbon electrodes for the voltammetric determination of free sulfide in alkaline solutions, Electrochim. Acta 205 (2016) 124–131.
[148] A. Diouf, M. Moufid, D. Bouyahya, L. Österlund, N. El Bari, B. Bouchikhi, An electrochemical sensor based on chitosan capped with gold nanoparticles combined with a voltammetric electronic tongue for quantitative aspirin detection in human physiological fluids and tablets, Mater. Sci. Eng. C 110 (2020) 110665.
[149] E. Núñez-Bajo, M.C. Blanco-López, A. Costa-García, M.T. Fernández-Abedul, In situ gold-nanoparticle electrogeneration on gold films deposited on paper for non-enzymatic electrochemical determination of glucose, Talanta 178 (2018) 160–165.
[150] J. Raveendran, R.G. Krishnan, B.G. Nair, T.G. Satheesh Babu, Voltammetric determination of ascorbic acid by using a disposable screen printed electrode modified with $Cu(OH)_2$ nanorods, Microchim. Acta 184 (2017) 3573–3579.
[151] B. Pérez-Fernández, D. Martín-Yerga, A. Costa-García, Galvanostatic electrodeposition of copper nanoparticles on screen-printed carbon electrodes and their application for reducing sugars determination, Talanta 175 (2017) 108–113.
[152] S. Kurbanoglu, C.C. Mayorga-Martinez, M. Medina-Sánchez, L. Rivas, S. A. Ozkan, A. Merkoçi, Antithyroid drug detection using an enzyme cascade blocking in a nanoparticle-based lab-on-a-chip system, Biosens. Bioelectron. 67 (2015) 670–676.
[153] A.A. Khorshed, M. Khairy, S.A. Elsafty, C.E. Banks, Disposable screen-printed electrodes modified with uniform iron oxide nanocubes for the simple electrochemical determination of meclizine, an antihistamine drug, Anal. Methods 11 (2019) 282.
[154] S. Palanisamy, B. Thirumalraj, S.M. Chen, M.A. Ali, F.M.A. Al-Hemaid, Palladium nanoparticles decorated on activated fullerene modified screen printed carbon electrode for enhanced electrochemical sensing of dopamine, J. Colloid Interface Sci. 448 (2015) 251–256.
[155] C. Karuppiah, M. Velmurugan, S.M. Chen, R. Devasenathipathy, R. Karthik, S.F. Wang, Electrochemical activation of graphite nanosheets decorated with palladium nanoparticles for high performance amperometric hydrazine sensor, Electroanalysis 28 (2016) 808–816.
[156] X. Yang, Y. Ouyang, F. Wu, Y. Hu, H. Zhang, Z. Wu, In situ & controlled preparation of platinum nanoparticles doping into graphene sheets@cerium oxide nanocomposites sensitized screen printed electrode for nonenzymatic electrochemical sensing of hydrogen peroxide, J. Electroanal. Chem. 777 (2016) 85–91.
[157] A. Popa, E.C. Abenojar, A. Vianna, C.Y.A. Buenviaje, J. Yang, C.B. Pascual, A.C.S. Samia, Fabrication of metal nanoparticle-modified screen printed carbon electrodes for the evaluation of hydrogen peroxide content in teeth whitening strips, J. Chem. Educ. 92 (2015) 1913–1917.

[158] S. Sanllorente-Méndez, O. Domínguez-Renedo, M.J. Arcos-Martínez, Determination of Arsenic(III) using platinum nanoparticle-modified screen-printed carbon-based electrodes, Electroanalysis 21 (2009) 635–639.
[159] K. Shim, J. Kim, M. Shahabuddin, Y. Yamauchi, M.S.A. Hossain, J.H. Kim, Efficient wide range electrochemical bisphenol-A sensor by self-supported dendritic platinum nanoparticles on screen-printed carbon electrode, Sens. Actuators B: Chem. 255 (2018) 2800–2808.
[160] L. Fu, K. Wu, J. Ji, J. Zhang, X. Guo, A highly sensitive disposable glucose biosensor based on platinum nanoflowers decorated screen printed carbon electrode, Proceedings of the IEEE Sensors, GLASGOW, SCOTLAND, UK, 2017.
[161] M.I. González-Sánchez, B. Gómez-Monedero, J. Agrisuelas, E. Valero, Recycling metals from spent screen-printed electrodes while learning the fundamentals of electrochemical sensing, J. Chem. Educ. 95 (2018) 847–851.
[162] V.A. Gatselou, D.L. Giokas, A.G. Vlessidis, M.I. Prodromidis, Rhodium nanoparticle-modified screen-printed graphite electrodes for the determination of hydrogen peroxide in tea extracts in the presence of oxygen, Talanta 134 (2015) 482–487.
[163] H. Cunha-Silva, M.J. Arcos-Martinez, A disposable rhodium nanoparticle-modified screen-printed sensor for direct determination of bromide anions, Sens. Actuators B Chem. 282 (2019) 603–608.
[164] D. Martín-Yerga, J. Carrasco-Rodríguez, J.L.G. Fierro, F.J. García Alonso, A. Costa-García, Copper-modified titanium phosphate nanoparticles as electrocatalyst for glucose detection, Electrochim. Acta 229 (2017) 102–111.
[165] C.H. Lien, J.C. Chen, C.C. Hu, D.S.H. Wong, Cathodic deposition of binary nickel-cobalt hydroxide for non-enzymatic glucose sensing, J. Taiwan Inst. Chem. Eng. 45 (2014) 846–851.
[166] C.C. Yang, A.S. Kumar, M.C. Kuo, S.H. Chien, J.M. Zen, Copper-palladium alloy nanoparticle plated electrodes for the electrocatalytic determination of hydrazine, Anal. Chim. Acta 554 (2005) 66–73.
[167] X. Niu, C. Chen, H. Zhao, Y. Chai, M. Lan, Novel snowflake-like Pt–Pd bimetallic clusters on screen-printed gold nanofilm electrode for H_2O_2 and glucose sensing, Biosens. Bioelectron. 36 (2012) 262–266
[168] A. Şavk, H. Aydın, K. Cellat, F. Şen, A novel high performance non-enzymatic electrochemical glucose biosensor based on activated carbon-supported Pt–Ni nanocomposite, J. Mol. Liq. 300 (2020) 112355.
[169] N.F.B. Azeredo, P.O. Rossini, J.M. Gonçalves, G.L. Assis, K. Araki, L. Angnes, Nanostructured mixed Ni/Pt hydroxides electrodes for BIA-amperometry determination of hydralazine, J. Taiwan Inst. Chem. Eng. 95 (2019) 475–480.
[170] L. Zhang, H. Li, J. Gu, X. Zhao, X. Wang, Facile one-step synthesis of Pt/Ni(OH) nanoflakes as sensitive electrode for detection of ammonia–nitrogen in drinking water, Mater. Lett. 328 (2022) 133090.
[171] M.L. Chelaghmia, M. Nacef, A.M. Affoune, Ethanol electrooxidation on activated graphite supported platinum–nickel in alkaline medium, J. Appl. Electrochem. 42 (2012) 819–826.
[172] M.L. Chelaghmia, M. Nacef, H. Fisli, A.M. Affoune, M. Pontié, A. Makhlouf, T. Derabla, O. Khelifi, F. Aissat, Electrocatalytic performance of Pt–Ni nanoparticles supported on an activated graphite electrode for ethanol and 2–propanol oxidation, RSC Adv. 10 (2020) 36941–36948.
[173] R. Zhu, Z. Zhao, J. Cao, H. Li, L. Ma, K. Zhou, Z. Yu, Q. Wei, Effect of Pt–Ni deposition sequence on the bimetal-modified boron-doped diamond on catalytic performance for glucose oxidation in neutral media, J. Electroanal. Chem. 907 (2022) 116084.
[174] M.T. Zhybak, L.Y. Fayura, Y.R. Boretsky, M.V. Gonchar, A.A. Sibirny, E. Dempsey, A.P.F. Turner, Y.I. Korpan, Amperometric L-arginine biosensor based on a novel recombinant arginine deiminase, Microchim. Acta 184 (2017) 2679–2686.
[175] J. Lee, K. Murugappan, D.W.M. Arrigan, D.S. Silvester, Oxygen reduction voltammetry on platinum macrodisk and screen-printed electrodes in ionic liquids: Reaction of the electrogenerated superoxide species with compounds used in the paste of Pt screen-printed electrodes?, Electrochim. Acta 101 (2013) 158–168.

[176] B. Rafiee, A.R. Fakhari, Electrocatalytic oxidation and determination of insulin at nickel oxide nanoparticles-multiwalled carbon nanotube modified screen printed electrode, Biosens. Bioelectron. 46 (2013) 130–135.
[177] Y.C. Luo, J.S. Do, C.C. Liu, An amperometric uric acid biosensor based on modified Ir-C electrode, Biosens. Bioelectron. 22 (2006) 482–488.
[178] W.Y. Jeon, Y.B. Choi, H.H. Kim, Disposable non-enzymatic glucose sensors using screen-printed nickel/carbon composites on indium tin oxide electrodes, Sensors 15 (2015) 31083–31091.
[179] L. Shi, M. Layani, X. Cai, H. Zhao, S. Magdassi, M. Lan, An inkjet printed Ag electrode fabricated on plastic substrate with a chemical sintering approach for the electrochemical sensing of hydrogen peroxide, Sens. Actuators B Chem. 256 (2018) 938–945.
[180] C.C. Mayorga-Martinez, M. Cadevall, M. Guix, J. Ros, A. Merkoçi, Bismuth nanoparticles for phenolic compounds biosensing application, Biosens. Bioelectron. 40 (2013) 57–62.
[181] H. Shamkhalichenar, J.W. Choi, An inkjet-printed non-enzymatic hydrogen peroxide sensor on paper, J. Electrochem. Soc. 164 (2017) B3101–B3106.
[182] A.V. Shabalina, V.A. Svetlichnyi, K.A. Ryzhinskaya, I.N. Lapin, Copper nanoparticles for ascorbic acid sensing in water on carbon screen-printed electrodes, Anal. Sci. 33 (2017) 1415–1419.
[183] M. Hjiri, R. Dhahri, N. Ben Mansour, L. El Mir, M. Bonyani, A. Mirzaei, S.G. Leonardi, G. Neri, Electrochemical properties of a novel Ni-doped nanoporous carbon, Mater. Lett. 160 (2015) 452–455.
[184] M. Chikae, K. Idegami, K. Kerman, N. Nagatani, M. Ishikawa, Y. Takamura, E. Tamiya, Direct fabrication of catalytic metal nanoparticles onto the surface of a screen-printed carbon electrode, Electrochem. Commun. 8 (2006) 1375–1380.
[185] T.K. Huang, K.W. Lin, S.P. Tung, T.M. Cheng, I.C. Chang, Y.Z. Hsieh, C.Y. Lee, H.T. Chiu, Glucose sensing by electrochemically grown copper nanobelt electrode, J. Electroanal. Chem. 636 (2009) 123–127.
[186] B. Pérez-Fernández, D. Martín-Yerga, A. Costa-García, Galvanostatic electrodeposition of copper nanoparticles on screen-printed carbon electrodes and their application for reducing sugars determination, Talanta 175 (2017) 108–113.
[187] M.Y. Lee, J. Peng, C.C. Wu, Geometric effect of copper nanoparticles electrodeposited on screen-printed carbon electrodes on the detection of α-, β- and γ-amino acids, Sens. Actuators B Chem. 186 (2013) 270–277.
[188] J.M. Zen, C.T. Hsu, A.S. Kumar, H.J. Lyuu, K.Y. Lin, Amino acid analysis using disposable copper nanoparticle plated electrodes, Analyst 129 (2004) 841–845.
[189] Niu, X.; Zhao, H.; Chen, C.; Lan, M. Platinum nanoparticle-decorated carbon nanotube clusters on screen-printed gold nanofilm electrode for enhanced electrocatalytic reduction of hydrogen peroxide, Electrochim. Acta 65 (2012) 97–103.
[190] G. Martínez-Paredes, M.B. González-García, A. Costa-García, In situ electrochemical generation of gold nanostructured screen-printed carbon electrodes: Application to the detection of lead underpotential deposition, Electrochim. Acta 54 (2009) 4801–4808.
[191] V. Sima, C. Cristea, E. Bodoki, G. Dutu, R. Sandulescu, Screen-printed electrodes modified with HRP–zirconium alcoxide film for the development of a biosensor for acetaminophen detection, Cent. Eur. J. Chem. 8 (2010) 1034–1040.
[192] B.G. Mahmoud, M. Khairy, F.A. Rashwan, C.E. Banks, Simultaneous voltammetric determination of acetaminophen and isoniazid (hepatotoxicity-related drugs) utilizing bismuth oxide nanorod modified screen-printed electrochemical sensing platforms, Anal. Chem. 89 (2017) 2170–2178.
[193] A.T.M. Gilmartin, J.P. Hart, Rapid detection of paracetamol using a disposable, surface-modified screen-printed carbon electrode, Analyst 119 (1994) 2431–2437.
[194] S. Abdi, M.L. Chelaghmia, R. Kihal, C.E. Banks, A.G.M. Ferrari, H. Fisli, M. Nacef, A.M. Affoune, M.E.H. Benhamza, Simultaneous determination of 4-aminophenol and paracetamol based on CS–Ni nanocomposite-modified screen-printed disposable electrodes, Monatsh, Chemie 154 (2023) 563–575.
[195] W. Kit-Anan, A. Olarnwanich, C. Sriprachuabwong, C. Karuwan, A. Tuantranont, A. Wisitsoraat, et al., Disposable paper-based electrochemical sensor utilizing inkjet-printed polyaniline modified screen-printed carbon electrode for ascorbic acid detection, J. Electroanal. Chem. 685 (2012) 72–78.

[196] A.G. Crevillén, M. Pumera, M.C. González, A. Escarpa, Carbon nanotube disposable detectors in microchip capillary electrophoresis for water-soluble vitamin determination: analytical possibilities in pharmaceutical quality control, Electrophoresis 29 (2008) 2997–3004.
[197] N. Ruecha, N. Rodthongkum, D.M. Cate, J. Volckens, O. Chailapakul, C.S. Henry, Sensitive electrochemical sensor using a graphene-polyaniline nanocomposite for simultaneous detection of Zn(II), Cd(II), and Pb(II), Anal. Chim. Acta 874 (2015) 40–48.
[198] U. Ngoensawat, T. Pisuchpen, Y. Sritana-anant, N. Rodthongkum, V.P. Hoven, Conductive electrospun composite fibers based on solid-state polymerized Poly (3,4-ethylenedioxythiophene) for simultaneous electrochemical detection of metal ions, Talanta 241 (2022) 123253.

Chapter III

Experimental procedures, equipment and characterization techniques

III.1. Introduction

This chapter presents the methods used for the development and characterization of new electrochemical sensors based on screen-printed electrodes, employing working electrodes made of either graphite (Pt–Ni/SPE) or graphene (Pt–Ni/SPGE) decorated with platinum and nickel bimetallic nanoparticles. These sensors are designed for the individual and simultaneous detection of PA, 4-AP, AA and Zn(II).

The first part outlines the operational protocol and experimental setup, including the preparation and functionalization of the electrode surfaces. The second part explores various structural and microstructural characterization techniques such as field-emission scanning electron microscopy (FE-SEM), transmission electron microscopy (TEM), energy-dispersive X-ray spectroscopy (EDX), X-ray diffraction (XRD), and atomic force microscopy (AFM), providing detailed information on the structure and composition of the Pt–Ni nanoparticles and the electrode surfaces.

Finally, electrochemical impedance spectroscopy, cyclic voltammetry, square wave voltammetry, and differential pulse voltammetry are employed to assess the performance of the sensors. These techniques allow for the characterization of electrochemical responses, reaction kinetics, and analysis of the sensors' sensitivity and selectivity for the target analytes. All experiments were conducted at the Laboratory of Industrial Analysis and Materials Engineering (LAIGM) at the University of 8 Mai 1945, Guelma, while the structural and microstructural characterization of the developed electrodes was performed at the University of Angers, France.

III.2. Reagents and preparation of solutions

III.2.1. Reagents

Chemicals were used as received, no purification of any kind was deemed useful in this study and doubly distilled water with a resistivity of 18 MΩ cm was used to prepare all aqueous solutions. The products used in the various experiments are listed in table III.1 below:

Table III.1. Properties of the chemicals used.

Product name	Molecular formula	Molar mass (g/mol)	Purity (%)	Producer
Sodium hydroxide	NaOH	40	98 %	Fluka
Hydrochloric acid	HCl	36.46	37 %	Sigma-Aldrich
Sulfuric acid	H_2SO_4	98.07	95-97 %	Sigma-Aldrich
Acetic acid	CH_3COOH	60.05	99 %	Sigma-Aldrich
Sodium acetate	CH_3COONa	82.03	≥ 99.5 %	Sigma-Aldrich
Di-Sodium hydrogen phosphate dihydrate	$Na_2HPO_4 \cdot 2H_2O$	177.99	99.5 %	Sigma-Aldrich
Sodium Di- hydrogen phosphate dihydrate	NaH_2PO_4 $2H_2O$	156.01	99.5 %	Sigma-Aldrich
Nickel sulfate hexahydrate	$NiSO_4$ $6H_2O$	262.84	99 %	Sigma-Aldrich
Sodium sulfate	Na_2SO_4	142.04	99 %	Sigma-Aldrich
Chloroplatinic acid	H_2PtCl_6 $6H_2O$	517.9	≥ 99.9 %	Sigma-Aldrich
Potassium chloride	KCl	74.551	99 %	Fluka
Potassium ferricyanide	$K_3[Fe(CN)_6]$	329.24	99 %	Fluka
Potassium ferrocyanide	$K_4[Fe(CN)_6]$	368.34	99 %	Fluka
Paracetamol	$C_8H_9NO_2$	151.163	99 %	Fluka
4-aminophenol	C_6H_7NO	109.13	99 %	Fluka
Ascorbic acid	$C_6H_8O_6$	176.12	99 %	Fluka
Caffeine	$C_8H_{10}N_4O_2$	194.19	99 %	Fluka
Glucose	$C_6H_{12}O_6$	180.156	99.5 %	Fluka
Fructose	$C_6H_{12}O_6$	180.16	≥ 99 %	Sigma-Aldrich
Galactose	$C_6H_{12}O_6$	180.16	≥ 98 %	Sigma-Aldrich
Citric acid	$C_6H_8O_7$	192.124	99 %	Fluka
Zinc	Zn(II)	65.38	99 %	PerkinElmer-Pure

III.2.2. Preparation of solutions

In the context of this research, various solutions were prepared and employed for specific purposes, with variations in composition, concentration, and functionality. It is important to note that these solutions were formulated using either distilled water at room temperature, phosphate buffer solution (PBS), or acetate buffer solution (ABS), depending on the solubility of the compounds in the solution.

III.2.2.1. Preparation of buffer solutions

The buffers used in this work were prepared by dissolving specific amounts of the appropriate compounds in distilled water while stirring, followed by adjusting the solution pH to the desired level using HCl or NaOH. The phosphate buffer solution (PBS, 0.1 M) at a pH of 7.4 was obtained by mixing 0.1 M NaH_2PO_4 and Na_2HPO_4, while the acetate buffer solution (ABS, 0.1 M) at a pH of 4.7 was prepared from a mixture of 0.1 M CH_3COONa and CH_3COOH.

III.2.2.2. Preparation of analytical solutions of 4-AP, PA, AA and Zn(II)

A stock solution of 10 mM was prepared using hot distilled water for 4-aminophenol, phosphate buffer solution at room temperature for paracetamol and ascorbic acid, and acetate buffer solution at room temperature for zinc. The stock solution was then diluted according to the application requirements. These solutions were stored in the refrigerator at 5°C until use.

III.2.2.3. Electrodeposition bath

The electrolyte bath is a complex composition containing metallic substances and electrolytes, designed to achieve the desired properties. The selection of the bath depends on its adherence to the following criteria: low cost and excellent performance.

The supporting electrolytes are highly dissociated ionic compounds that do not react with the electrode surface. Their role is to enhance the stability of the ions in solution, which leads to improved distribution capabilities of the deposit. Platinum and nickel (Pt–Ni) were simultaneously electrodeposited from a 1.0 M H_2SO_4 solution containing a mixture of 8.0 mM H_2PtCl_6 and 128 mM $NiSO_4$.

III.2.2.4. Preparation of real samples

Three tablets of each chosen pharmaceutical product (Doliprane or Efferalgan Vitamin C or Vitamin C with Zinc complementary dietary supplement) were carefully grinded in an agate mortar and precisely weighed. Their solutions were then made by ultrasonically dissolution in distilled water**.** Following centrifugation at 3500 rpm for 20 min, each resulting filtrate was gathered in a 50 ml graduated flask and further diluted with a 0.1 mol. L^{-1} buffer solution (either PBS or ABS, depending on the analyte). In the subsequent step, precise volumes of the resultant solutions were transferred to the electrolytic cell for SWV measurements.

Notably, for the paracetamol sample, fortification with 4-AP was conducted prior to assay. The human blood serum samples of two healthy people were kindly provided by a local hospital. These samples were pretreated in compliance with our previous work **[1]**.

III.3. Electrochemical Setup

In the context of this study, two experimental setups are employed to investigate the performance of the developed electrochemical sensors. The first setup (Figure III.1) is used for conducting kinetic studies and assessing the ideal electrochemical behavior of the system through cyclic voltammetry and electrochemical impedance spectroscopy. This setup consists

of an electrochemical cell connected to a Versa STAT 3 potentiostat from Princeton Applied Research, AMETEK, USA. The potentiostat is operated using software called "Versa Studio."

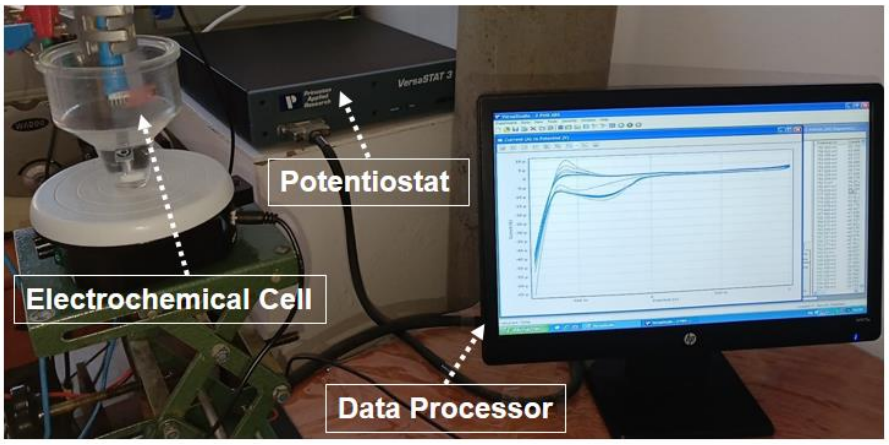

Figure III.1. Experimental setup 1.

The second setup is used to characterize the sensitivity of the sensors through differential pulse voltammetry and square wave voltammetry (Figure III.2). It is also utilized for electrochemical deposition tests via linear sweep voltammetry. This is performed in the same electrochemical cell using a 273A potentiostat-galvanostat from Princeton Applied Research. The potentiostat is operated with software called "Power Suite."

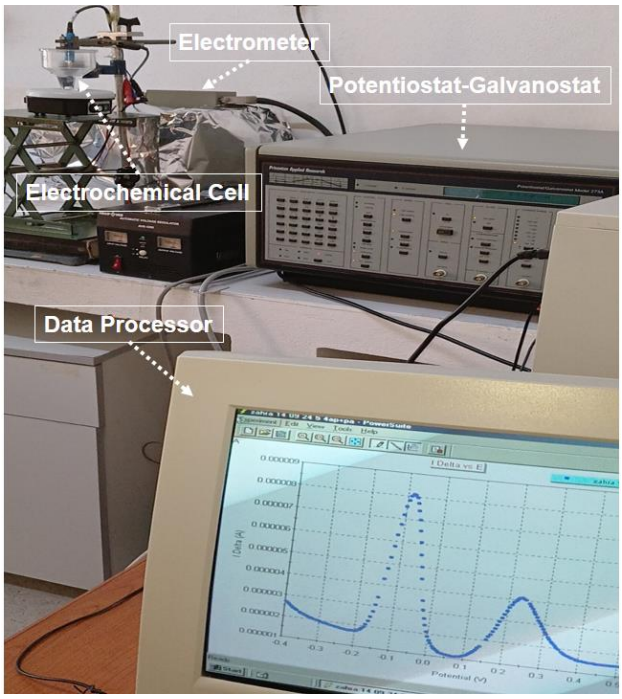

Figure III.2. Experimental setup 2.

The electrochemical cell used is illustrated in figure III.3. It is a 75 mL PYREX glass cell, providing sufficient volume to maintain a constant concentration of electroactive species during experimentation. This cell accommodates a screen-printed electrode that incorporates all three electrodes: the reference electrode (RE), the counter electrode (CE), and the working electrode (WE).

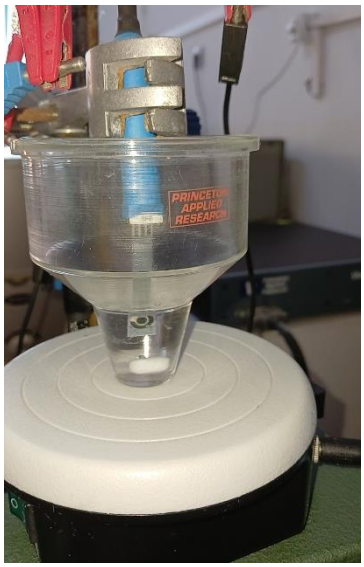

Figure III.3. The electrochemical cell used.

- ✓ **Reference Electrode**: This electrode maintains a constant potential in the medium in which it is placed. Thus, the potential measured between the working electrode (WE) and the reference electrode (RE) exclusively reflects the response of the WE. All potential measurements are referenced to a silver/silver chloride (Ag/AgCl) electrode.
- ✓ **Counter Electrode**: The counter electrode, or auxiliary electrode, has a surface area significantly larger than that of the working electrode to prevent the reaction occurring at the counter electrode from becoming the rate-limiting step in electrochemical processes. It facilitates current flow. A graphite auxiliary electrode was used.
- ✓ **Working Electrode**: The working electrode, also referred to as the indicator electrode, is where the oxidation or reduction reaction of the analyte occurs in response to changes in potential. The working electrode used has a diameter of 3.1 mm and can be made of graphite, graphite decorated with Pt-Ni nanoparticles, graphene, or graphene decorated with Pt-Ni nanoparticles. Visually, there is no discernible difference between the screen-printed electrode (SPE) based on graphite and that based on graphene, as they share the same shape (Figure III.4). All screen-printed electrodes, regardless of their type, were purchased from Kanichi Research Limited (Manchester, UK).

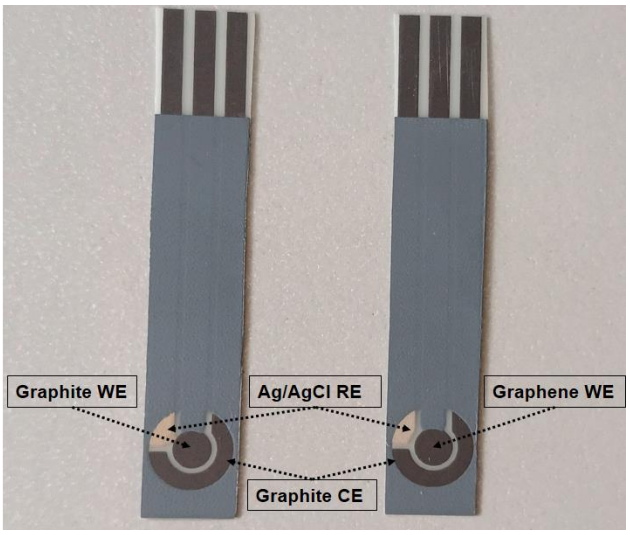

Figure III.4. Comparison of SPE with graphite working electrode vs. SPE with graphene working electrode.

III.4. Elaboration of modified screen-printed electrodes

The screen-printed electrodes (SPEs) were produced using stencil designs and a micro DEK 1760RS screen-printing machine (DEK, Weymouth, UK). The process began with the application of a carbon-graphite ink formulation, which has been extensively utilized in previous studies **[2–5]**. This ink was screen-printed onto a flexible polyester film (Autostat, 250 µm thickness). The curing process involved placing the printed film in a fan oven at 60°C for 30 minutes.

Next, an Ag/AgCl reference electrode was created by screen-printing Ag/AgCl paste (Gwent Electronic Materials Ltd., UK) onto the plastic substrate. The 3.1 mm diameter graphite working electrode was then defined by printing a dielectric paste ink (Gwent Electronic Materials Ltd., UK). Following a final curing process at 60°C for 30 minutes, the screen-printed graphite electrodes were ready for use. A similar procedure was followed to fabricate screen-printed graphene electrodes, with the only modification being the replacement of the carbon-graphite ink formulation with a carbon-graphene ink formulation.

The working electrodes, either graphite or graphene-based, were further modified with Pt–Ni nanostructures through an electrodeposition technique utilizing linear sweep voltammetry. This process involved cycling in the cathodic direction from 0 V to –0.95 V for a total of five repetitions in an aqueous solution. The innovative application of this electrodeposition technique not only minimized concentration polarization but also significantly enhanced grain refinement. The platinum and nickel (Pt–Ni) were simultaneously

electrodeposited from a 1.0 M H_2SO_4 solution containing a mixture of 8.0 mM H_2PtCl_6 and 128 mM $NiSO_4$.

After the deposition, the modified electrode was thoroughly washed with distilled water and allowed to air-dry at room temperature. Prior to use, the Pt–Ni/SPE electrodes underwent at least fifty cyclic voltammetry (CV) cycles in a 0.1 M phosphate-buffered saline (PBS) solution (pH 7.4) at a scan rate of 50 mV s^{-1} until a stable peak response was achieved. For comparative purposes, SPEs modified with platinum nanoparticles (PtNPs) were also prepared following the same procedure, using only 8.0 mM H_2PtCl_6 as a precursor.

The modification process for the SPEs, as illustrated in figure III.5, is straightforward and essentially a one-step procedure. Although the electrodeposition must be performed individually for each sensor, this step remains efficient and not time-consuming, particularly in the context of large-scale batch production.

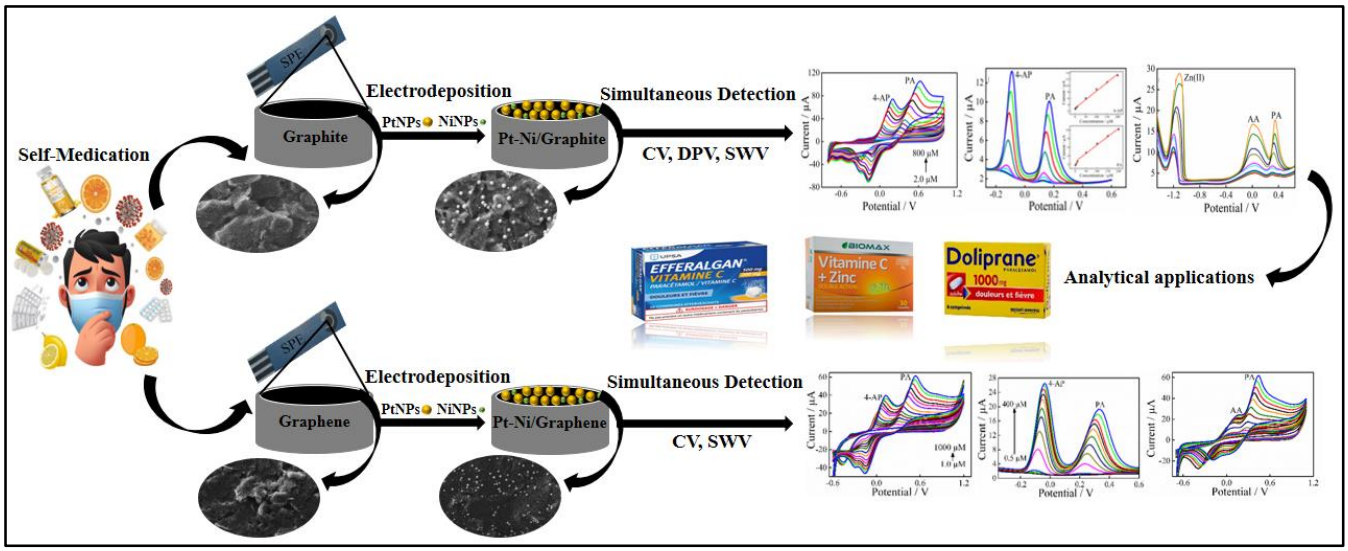

Figure III.5. Schematic representation of the modification and application of screen-printed electrodes.

III.5. Techniques for characterizing modified electrode surfaces

III.5.1. Structural and microstructural characterization techniques

In this thesis, a range of characterization techniques were employed to physically describe and investigate the modified electrodes. The development of these electrodes took place at the Laboratory of Industrial Analysis and Materials Engineering, while their structural and microstructural characterization was conducted at the University of Angers. This section provides a brief introduction to each technique and the equipment utilized, offering insights into the methodologies that underpin our investigations. These techniques are crucial for

understanding the properties and performance of the developed electrodes, setting the stage for further exploration of their applications in the following chapter.

III.5.1.1. Scanning electron microscopy and X-ray microanalysis

Scanning electron microscopy (SEM) enables morphological, structural and chemical analysis of solid materials at the micrometric scale for standard SEM and nanometric scale for high-resolution SEM. This microscopy is based primarily on the detection of secondary electrons stripped from the sample material under the impact of a very fine beam of monokinetic primary electrons that scans the surface; the energy of the secondary electrons is much lower than that of the incident electrons. Other interactions take place (Figure III.6 and figure III.7): backscattered electrons (BSE) - of comparable energy to incident electrons; Auger electrons - of very low energy and can only be studied under ultra-high vacuum conditions; visible photons - specific cathodoluminescence of certain materials or impurities; X-ray photons giving access to analysis of the sample's atomic composition **[6]**.

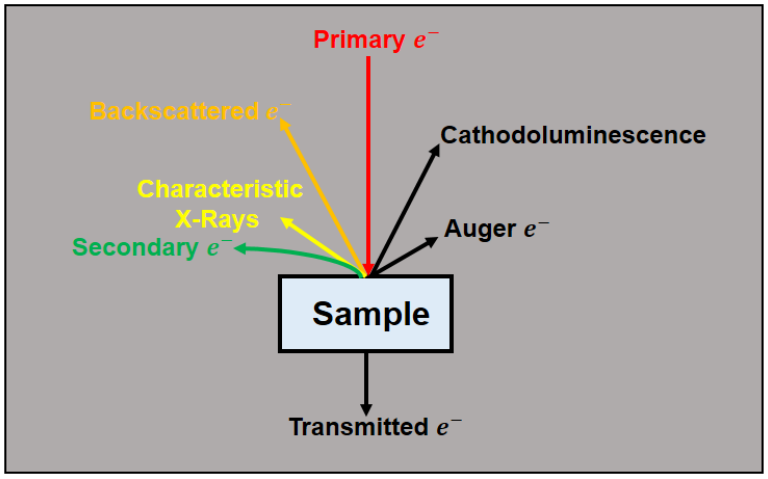

Figure III.6. Signals produced by the interaction of a primary electron with the sample in a scanning electron microscope.

The detection of secondary electrons provides information on the topography of the sample to a depth of 10 nm. Analysis of these electrons provides a characteristic image of the surface.

In the SEM, when the sample is bombarded by the fine brush of electrons, an X-ray emission characteristic of existing atoms appears, coming from the almost punctual zone located under the surface subjected to electron bombardment. For this reason, the modern SEM is often equipped with an analytical system for X-ray microanalysis of the spectrum emitted by

the observed sample, using two spectrometric techniques: wavelength-dispersive (WDS) and energy-dispersive (EDS or EDX).

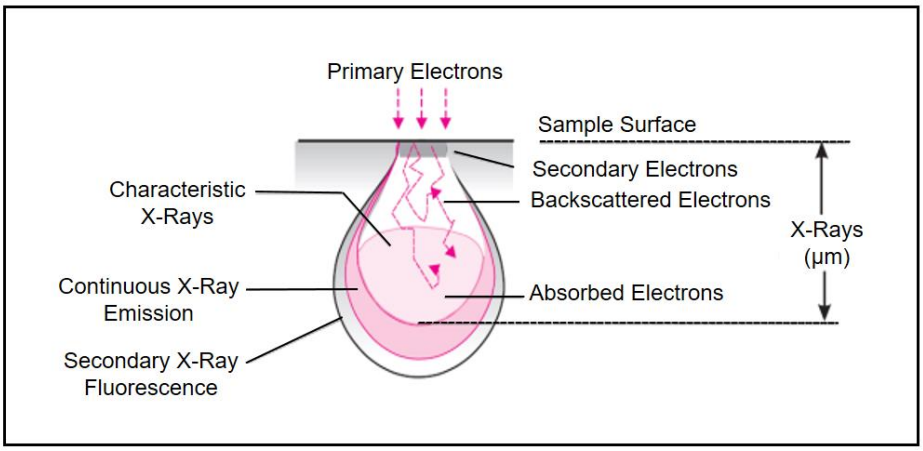

Figure III.7. Diffusion bulb of various interactions in a sample (SEM).

In an EDX system, the spectrometer analyzes the entire X-ray spectrum, and the distinction between the various X-rays received (energy sorting) is subsequently made by energy selection in the electronic chain. The energy (or wavelength) position of the characteristic lines in the X-ray spectrum enables qualitative analysis of the sample, i.e. identification of the elements present in the volume bombarded by the incident electrons. Quantitative analysis involves measuring the intensities of the characteristic lines for each element in the sample and for the same elements in standards of known composition. This is demonstrated using various examples of nanostructures. Advanced data processing of the results paves the way for automated classification of NPs by feature analysis. This method combines morphological structure detection by image processing of TEM/SEM micrographs with chemical classification by EDX **[7, 8]**.

The morphological characteristics and elemental composition of the SPE-modified electrodes from this thesis work were obtained via a field emission scanning electron microscope (FE-SEM), ZEISS EVO LS10 (Figure III.8), coupled to energy dispersive X-ray spectroscopy (EDX), (Inca, OXFORD Instruments).

Figure III.8. Field emission scanning electron microscope coupled with energy dispersive X–ray spectroscopy ZEISS EVO LS10.

III.5.1.2. Transmission electron microscopy

The transmission electron microscope (TEM) is a characterization tool that can be used to explore matter on an atomic scale, in particular to analyze the distribution of nanoparticles according to their nature and morphology. Not only can the size of these nanoparticles be measured, but electron diffraction can also be used to identify their structure.

Transmission electron microscopy is a microscopy technique in which a beam of electrons is "transmitted" through a very thin sample. The interaction between the electrons and the sample produces an image with a resolution of up to 0.8 Å. The images obtained are generally not self-explanatory, and must be interpreted with the aid of theoretical support **[9]**. A beam of electrons transmitted through a sample forms a diffraction pattern in the local plane to form the image, thanks to magnetic lenses (electromagnets that deflect the electrons) as shown in figure III.9.

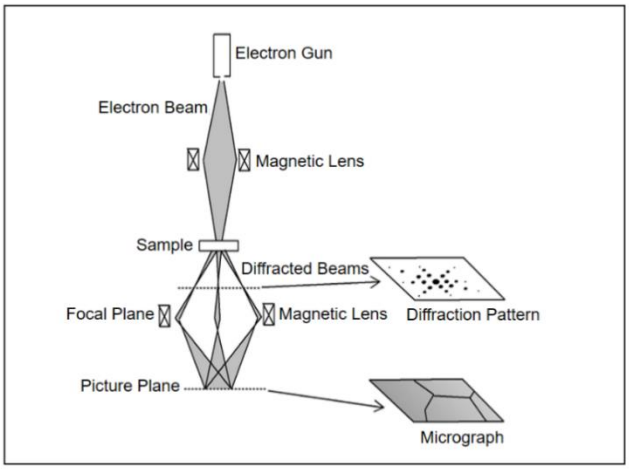

Figure III.9. Principle of the TEM imaging process.

In our study, the transmission electron microscope images were obtained at JEOL, JEM-1400 TEM (Japan). A photograph of this microscope is shown in figure III.10.

Figure III.10. Transmission electron microscope model JEOL, JEM-1400.

III.5.1.3. Atomic force microscopy

Atomic force microscopy (AFM) is ideal for characterizing surface morphology and topographical features at the nanoscale. It provides qualitative and quantitative information on numerous physical properties such as size, morphology, surface texture and roughness. This technique enables three-dimensional images of a surface to be obtained with nanometric resolution. A wide range of particle sizes can be characterized in the same scan, from 1 nanometer to 8 micrometers. What's more, AFM can characterize nanoparticles in multiple media, including ambient air, controlled environments and even liquid dispersions. AFM provides spatial information both parallel and perpendicular to the surface. In addition to high-resolution topographical information, local material properties such as adhesion and stiffness can be studied by analyzing the interaction forces between tips and samples **[10, 11]**.

AFM belongs to a family of very high-resolution local probe microscopes. Not only does it make it possible to observe atoms on the surface of a sample in a vacuum or in air, it also makes it possible to manipulate the surface of the sample very precisely. The device consists of a fine tip placed at the end of a highly sensitive spring blade called a lever, an optical lever deflection detector and a piezoelectric positioning system enabling displacements in 3 directions in space (Figure III.11). When the device is moved horizontally, in the x and y

directions, at a constant height above the sensitive element to be analyzed, the tip will move vertically to follow the very slight variations on the surface. The forces acting between the tip and the surface cause deflections of the lever supporting the tip in the z direction, which are recorded as a function of the position in x and y. Lever deflections are detected using an optical method. A laser beam is focused on the rear face of the lever and reflected towards a detector consisting of a photodiode with two or four dials. Each dial delivers a voltage proportional to its illuminated area, so that the vertical and horizontal movements of the laser beam associated with the lever's deflections and torsions, respectively, can be tracked. This system achieves vertical resolution of less than one Å **[12]**.

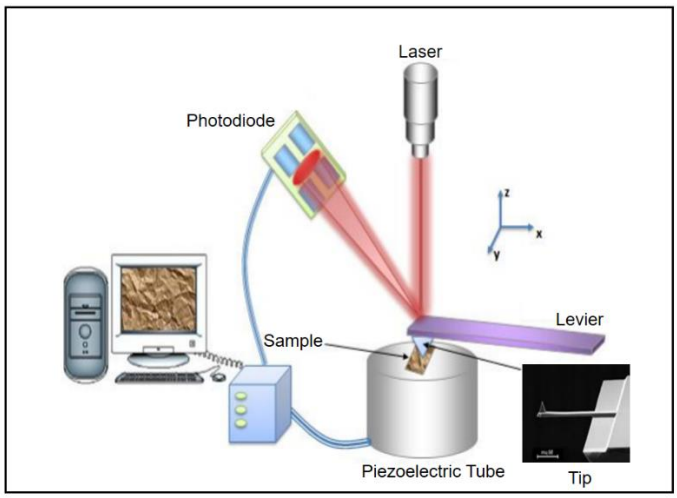

Figure III.11. Schematic of the principle of AFM measurement.

To study a surface using an AFM, there are different working modes that provide access not only to the topography of the surface being probed, but also to its mechanical properties. There are 3 main modes: contact mode, non-contact mode and intermittent contact mode (known as "tapping") **[13, 14]**.

In this work, AFM measurements were carried out in air at room temperature using an Autoprobe CP-R Thermomicroscopes (Figure III.12). AFM images are taken in tapping mode, and processed by the «*Gwyddion*» software.

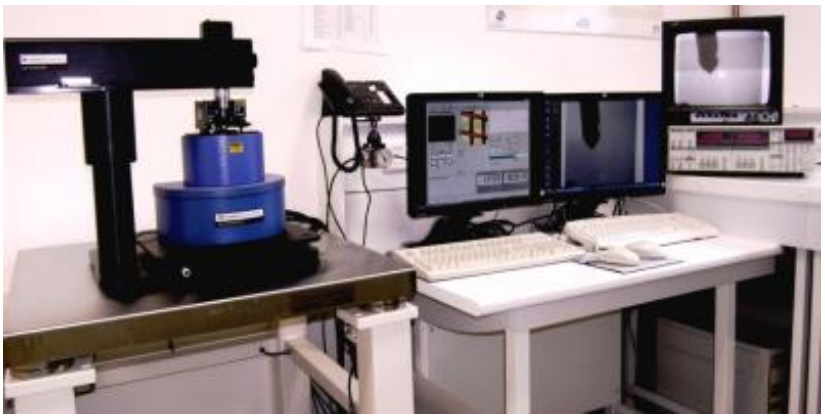

Figure III.12. Autoprobe CP-R Thermomicroscopes.

III.5.1.4. X-ray diffraction

The properties of a material are conditioned by its structure, i.e. the way its atoms are arranged. If this arrangement is a triply periodic repetition, the material is crystalline, but it may be little or well crystallized. Amorphous materials, on the other hand, have a totally disorganized structure. In nature, almost all the solid matter around us is in a crystalline state, hence the importance of knowing the crystalline medium and its structure.

X-ray diffractometry (XRD) is a non-destructive characterization technique for determining a sample's composition, crystalline structure and crystallite size. A crystal is a three-dimensional periodic repetition of the elements shown in figure III.13a XRD involves irradiating the crystalline sample with a monochromatic, parallel beam of X-rays and measuring the intensity of the X-rays scattered according to their orientation in space using a detector (Figure III.13b). In fact, when the sample is irradiated with an X-ray beam, the elements of the crystal scatter waves, which propagate in all directions and interfere with each other **[15, 16]**.

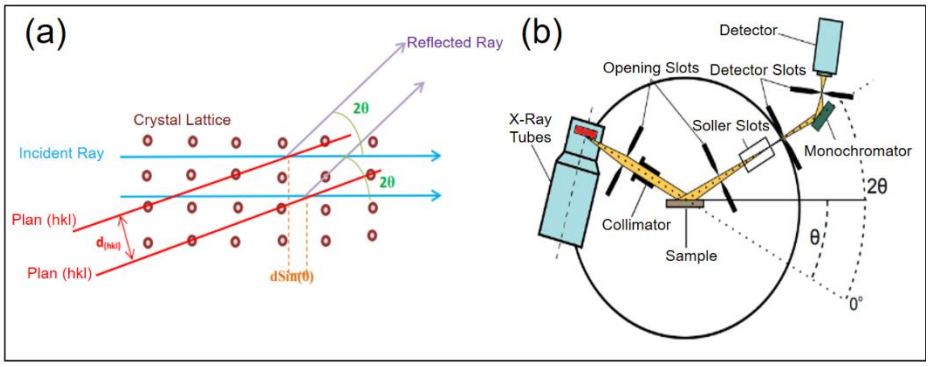

Figure III.13. (a) Diffraction of an X-ray beam, (b) Operation of an X-ray diffractometer.

The intensity of the X-rays detected is plotted as a function of the beam's deflection angle 2θ, providing a diffractogram. Moreover, two particular light rays interfere constructively

when the optical path difference is equal to an integer n wavelength. Using Bragg's law and a database of JCPDS (Joint Comittee on Powder Diffraction Standards) spectra, it is possible to identify the peaks obtained and relate them to the crystalline phase of the sample analyzed (orientation and inter-planar distance).

Bragg's law relates the beam deflection angle to the interplanar distance and is written as **[17]**:

$$2\, d_{hkl} \sin\theta = n\, \lambda \qquad \text{Eq.III.1}$$

Where:

d: interplanar distance (nm)

h,k,l: Miller indices.

θ: Bragg angle (°)

n: diffraction order (unitless)

λ: X-ray wavelength (nm)

The Bragg angle θ is the angle of incidence of the parallel X-ray beam on the reticular planes of the analyzed sample and is equal to half the beam deflection angle.

For our work, DRX analyses were carried out with a Bruker D8 Discover diffractometer equipped with a Cu-Kα source (λ= 1.5418) (Figure III.14).

Figure III.14. Bruker D8 diffractometer.

III.5.2. Electrochemical characterization techniques

Electrochemical characterization techniques are the tools used in electroanalytical chemistry to identify and quantify the analyte on the basis of signals generated by oxidation/reduction, adsorption/desorption and incorporation/exclusion processes at the electrode-solution interface.

III.5.2.1. Voltammetric techniques

Voltammetry is the most widely used group of electroanalytical techniques. Voltammetry involves measuring the current (I) flowing over an electrode as a function of potential (E) and time (t). Consequently, voltammetry can be considered a function of E, I and time (t) **[18]**. A plot of I versus E is called a voltamogram. The techniques used in voltammetry are distinguished from one another by the function of the potential applied to the working electrode to drive the electrochemical reaction **[19]**.

Here, we present the theoretical background required to understand the different voltammetric techniques used in this work.

III.5.2.1.1. Pulse voltammetry

Pulse voltammetry techniques were developed by Barker and Jenkin in the 1950s **[20]**. Applying a pulse to an electrode maximizes flux by reducing the thickness of the diffusion layer **[21]**. This leads to an increase in sensitivity. Various pulse techniques are available. The techniques applied in this work are:

III.5.2.1.1.1. Differential pulse voltammetry

Differential pulse voltammetry (DPV) consists of fixed low-amplitude pulses superimposed on the linear potential. A ramp or staircase potential is applied to the electrode. The current is measured twice: immediately before the pulse, giving a current (I_1), and at the end of the pulse, giving a current (I_2). The difference between the two currents ($\Delta I = I_2 - I_1$) is then recorded as a function of the imposed potential, hence the name differential voltammetry. The resulting peak-shaped profile is called a differential pulse voltamogram (Figure III.15). DPV is 10 to 100 times more sensitive than CV. The peak current (I_p) is proportional to the analyte concentration **[22]**. Reversible systems provide narrow, symmetrical peaks, while irreversible systems generate wider peaks with lower sensitivity.

In this work, DPV measurements were used for the individual and simultaneous analysis of 4-AP and PA and to characterize the sensitivity of the sensors developed. DPV measurements

are performed over a potential range from -0.5 to 0.6 V, employing the following parameters: increment, 0.005 V; pulse amplitude, 0.05 V; pulse width, 0.2 s, and pulse period, 0.5 s.

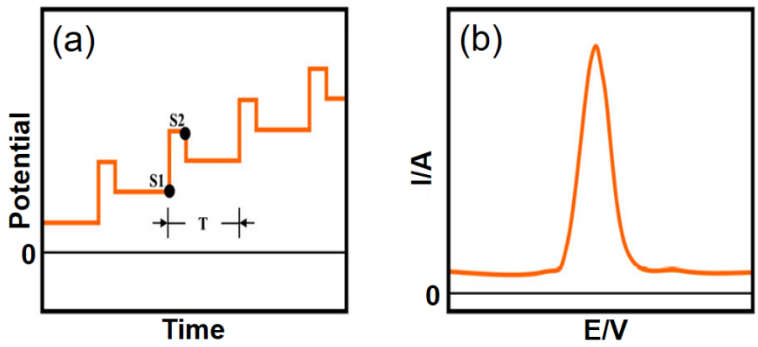

Figure III.15. Sequence of potential sweeps employed in DPV (a) and an example of the resulting current-potential curve (b); T represents the waveform period, and S1 and S2 indicate the two current sampling points.

III.5.2.1.1.2. Square-wave voltammetry

Square-wave voltammetry (SWV) has received increasing attention as a voltammetric technique for frequent quantitative analysis, although it has been reported since 1957 by Barker **[23]**. It is a high-amplitude pulse technique offering the advantage of high speed and sensitivity. The excitation waveform consists of a symmetrical square wave superimposed on a staircase base potential applied to the electrode. The current is sampled twice per square wave cycle, at the end of the two half-cycles; forward ($I_{forward}$) and reverse ($I_{inverse}$). The difference between these two measurements (net current, ΔI) is plotted against the staircase base potential. The resulting peak-shaped profile is called a square-wave voltamogram (Figure III.16). I_p is proportional to analyte concentration. Voltamograms can be recorded in a few seconds or less. The effective scan rate is given by f ΔE, where f is the frequency of the square wave and ΔE the height of the staircase potential **[24]**.

In this work, SWV measurements were also used for the simultaneous analysis of different target analytes and to characterize the sensitivity of the sensors developed. SWV measurements are performed employing the same parameters used in DPV measurments: increment, 0.005 V; pulse amplitude, 0.05 V; and pulse width, 0.2 s

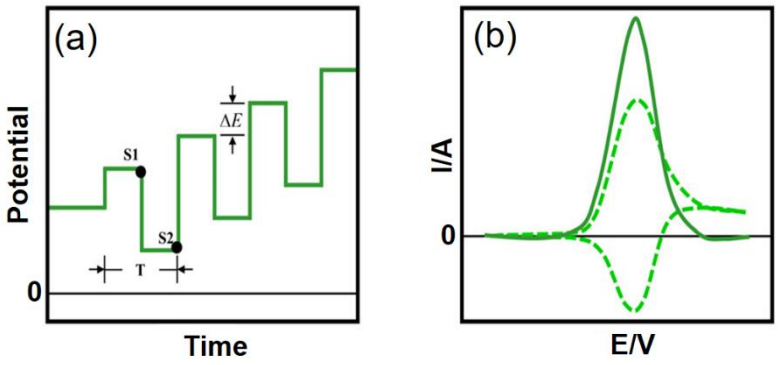

Figure III.16. Voltammogram resulting from a square wave pulse: (a) excitation signal for square wave voltammetry, where ΔE represents the potential increment and T is the potential period; (b) current-potential curve showing the response current, which includes forward (anodic) and reverse (cathodic) components (dashed line), with their difference yielding a net current.

III.5.2.1.2. Cyclic voltammetry

Cyclic voltammetry (CV) is the most versatile and widely used electroanalytical technique for characterizing electroactive species. CV is usually the first experiment to be carried out in an electrochemical study. The popularity of CV lies in its ability to provide the thermodynamics and kinetics of redox processes in a form that is easy to obtain and interpret **[25]**. CV allows us to quickly locate the redox potential of an electroactive species. It was first reported in 1938 and described theoretically by *Randles* and *Ševčík* **[26, 27]**. In CV, the control potential applied to the working electrode (ET) and reference electrode (ER) is called the excitation signal, is a triangular waveform (E/t) (Figure III.17a) in which the electrode potential has been swept from $E_{initial}$ to E_{final}, the direction of sweep has been reversed to the switching potential (E_f) at a constant sweep rate (ν). The potential limits must be chosen so that at E_i there is no electrochemical activity and at E_f the reaction is controlled by mass transport. The current measured during this process is plotted against the applied potential, and the result is called the cyclic voltamogram. Figure III.17b shows a typical cyclic voltamogram obtained for a reversible electrochemical system.

In this work, cyclic voltammetry is used for individual and simultaneous detection of target analytes also for monitoring processes occurring on the surface of the modified electrode as well as evaluating the effect of pH and scan rate. CV measurements are performed in 0.1 M PBS solution (pH 7.4) at a scan rate of 50 mVs^{-1}.

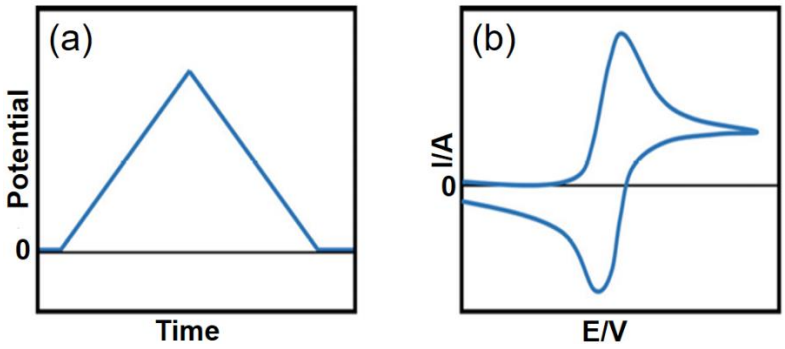

Figure III.17. (a) Excitation potential signal used for CV, (b) Typical CV response for an electrochemically reversible system.

III.5.2.2. Electrochemical impedance spectroscopy

Electrochemical impedance spectroscopy (EIS) is a reliable and powerful technique for studying the electrical properties of electrochemical systems. As such, it is widely used in various fields of research, such as corrosion **[28]**, thin-film characterization, electrode kinetics and batteries **[29]**. In the last decade, EIS has become increasingly important in the fields of biophysical and biosensor technologies **[30, 31]**. This popularity is due to its ability to provide a wide range of information. It provides a better and more complete understanding of an electrochemical system than other electrochemical techniques.

All physical or chemical systems can be modeled by electrical circuits made up of resistors, capacitors, inductors, current sources, voltage sources, etc. An electrochemical cell can be considered as an electrical dipole with impedance Z.

This method of analyzing electrochemical systems using impedancemetric measurements was introduced in 1960 by *Sluyters* **[32]**. It involves analyzing the system response as a function of the frequency of the alternating excitation signal. The low-amplitude frequency signal may or may not be superimposed on a DC bias voltage. An impedance Z(ω) can be presented in either polar or Cartesian coordinate form.

$$Z(\omega) = |Z|.\exp(j\,\varphi) = R_s\,(Z) + j.\,I_m\,(Z) \qquad \text{Eq.III.2}$$

With, $j = \sqrt{-1}$ and ω the signal pulsation.

This gives rise to two types of diagram, the *Nyquist* diagram and the *Bode* diagram. The current is due to charge transport, giving a faradic current I_F and a capacitive current I_C due to the variation in interfacial charges. The equivalent circuit, also known as the Randles diagram, is shown in figure III.18 **[33]**.

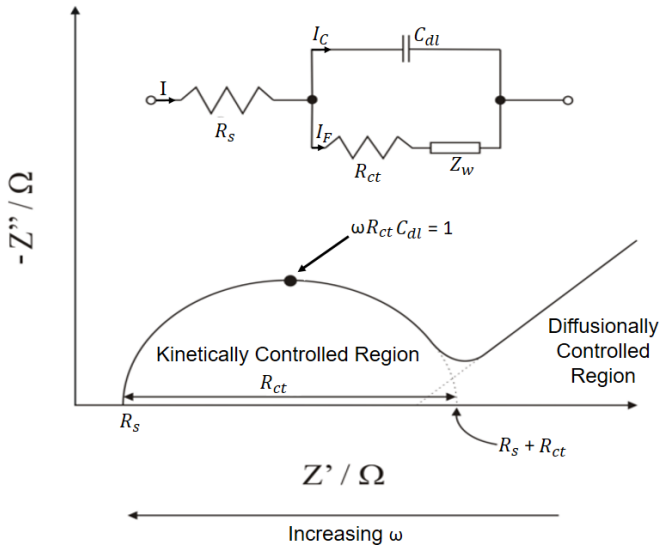

Figure III.18. Equivalent circuit and appropriate *Nyquist* trace for an "ideal" electrochemical cell (*Randles* diagram).

At high frequencies: the *Warburg* impedance Z_w is negligible, so Z tends towards R_{ct}; consequently, the equivalent circuit is a parallel combination of the charge transfer resistor R_{ct} and the double-layer capacitor C_{dl} in series with the resistor corresponding to the ohmic drop R_s.

At low frequencies: the system is driven by diffusion processes, which means that Warburg impedance is predominant.

In this work, impedance measurements were carried out at room temperature. The frequency range is from 100 KHz to 0.1 Hz with an amplitude of 10 mV. All measurements were performed in a 0.1 M KCl solution containing 0.5 mM $K_3[Fe(CN)_6]/K_4[Fe(CN)_6]$ (1:1). Analysis of impedance spectrum data is performed using «*EC-Lab*» software.

III.6. Conclusion

In chapter III, we delved into the essential experimental procedures, equipment, and characterization techniques that underpin our study. We discussed the preparation of various solutions, including buffer solutions and analytical solutions for 4-AP, PA, AA, and Zn(II), as well as the specifics of the electrodeposition bath and the preparation of real samples. The electrochemical setup was thoroughly outlined, alongside the structural, microstructural, and electrochemical characterization techniques employed. This foundation sets the stage for our subsequent investigations.

In the next chapter, the diverse results obtained using the developed electrodes will be presented, with an emphasis on their performance and potential applications.

.

References

[1] W. Drissi, M.L. Chelaghmia, M. Nacef, A.M. Affoune, H. Satha, R. Kihal, H. Fisli, C. Boukharouba, M. Pontié, In situ growth of $Ni(OH)_2$ nanoparticles on 316L stainless steel foam: an efficient three-dimensional non-enzymatic glucose electrochemical sensor in real human blood serum samples, Electroanalysis 34 (2022) 1735–1744.
[2] M. Khairy, A.A. Khorshed, F.A. Rashwan, G.A. Salah, H.M. Abdel-Wadood, C.E. Banks, Sensitive determination of amlodipine besylate using bare/unmodified and DNA-modified screen-printed electrodes in tablets and biological fluids, Sens. Actuators B Chem. 239 (2017) 768–775.
[3] M. Khairy, H.A. Ayoub, C.E. Banks, Non-enzymatic electrochemical platform for parathion pesticide sensing based on nanometer-sized nickel oxide modified screen-printed electrodes, Food Chem. 255 (2018) 104–111.
[4] N. Hernández-Ibáñez, I. Sanjuán, M.Á. Montiel, C.W. Foster, C.E. Banks, J. Iniesta, L-Cysteine determination in embryo cell culture media using Co(II)-phthalocyanine modified disposable screen-printed electrodes, J. Electroanal. Chem. 780 (2016) 303–310.
[5] E. Bernalte, M. Carroll, C.E. Banks, New electrochemical approach for the measurement of oxidative DNA damage: Voltammetric determination of 8-oxoguanine at screen-printed graphite electrodes, Sens. Actuators B Chem. 247 (2017) 896–902.
[6] W. Zhou, R. Apkarian, Z.L. Wang, D. Joy, Fundamentals of Scanning Electron Microscopy (SEM), in: Scanning Microscopy for Nanotechnology, Springer, New York (2006).
[7] T. Brouri, Élaboration et étude des propriétés électriques de couches minces et de nanofils de ZnO, PhD thesis in materials science, University of PARIS-EST, 2011.
[8] C. Esnouf, Chemical analysis using X-ray and electron spectroscopies, Rev. Metall. 100 (2003) 495–506.
[9] P. Shindo, Y. Murakami, Fundamentals of characterization, in: Morphology Control of Materials and Nanoparticles, Springer (2004).
[10] D. Johnson, N. Hilal, W.R. Bowen, Basic principles of atomic force microscopy, in: Atomic Force Microscopy in Process Engineering, Elsevier Ltd. (2009).
[11] V. Bellitto, Atomic Force Microscopy: Imaging, Measuring and Manipulating Surfaces at the Atomic Scale, BoD–Books (2012).
[12] B. Voigtländer, Static Atomic Force Microscopy, Atomic Force Microscopy, Springer International Publishing, Cham (2019).
[13] G. Coulon, Imagerie de surface de polymères: microscopie à force atomique, 2000.
[14] M. Boutamine, Etude et caracterisation d'un capteur chimique a base de couches minces, PhD thesis, University of FRERES MENTOURI, CONSTANTINE, 2014.
[15] B.D. Cullity, Elements of X-ray Diffraction, Addison-Wesley, Reading, MA, 2nd Ed. (1978).
[16] F.C. Krebs, Fabrication and processing of polymer solar cells: A review of printing and coating techniques, Sol. Energy Mater. Sol. Cells 93 (2009) 394–412.
[17] H. Tebani, Elaboration et caractérisation d'alliage ni-fe par electrodéposition, University of 8 MAI 1945, GUELMA, 2019.
[18] A.J. Bard, L.R. Faulkner, Electrochemical Methods – Fundamentals and Applications, John Wiley & Sons, Inc, 2nd Ed. (2001).
[19] J. Barek, A.C. Fogg, A. Muck, J. Zima, Crit. Rev. Anal. Chem. 31 (2001) 291.
[20] G.C. Barker, I.L. Jenkins, Square-wave polarography, Analyst 77 (1952) 685.
[21] D.A. Skoog, F.J. Holler, S.R. Crouch, Instrumental Analysis, Cengage Learning India Pvt. Ltd., 6th Ed. (2010).
[22] J. Wang, Analytical Electrochemistry, Wiley-VCH, 3rd Ed. (2010).
[23] V. Mirceski, S. Komorsky-Lovric, M. Lovric, Square-wave voltammetry: theory and application, Springer Science & Business Media, 2007.
[24] A. Sbartaï, Conception et développement de nouveaux microcapteurs chimiques pour la détection des métaux lourds dans les eaux, PhD thesis in chemistry, co-tutelle thesis between university of CLAUDE BERNARD, LYON 1, and BADJI MOKHTAR, ANNABA, 2014.

[25] M. Noel, K.I. Vasu, Cyclic voltammetry and the frontiers of electrochemistry, Oxford and IBH publishing Co. Pvt. Ltd., 1st Ed. (1990).
[26] J.E.B. Randles, A cathode ray polarograph. Part II. —The current-voltage curves, Trans. Faraday Soc. 44 (1948) 327.
[27] A. Ševčík, Oscillographic polarography with periodical triangular voltage, Czech. Chem. Commun. 13 (1948) 349–377.
[28] C.F. Dong, H.B. Xue, X.G. Li, H.B. Qi, Y.F. Cheng, Electrochemical corrosion behavior of hot-rolled steel under oxide scale in chloride solution, Electrochim. Acta 54 (2009) 4223–4228.
[29] S. Hong, L. Tai-Chin, Electrochemical impedance spectroscopy EIS for battery research and development. Rapport technique 31, Solartron, 1996.
[30] B. Pejcic, R. De Marco, Impedance spectroscopy: Over 35 years of electrochemical sensor optimization, Electrochim. Acta 51 (2006) 6217–6229.
[31] S. Helali, conception et réalisation de matériaux bifonctionnel pour des dispositifs capteurs impédimétriques, PhD thesis, co-tutelle thesis between Central School of Lyon, and Faculty of Science of Tunis, 2005.
[32] J.H. Sluyters, On the impedance of galvanic cells, Rec. Trav. Chim. 79 (1960) 1092–1100.
[33] H. Herrera Hernández, A.M. Ruiz Reynoso, J.C. Trinidad González, C.O. González Morán, J.G. Miranda Hernández, A. Mandujano Ruiz, J. Morales Hernández, R. Orozco Cruz, Electrochemical Impedance Spectroscopy (EIS): A review study of basic aspects of the corrosion mechanism applied to steels, in: Electrochemical Impedance Spectroscopy, 2020.

Chapter IV

Results and discussion

Part A

Development of a novel electrochemical sensor based on Pt-Ni nanostructured screen-printed graphite electrode for the simultaneous detection of paracetamol with 4-aminophenol, as well as with zinc and ascorbic acid in real samples

IV.1. Introduction

The primary objective of this study is to design and develop a novel electrochemical sensor utilizing platinum and nickel nanoparticles (PtNiNPs) deposited on a screen-printed graphite electrode through an innovative electrodeposition method. This sensor aims to detect paracetamol, 4-aminophenol, ascorbic acid, and zinc.

Following the characterization of the synthesized material, we investigated the electrochemical behavior of the target analytes on the Pt-Ni/SPE electrodes using various techniques, including electrochemical impedance spectroscopy (EIS), cyclic voltammetry (CV), differential pulse voltammetry (DPV), and square wave voltammetry (SWV).

IV.2. Electrochemical activation of Pt-Ni NPs modified screen-printed electrodes

Prior to use, the modified Pt–Ni/SPE electrodes were subjected to at least fifty CV cycles in the potential window of –0.8 to 1.0 V in 0.1 M PBS solution (pH 7.4) at 50 mV s^{-1} until a stable peak response was reached (Figure IV.1).

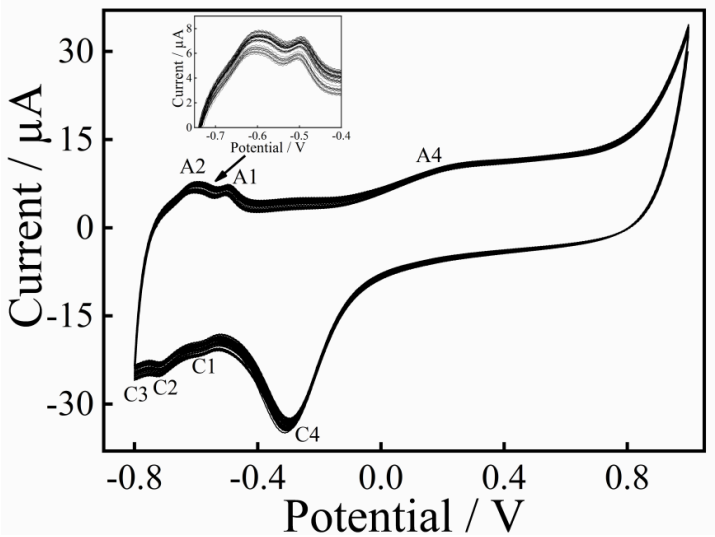

Figure IV.1. Cyclic voltammograms of Pt−Ni modified SPE in 0.1 M PBS solution (pH 7.4) at 50 mV s^{-1}, showing characteristic hydrogen and oxygen electrochemical processes and stability of the modified electrode after activation.

Figure IV.1 showed a typical CVs of Pt–Ni in 0.1 M PBS previously reported by some authors **[1–6]**. Relevant features were denoted as C1, C2, C3, C4 in the cathodic direction and A1, A2, A4 in the anodic region. We observed the hydrogen adsorption/ desorption process which took place in the potential region [–0.76, –0.50] V. C1 and A1 at about –0.58 V and –0.49 V, respectively, were due to adsorption/desorption of hydrogen with strong adsorption between hydrogen and metal, while C2 and A2 at around –0.71 and –0.6 V, respectively, were due to the adsorption/desorption of hydrogen with weak adsorption between hydrogen and

metal. C3 at around –0.79 V corresponded to hydrogen evolution reaction. A4 and C4 at around 0.21 V and –0.3 V were attributed to the adsorption and desorption of oxygen on Pt or the formation and reduction of Pt-Ni hydroxide layer, respectively.

Between the hydrogen and oxygen region, there was a so-called double layer region. In this region, only small current was observed due to the charging of double layer.

IV.3. Characterization of Pt−Ni modified SPEs

IV.3.1. Structural and morphological characterization

The structure and morphology of the modified electrodes were characterized using FE–SEM, TEM, EDX, XRD and AFM techniques.

FE–SEM images of the modified electrode (Pt–Ni/SPE) prepared by simultaneous electrodeposition technique were illustrated in figure IV.2. The surface morphology of SPE became homogeneous after the incorporation of highly uniform and well-dispersed Pt and Ni spherical particles as illustrated in figure IV.2a. The high-magnification FE–SEM image (Figure IV.2b) revealed that many Pt nanodeposits were homogenously distributed throughout the substrate, with an average–dimension up to ca. 300 nm. In contrast, only a few Ni nanoparticles with a smaller diameter were present. Within the experimental conditions outlined in this study, the electrodeposited Pt particles were found to be bigger in size compared to the Ni particles.

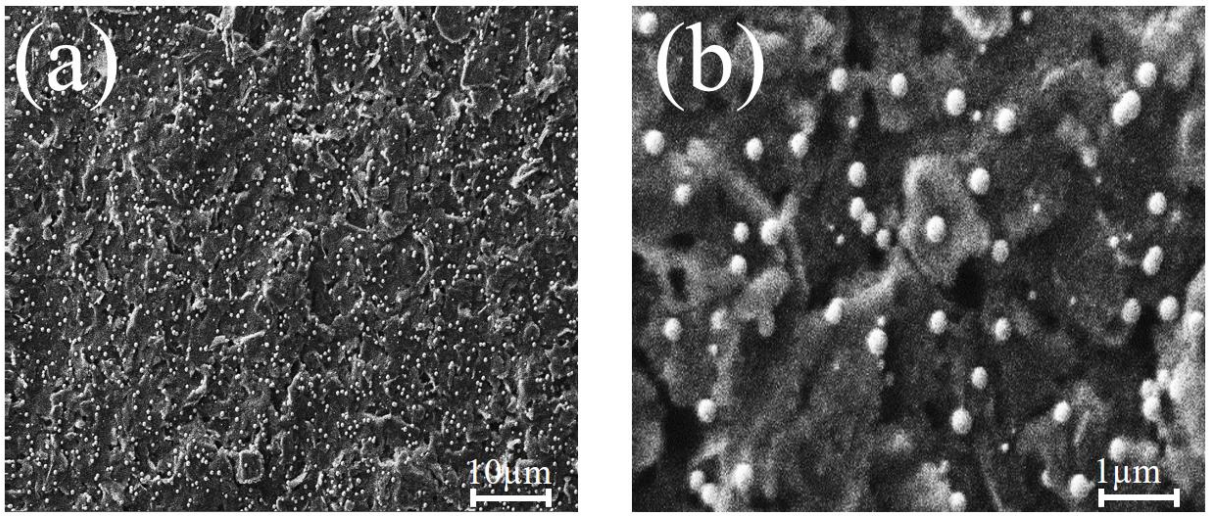

Figure IV.2. (a) FE–SEM image of Pt–Ni/SPE, (b) high-magnification FE–SEM image of Pt–Ni/SPE.

Moreover, the TEM image of the modified electrode further proved its successful preparation (Figure IV.3).

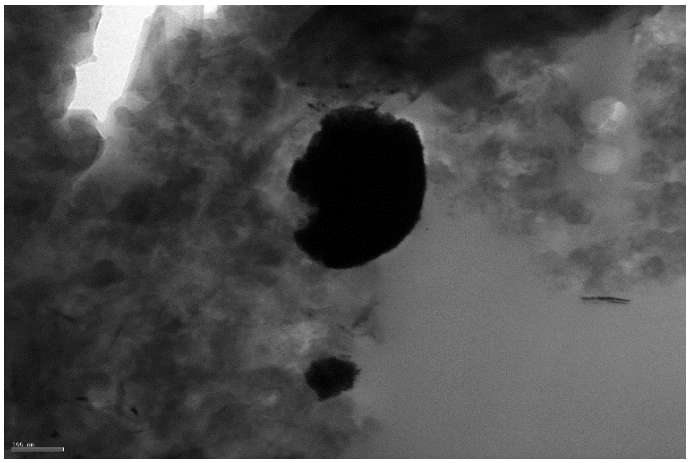

Figure IV.3. TEM image of Pt−Ni modified SPE.

The EDX spectrum of the as-fabricated Pt–Ni/SPE electrode (Figure IV.4) also provided elemental proof to confirm this result, with the atomic ratios of Pt and Ni estimated to be about 97.17% and 2.83 %, respectively.

The high percentage of Pt particles compared to Ni particles was attributed to the fact that the highest electro-catalytic activity of platinum particles was achieved when the amount of nickel in the modified electrode is up to about 5% **[7]**.

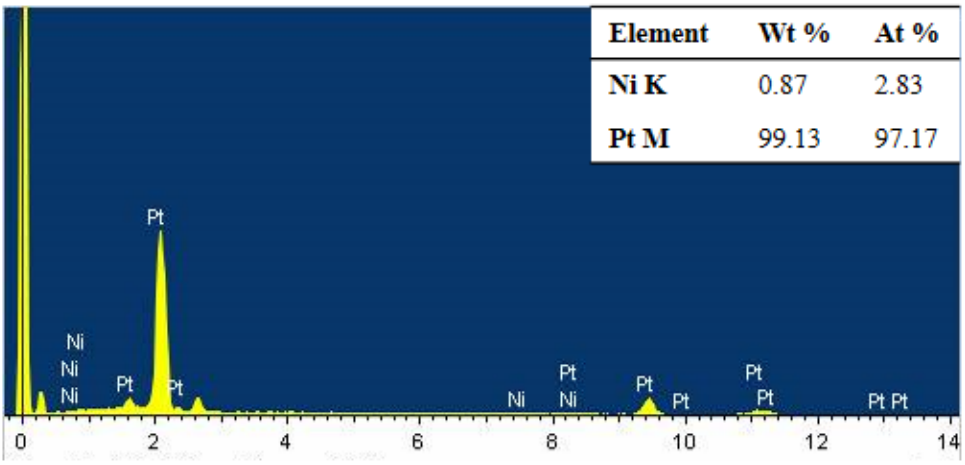

Figure IV.4. EDX spectrum of Pt–Ni/SPE electrode.

The above results demonstrated the successful synthesis of Pt–Ni/SPE. Additionally, as illustrated in figure IV.5, the crystal structure of Pt–Ni/SPE electrode was further examined by XRD. The peaks occurring in this figure at angular positions of 26.6°, 44.7°, and 54.8° corresponded to (002), (101), and (004) diffractions of hexagonal graphite (JCPDS No. 00–026–1080).

Furthermore, three crystalline peaks were observed at 2θ values of 40.2°, 46.7°, and 68.2°, which could be indexed to the (111), (200), and (220) diffractions of face-centered cubic

of pure Pt (JCPDS No. 00–001–1194). In addition, other three characteristic peaks at 44.7°, 52.1°, and 76.6°, matched well with the (111), (200), and (220) crystalline planes of cubic phase Ni (JCPDS No. 00–004–0850).

The XRD results also testified that Pt–Ni nanodeposits were formed and successfully loaded onto the graphite SPE electrode surface.

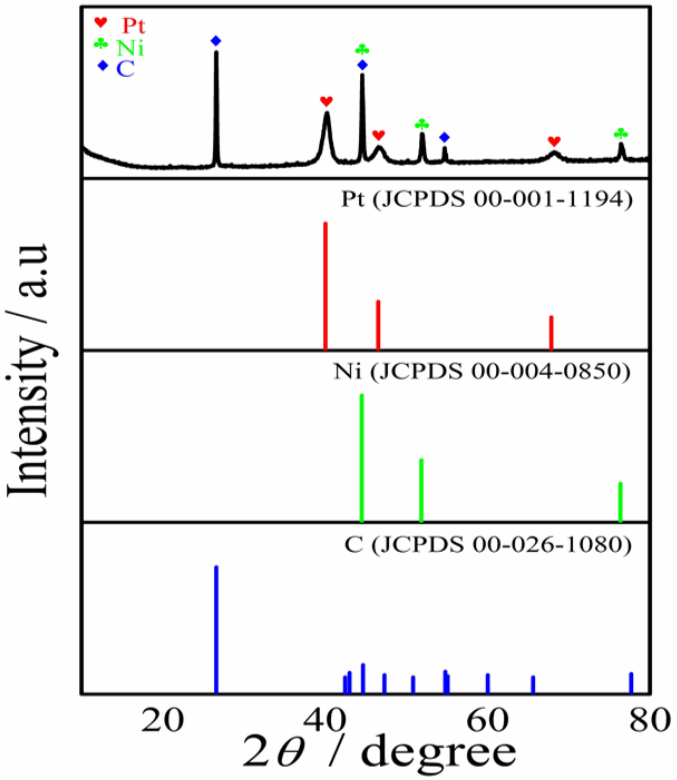

Figure IV.5. XRD pattern of Pt–Ni/SPE electrode.

Moreover, AFM analysis was performed on both unmodified and Pt–Ni modified SPE. Figure IV.6a and b presented two-dimensional (2D) and three-dimensional (3D) AFM images of the unmodified SPE, while figure IV.6c and d depicted the 2D and 3D views of the Pt–Ni modified SPE, respectively.

Comparison of the 3D AFM images in figure IV.6b and d revealed the relatively rough surface of the unmodified SPE, whereas the modified electrode surface appeared moderately homogeneous, indicating the smooth distribution of Pt–Ni particles. This supported previous findings of successful Pt–Ni nanodeposits loading onto the graphite screen-printed electrode surface.

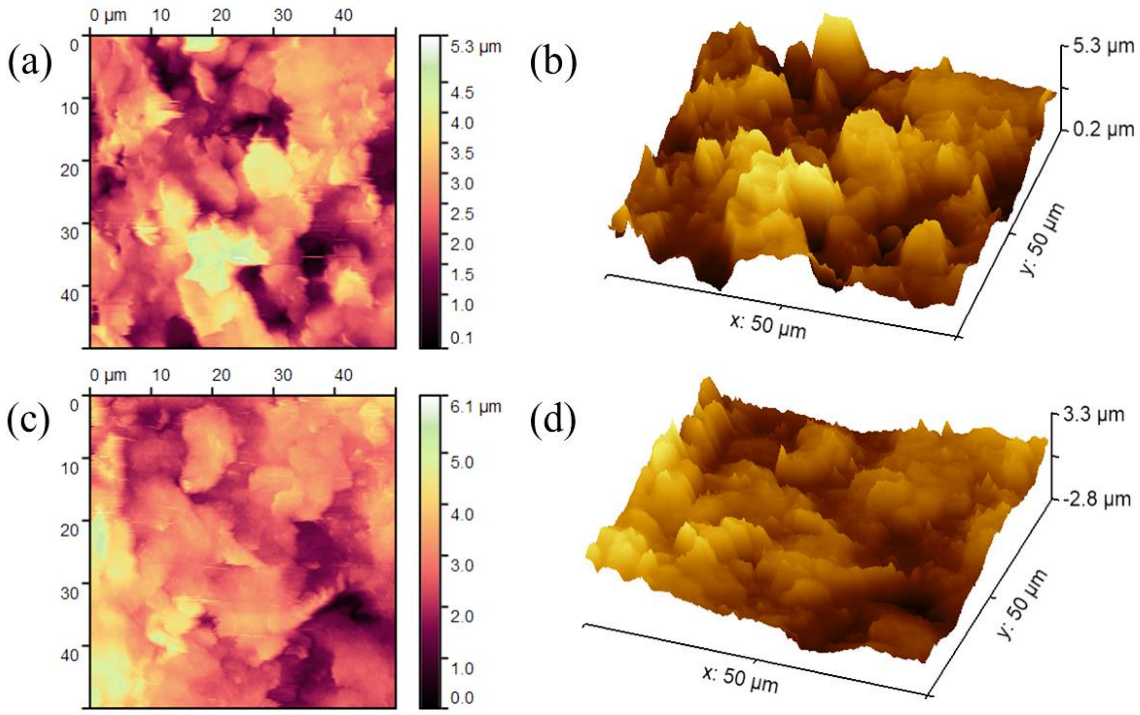

Figure IV.6. (a) 2D, (b) 3D AFM images of SPE; (c) 2D, (d) 3D AFM images of Pt–Ni/SPE.

IV.3.2. Electrochemical characterization

The electrochemical properties of the modified electrodes were studied using CV and EIS techniques.

IV.3.2.1. Electrochemical characterization by cyclic voltammetry

To investigate the electrochemical behavior of the bare SPE, Pt/SPE and Pt–Ni/SPE through $Fe(CN)_6^{-3/-4}$redox probe, CV technique was performed in 0.1 M KCl solution containing 0.5 mM $Fe(CN)_6^{-3/-4}$on the surface of these electrodes (Figure IV.7).

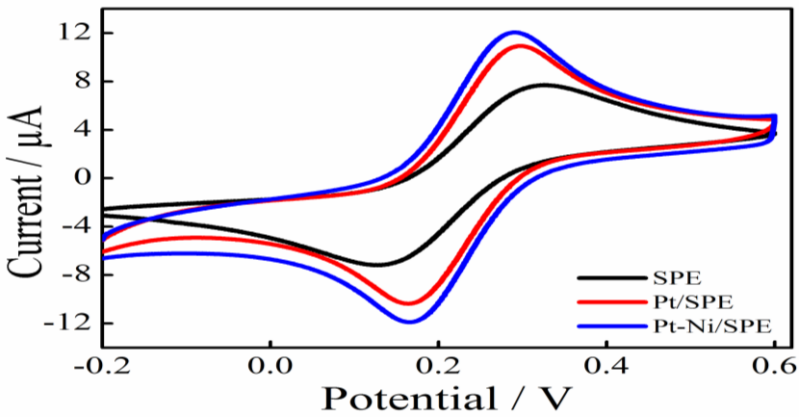

Figure IV.7. CVs for bare SPE, Pt/SPE and Pt–Ni/SPE electrodes in 0.5 mM $Fe(CN)_6^{3-/4-}$ comprising 0.1 M KCl, recorded at a scan rate of 50 mV s^{-1}.

Figure IV.7 illustrated the CVs of unmodified and modified SPEs, respectively. From this figure, it was found that the potential peak separation (ΔE_p) was 197 mV for the unmodified SPE, 133 mV for Pt/SPE, and 122 mV for Pt–Ni/SPE at a scan rate of 50 mV s^{-1}.

The impact of Pt and Pt–Ni nanoparticles upon the SPE's heterogeneous electron transfer characteristics was studied by employing Nicholson's method **[8]**. This method was routinely used estimate the heterogeneous electron transfer rate constant (k°) for quasi-reversible reactions using the following formula:

$$\psi = k^{\circ} [\pi D n \upsilon F/RT]^{-1/2} \qquad \text{Eq.IV.1}$$

Where:

$\boldsymbol{\psi}$ is a kinetic parameter;

$\boldsymbol{D}$ is the diffusion coefficient (D = 7.6 × 10^{-6} cm^2 s^{-1} for $Fe(CN)_6^{-3/-4}$);

$\boldsymbol{\upsilon}$ is the voltammetric scanning rate;

$\boldsymbol{n}$ is the number of electrons involved in the process;

$\boldsymbol{R}$, $\boldsymbol{F}$, and $\boldsymbol{T}$ denoted constants, with T being the temperature in Kelvin, R being the universal gas constant (8.314 J mol^{-1} K^{-1}), and F being the Faraday constant (96485.33 C mol^{-1}).

ψ was deduced from (ΔE_p) at a set temperature (298K) for a one-step, one electron process with the transfer coefficient α equal to 0.5. The function of ψ (ΔE_p), which fitted Nicholson's data, for practical usage (rather than producing a working curve) was given by **[9]**:

$$\psi = (-0.6288 + 0.0021X)/(1 - 0.017X) \qquad \text{Eq.IV.2}$$

where X=ΔE_p was used to determine ψ as a function of ΔE_p from the experimentally obtained voltammetric curves. From this, a plot of ψ against $[\pi D n \upsilon F/RT]^{-1/2}$ allowed the k° to be readily determined.

Using this approach, the corresponding k° values were estimated to be 2.4×10^{-4}, 5.3 ×10^{-4} and 5.9×10^{-4} for the unmodified SPE, Pt/SPE and Pt–Ni/SPE, respectively. Moreover, the redox peak currents observed over the various electrodes increased in the subsequent arrangement: SPE < Pt/SPE < Pt–Ni/SPE. Consequently, these changes demonstrated the electro-catalytic efficiency of Pt and Pt–Ni nanoparticles as modifiers, effectively enhancing and facilitating the electron transfer rate of the graphite SPE by factors of 2.2 and 2.5, respectively.

IV.3.2.1.1. Determination of the electroactive surface area of the modified electrodes

The electroactive surfaces of the unmodified and modified SPE were calculated to determine the efficiency of the modified surfaces.

Figure IV.8 showed cyclic voltammograms of bare SPE, Pt/SPE and Pt-Ni/SPE electrodes recorded for 0.5 mM $Fe(CN)_6^{3-/4-}$ solution comprising 0.1 M KCl at scan rate ranging from 10 to 120 mV s^{-1}. The results showed that peak currents increased linearly as a function of $v^{1/2}$ on both unmodified and modified SPE, reflecting a diffusion-controlled reaction. The regression equations obtained for the three electrodes were as follows:

$$I_{pa}(A) = 0.000027\ v^{1/2}\ (Vs^{-1})^{1/2} + 0.000001\ (R^2 = 0.997) \quad \text{Eq.IV.3}$$

$$I_{pa}(A) = 0.000045\ v^{1/2}\ (Vs^{-1})^{1/2} + 0.0000006\ (R^2 = 0.998) \quad \text{Eq.IV.4}$$

$$I_{pa}(A) = 0.000057\ v^{1/2}\ (Vs^{-1})^{1/2} + 0.0000007\ (R^2 = 0.999) \quad \text{Eq.IV.5}$$

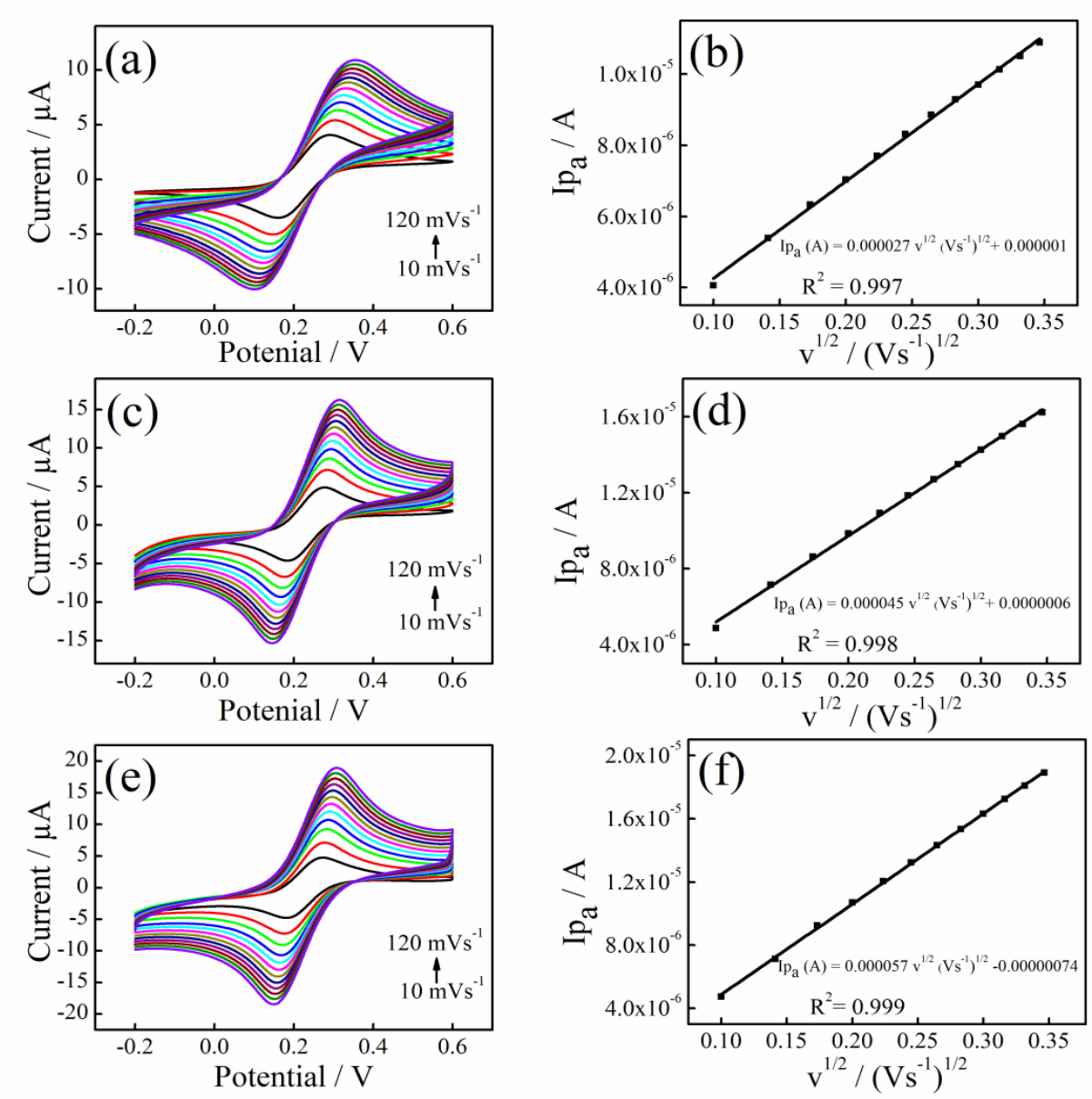

Figure IV.8. CVs of 0.5 mM $Fe(CN)_6^{3-/4-}$solution comprising 0.1 M KCl at scan rate ranging from 10 to 120 mV s^{-1} on (a) SPE, (c) Pt/SPE, (e) Pt–Ni/SPE, (b),(d) and (f) The variation of anodic peak currents (I_{pa}) vs square root of the scan rate ($v^{1/2}$).

The specific surface areas of bare SPE, Pt/SPE and Pt–Ni/SPE were calculated using *Randles–Ševčík* formula **[10]**:

$$I_p = \pm\, 0.436\, nFAC\sqrt{\frac{nFDv}{RT}} \qquad \text{Eq.IV.6}$$

where:

$\boldsymbol{I_P}$ was the anodic peak current (A);

n was the number of electron transformed;

$\boldsymbol{A}$ was the electroactive area of working electrode (cm^2);

$\boldsymbol{D}$ was the diffusion coefficient ($cm^2\ s^{-1}$);

$\boldsymbol{\upsilon}$ was the scan rate ($V\ s^{-1}$);

$\boldsymbol{C}$ was the bulk concentration ($mol\ cm^{-3}$).

Based on equation eq.IV.6, the electroactive surface areas were determined to be 5.1×10^{-2}, 6.7×10^{-2} and $6.9\times10^{-2}\ cm^2$ for the bare SPE, Pt/SPE and Pt–Ni/SPE, respectively. These results confirm the successful modification of the SPE surface with metallic nanoparticles. The moderate increase from the bare SPE to the Pt/SPE can be attributed to the deposition of Pt nanoparticles, which provided a greater number of electroactive sites and improved the electrode's surface accessibility, thus increasing the effective surface area. The relatively small difference between Pt/SPE and Pt–Ni/SPE suggests that the addition of Ni only slightly influenced the geometric surface area, likely due to a limited Ni content or minimal changes in surface morphology. However, the incorporation of Ni may still play a crucial role in enhancing catalytic activity through electronic effects and synergistic interactions with Pt.

IV.3.2.2. Electrochemical characterization by electrochemical impedance spectroscopy

Electrochemical impedance spectra proved to be a powerful approach employed to investigate the interface characteristics of surface modified electrodes in the frequency ranging from 0.1 to 10^5 Hz.

Figure IV.9 showed the EIS typical spectra of the unmodified SPE, Pt/SPE and Pt–Ni/SPE, consisting of two parts, semicircle portion at higher frequencies, indicative of the electron transfer process with a diameter equal to the charge transfer resistance (R_{ct}), and a straight line at lower frequencies reflecting the diffusion control process **[11]**.

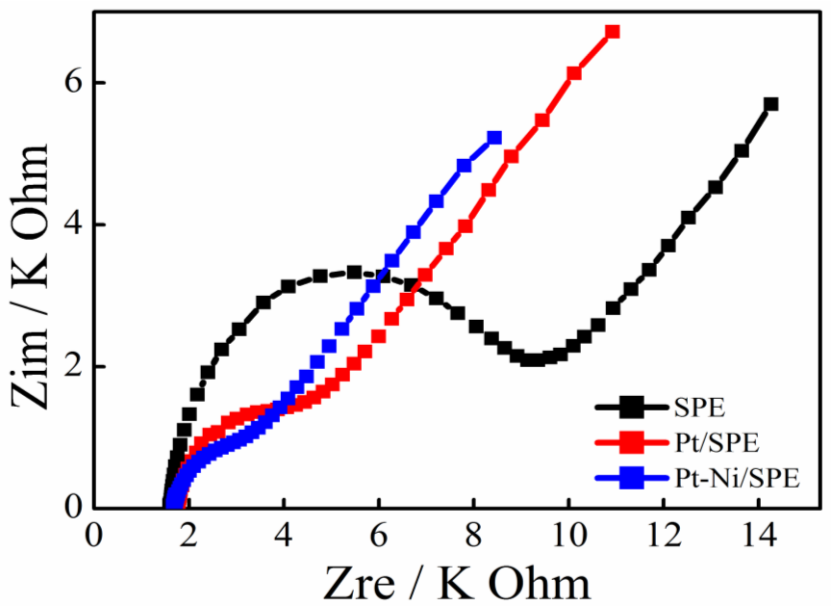

Figure IV.9. Nyquist EIS plots for bare SPE, Pt/SPE and Pt–Ni/SPE electrodes in 0.5 mM $Fe(CN)_6^{3-/4-}$ comprising 0.1 M KCl, recorded at a scan rate of 50 mV s^{-1} and within an applied frequency range spanning from 100 kHz to 0.1 Hz.

The EIS spectra were theoretically fitted to a suitable equivalent circuit (as shown in figure IV.10), which is composed of solution resistance (R_1), Warburg element (W), charge transfer resistance (R_2) and the constant phase element (CPE_1).

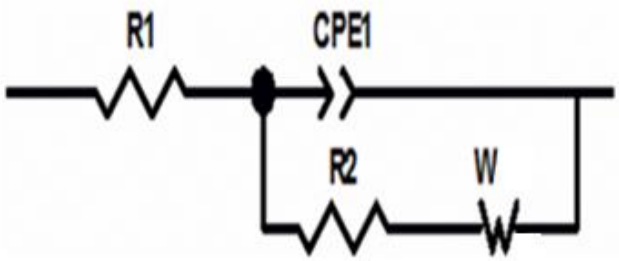

Figure IV.10. *Randles* equivalent circuit model.

The fitted R_2 values for the bare SPE, Pt/SPE and Pt–Ni/SPE were found to be 6.99 KΩ (χ^2=0.0302), 2.68 KΩ (χ^2=0.0384) and 1.59 KΩ (χ^2=0.0385), respectively. Notably, the lowest R_2 value was observed for the Pt–Ni/SPE, indicating a more efficient charge transfer process at the electrode–electrolyte interface. This suggests enhanced electrocatalytic activity of the Pt–Ni modified electrode compared to the other electrodes.

Hence, the EIS results were in agreement with both CV data and physical characterization results, demonstrating the effective modification of the screen-printed electrode surface with Pt–Ni nanoparticles.

IV.4. Electrochemical behaviors of 4-aminophenol and paracetamol at different modified electrodes

The electrochemical behaviors of 4-AP and PA were investigated on various modified electrodes (bare SPE, Pt/SPE and Pt–Ni/SPE) in 0.1 M PBS (pH = 7.4) containing 300 µM 4-AP and PA, respectively. The CV technique was employed for this analysis.

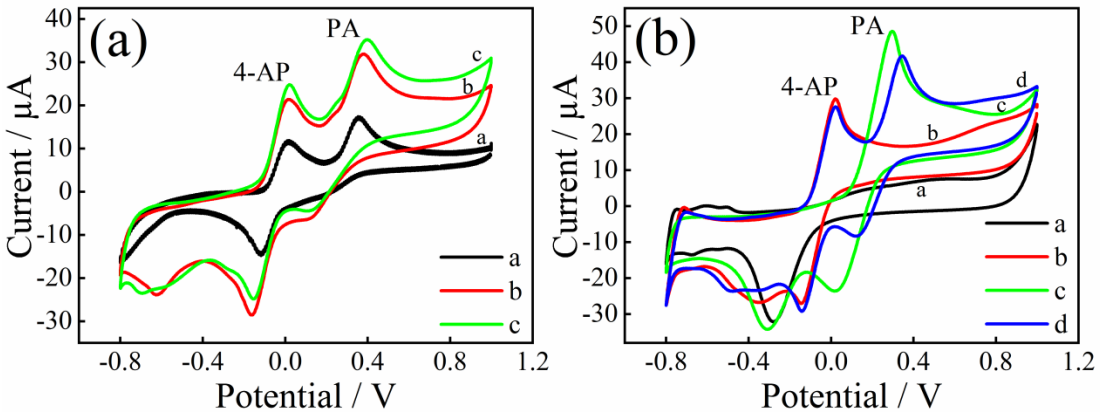

Figure IV.11. (a) CVs of bare SPE (a), Pt/SPE (b), Pt–Ni/SPE (c) in PBS (0.1 M, pH = 7.4) containing a mixture of 300 µM 4-AP and PA. (b) CVs of the Pt–Ni/SPE electrode in 0.1 M PBS solution (pH = 7.4) without 4-AP and PA (a), with 300 µM 4-AP (b), 300 µM PA (c) and their mixture (d), respectively.

As observed in figure IV.11a, the bare SPE depicted in the potential range of –0.8 to 1.0 V a pair of weak and broad redox peaks for 4-AP and PA (curve a). In comparison, the Pt/SPE exhibited an increase in the redox peak currents for both targets (curve b) by approximately 2 times, possibly due to the electro-catalytic activity of Pt particles.

Upon the surface modification of the Pt/SPE electrode through the co-deposition of Pt with Ni, as described in the experimental section, the oxidation peak currents density for both target analytes (curve c) exhibited a remarkable enhancement, surpassing that of the single metal modified electrode (Pt/SPE). This enhancement was attributed to the abundant heterogeneous electron transfer properties of nickel particles, which further improved the sensing characteristics of the fabricated electrode by enhancing electrical conductivity of platinum particles. This assumption was consistent with previously reported works on the oxidation of other analytes by the bi-metal (Pt–Ni) systems **[12–14]**.

CV measurements were also used to study the electrochemical detection of 4-AP and PA individually and simultaneously using the Pt–Ni/SPE modified electrode.

In figure IV.11b, the modified electrode was immersed in various solutions: blank PBS (a), 300 µM 4-AP (b), 300 µM PA (c) and their mixture solution (d).

In the blank PBS solution (0.1 M, pH = 7.4), no redox peaks were observed, and only the characteristic signals associated with the Pt–Ni/SPE were present (curve a). When 4-AP was introduced, a pair of well-defined redox peaks, corresponding to the electrochemical behavior of 4-AP, appeared at 0.02 V for the anodic peak potential and –0.14 V for the cathodic peak potential (curve b). Subsequently, when the prepared Pt–Ni/SPE electrode was immersed in the PA solution, a pair of distinct redox peaks showed at 0.29 V and 0.02 V for anodic and cathodic peak potential, respectively (curve c), certainly corresponding to the electrochemical behavior of PA.

As seen in curve d, the CV of the mixture containing both 4-AP and PA exhibited four distinct redox peaks related to the redox processes of 4-AP and PA, showing an anodic peak-to-peak separation up to 0.32 V.

These data indicated that the redox peaks of 4-AP and PA were clearly separated, demonstrating the capability of the Pt–Ni/SPE modified electrode for the simultaneous and selective determination of these target species.

IV.5. Optimization of analytical detection parameters

Before constructing the calibration voltammogram, it was necessary to optimize the conditions for measuring the electrode response in a solution containing the two molecules, while varying the pH of the electrolyte and the scan rate.

IV.5.1. The pH value effect

The electrochemical oxidation of phenolic compounds to form quinone is fundamentally reliant on the process of proton transfer **[15]**. Consequently, variations in the buffer solution's pH can directly influence the electrochemical response of 4-AP and PA. Thus, the effect of the supporting electrolyte pH ranging between 6.0 and 9.0 on the redox response of 100 µM 4-AP and PA mixture at Pt–Ni/SPE with a scan rate of 50 mV s^{-1} was carried out by CV.

As shown in figure IV.12a and b, as the pH increased from 6.0 to 7.4, the oxidation peak currents of both 4-AP and PA consistently increased. However, beyond this range, further increases in pH resulted in a decrease in peak currents. This behavior was attributed to the nature of the oxidation mechanism of phenolic compounds such as 4-AP and PA, which involves the loss of electrons and protons, typically forming quinone-like products. In mildly acidic to neutral conditions (pH 6.0-7.4), the presence of sufficient protons facilitated the proton-coupled electron transfer process, enhancing reaction kinetics and thereby increasing the peak currents. Moreover, the electrode surface remained stable and favorable for electron transfer near physiological pH. In contrast, at higher pH values (above 7.4), the reduced proton

concentration hindered the proton transfer steps, making the oxidation process less efficient. Additionally, deprotonation of either the analytes or surface functional groups may have altered the surface charge, weakening the interaction between the analytes and the electrode. Furthermore, in strongly basic conditions, side reactions or polymerization of oxidation products might have led to electrode fouling, contributing to the decline in current response.

Therefore, pH 7.4 was selected for subsequent experiments, as it provided the highest oxidation current, reflecting optimal reaction kinetics and maximum sensitivity for both 4-AP and PA detection. This pH also closely resembled physiological conditions, enhancing the potential of the sensor for biological or clinical applications. Notably, at pH 6.0, a strong current was observed, attributed to the hydrogen evolution reaction at the Pt surface; however, this current decreased for pH values above 6.0.

In figure IV.12c, it was evident that the E_{pa} values for 4-AP and PA exhibited a linear shift towards more negative directions as the pH increased within the range of 6.0 to 9.0. This was indicative of the direct involvement of protons in the redox process of both 4-AP and PA **[16]**. The displayed regression equations were as follows:

For 4-AP

$$E_{pa} = -0.058\,pH + 0.388\ (R^2 = 0.99) \qquad \text{Eq.IV.7}$$

For PA

$$E_{pa} = -0.05\,pH + 0.6\ (R^2 = 0.991) \qquad \text{Eq.IV.8}$$

Moreover, the slopes of the calibration curves, measuring 58.8 mV/pH for 4-AP and 50 mV/pH for PA, closely approximated the theoretical Nernstian value of 59 mV/pH **[17]**. This suggested that an equal number of protons and electrons had been participated in the oxidation-reduction mechanism of both phenolic analytes at the Pt–Ni/SPE modified electrode.

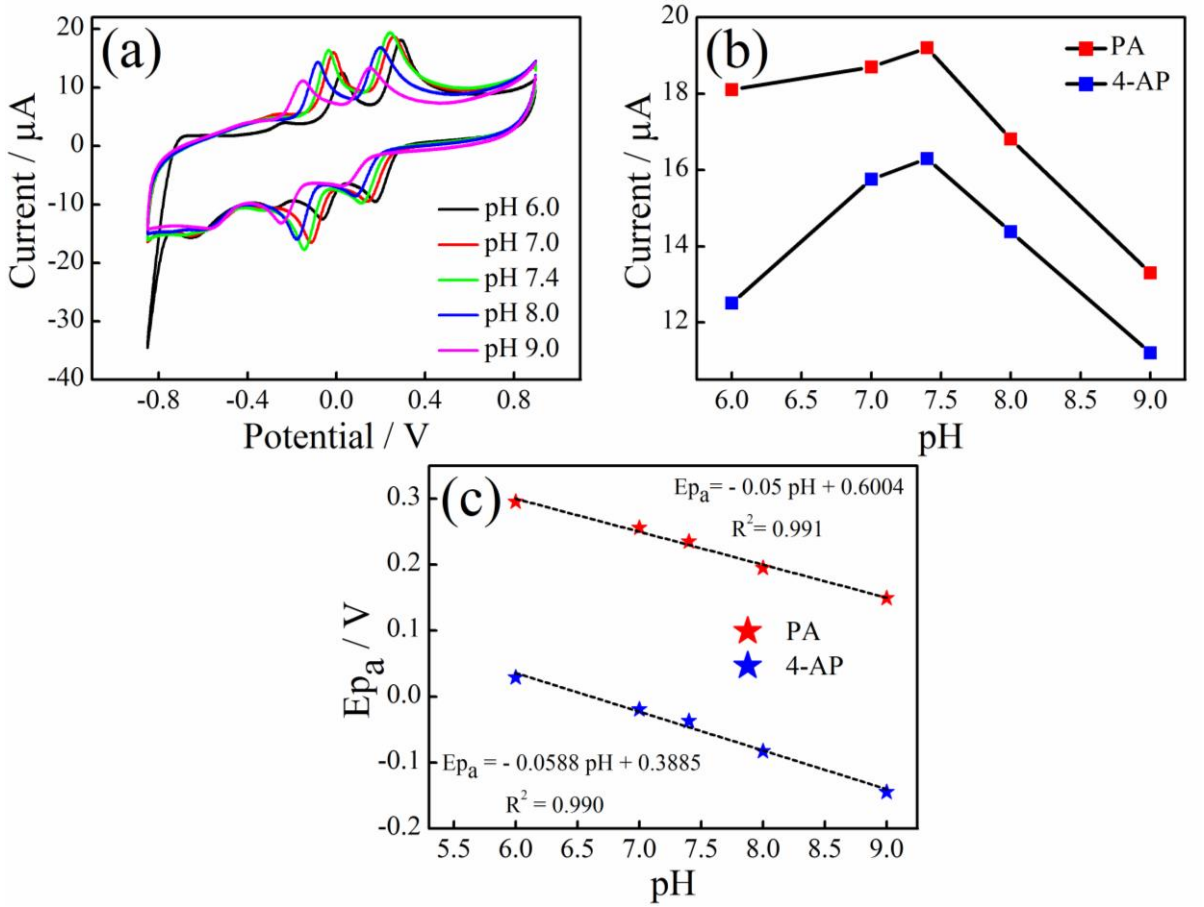

Figure IV.12. (a) CVs of the modified Pt−Ni/SPE electrode in 0.1M PBS comprising 100 µM 4-AP and PA mixture with different pH values from 6.0 to 9.0, at fixed scan rate of 50 mVs^{-1}; (b) The influence of solution pH on the anodic peak currents of 4-AP and PA;(c) The influence of pH on the anodic peak potentials of 4-AP and PA.

IV.5.2. The scan rate influence

To provide more information about the charge transfer proprieties of 4-AP and PA, the impact of scan rate on the electrochemical reaction of 4-AP and PA at the surface of the Pt–Ni/SPE proposed electrode was examined through CV at various scan rates from 5.0 to 1000 mVs^{-1} using a concentration of 300 µM for both analytes.

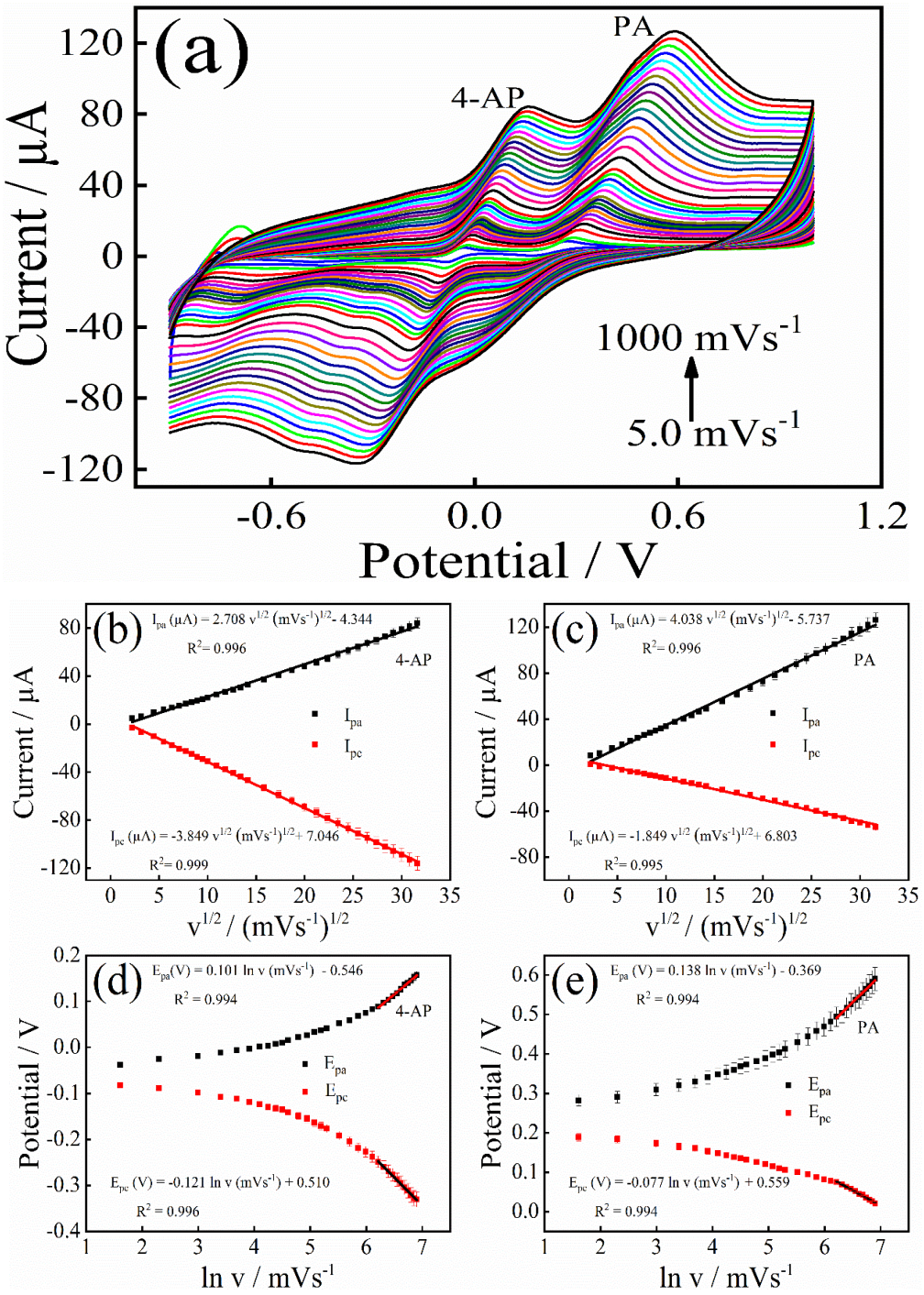

Figure IV.13. (a) CVs of Pt–Ni/SPE electrode in 0.1 M PBS (pH 7.4) with a combination of 300 µM 4-AP and PA at various scan rates from 5.0 to 1000 mVs^{-1}, (b, c) Calibration plots of redox peak currents vs $\upsilon^{1/2}$, (d, e) Plots of redox peak potentials vs. ln υ. The error bars indicate the standard deviations of three repeated measurements.

Figure IV.13a revealed that as the scan rate increased, the electrochemical signals of both 4-AP and PA exhibited a gradual increase.

At the same time, figure IV.13b and c showed that the anodic and cathodic peak currents (I_{pa} and I_{pc}) of the two phenolic compounds exhibited a proportional relationship with the

square root of the scan rate ($\upsilon^{1/2}$). The fitting equations assumed for this relationship were as follows:

For 4-AP:

$$I_{pa}\ (\mu A) = 2.708\ \upsilon^{1/2}\ (mV\ s^{-1})^{1/2} - 4.344\ (\ R^2 = 0.996), \qquad \text{Eq.IV.9}$$

$$I_{pc}\ (\mu A) = -3.849\ \upsilon^{1/2}\ (mV\ s^{-1})^{1/2} + 7.046\ (\ R^2 = 0.999) \qquad \text{Eq.IV.10}$$

For PA:

$$I_{pa}\ (\mu A) = 4.038\ \upsilon^{1/2}\ (mV\ s^{-1})^{1/2} - 5.737\ (\ R^2 = 0.996), \qquad \text{Eq.IV.11}$$

$$I_{pc}\ (\mu A) = -1.849\ \upsilon^{1/2}\ (mV\ s^{-1})^{1/2} + 6.803\ (\ R^2 = 0.995) \qquad \text{Eq.IV.12}$$

These phenomena clearly suggested that all electrochemical reactions at the surface of Pt–Ni/SPE modified electrode were diffusively controlled **[18]**.

On the other hand, a slight positive and negative shift in the oxidation and reduction peak potentials (E_{pa} and E_{pc}), respectively, was observed as the scan rate increased, implying a kinetic limitation of the modified Pt–Ni/SPE towards 4-AP and PA oxidation.

Figure IV.13d and e showed the linear dependence between E_{pa}, E_{pc} and the natural logarithm of the scanning speed ($\ln \upsilon$). This linear relationship was expressed through the following corresponding linear equations:

For 4-AP:

$$E_{pa}(V) = 0.101 \ln \upsilon\ (mV\ s^{-1}) - 0.546\ (R^2 = 0.994), \qquad \text{Eq.IV.13}$$

$$E_{pc}(V) = -0.121 \ln \upsilon\ (mV\ s^{-1}) + 0.510\ (R^2 = 0.996) \qquad \text{Eq.IV.14}$$

For PA:

$$E_{pa}(V) = 0.138\ \ln \upsilon\ (mV\ s^{-1}) - 0.369\ (R^2 = 0.994), \qquad \text{Eq.IV.15}$$

$$E_{pc}(V) = -0.077\ \ln \upsilon\ (mV\ s^{-1}) + 0.559\ (R^2 = 0.994) \qquad \text{Eq.IV.16}$$

Referring to Laviron's theory **[19]**:

$$E_{pa} = E^0 + A\ ln\ v \qquad \text{Eq.IV.17}$$

$$E_{pc} = E^0 + B\,ln\,v \qquad \text{Eq.IV.18}$$

$A = RT/(1-\alpha)nF$

$B = RT/\alpha nF$,

where all constants remained consistent with the previous description, except for the standard redox potential E°.

By analyzing the linear relationships between E_{pa}, E_{pc} and $\ln v$, it was observed that the slopes of the linear regressions corresponded to $RT/\alpha nF$ and $RT/(1-\alpha)nF$, respectively.

Following the calculations, the values of *n* and α were found to be (2.45 and 0.47) for 4-AP and (2.41 and 0.55) for PA, respectively.

Hence, the redox mechanism of the two phenolic compounds at the surface of our newly modified electrode involved the transfer of two electrons and two protons ($2e^-/2H^+$). The probable reaction mechanism of 4-AP and PA is described in figure IV.14, consistent with those previously reported **[20, 21]**.

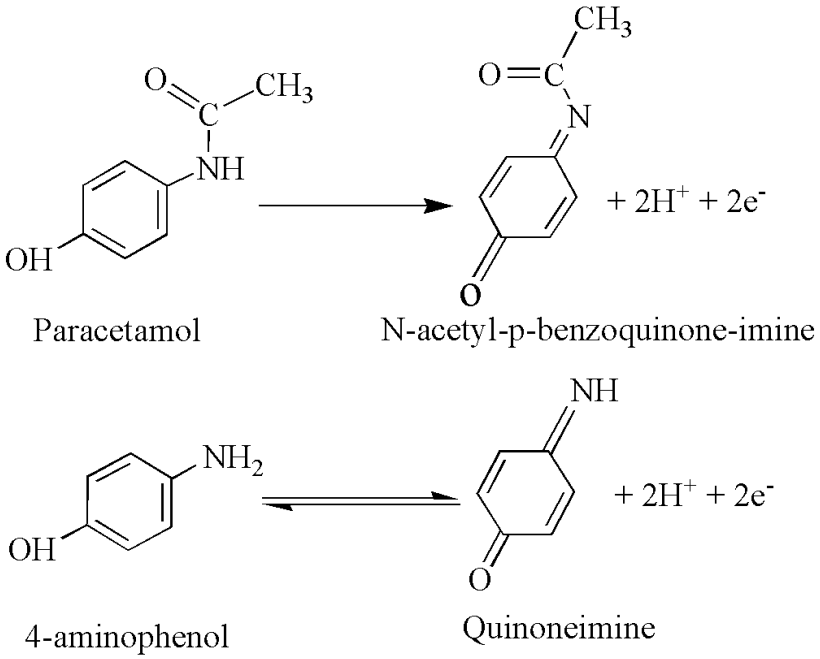

Figure IV.14. Electrochemical reaction mechanism of 4-AP and PA on the Pt–Ni/SPE.

IV.6. Individual and simultaneous electrochemical detection of 4-aminophenol and paracetamol

Cyclic voltammetry and differential pulse voltammetry methods were both performed to study the analytical performances of the developed electrochemical Pt–Ni/SPE sensor for the detection of 4-AP and PA.

IV.6.1. Simultaneous electrochemical detection via cyclic voltammetry

The concentration influence of 4-AP and PA at Pt–Ni/SPE was firstly tested by CV, as given in figure IV.15a. As can be seen, a good separation of 0.42 V is evident between the oxidation peaks of 4-AP and PA, where the current values for the oxidation of both compounds demonstrated a proportional increase corresponding to their respective concentrations.

The linearity between the anodic peak current (I_{pa}) and concentration was demonstrated by plotting them against each other; as depicted in figure IV.15b.

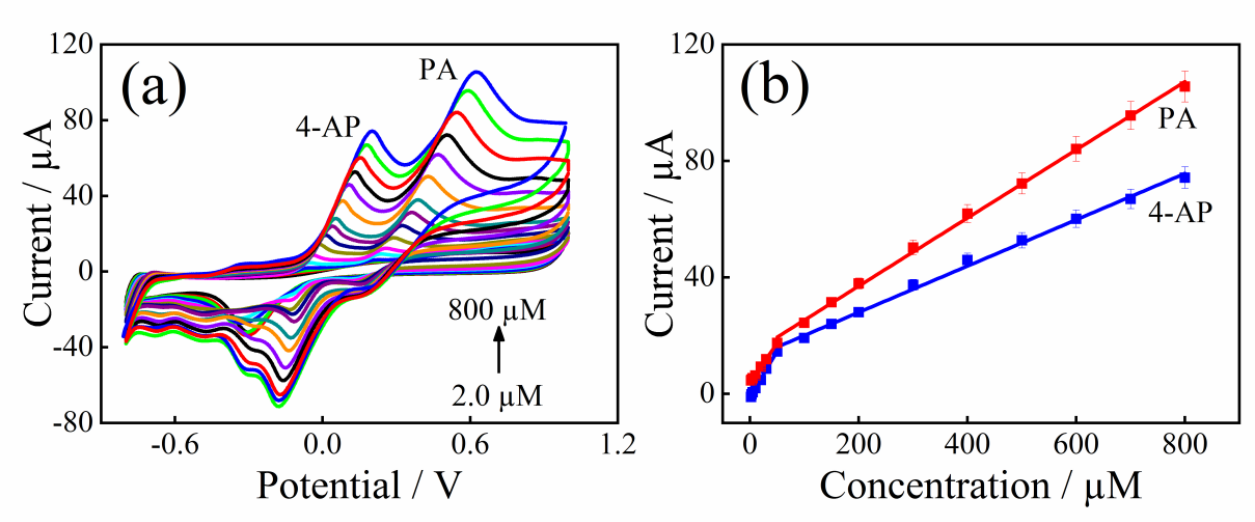

Figure IV.15. (a) CVs of Pt–Ni/SPE for various concentrations of both 4-AP and PA (2.0–800 µM) in PBS (0.1 M, pH 7.4) at 50 mVs^{-1}. (b) Represents the plots of anodic peak currents *vs.* 4-AP and PA concentrations.

The plot clearly showed two distinct linear ranges for each analyte. The first range spanned from 2.0 to 50 µM, and the subsequent range extended from 50 to 800 µM. This behavior could be explained by the interaction between the analyte concentration and the surface characteristics of the modified electrode. At low concentrations of PA, the electrode surface had an abundance of active sites available, allowing for efficient and rapid electron transfer, which resulted in a strong and linear current response. However, at higher concentrations, the electrode surface might have become partially fouled or saturated by the analyte or its oxidation products. This could have hindered electron transfer, thereby reducing sensitivity and leading to the appearance of a second, less steep linear range **[22]**.

Furthermore, the limits of detection (LODs) (*S/N*=3) of the modified Pt–Ni/SPE towards the electro-oxidation process of the two target analytes were estimated as follows: 1.42 µM for 4-AP and 1.47 µM for PA, respectively. Their corresponding linear regression equations and correlation coefficients are listed in table IV.1.

Table IV.1. Linearity ranges, their corresponding linear regression equations and correlation coefficients for 4-AP and PA.

Analyte	Linearity Range	Linear regression equations	Correlation coefficients
4-AP	2.0−50 µM	$I_{4-AP}(\mu A) = 0.316 \times [C_{4-AP}]\ (\mu M) - 1.189$	$R^2 = 0.997$
	50−800 µM	$I_{4-AP}(\mu A) = 0.079 \times [C_{4-AP}]\ (\mu M) + 12.117$	$R^2 = 0.996$
PA	2.0−50 µM	$I_{PA}(\mu A) = 0.266 \times [C_{PA}]\ (\mu M) + 4.02$	$R^2 = 0.997$
	50−800 µM	$I_{PA}(\mu A) = 0.117 \times [C_{PA}]\ (\mu M) + 13.634$	$R^2 = 0.998$

According to these results, the developed Pt–Ni/SPE sensor demonstrated the capability for the simultaneous detection of 4-AP and PA with high sensitivity.

IV.6.2. Individual and simultaneous electrochemical detection via differential pulse voltammetry

The DPV method was also performed in PBS buffer pH 7.4 under optimal experimental conditions to investigate the electrochemical applicability of the recently developed Pt–Ni/SPE sensor for the individual as well as simultaneous determination of 4-AP and PA.

Throughout the individual detection of the two target components within their combined solution, one component's concentration kept changing linearly, while the other maintained constant. In figure IV.16a, it is evident that the DPV peak currents of 4-AP exhibited a linear increase in response to varying concentrations ranging from 1.0 to 250 µM, while the peak currents and potentials of 40 µM PA remained relatively unchanged. The regression equation for 4-AP was derived as:

$$I_p(\mu A) = 0.049\ C\ (\mu M) + 3.445\ (R^2 = 0.995) \qquad \text{Eq.IV.19}$$

With a LOD of 0.95 µM (*S/N* = 3).

Similarly, as depicted in figure IV.16b, when the 4-AP concentration was fixed at 40 µM, the oxidation peak current of PA demonstrated two linear ranges: one from 0.5 to 10 µM and another from 10 to 250 µM. The corresponding regression equations are respectively:

$$I_p(\mu A) = 0.097C\ (\mu M) + 2.280\ (R^2 = 0.994) \qquad \text{Eq.IV.20}$$

$$I_p(\mu A) = 0.035\ C\ (\mu M) + 3.103\ (R^2 = 0.996) \qquad \text{Eq.IV.21}$$

Using the first linear fitting equation, the corresponding LOD was determined to be 0.25 µM (*S/N* = 3).

These results undeniably demonstrated that the addition of one component has minimal impact on the detection of the other.

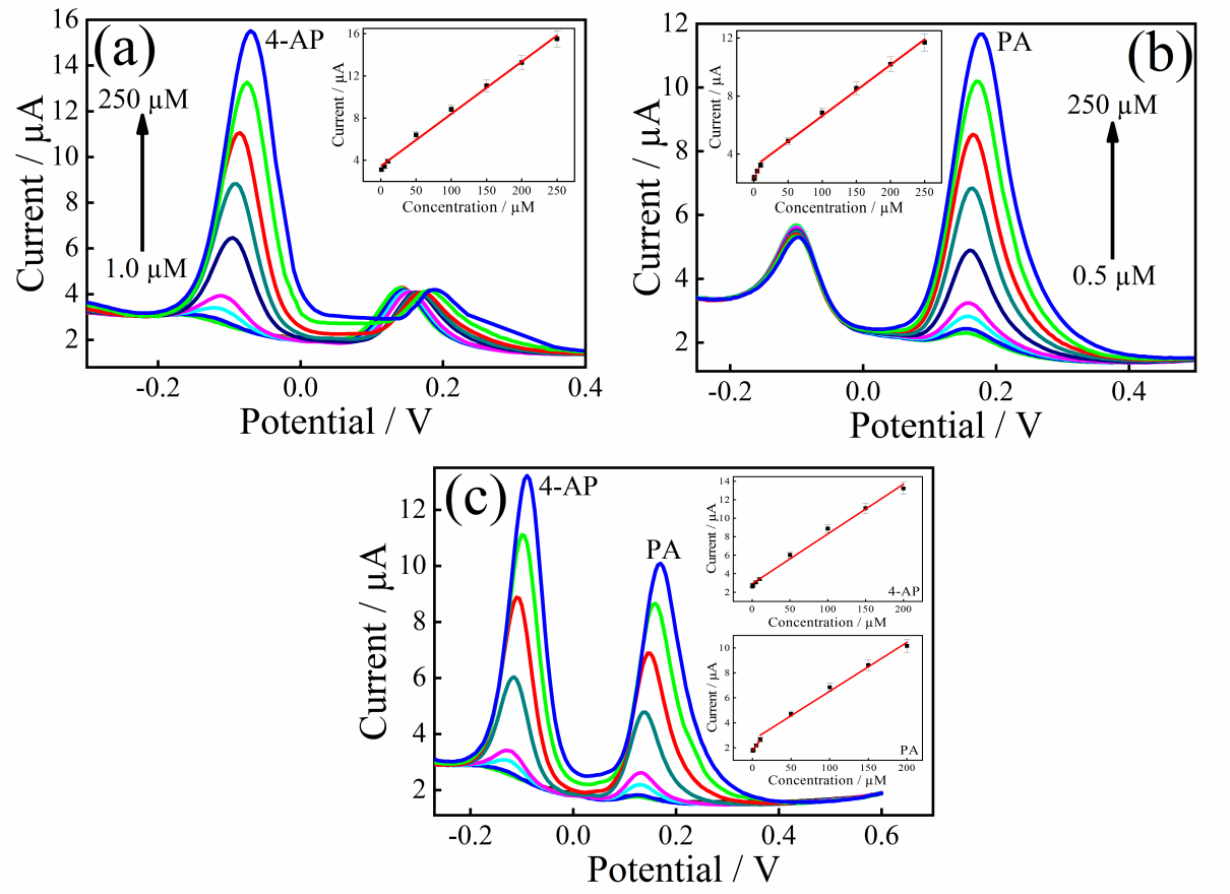

Figure IV.16. DPV profiles of different mixtures of 4-AP and PA. (a) 4-AP (1.0–250 µM) and 40 µM PA, (b) PA (0.5–250 µM) and 40 µM 4-AP, (c) 4-AP and PA (0.5–200 µM) on Pt–Ni/SPE in 0.1 M PBS (pH = 7.4). The insets show the corresponding calibration curves.

In a subsequent step, the Pt–Ni/SPE was used for the simultaneous detection of 4-AP and PA by changing their concentrations synchronously (Figure IV.15c). As evident, the peak-to-peak separation of 0.26 V was sufficiently enough for the simultaneous determination of 4-AP and PA. Moreover, their oxidation peak currents displayed good linear relationships as their concentrations were gradually increased. The corresponding linear equations were depicted as follows:

For 4-AP:

$$I_p(\mu A) = 0.053\ C\ (\mu M) + 2.912\ (0.5 - 200\ \mu M, R^2 = 0.992), \qquad \text{Eq.IV.22}$$

For PA:

$$I_p(\mu A) = 0.089\ C\ (\mu M) + 1.734\ (0.5 - 10\ \mu M, R^2 = 0.998), \quad \text{Eq.IV.23}$$

$$I_p(\mu A) = 0.039\ C\ (\mu M) + 2.611\ (10 - 200\ \mu M, R^2 = 0.991). \quad \text{Eq.IV.24}$$

The determined LOD and sensitivity values of the newly modified Pt–Ni/SPE for 4-AP and PA detection were 0.33 µM, $0.768 \pm 0.01\ \mu A\ \mu M^{-1}\ cm^{-2}$ and 0.23 µM, $1.289 \pm 0.01\ \mu A\ \mu M^{-1}\ cm^{-2}$ correspondingly.

Based on these results, individual or simultaneous determination of 4-AP and PA on Pt–Ni/SPE can be realized with high sensitivity and selectivity.

A similar behavior was observed in the DPV results, as shown in figure IV.16b and c, where PA also exhibited two linear ranges. This trend was consistent with the earlier CV findings, which had already shown two linear segments for both analytes. As previously explained, the initial increase in current at low PA concentrations was likely due to the abundance of active sites on the electrode surface, while the decrease in sensitivity at higher concentrations may have resulted from surface fouling or saturation effects caused by the analyte or its oxidation products.

In comparison to some previous reports in the literature for 4-AP and PA simultaneous detection, our newly Pt–Ni/SPE sensor developed in this work offered several advantages such as a widest linear range, lower detection limit and higher sensitivity, as shown in table IV.2. These results highlighted the immense potential of our novel electrode as a compelling candidate for the simultaneous determination of 4-AP and PA.

Table IV.2. Analytical performances comparison with previously reported modified electrodes for 4-AP and PA determination.

Electrode	Modifier	Technique	pH	Analyte	Linear range (µM)	Detection limit (µM)	Sensitivity (µA µM^{-1})	Ref.
Glassy carbon	Poly(PE)bis-8(hq)[a]	SWV	4.0	PA	0.5−200	0.07	0.0431	**[23]**
				4-AP	3.0−150	0.45	0.096	
Glassy carbon	PEDOT[b]	DPV	7.0	PA	1.0−100	0.4	0.284	**[24]**
				4-AP	4.0−320	1.2	0.094	
Paper-based devices	-	Amp	4.5	PA	0.05−2000	25	-	**[25]**
				4-AP	0.05−2000	10	-	
Glassy carbon	Bis-schiff Base Cobalt	DPV	7.0	PA	5.0−30	1.86	-	**[26]**
				4-AP	5.0-30	2.08	-	
Glassy carbon	CS/Au/Pd/rGO[c]	DPV	8.0	PA	1.0−250	0.3	0.052	**[27]**
				4-AP	1.0−300	0.12	0.134	
Carbon paste	MoO_3-GO[d]	DPV	7.0	PA	1.0−90	0.39	-	**[28]**
				4-AP	1.0−70	0.16	-	
Glassy carbon	CS/Ag-Pd@rGO	DPV	8.0	PA	0.5 −300	0.23	0.009	**[29]**
				4-AP	1.0 −300	0.013	0.024	
Glassy carbon	AuNPs/CNTs-CONH TAPP[e]	DPV	7.0	PA	4.5−500	0.44	0.037	**[30]**
				4-AP	0.08−60	0.025	0.278	
Glassy carbon	S-CTFs@$NiCo_2O_4$[f]	DPV	6.0	PA	2.0−360	0.18	0.031	**[31]**
				4-AP	2.0−360	0.35	0.065	
Graphene oxide	Bio-AgO	DPV	-	PA	1.0−250	0.3	-	**[32]**
				4-AP	1.0−300	12	-	
Screen printed	**Pt−Ni**	**DPV**	**7.4**	**PA**	**0.5−200**	**0.23**	**1.289**	**This work**
				4-AP	**0.5−200**	**0.33**	**0.768**	

[a]Poly(PE)bis-8(hq): Poly (2,2'-(1,4-phenylenedivinylene) bis-8-hydroxyquinaldine);

[b]PEDOT: poly (3,4-ethylenedioxythiophene);

[c]CS/Au/Pd/rGO: Chitosan/gold nanoparticles/palladium/reduced graphene oxide;

[d]MoO_3-GO: MoO_3 nanobelt-graphene oxide;

[e]CNTs-CONH-TAPP: multi-walled carbon nanotubes-tetraaminophenyl porphyrin;

[f]S-CTFs@$NiCo_2O_4$: sulfurbridged-covalent triazine frameworks/nickel cobaltite nanoflowers

IV.7. Simultaneous electrochemical detection of ascorbic acid and paracetamol

The simultaneous analysis of AA and PA at the modified Pt–Ni/SPE electrode was further performed. Figure IV.17a illustrated SWVs obtained from the concurrent addition of different concentrations of AA and PA in 0.1 M acetate buffer (ABS, pH 4.7).

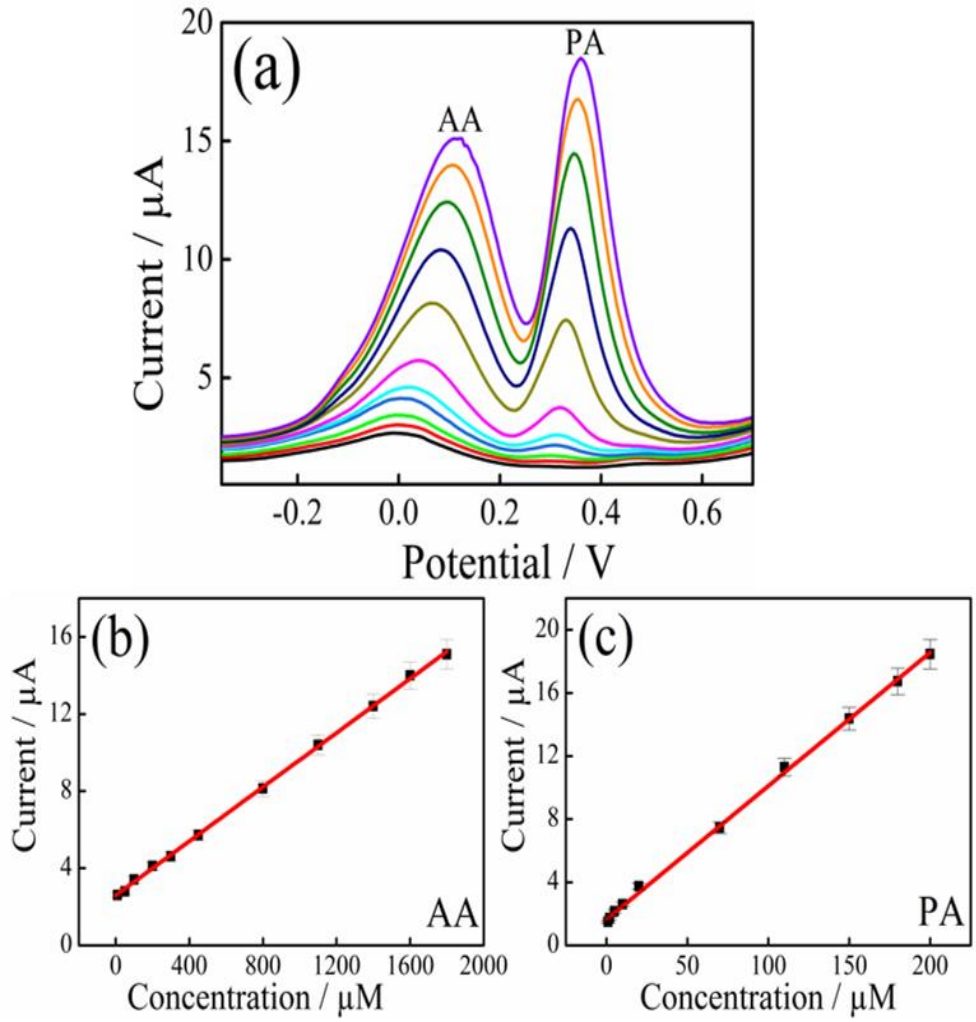

Figure IV.17. (a) SWV profiles at Pt–Ni/SPE in 0.1 M ABS (pH 4.7) containing a mixture of 10–1800 µM AA and 1.0–200 µM PA, (b and c) illustrate the corresponding calibration curves.

The presence of two well-defined oxidation peaks was clearly evident in the data at potential values of 0.11 V and 0.36 V, corresponding to AA and PA, respectively. The observed peak-to-peak separation of 0.25 V was sufficient for the simultaneous quantification of both above species, analogous to the prior determination of 4-AP and PA conducted simultaneously.

In addition, there was a good linear correlation observed between the concentrations of AA and PA and their respective oxidation peak currents. The corresponding linear regression equations were as follows (see figure IV.17b and c):

For AA:

$$I_p(\mu A) = 0.007\ C\ (\mu M) + 2.586\ (10 - 1800\ \mu M, R^2 = 0.999), \qquad \text{Eq.IV.25}$$

For PA:

$$I_p(\mu A) = 0.085\ C\ (\mu M) + 1.631\ (1.0 - 200\ \mu M, R^2 = 0.998) \qquad \text{Eq.IV.26}$$

With the calculated LODs were 7.0 µM and 0.66 µM (*S/N* = 3) for AA and PA, respectively.

IV.8. Simultaneous electrochemical detection of zinc, ascorbic acid and paracetamol

Under the optimal conditions, Pt–Ni/SPE proposed electrode was also employed for the simultaneous quantification of three analytes.

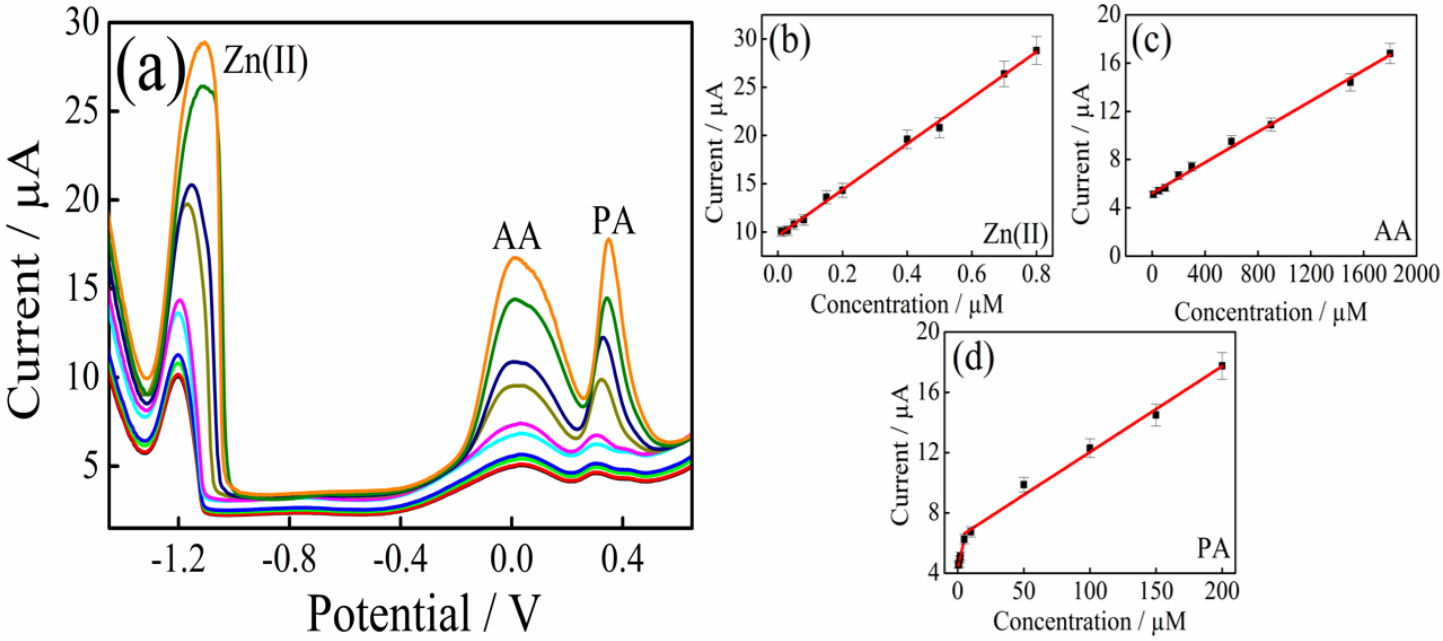

Figure IV.18. (a) SWV profiles at Pt–Ni/SPE in 0.1 M ABS (pH 4.7) containing a mixture of 0.01–0.8 µM Zn(II), 10–1800 µM AA and 0.5–200 µM PA. From b to d illustrate the corresponding calibration curves.

Figure IV.18a displayed the recorded SWVs for a ternary mixture solution comprising varying concentrations of Zn(II), AA, and PA in 0.1 M ABS (pH 4.7).

As observed, each analyte in the mixture displayed distinct oxidation current peaks, and the oxidation peak current intensities increased proportionally with the rising concentrations of all three analytes. The corresponding regression equations were expressed as (see figure IV.18b, c and d):

For Zn(II):

$$I_p(\mu A) = 23.816\ C\ (\mu M) + 9.620\ (0.01 - 0.8\ \mu M, R^2 = 0.997) \qquad \text{Eq.IV.27}$$

For AA:

$$I_p(\mu A) = 0.006\ C\ (\mu M) + 5.213\ (10 - 1800\ \mu M, R^2 = 0.996) \quad \text{Eq.IV.28}$$

For PA:

$$I_p(\mu A) = 0.388\ C\ (\mu M) + 4.322\ (0.5 - 5.0\ \mu M, R^2 = 0.995), \quad \text{Eq.IV.29}$$

$$I_p(\mu A) = 0.0569\ C\ (\mu M) + 6.350\ (5.0 - 200\ \mu M, R^2 = 0.992) \quad \text{Eq.IV.30}$$

The two linear ranges of PA were probably due to the fact that the sensor starts oxidizing Zn(II) and AA first. It was also noteworthy that the sensor exhibited an excellent separation of the detection potential of Zn(II) from that of AA and PA, with an inter-peak potential difference of 1.12 V. This provided the opportunity of detecting of other electroactive analytes within this range.

The estimated LODs values for Zn(II), AA and PA were determined as follows: 0.004 µM; 9.0 µM; and 0.15 µM; respectively.

The outcomes showed that this constructed electrode as a sensor was capable of effectively detecting Zn(II), AA, and PA simultaneously in a single analytical run. When compared to various sensors reported in previous studies (Table IV.3), this sensor exhibited satisfactory linear ranges and detection limits for the target analytes.

Table IV.3. Comparison of the fabricated Pt–Ni/SPE electrode's features with other related sensors reported in the literature for the detection of Zn(II), AA and PA.

Analyte	Electrode	Modifier	Technique	pH	Linear range (µM)	Detection limit (µM)	Ref.
Zn(II)	Screen-printed	Nafion/G/PANI[a]	SWASV	4.5	0.01–4.58	0.01	**[33]**
	Screen-printed carbon nanotubes	Bi[b]	SIA–ASV	4.0	0.18–1.52	0.17	**[34]**
	Carbon paste	$TbFeO_3$/CuO	SWASV	4.8	0.01–1.68	0.007	**[35]**
	Screen-printed carbon	PEDOT/PVA/AgNPs[c]	SWASV	4.6	0.15–1.22	0.09	**[36]**
	Glassy carbon	BiFE[d]	DP–ASV	4.5	0.07–1.68	0.016	**[37]**
	Screen-printed	**Pt–Ni**	**SWV**	**4.7**	**0.01–0.8**	**0.004**	**This work**
AA	Carbon fiber	GEF[e]	DPV	7.0	45.4–1489	24.70	**[38]**
	Glassy carbon	rGO–SnO_2	DPV	7.0	400–1600	38.70	**[39]**
	Carbon fiber paper	Pt@NP–AuSn/Ni	DPV	7.0	200–1200	13.4	**[40]**
	Glassy carbon	GS[f]	DPV	6.8	100–1000	100	**[41]**
	Glassy carbon	MLN[g]/Ag	Amp	7.0	30–1000	15	**[42]**
	Screen-printed	**Pt–Ni**	**SWV**	**4.7**	**10–1800**	**9.0**	**This work**

Table IV.3. Cont.

Analyte	Electrode	Modifier	Technique	pH	Linear range (µM)	Detection limit (µM)	Ref.
	Glassy carbon	MWCNTs/poly(Gly)[h]	DPV	7.0	0.5–10	0.5	**[43]**
	Carbon paste	CNT–P[i]	SWV	5.0	10–100	1.1	**[44]**
PA	Glassy carbon	MWCNT/GO/Poly(Thr)[j]	DPV	7.0	5.0–200	0.16	**[45]**
	Single walled carbon nanotube	AuNP–PGA[k]	DPV	7.2	8.3–145.6	1.18	**[46]**
	Carbon paste	NiCoSalenA[l]	DPV	3.0	1.71–137.6	0.51	**[47]**
	Screen-printed	**Pt–Ni**	**SWV**	**4.7**	**0.5–200**	**0.15**	**This work**

[a]G/PANI: graphene/polyaniline nanocomposite;

[b]Bi: bismuth;

[c]PEDOT/PVA/AgNPs: poly (3,4–ethylenedioxythiophene)/poly vinyl alcohol/silver nanoparticles;

[d]BiFE: bismuth film electrode;

[e]GEF: graphene flower;

[f]GS: graphene/SnO_2 nanocomposite;

[g]MLN: molybdenite;

[h]MWCNTs/ poly(Gly): multi–walled carbon nanotubes/poly (glycine);

[i]CNT–P : carbon nanotube/poly (3–aminophenol);

[j]GO/Poly(Thr): graphene oxide/poly (threonine);

[k]PGA: glutamic acid;

[l]NiCoSalenA: nickel–cobalt salen complexes/NaA nanozeolite

IV.9. Method validation

The square wave voltammetry was used in all the following experiments because of its higher sensitivity than CV and DPV.

IV.9.1. Reproducibility, repeatability, stability and interference of Pt–Ni/SPE sensors

Reproducibility, repeatability, stability and interference studies were used to identify the performance of the proposed detection electrode.

IV.9.1.1. Reproducibility

Screen-printed electrodes are widely used in various biomedical and environmental analyses, which are unfortunately disposable with only one use. Thus, the development of sensors with multiple uses was considered desirable. For this reason the fabrication reproducibility of Pt-Ni/SPE was studied by analyzing the electrochemical responses of 0.6 µM Zn(II), 900 µM AA and 50 µM PA on five modified electrodes. The electrodes were prepared separately under identical conditions, and the results were shown in figure IV.19.

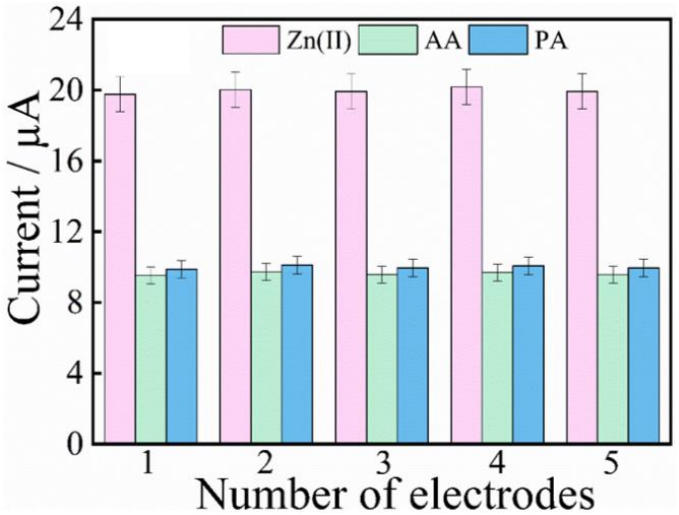

Figure IV.19. Reproducibility test on Pt–Ni/SPE in the presence of a ternary mixture containing 0.6 µM Zn(II), 900 µM AA and 50 µM PA.

Figure IV.19 showed that the peak oxidation currents of Zn(II), AA and PA were identical for all five screen-printed electrodes modified with Pt-Ni NPs. This consistency in electrochemical responses among different electrodes was an indicator of the sensor's reproducibility. The relative standard deviation (RSD) of SWV response was 4.0% for Zn(II), 2.3% for AA, and 1.5% for PA, separately, indicating that the Pt–Ni/SPE possessed outstanding fabrication reproducibility, which is essential for ensuring the reliability and the accuracy of electrochemical measurements in the applications of detection of Zn(II), AA, and PA.

IV.9.1.2. Repeatability

The repeatability of the developed electrode was also investigated using a single Pt–Ni/SPE electrode for five successive measurements in ABS samples containing the same ternary mixture (see figure IV.20). Pt-Ni/SPE electrode produced consistent current responses across all five tests, and the RSD values for Zn(II), AA and PA were 1.5 %, 1.1 % and 1.2%, respectively, confirming the decent repeatability of the fabricated sensor.

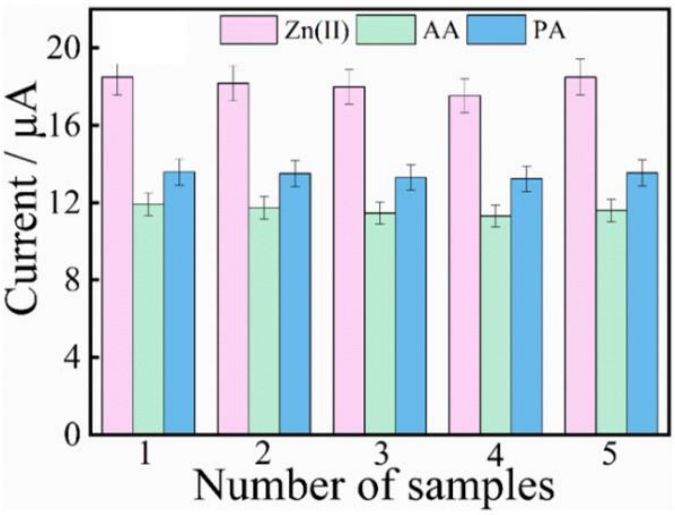

Figure IV.20. Repeatability test on Pt–Ni/SPE in the presence of a ternary mixture containing 0.6 µM Zn(II), 900 µM AA and 50 µM PA.

IV.9.1.3. Stability

Stability is an important property for long-term sensor operation. To measure the long term stability of the proposed modified electrode, Pt–Ni/SPE was stored at room temperature for 8 weeks, and only a slight decrease in the oxidation peak currents of Zn(II), AA and PA was observed (see figure IV.21), with reductions of around 2.92%, 2.85% and 3.0% of the initial SWV responses respectively, clarifying the excellent long-term stability of the modified electrode.

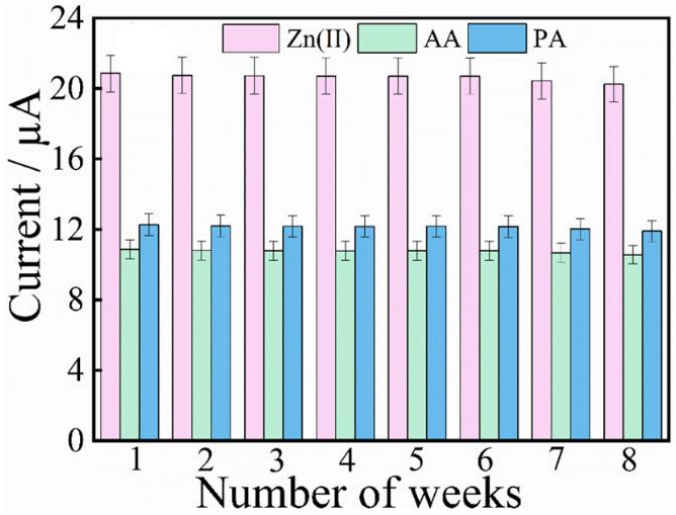

Figure IV.21. Stability test on Pt–Ni/SPE in the presence of a ternary mixture containing 0.6 µM Zn(II), 900 µM AA and 50 µM PA.

IV.9.1.4. Interference

The selectivity of the Pt–Ni/SPE fabricated sensor was also investigated by adding potential foreign substances commonly found in food, beverages, or possibly present in pharmaceutical tablets. These substances comprised diverse ions and organic substances, including but not limited to Na^+, K^+, Cl^-, SO_4^{2-}, caffeine, glucose, fructose and galactose. Additionally, examination included physiological interfering compounds, such as citric acid. All of these substances may exist in similar environment with the target analytes.

As presented in figure IV.22, 1.0 mM of Na^+, K^+, Cl^-, SO_4^{2-}, Caf, Cit, and 0.5 mM of Glu, Fru, and Gal did not affect the oxidation signals of 0.6 µM Zn(II), 900 µM AA and 50 µM PA (changes in signal remained under 10%). The results demonstrated that the Pt–Ni/SPE sensor had no interfering ability and good selectivity toward Zn(II), AA and PA simultaneous detection.

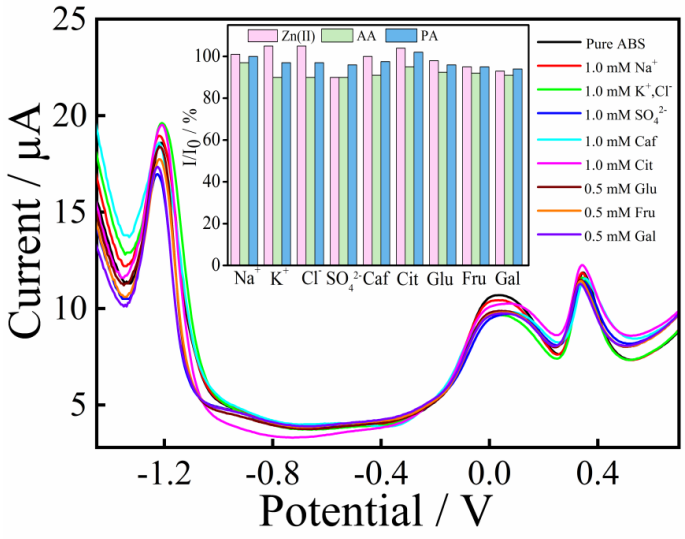

Figure IV.22. Selectivity test of Pt–Ni/SPE sensor by SWV for the simultaneous determination of Zn(II), AA and PA. The inset illustrates the corresponding calibrated histogram of peak current.

IV.9.2. Analytical applications in pharmaceutical tablet and blood samples

IV.9.2.1. Analytical applications in pharmaceutical tablet samples

The feasibility of the designed electrochemical sensor was evaluated using both pharmaceutical tablet samples and corresponding standard samples with identical analyte concentrations. Specifically, the pharmaceutical tablet samples included Efferalgan Vitamin C tablet (200 mg AA + 500 mg PA), a Vitamin C with Zinc complementary dietary supplement (10 mg Zn(II) + 250 mg AA), and Doliprane tablet (1000 mg PA).

As shown in figure IV.23, the Pt–Ni/SPE modified electrode exhibited consistent current responses across all sample types, indicating its robust performance. These findings suggested the potential suitability of the sensor for real applications.

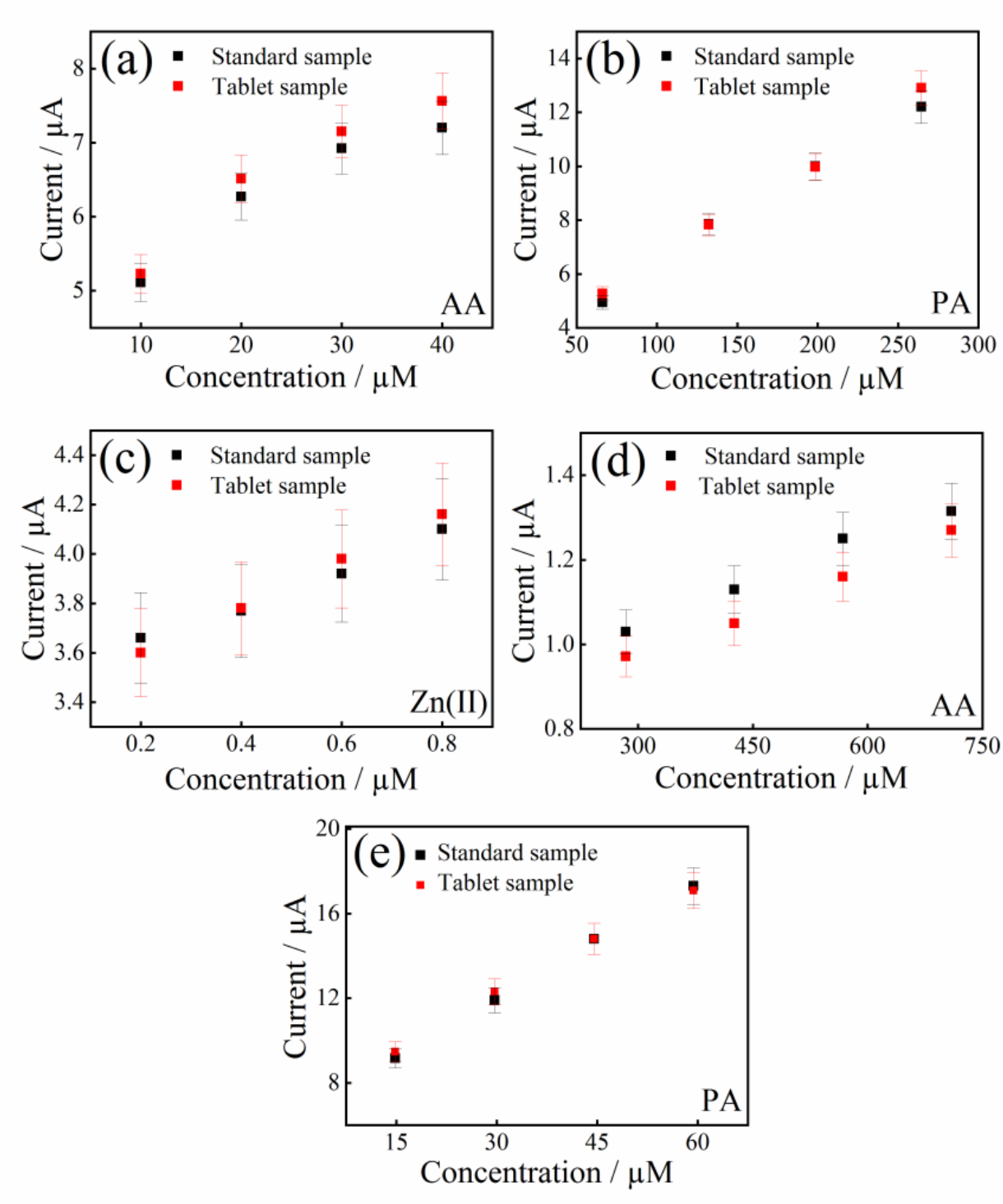

Figure IV.23. (a–e) Sensor responses to identical analyte concentrations in tablet samples (red) *vs.* standard samples (black).

To further validate the practical utility of the Pt–Ni/SPE sensor, the concentrations of various analytes in the aforementioned pharmaceutical tablets were determined using the standard addition method, facilitated by SWV technique under optimized conditions. The obtained results were summarized in table IV.4 and the samples pre-treatment process was detailed in Chapter III.

It can be seen that the determination results were in quite agreement with the specified target contents given by the manufacturer with the recoveries ranged from 96.2 to 109%. In addition, the RSD values of each sample for three time's parallel detections were less than 2.89%. It is noteworthy that the additives contained in the tablets did not exhibit any interference effect on the determination of analytes in the commercial samples.

These results illustrated that the Pt–Ni/SPE developed sensor possessed reliability and accuracy in the determination of PA, AA and Zn(II) in pharmaceutical tablets.

Table IV.4. Results for the determination of 4-AP, PA, AA and Zn(II) in pharmaceutical tablet samples using Pt–Ni/SPE proposed sensor (n=3).

Sample	Species	Reported content (mg per tablet)	Determined (mg per tablet)	Recovery (%)	RSD (%) (n = 3)
Efferalgan	PA	500	481	96.2	0.68
Vitamin C	AA	200	195.8	97.9	1.41
Vitamin C	Zn(II)	10	10.9	109	0.25
with Zinc	AA	250	263	105.2	2.89
Doliprane	PA	1000	987	98.7	0.94
	4-AP	ND	ND	-	-

ND: not detected

IV.9.2.2. Analytical applications in blood samples

Furthermore, recovery experiments for the simultaneous determination of Zn(II), AA, and PA in human serum samples were conducted using the same parameters as those employed in the SWV experiment with the Pt–Ni/SPE sensor. Certain amounts of Zn(II), AA and PA were spiked in human serum sample, and the analysis results were listed in table IV.5. The recovery rates were in the range of 95.4–103.5% and the correlation standard deviation was less

than 4%. The results confirmed that the Pt–Ni/SPE had great potential for the detection of Zn(II), AA and PA in practical serum.

Table IV.5. The obtained recovery values of Zn(II), AA, and PA in human plasma samples.

Sample	Analyte (µM)						Recovery (%)		
	Added			Found					
	Zn(II)	AA	PA	Zn(II)	AA	PA	Zn(II)	AA	PA
Serum 1	0 0.15	0 1000	0 100	ND 0.14	ND 1033	ND 95.6	- 96.1	- 103.5	- 95.8
Serum 2	0 0.10	0 500	0 50	ND 0.098	ND 489	ND 47.7	- 98	- 97.8	- 95.4

IV.10. Conclusion

In the first part of this chapter, we characterized screen-printed electrodes modified with platinum and nickel nanoparticles using various physicochemical techniques, including FE-SEM, TEM, EDX, XRD, and AFM, to ascertain their morphology, structure, and crystallography. The electrodeposition technique successfully created a bimetallic sensor architecture with Pt and Ni nanodeposits, which exhibited remarkable electrochemical properties.

The FE–SEM images demonstrated a uniform distribution of numerous platinum (Pt) nanodeposits across the substrate, with an average size of around 300 nm. In contrast, nickel (Ni) nanoparticles were present in limited quantities and had a smaller diameter. Additionally, the TEM images of the modified electrode further validated the successful synthesis of the nanocomposite. The EDX spectrum of the fabricated Pt–Ni/SPE electrode provided clear elemental evidence, revealing a substantial platinum content of 97.17%, while nickel accounted for only 2.83%. Moreover, XRD analysis confirmed the successful formation of Pt–Ni nanodeposits on the surface of the graphite SPE electrode. AFM imaging of both the unmodified and Pt–Ni modified SPE indicates that the surface of the modified electrode exhibited moderate homogeneity, reflecting a smooth and even distribution of the Pt–Ni particles.

Cyclic voltammetry and electrochemical impedance spectroscopy were employed to elucidate the electrochemical properties of the various modified electrodes in a 0.1 M KCl solution containing 0.5 mM $Fe(CN)_6^{-3/-4}$ as a redox probe. The results confirmed that the Pt–Ni/SPE electrode possessed a larger active surface area and enhanced conductivity compared to the other electrodes.

In summary, the first part of this chapter presented the development of a novel and effective electrochemical strategy for the simultaneous detection of paracetamol in the presence of its toxic impurities (4-aminophenol) and commonly co-formulated drugs (ascorbic acid and zinc) in pharmaceutical formulations and human blood samples. This was achieved using a pioneering Pt–Ni/SPE sensor in conjunction with differential pulse voltammetry and square wave voltammetry techniques.

The designed Pt–Ni/SPE sensor demonstrated exceptional electro-catalytic activity for the electrochemical sensing of 4-aminophenol, paracetamol, ascorbic acid, and zinc(II), exhibiting high sensitivity, low limits of detection, and a wide linear range, making it particularly suitable for sensor applications. By leveraging a dual-effect approach, the sensor effectively detected Zn(II) via Pt and 4-aminophenol, ascorbic acid, and paracetamol through Pt–Ni interactions. Moreover, the sensor adeptly separated the detection potentials of Zn(II), ascorbic acid, and paracetamol, achieving a notable inter-peak difference of 1.12 V, which facilitated the detection of other electroactive analytes within this range.

Overall, the Pt–Ni/SPE sensor exhibited excellent sensitivity, stability, repeatability, and reproducibility, with minimal interference observed in the detection of target analytes, as corroborated by interference studies. Consequently, the sensor effectively analyzed paracetamol, 4-aminophenol, ascorbic acid, and zinc in pharmaceutical and human blood samples, yielding satisfactory recovery rates.

References

[1] Y. Zhao, Y. E, L. Fan, Y. Qiu, S. Yang, A new route for the electrodeposition of platinum–nickel alloy nanoparticles on multi-walled carbon nanotubes, Electrochim. Acta 52 (2007) 5873–5878.
[2] M.L. Chelaghmia, M. Nacef, A.M. Affoune, Ethanol electrooxidation on activated graphite supported platinum–nickel in alkaline medium, J. Appl. Electrochem. 42 (2012) 819–826.
[3] R. Velayutham, K. Palanisamy, R. Manikandan, T. Velumani, S.K. AP, J. Puigdollers, B.C. Kim, Synergetic effect induced/tuned bimetallic nanoparticles (Pt-Ni) anchored graphene as a catalyst for oxygen reduction reaction and scalable SS-314L serpentine flow field proton exchange membrane fuel cells (PEMFCs), Mater. Sci. Eng. B. 282 (2022) 115780.
[4] Q. Liu, W. Qin, Z. Yan, J. Gao, E. Wang, Porous $Ni(OH)_2$ permselective membrane to identify the mechanism of hydrogen evolution reaction in buffered solution, Electrochim. Acta 401 (2022) 139444.
[5] L. Zhang, X. Ma, J. Liu, J. Gu, H. Suo, C. Zhao, X. Wang, Achieving Ni@(Pt/$Ni(OH)_2$) ternary nanoflowers derived from Ni nanoflowers for electrochemical ammonia–nitrogen detection in the aqueous environment, Microchem. J. 200 (2024) 110401.
[6] S. Liu, Y. Xiang, J. Liu, Z. Du, S. Fang, L. Gao, F. Fu, X. Gao, X. Jian, Hydrogen spillover in Pt/$Ni(OH)_2$/$Mo_2TiC_2T_x$ electrocatalyst improves pH-universal hydrogen evolution reaction, Int. J. Hydrogen Energ. 63 (2024) 500–509.
[7] M.A.A. Rahim, H.B. Hassan, R.M.A. Hameed, Graphite electrodes modified with platinum–nickel nano-particles for methanol oxidation, Fuel Cells 4 (2007) 298–305.
[8] R.S. Nicholson, Theory and application of cyclic voltammetry for measurement of electrode reaction kinetics, Anal. Chem. 37 (1965) 1351–1355.
[9] L.R. Cumba, C.W. Foster, D.A.C. Brownson, J.P. Smith, J. Iniesta, B. Thakur, D. R. do Carmo, C.E. Banks, Can the mechanical activation (polishing) of screen printed electrodes enhance their electroanalytical response? Analyst 141 (2016) 2791–2799.
[10] R.D. Crapnell, C.E. Banks, Perspective: what constitutes a quality paper in electroanalysis? Talanta 4 (2021) 100065.
[11] P. Shaikshavali, T.M. Reddy, V.N. Palakollu, R. Karpoormath, Y.S. Rao, G. Venkataprasad, T.V. Gopal, P. Gopal, Multi walled carbon nanotubes supported CuO–Au hybrid nanocomposite for the effective application towards the electrochemical determination of acetaminophen and 4-aminophenol, Synth. Met. 252 (2019) 29–39.
[12] Y. Sun, H. Yang, X. Yu, H. Meng, X. Xu, A novel non-enzymatic amperometric glucose sensor based on hollow Pt–Ni alloy nanotubes array electrode with enhanced sensitivity, RSC Adv. 86 (2015) 69899–70702.
[13] Q. Sheng, D. Liu, J. Zheng, A nonenzymatic electrochemical nitrite sensor based on Pt nanoparticles loaded Ni(OH) 2 /multi-walled carbon nanotubes nanocomposites, J. Electroanal. Chem. 796 (2017) 9–16.
[14] Y.V.M. Reddy, B. Sravani, H. Maseed, T. Łuczak, M. Osi´ nska, L. SubramanyamSarma, V.V.S.S. Srikanth, G. Madhavi, Ultrafine Pt–Ni bimetallic nanoparticles anchored on reduced graphene oxide nanocomposites for boosting electrochemical detection of dopamine in biological samples, New J. Chem. 20 (2018) 16387–17140.
[15] J. Ahmed, M.M. Rahman, I.A. Siddiquey, A.M. Asiri, M.A. Hasnat, Efficient hydroquinone sensor based on zinc, strontium and nickel based ternary metal oxide (TMO) composites by differential pulse voltammetry, Sens. Actuators B Chem. 256 (2018) 383–392.
[16] N.F. Atta, A. Galal, D.M. El-Said, A novel electrochemical sensor for paracetamol based on β-cyclodextrin/nafion®/polymer nanocomposite, Int. J. Electrochem. Sci. 10 (2015) 1404–1419.
[17] Y. Song, Y. Zhang, J. Li, C. Tan, Y. Li, Preparation of poly ionic liquid-mesoporous carbon nanospheres and its application in simultaneous determination of hydroquinone and catechol, and detection of paracetamol, J. Electroanal. Chem. 865 (2020) 114157.
[18] Q. Guan, H. Guo, N. Wu, Y. Cao, M. Wang, L. Zhang, W. Yang, Highly sensitive determination of acetaminophen and 4-aminophenol based on COF/3D NCNF-T/ Au NPs composite electrochemical sensing platform, Colloids Surf. A Physicochem. Eng. Asp. 630 (2021) 127624.
[19] E. laviron, General expression of the linear potential sweep voltammogram in the case of diffusionless electrochemical systems, J. Electroanal. Chem. 101 (1979) 19–28.

[20] Q. Guan, H. Guo, N. Wu, Y. Cao, M. Wang, L. Zhang, W. Yang, Highly sensitive determination of acetaminophen and 4-aminophenol based on COF/3D NCNF-T/ Au NPs composite electrochemical sensing platform, Colloids Surf. A Physicochem. Eng. Asp. 630 (2021) 127624.
[21] Abdi, M.L. Chelaghmia, R. Kihal, C.E. Banks, A.G.M. Ferrari, H. Fisli, M. Nacef, A.M. Affoune, M.E.H. Benhamza, Simultaneous determination of 4-aminophenol and paracetamol based on CS–Ni nanocomposite-modified screen-printed disposable electrodes, Monatsh, Chemie 154 (2023) 563–575.
[22] H. Guo, T. Fan, W. Yao, W. Yang, N. Wu, H. Liu, M. Wang, W. Yang, Simultaneous determination of 4-aminophenol and acetaminophen based on high electrochemical performance of ZIF–67/MWCNT–COOH/Nafion composite, Microchem. J. 158 (2020) 105262.
[23] H. Filik, S. Aydar, A.A. Avan, Poly(2,2′-(1,4-phenylenedivinylene) Bis-8-hydroxyquinaldine) modified glassy carbon electrode for the simultaneous determination of paracetamol and p-aminophenol, Anal. Lett. 48 (2015) 2581−2596.
[24] S. Mehretie, S. Admassie, T. Hunde, M. Tessema, T. Solomon, Simultaneous determination of N-acetyl-p-aminophenol and p-aminophenol with poly(3,4-ethylenedioxythiophene) modified glassy carbon electrode, Talanta 85 (2011) 1376−1382.
[25] L.Y. Shiroma, M. Santhiago, A.L. Gobbi, L.T. Kubota, Separation and electrochemical detection of paracetamol and 4-aminophenol in a paper-based microfluidic device, Anal. Chim. Acta 725 (2012) 44−50.
[26] Q. Liang, Z. Liu, C. Liang, G.C. Han, S. Zhang, X.Z. Feng, Electrochemical simultaneous detection of paracetamol and 4-aminophenol based on bis-schiff base cobalt complex, Int. J. Electrochem. Sci. 14 (2019) 7178−7201.
[27] H. Wang, S. Zhang, S. Li, J. Qu, Electrochemical sensor based on palladium-reduced graphene oxide modified with gold nanoparticles for simultaneous determination of acetaminophen and 4-aminophenol, Talanta 178 (2018) 188−194.
[28] M. Vazan, J. Tashkhourian, B. Haghighi, A novel electrochemical sensor based on MoO_3 nanobelt-graphene oxide composite for the simultaneous determination of paracetamol and 4-aminophenol, Diam. Relat. Mater. 140 (2023) 110549.
[29] N. Dou, S. Zhang, J. Qu, Simultaneous detection of acetaminophen and 4-aminophenol with an electrochemical sensor based on silver-palladium bimetal nanoparticles and reduced graphene oxide, RSC Adv. 9 (2019) 31440−31446.
[30] P. Shi, R. Xue, Y. Wei, X. Lei, J. Ai, T. Wang, Z. Shi, X. Wang, Q. Wang, F.M. Soliman, H. Guo, W. Yang, Gold nanoparticles/tetraaminophenyl porphyrin functionalized multiwalled carbon nanotubes nanocomposites modified glassy carbon electrode for the simultaneous determination of p-acetaminophen and p-aminophenol, Arab. J. Chem. 13 (2020) 1040−1051.
[31] L. Sun, H. Guo, Z. Pan, B. Liu, N. Wu, Y. Liu, Z. Lu, X. Wei, W. Yang, Design of $NiCo_2O_4$ nanoflowers decorated sulfurbridged covalent triazine frameworks nanocomposites for electrochemical simultaneous detection of acetaminophen and 4-aminophenol, Microchem. J. 182 (2022) 107879.
[32] S.Y. Ahmed, P. Emerson, M. Selvaraj, W. Sultana, D. Bharathi, Effects of AgO incorporation with 2D rGO nanocomposite characteristics and its beneficial electrochemical detection of acetaminophen, Inorg. Chem. Commun. 164 (2024) 112453.
[33] N. Ruecha, N. Rodthongkum, D.M. Cate, J. Volckens, O. Chailapakul, C.S. Henry, Sensitive electrochemical sensor using a graphene-polyaniline nanocomposite for simultaneous detection of Zn(II), Cd(II), and Pb(II), Anal. Chim. Acta 874 (2015) 40–48.
[34] U. Injang, P. Noyrod, W. Siangproh, W. Dungchai, S. Motomizu, O. Chailapakul, Determination of trace heavy metals in herbs by sequential injection analysis anodic stripping voltammetry using screen-printed carbon nanotubes electrodes, Anal. Chim. Acta 668 (2010) 54–60.
[35] H.M. Moghaddam, M. Amiri, H.A. Javar, Q.A. Yousif, M.S. Niasari, Green synthesis and characterization of Tb-Fe-O-Cu ceramic nanocomposite and its application in simultaneous electrochemical sensing of zinc, cadmium and lead, Arab. J. Chem. 15 (2022) 103988.
[36] U. Ngoensawat, T. Pisuchpen, Y. Sritana-anant, N. Rodthongkum, V.P. Hoven, Conductive electrospun composite fibers based on solid-state polymerized Poly (3,4-ethylenedioxythiophene) for simultaneous electrochemical detection of metal ions, Talanta 241 (2022) 123253.
[37] N.M. Thanh, N.V. Hop, N.D. Luyen, N.H. Phong, T.T.T. Toan, Simultaneous determination of Zn(II), Cd(II), Pb(II), and Cu(II) using differential pulse anodic stripping voltammetry at a bismuth film-modified electrode, Adv. Mater. Sci. Eng. 11 (2019) 1826148.

[38] J. Du, R. Yue, F. Ren, Z. Yao, F. Jiang, P. Yang, Y. Du, Novel graphene flowers modified carbon fibers for simultaneous determination of ascorbic acid, dopamine and uric acid, Biosens. Bioelectron. 53 (2014) 220–224.
[39] R. Sha, S. Badhulika, Facile green synthesis of reduced graphene oxide/tin oxide composite for highly selective and ultra-sensitive detection of ascorbic acid, J. Electroanal. Chem. 816 (2018) 30–37
[40] H. Yang, J. Zhao, M. Qiu, P. Sun, D. Han, L. Niu, G. Cui, Hierarchical bi-continuous Pt decorated nanoporous Au–Sn alloy on carbon fiber paper for ascorbic acid, dopamine and uric acid simultaneous sensing, Biosens. Bioelectron. 124–125 (2019) 191–198.
[41] Y.L. Xie, J. Yuan, H.L. Ye, P. Song, S.Q. Hu, Facile ultrasonic synthesis of graphene/ SnO nanocomposite and its application to the simultaneous electrochemical determination of dopamine, ascorbic acid, and uric acid, J. Electroanal. Chem. 749 (2015) 26–30.
[42] R. Zhao, Y. Wang, Z. Zhang, Y. Hasebe, D. Tao, A glassy carbon electrode modified with molybdenite and Ag nanoparticle composite for selectively sensing of ascorbic acid, Anal. Sci. 35 (2019) 733–738.
[43] P.V. Narayana, T.M. Reddy, P. Gopal, G.R. Naidu, Electrochemical sensing of paracetamol and its simultaneous resolution in the presence of dopamine and folic acid at a multi-walled carbon nanotubes/poly(glycine) composite modified electrode, Anal. Methods 6 (2014) 9459–9468.
[44] I. Noviandri, R. Rakhmana, Carbon paste electrode modified with carbon nanotubes and poly(3–aminophenol) for voltammetric determination of paracetamol, Int. J. Electrochem. Sci. 7 (2012) 4479–4487.
[45] G.V. Prasad, V. Vinothkumar, S.J. Jang, D.E. Oh, T.H. Kim, Multi-walled carbon nanotube/graphene oxide/poly(threonine) composite electrode for boosting electrochemical detection of paracetamol in biological samples, Microchem. J. 184 (2023) 108205.
[46] M.P.N. Bui, C.A. Li, K.N. Han, X.H. Pham, G.H. Seong, Determination of acetaminophen by electrochemical co-deposition of glutamic acid and gold nanoparticles, Sens. Actuators B Chem. 174 (2012) 318–324.
[47] N. Masihpour, S.K. Hassaninejad-Darzi, A. Sarvary, Nickel–cobalt salen organometallic complexes encapsulated in mesoporous NaA nanozeolite for electrocatalytic quantification of ascorbic acid and paracetamol, J. Inorg. Organomet. Polym Mater. 33 (2023) 2661–2680.

Part B

Development of an innovative electrochemical sensor utilizing Pt-Ni nanostructured screen-printed graphene electrode for the simultaneous and individual electrochemical detection of 4-aminophenol, paracetamol, and ascorbic acid

IV.1. Introduction

As part of a complementary study, screen-printed graphene electrodes were modified with platinum and nickel nanoparticles (Pt-Ni NPs) through the electrodeposition method outlined in Part A. This sensor is designed to detect 4-aminophenol, paracetamol, and ascorbic acid both individually and simultaneously.

After characterizing the structural and morphological properties of the synthesized material, electrochemical detection of the target analytes was conducted using the Pt-Ni modified graphene screen-printed electrodes (Pt-Ni/SPGE) through cyclic voltammetry (CV) and square wave voltammetry (SWV) techniques.

IV.2. Structural and morphological characterization of Pt−Ni modified graphene SPEs

The structure and morphology of the modified graphene screen-printed electrodes were characterized using FE-SEM, EDX, and AFM techniques.

FE-SEM images of the modified graphene screen-printed electrode (Pt-Ni/SPGE), prepared by the simultaneous electrodeposition technique—identical to the method used for modifying graphite screen-printed electrodes—were shown in figure IV.1. Figure IV.1a demonstrated that the graphene surface is uniformly covered with well-dispersed Pt and Ni spherical particles. The high-magnification FE-SEM image (Figure IV.1b) revealed a homogeneous distribution of Pt nanodeposits across the substrate, with an average size of approximately 155 nm. In contrast, fewer Ni nanoparticles with a smaller diameter of 51.6 nm were observed.

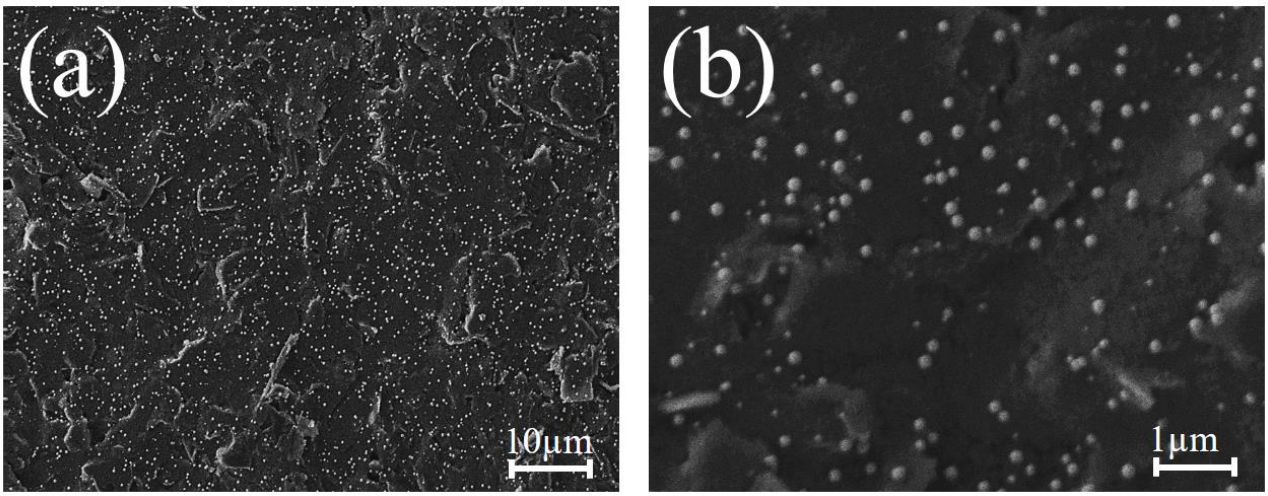

Figure IV.1. (a) FE–SEM image of Pt–Ni modified graphene SPE, (b) high-magnification FE–SEM image of Pt–Ni modified graphene SPE.

Similarly, the EDX spectrum of the Pt–Ni/SPGE (Figure IV.2) was consistent with the results obtained in Part A and provided elemental evidence confirming the successful modification of graphene with the bimetallic nanoparticles. The atomic ratios of Pt and Ni were estimated to be approximately 98.28% and 1.72%, respectively.

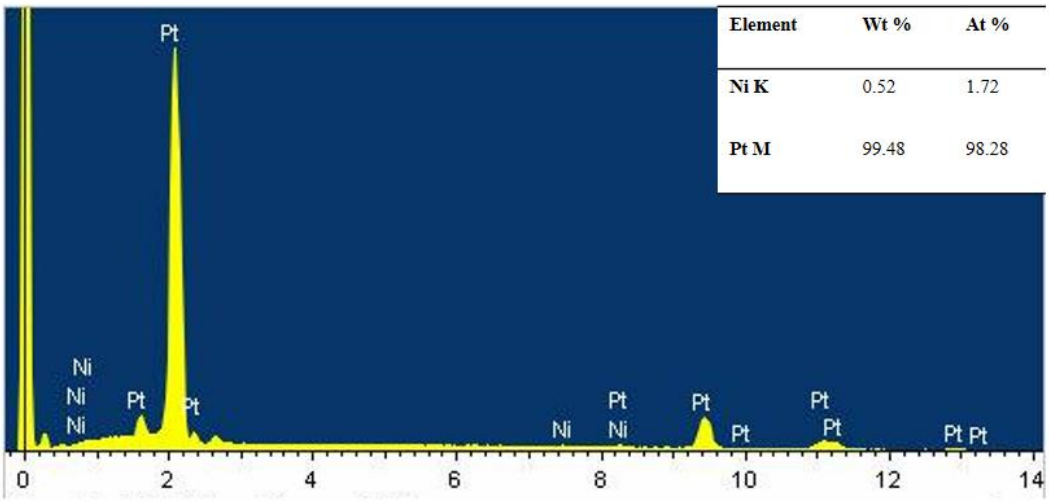

Figure IV.2. EDX spectrum of Pt–Ni/SPGE.

Additionally, AFM analysis was conducted on both unmodified and Pt-Ni modified graphene SPE. Figures IV.3a and b showed the two-dimensional (2D) and three-dimensional (3D) AFM images of the unmodified SPE, while figures IV.3c and d displayed the 2D and 3D images of the Pt-Ni modified graphene SPE, respectively. A comparison of the 3D AFM images in figures IV.3b and d revealed the relatively rough surface of the unmodified SPE, while the modified electrode surface appeared more homogeneous, indicating the smooth distribution of Pt-Ni particles. This observation supported previous findings of successful Pt-Ni nanodeposit loading onto the graphene screen-printed electrode surface and aligned with the graphite modification results, demonstrating the effectiveness of the electrodeposition technique developed in this study.

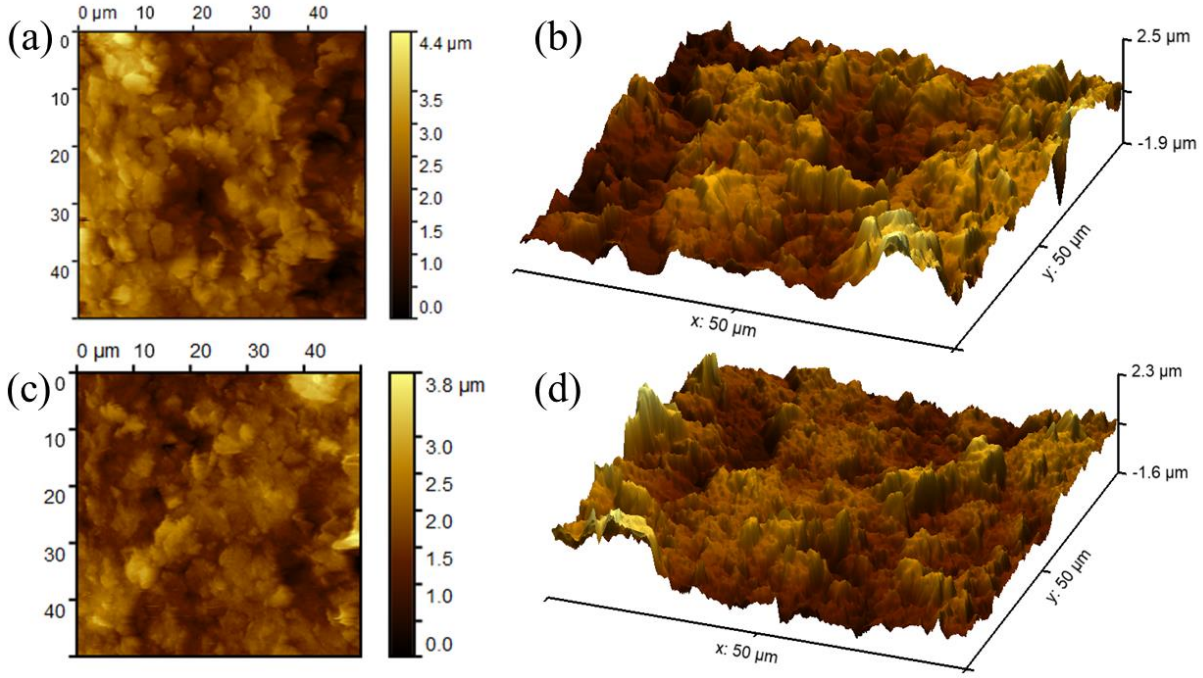

Figure IV.3. (a) 2D, (b) 3D AFM images of bare SPE; (c) 2D, (d) 3D AFM images of Pt–Ni modified graphene SPE.

IV.3. Individual and simultaneous electrochemical detection of target analytes

To assess the analytical performance of the modified graphene screen-printed sensor (Pt-Ni/SPGE) developed in this study for the detection of AA, 4-AP, and PA, cyclic voltammetry and square wave voltammetry techniques were employed.

IV.3.1. Individual electrochemical detection of ascorbic acid, 4-aminophenol and paracetamol

The electrooxidation of different concentrations of AA, 4-AP, and PA on the modified graphene electrode (Pt–Ni/SPGE) was investigated in PBS buffer at pH 7.4. The resulting CVs were shown in figures IV.4a-c.

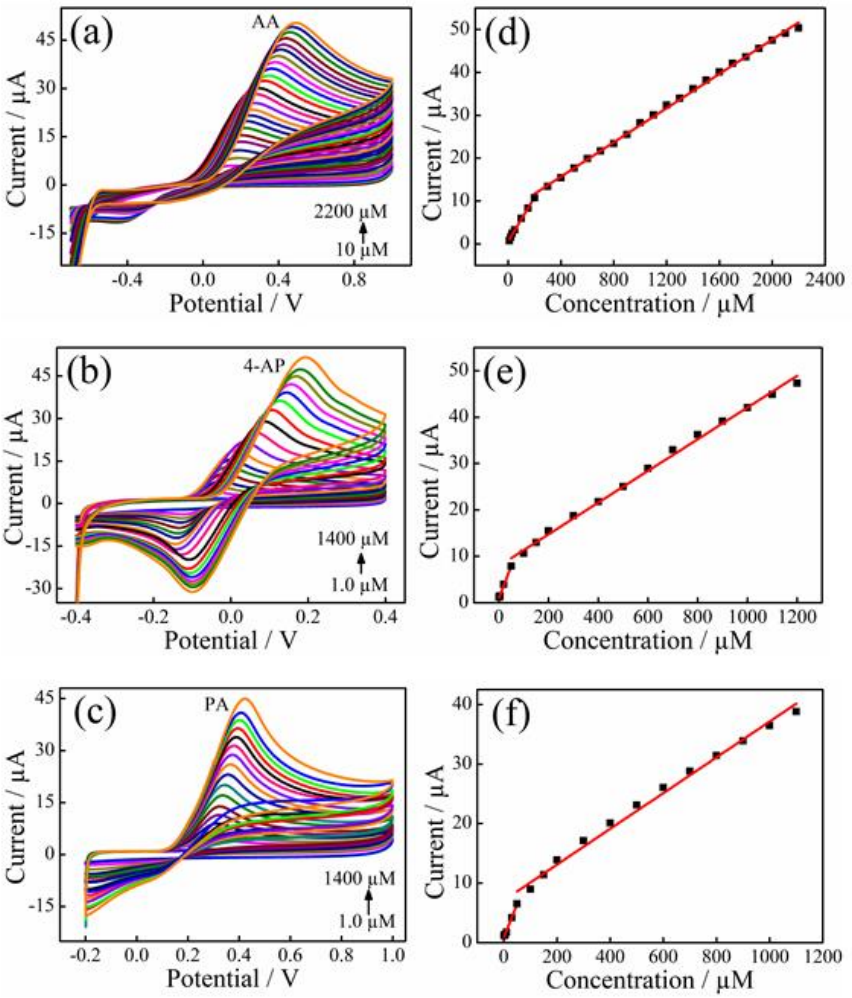

Figure IV.4. CVs for different concentrations of AA (a), 4-AP (b), and PA (c) on Pt-Ni/SPGE in 0.1 M PBS (pH 7.4) at 50 mV s^{-1}. (d), (e), and (f) Variation of anodic peak currents (I_{pa}) as a function of concentration.

Figure IV.4a illustrated the irreversible oxidation behavior of AA on the nanocomposite surface (Pt–Ni/SPGE); with current peaks increased as the AA concentration rose. As seen in figure IV.4d, the oxidation current was proportional to the AA concentration, demonstrating two distinct linear ranges: one from 10 to 200 µM and another from 200 to 2200 µM. The corresponding regression equations were as follows:

$$I_p(\mu A) = 0.051\ C\ (\mu M) + 0.628\ (R^2 = 0.996) \qquad \text{Eq.IV.1}$$

$$I_p(\mu A) = 0.02\ \ C\ (\mu M) + 7.699\ (R^2 = 0.998) \qquad \text{Eq.IV.2}$$

Using the first linear fitting equation, the corresponding limit of detection (LOD) of the modified graphene SPE was calculated to be 9.84 µM (S/N = 3).

Figure IV.4b showed the quasi-reversible response of 4-AP oxidation on the surface of the new sensor (Pt–Ni/SPGE). It was observed that the oxidation current peak progressively increased with the concentration of 4-AP. According to figure IV.4e, the oxidation current was proportional to the 4-AP concentration, demonstrating linearity in two ranges: 1-50 µM and 50-1200 µM, described by the following linear equations:

$$I_p(\mu A) = 0.139\ C\ (\mu M) + 0.968\ (R^2 = 0.997) \qquad \text{Eq.IV.3}$$

$$I_p(\mu A) = 0.034\ C\ (\mu M) + 7.915\ (R^2 = 0.995) \qquad \text{Eq.IV.4}$$

The corresponding limit of detection (LOD) of the new sensor was calculated to be 2.36 µM (S/N = 3).

Similarly, figure IV.4c illustrated the CVs of the quasi-reversible response of PA oxidation on the Pt-Ni/SPGE in 0.1 M PBS at different PA concentrations. It was observed that the oxidation peak current (I_p) increased progressively with the PA concentration. The corresponding calibration curve (current density versus PA concentration) was shown in figure IV.4f. This demonstrated a strong linear relationship for concentrations within the 1-50 µM range and between 50 and 1100 µM. The observed linear responses were given by the following equations:

$$I_p(\mu A) = 0.112\ C\ (\mu M) + 0.875\ (R^2 = 0.995) \qquad \text{Eq.IV.5}$$

$$I_p(\mu A) = 0.030\ C\ (\mu M) + 7.098\ (R^2 = 0.990) \qquad \text{Eq.IV.6}$$

With the calculated limit of detection (LOD) of 2.0 µM (S/N = 3).

The CVs revealed an irreversible oxidation reaction for AA, while PA and 4-AP exhibited a quasi-reversible process (Figure IV.5), consistent with the behavior previously observed at the surface of the Pt-Ni modified graphite screen-printed electrode.

The oxidation mechanism of AA involved irreversible electrochemical reactions that facilitated electron transfer, released electrons and protons, lead to the formation of dehydroascorbic acid as the product.

The electrochemical oxidation mechanism of 4-AP involved a quasi-reversible reaction, where two electrons and two protons were transferred. Initially, 4-AP lost electrons from the aromatic ring, followed by the release of protons. This resulted in the formation of quinoneimine, an intermediate product of the oxidation.

The electrochemical oxidation of PA induced electrolysis in the aromatic ring, removed two electrons and two protons irreversibly, and led to the formation of the intermediate N-acetyl-p-benzoquinone-imine.

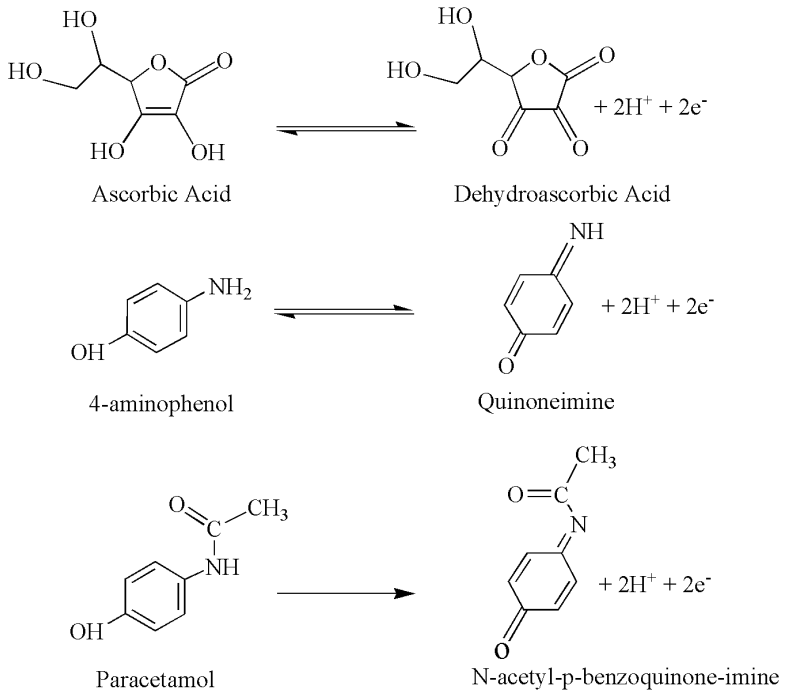

Figure IV.5. Mechanism of oxidation of AA, 4-AP, and PA at the electrode surface.

IV.3.2. Simultaneous electrochemical detection of target analytes

IV.3.2.1. Simultaneous electrochemical detection of ascorbic acid and paracetamol

The electro-catalytic properties of the Pt-Ni modified graphene SPE developed were examined by measuring the CV response of AA and PA at different concentrations in a 0.1M PBS solution (pH 7.4) (Figure IV.6).

Clear and easily interpretable curves were obtained again, with the oxidation peaks of both species distinctly separated. In figure IV.6a, we observe that the cyclic voltammetry responses showed that the simultaneous detection of paracetamol and ascorbic acid was highly concentration-dependent, with the oxidation peak currents of both analytes steadily increasing as the concentration rose.

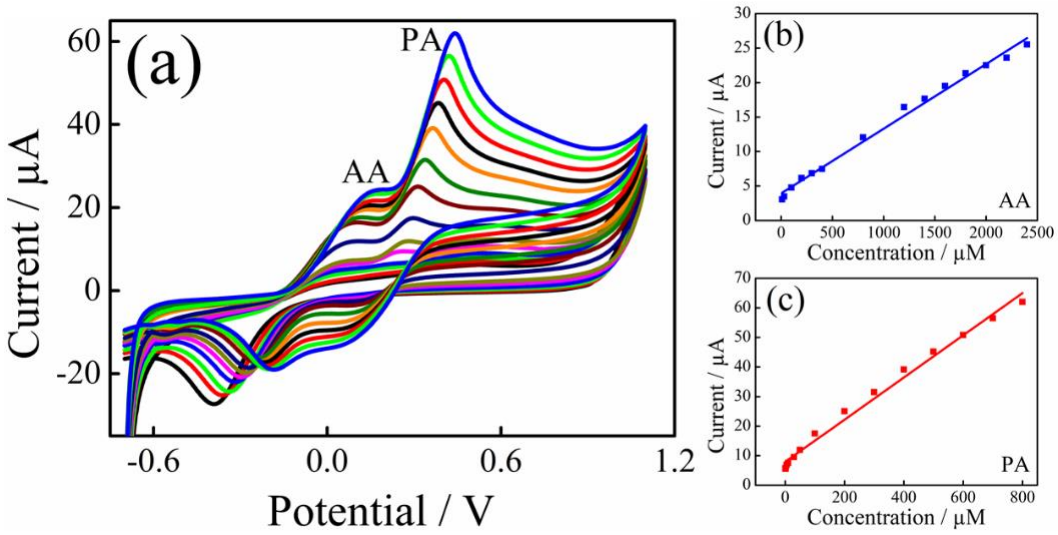

Figure IV.6. (a) CVs for the simultaneous analysis of AA and PA on Pt–Ni/SPGE in 0.1 M PBS solution (pH 7.4) at 50 mV s^{-1}. (b) and (c) Variation of anodic peak currents (I_{pa}) as a function of concentration.

After processing all the curves, the variation in current intensity for both peaks was plotted as a function of the concentration of each substance. Figures IV.6b and c presented the calibration curves obtained. Linearity was validated for both substances within concentration ranges of 10 µM to 2400 µM for ascorbic acid and 1.0 µM to 800 µM for paracetamol. The resulting equations were as follows:

$$I_p(\mu A) = 0.009\ C\ (\mu M) + 3.92\ (R^2 = 0.993) \qquad \text{Eq.IV.7}$$

With a sensitivity of $0.45 \pm 0.01\ \mu A\ \mu M^{-1}\ cm^{-2}$ and a LOD of 30 µM (S/N = 3) for AA and,

$$I_p(\mu A) = 0.071\ C\ (\mu M) + 7.90\ (R^2 = 0.990) \qquad \text{Eq.IV.8}$$

With a sensitivity of $2.44 \pm 0.01\ \mu A\ \mu M^{-1}\ cm^{-2}$ and a LOD of 5.0 µM (S/N = 3) for PA.

The results obtained suggested that the Pt-Ni modified graphene SPE was promising for the electrochemical analysis of ascorbic acid and paracetamol, demonstrating high selectivity and sensitivity.

IV.3.2.2. Simultaneous electrochemical detection of 4-aminophenol and paracetamol

IV.3.2.2.1. Simultaneous electrochemical detection via cyclic voltammetry

The analytical performance of the proposed Pt–Ni/SPGE sensor for the simultaneous determination of 4-AP and PA was first studied using cyclic voltammetry, as shown in figure

IV.7a. As observed, the current peaks for 4-AP were clearly separated from those of PA, with increasing values.

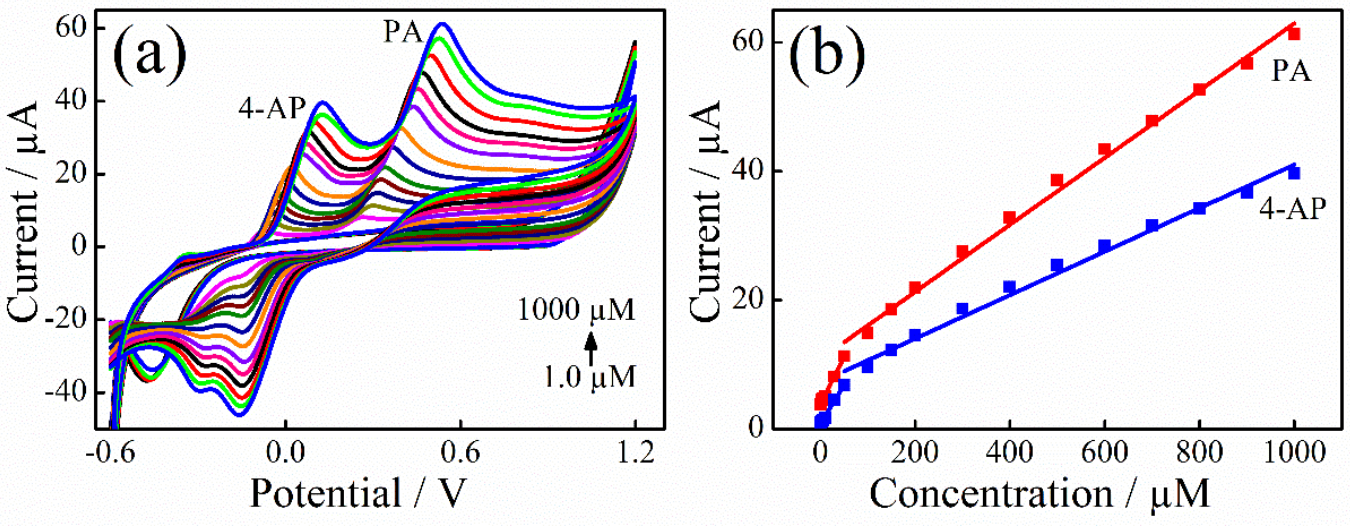

Figure IV.7. (a) CVs for the simultaneous analysis of 4-AP and PA on Pt–Ni/SPGE in 0.1 M PBS solution (pH 7.4) at 50 mV s^{-1}. (b) Variation of anodic peak currents (I_{pa}) as a function of concentration.

The linearity between the anodic peak current (I_{pa}) and concentration was established by plotting them against each other, as shown in figure IV.7b. The plot clearly illustrated two distinct linear ranges for each analyte. The first range extended from 1.0 to 50 µM, while the second range spanned from 50 to 1000 µM. The corresponding linear regression equations and correlation coefficients were as follows:

For 4-AP:

$$I_p(\mu A) = 0.122\ C\ (\mu M) + 0.752\ (1.0 - 50\ \mu M, R^2 = 0.997), \qquad \text{Eq.IV.9}$$

$$I_p(\mu A) = 0.034\ C\ (\mu M) + 7.271\ (50 - 1000\ \mu M, R^2 = 0.990), \qquad \text{Eq.IV.10}$$

For PA:

$$I_p(\mu A) = 0.147\ C\ (\mu M) + 3.817\ (1.0 - 50\ \mu M, R^2 = 0.995), \qquad \text{Eq.IV.11}$$

$$I_p(\mu A) = 0.052\ C\ (\mu M) + 10.85\ (50 - 1000\ \mu M, R^2 = 0.995). \qquad \text{Eq.IV.12}$$

Furthermore, the LODs (*S/N*=3) and sensitivities of the modified graphene Pt–Ni/SPGE towards the electro-oxidation process of the two target analytes were calculated as follows: 2.0 µM and 2.8 $\pm$ 0.01 $\mu A\ \mu M^{-1}\ cm^{-2}$ for 4-AP, and 2.0 µM and 1.4 $\pm$ 0.01 $\mu A\ \mu M^{-1}\ cm^{-2}$ for PA, respectively.

The results of the simultaneous detection of both analytes, 4-AP and PA, were similar to those obtained in individual analyses. This suggested that the Pt–Ni modified graphene SPE sensor was capable of detecting these two analytes with high sensitivity, whether they were analyzed individually or simultaneously.

Furthermore, when comparing the graphite and graphene-modified SPE, the sensitivity of the graphene micro-sensor was slightly enhanced for 4-AP and PA, in terms of linearity. Additionally, for the same concentration, the current intensity was higher with graphene than with the graphite-modified SPE, indicating a superior catalytic effect.

IV.3.2.2.2. Simultaneous electrochemical detection via square wave voltammetry

The SWV method was also conducted in PBS buffer at pH 7.4 under optimal experimental conditions to investigate the electrochemical applicability of the newly developed Pt–Ni modified graphene SPE sensor for the simultaneous quantification of 4-AP and PA by synchronously varying their concentrations, as shown in figure IV.8.

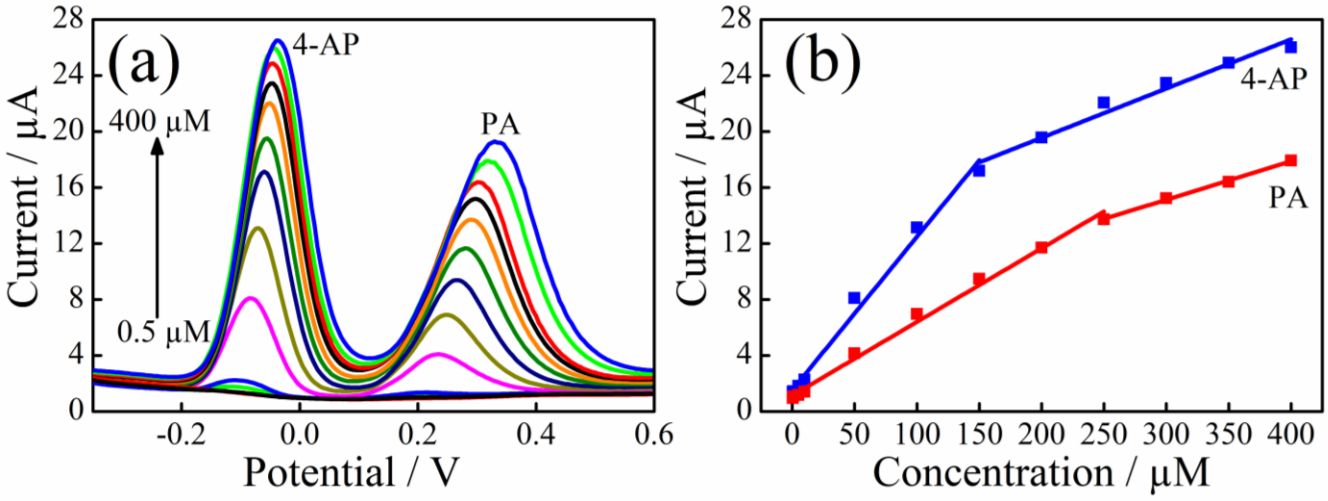

Figure IV.8. (a) SWV profiles for the simultaneous analysis of 4-AP and PA on Pt–Ni/SPGE in 0.1 M PBS solution (pH 7.4). (b) illustrate the corresponding calibration curves.

As observed, the peak-to-peak separation of 0.37 V was sufficiently large for the simultaneous determination of 4-AP and PA. Moreover, their oxidation peak currents exhibited strong linear relationships as their concentrations were gradually increased (Figure IV.8b). The corresponding linear equations were as follows:

For 4-AP:

$$I_p(\mu A) = 0.109\ C\ (\mu M) + 1.521\ (0.5 - 150\ \mu M, R^2 = 0.990), \qquad \text{Eq.IV.13}$$

$$I_p(\mu A) = 0.026\ C\ (\mu M) + 15.465\ (150 - 400\ \mu M, R^2 = 0.996), \quad \text{Eq.IV.14}$$

For PA:

$$I_p(\mu A) = 0.053\ C\ (\mu M) + 1.141\ (0.5 - 250\ \mu M, R^2 = 0.994), \quad \text{Eq.IV.15}$$

$$I_p(\mu A) = 0.027\ C\ (\mu M) + 6.855\ (250 - 400\ \mu M, R^2 = 0.997). \quad \text{Eq.IV.16}$$

The determined LOD and sensitivity values for the newly developed Pt–Ni/SPGE sensor for 4-AP and PA detection were 2.3 µM and 1.1 $\pm$ 0.01 µA µM^{-1} cm^{-2} for 4-AP, and 2.6 µM and 2.18 $\pm$ 0.01 µA µM^{-1} cm^{-2} for PA.

Additionally, consistent with the results from the previous CV analysis, the sensitivity of the modified graphene SPE showed a slight improvement for both 4-AP and PA, particularly in terms of linearity, with a wider linear range. For instance, at a concentration of 200 µM 4-AP, the current intensity for the graphene-modified SPE was higher (19.620 µA) compared to the graphite-modified SPE (13.262 µA), indicating an approximately 1.5-fold enhancement in catalytic activity. A similar trend was observed for PA as well.

Based on these results, the Pt–Ni modified graphene SPE (Pt–Ni/SPGE) allowed for the individual or simultaneous determination of target analytes with high sensitivity.

IV.4. Comparison of the analytical performance of the fabricated sensor with sensors reported in the literature

The analytical performance of the newly fabricated Pt-Ni modified graphene SPE sensor, compared to other electrodes reported for the detection of 4-AP, PA, and AA, was presented in table IV.1. These results demonstrated that the Pt-Ni modified graphene SPE developed in this study exhibited a wider linear range, lower detection limits, and higher sensitivity for the detection of the target analytes, both individually and simultaneously, compared to the values previously reported by various authors.

Table IV.1. Comparison of analytical performance of the newly developed Pt-Ni modified graphene SPE with other sensors for detecting 4-AP, PA, and AA.

Electrode	Technique	Linear Range (µM)			Detection Limit (µM)			Ref.
		4-AP	PA	AA	4-AP	PA	AA	
Pt/ZnO	CA	100-900	-	-	4.11	-	-	**[1]**
AuPt/ZnO	CA	100-900	-	-	3.6	-	-	
Graphene/PANI/CPE	Amp	50-500	-	-	15.68	-	-	**[2]**
Hemin/MIP	Amp	10-90	-	-	3.0	-	-	**[3]**
NiO/CuO/GR/GCE	SWV	-	4-400	-	-	1.33	-	**[4]**
Carbon coated nickel nanoparticles/GCE	DPV	-	7.8-110	-	-	2.3	-	**[5]**
AuNP-PGA/SWCNT	DPV	-	8.3-145.6	-	-	1.18	-	**[6]**
SPCE/CB-ERGO	CV	-	10-200	-	-	5.3	-	**[7]**
GR-CS	DPV	-	1.0-100	-	-	3.0	-	**[8]**
ERGO/ZrO_2/GCE	LSV	-	9-231	-	-	-	-	**[9]**
(ERGO)/NHCF	LSV	-	-	-	-	14.2	-	**[10]**
Graphite electrode	DPV	-	6.10-66.10	-	-	2.2	-	**[11]**
GS-PTCA	DPV	-	-	20-420	-	-	5.6	**[12]**
AgNPs/RGO/GCE	LSV	-	-	10-800	-	-	9.6	**[13]**
Poly(rhodamineB)/MWCNTs/GCE	DPV	-	-	200-5000	-	-	20	**[14]**
Au on paper	Amp	0.05-2000	0.05-2000	-	10	25	-	**[15]**
PEDOT/GCE	DPV	4.0-320	1.0-100	-	1.2	0.4	-	**[16]**
Carbon Ionic Liquid Electrode	DPV	0.3-100	2.0-220	-	0.1	0.5	-	**[17]**
Pt-Ni/SPGE	**CV**	**1.0-1200**	**-**	**-**	**2.36**	**-**	**-**	**This work**
	CV	**-**	**1.0-1100**	**-**	**-**	**2.0**	**-**	
	CV	**-**	**-**	**10-2200**	**-**	**-**	**9.84**	
	CV		**1.0-800**	**10-2400**	**-**	**5.0**	**30**	
	CV	**1.0-1000**	**1.0-1000**	**-**	**2.0**	**2.0**	**-**	
	SWV	**0.5-400**	**0.5-400**	**-**	**2.3**	**2.6**	**-**	

IV.5. Conclusion

A second sensor was developed using a graphene screen-printed electrode modified with the same electrodeposition technique employed previously in Chapter IV, Part A. This sensor was used for the individual as well as simultaneous electrochemical detection of 4-aminophenol (4-AP), ascorbic acid (AA), and paracetamol (PA).

The sensor was characterized using FE-SEM, EDX, and AFM techniques. The FE-SEM images showed that the graphene surface was covered with highly uniform and well-dispersed spherical Pt and Ni particles. The EDX spectrum further confirmed this result by providing elemental proof. The 3D AFM images revealed the relatively rough surface of the unmodified SPE, while the modified electrode surface appeared more homogeneous, indicating the smooth distribution of Pt–Ni particles. Additionally, the electrochemical behavior of 4-AP, AA, and

PA on the modified electrode was studied primarily using cyclic voltammetry and square wave voltammetry (in the case of simultaneous detection of 4-AP and PA). The results indicated that the developed sensor (Pt–Ni/SPGE) was capable of detecting 4-AP, AA, and PA both individually and simultaneously.

References

[1] G. Fiaschi, S. Cosentino, R. Pandey, S. Mirabella, V. Strano, L. Maiolo, D. Grandjean, P. Lievens, Y. Shacham-Diamand, A novel gas-phase mono and bimetallic clusters decorated Zno nanorods electrochemical sensor for 4-aminophenol detection, J. Electroanal. Chem. 811 (2018) 89–95.
[2] P. Rattanarat, A. Suea-Ngam, N. Ruecha, W. Siangproh, C.S. Henry, M. Srisa-Art, O. Chailapakul, Graphene-polyaniline modified electrochemical droplet-based microfluidic sensor for high-throughput determination of 4-aminophenol, Anal. Chim. Acta 925 (2016) 51–60.
[3] J.R.M. Neto, W.J.R. Snatos, P.R. Lima, S.M.C.N. Tanaka, A.A. Tanaka, L.T. Kubota, A hemin-based molecularly imprinted polymer(MIP) grafted onto a glassy carbon electrode as a selective sensor for 4-aminophenol amperometric, Sens. Actuators B: Chem. 152 (2011) 220–22.
[4] B. Liu, X. Ouyang, Y. Ding, L. Luo, D. Xu, Y. Ning, Electrochemical preparation of nickel and copper oxides-decorated graphene composite for simultaneous determination of dopamine, acetaminophen and tryptophan, Talanta 146 (2016) 114–121.
[5] S.F. Wang, F. Xie, R.F. Hu, Carbon-coated nickel magnetic nanoparticles modified electrodes as a sensor for determination of acetaminophen, Sens. Actuators B: Chem. 123 (2007) 495–500.
[6] M.P.N. Bui, C.A. Li, K.N. Han, X.H. Pham, G.H. Seong, Determination of acetaminophen by electrochemical co-deposition of glutamic acid and gold nanoparticles, Sens. Actuators B: Chem. 174 (2012) 318–324.
[7] G. Ibáñezredín, D. Wilson, D. Gonçalves, J. Colloid Interface Sci. 9 (2017) 101–108.
[8] M. Zheng, F. Gao, Q. Wang, X. Cai, S. Jiang, L. Huang, F. Gao, Electrocatalytical oxidation and sensitive determination of acetaminophen on glassy carbon electrode modified with graphene–chitosan composite, Mat. Sci. Eng. C Mater. 33 (2013) 1514–1520.
[9] A.T. Ezhil Vilian, M. Rajkumar, Sh.M. Chen, In situ electrochemical synthesis of highly loaded zirconium nanoparticles decorated reduced graphene oxide for the selective determination of dopamine and paracetamol in presence of ascorbic acid, Colloids Surf. B 115 (2014) 295–301.
[10] B. Devadas, M. Rajkumar, S.M. Chen, R. Saraswathi, Electrochemically reduced graphene oxide/ neodymium hexacyanoferrate modified electrodes for the electrochemical detection of paracetomol, Int. J. Electrochem. Sci. 7 (2012) 3339–3349.
[11] I. Baranowska, P. Markowski, A. Gerle, J. Baranowski, Determination of selected drugs in human urine by differential pulse voltammetry technique, Bioelectrochemistry 73 (2008) 5–10.
[12] W. Zhang, Y. Chai, R. Yuan, Sh. Chen, J. Han, D. Yuan, Facile synthesis of graphene hybrid tube-like structure for simultaneous detection of ascorbic acid, dopamine, uric acid and tryptophan, Anal. Chim. Acta 756 (2012) 7–12.
[13] B. Kaura, T. Pandiyanb, B. Satpatic, R. Srivastava, Simultaneous and sensitive determination of ascorbic acid, dopamine, uric acid, and tryptophan with silver nanoparticles decorated reduced graphene oxide modified electrode, Colloids Surf. B 111 (2013) 97–106.
[14] H. Filik, A.A. Avan, S. Aydar, R. Apak, Poly(Rhodamine B) and MWCNTS composite film for the separation and simultaneous voltammetric quantification of tryptophan, paracetamol, uric acid, dopamine and ascorbic acid, Curr. Anal. Chem. 11 (2015) 87–95.
[15] L.Y. Shiroma, M. Santhiago, A.L. Gobbi, L.T. Kubota, Separation and electrochemical detection of paracetamol and 4-aminophenol in a paper-based micro fluidic device, Anal. Chim. Acta 725 (2012) 44–50.
[16] S. Mehretie, S. Admassie, T. Hunde, M. Tessema, T. Solomon, Simultaneous determination of N-acetyl-p-aminophenol and p-aminophenol with poly(3,4-ethylenedioxythiophene) modified glassy carbon electrode, Talanta 85 (2011) 1376−1382.
[17] A. Safavi, N. Maleki, O. Moradlou, A Selective and Sensitive Method for Simultaneous Determination of Traces of Paracetamol and p-Aminophenol in Pharmaceuticals Using Carbon Ionic Liquid Electrode, Electroanalysis 20 (2008) 2158−2162.

General conclusion

General conclusion

The primary objective of the research undertaken in this thesis was to develop novel electrochemical sensors that are simple, rapid, and cost-effective for monitoring self-medication practices, utilizing bimetallic nanoparticle systems. The new approach leverages the properties of Pt-Ni nanoparticles for the individual and simultaneous detection of paracetamol (PA), 4-aminophenol (4-AP), ascorbic acid (AA), and zinc (Zn(II)).

To achieve this goal, an electrochemical sensor was developed using a screen-printed graphite electrode modified with platinum-nickel (Pt-Ni) nanoparticles. This sensor allows for the simultaneous detection of 4-aminophenol and paracetamol on one hand, and the simultaneous detection of zinc, ascorbic acid, and paracetamol on the other. The prepared sensors underwent both structural and morphological characterization using FE-SEM, TEM, EDX, XRD, and AFM techniques, as well as electrochemical characterization through cyclic voltammetry (CV) and electrochemical impedance spectroscopy (EIS).

FE-SEM images of the modified Pt-Ni/SPE electrode revealed the formation of highly uniform and well-dispersed Pt and Ni spherical nanoparticles. Many Pt nanodeposits were evenly distributed across the substrate, while only a few smaller Ni nanoparticles were present. TEM images further confirmed the successful preparation of the modified electrode. The EDX spectrum provided elemental proof, confirming the presence of Pt and Ni in the electrode with atomic ratios of approximately 97.17% and 2.83%, respectively. The XRD analysis confirmed the successful formation of Pt-Ni nanodeposits on the graphite SPE surface. Furthermore, AFM analysis revealed a relatively rough surface for the bare SPE, whereas the modified electrode surface exhibited a more homogeneous distribution of Pt-Ni particles, indicating improved surface smoothness.

The electrochemical properties of the modified electrodes were studied using CV and EIS techniques. The heterogeneous electron transfer rate constant (k°) was calculated using Nicholson's method, yielding values of 2.4×10^{-4}, 5.3×10^{-4}, and 5.9×10^{-4} for the bare SPE, Pt/SPE, and Pt-Ni/SPE, respectively. Redox peak currents increased in the following order: SPE < Pt/SPE < Pt-Ni/SPE, which demonstrates the enhanced electro-catalytic efficiency of Pt and Pt-Ni nanoparticles as modifiers. These nanoparticles facilitated the electron transfer rate of the graphite SPE by factors of 2.2 and 2.5, respectively. The electroactive surface areas of the bare SPE, Pt/SPE, and Pt-Ni/SPE electrodes were determined to be 5.1×10^{-2}, 6.7×10^{-2}, and 6.9×10^{-2} cm², respectively, confirming the successful growth of Pt-Ni nanoparticles on the electrode surface and the resultant increase in the electroactive surface area. EIS spectra were analyzed using a suitable equivalent circuit, and the fitted R_2 values for the unmodified SPE,

Pt/SPE, and Pt-Ni/SPE electrodes were 6.99 kΩ (χ^2 = 0.0302), 2.68 kΩ (χ^2 = 0.0384), and 1.59 kΩ (χ^2 = 0.0385), respectively. The lowest R_2 value observed for the Pt-Ni/SPE electrode confirmed its superior electrical conductivity compared to the other electrodes.

The simultaneous detection of 4-AP and PA was achieved using cyclic voltammetry and differential pulse voltammetry, while the simultaneous detection of zinc, ascorbic acid, and paracetamol was performed using square wave voltammetry. The sensor demonstrated excellent analytical performance, including high sensitivity, a wide linear range, and very low detection limits. Moreover, the sensor exhibited outstanding reproducibility, repeatability, stability, and selectivity. The practical application of the sensor was successfully demonstrated by detecting AA and PA simultaneously, as well as Zn(II) and AA, for quality control of pharmaceutical products. Additionally, the triple simultaneous detection of Zn(II), AA, and PA in human blood samples was achieved without significant interference, resulting in satisfactory recovery rates.

The second part of this work focused on the development of a similar electrochemical sensor, with the only difference being the use of a graphene-based working electrode instead of graphite. This electrode was modified with Pt-Ni nanoparticles (Pt–Ni/SPGE) for the individual and simultaneous detection of 4-aminophenol, paracetamol, and ascorbic acid. The sensors developed in this section underwent comprehensive structural and morphological characterization using FE-SEM, EDX, and AFM techniques.

FE-SEM images revealed that the graphene surface was covered with highly uniform and well-dispersed spherical Pt and Ni nanoparticles. Numerous Pt nanodeposits were homogeneously distributed across the substrate, with an average size of approximately 155 nm. In contrast, only a few Ni nanoparticles were present, with a smaller diameter of 51.6 nm. The EDX spectrum confirmed this observation, with the atomic ratios of Pt and Ni estimated to be approximately 98.28% and 1.72%, respectively. 3D AFM images demonstrated that the unmodified SPE surface was relatively rough, while the modified electrode surface appeared more homogeneous, suggesting a smooth distribution of Pt-Ni particles. Furthermore, the electrochemical behavior of 4-aminophenol, ascorbic acid, and paracetamol on the modified electrode was studied using cyclic voltammetry and square wave voltammetry (in the case of the simultaneous detection of 4-AP and PA). The results indicated that the developed sensor (Pt–Ni/SPGE) was capable of detecting 4-AP, AA, and PA both individually and simultaneously.

The results obtained have opened several promising avenues for future research in this field:

- Conduct a more in-depth study of the properties of graphene and develop new hybrid sensors based on graphene modified with inorganic nanoparticles and biofilms.
- Explore and develop novel deposition methods for electrodes.
- Develop wearable smart sensors, similar to watches that make it easy for anyone to simultaneously detect multiple pharmaceutical products, with the aim of addressing issues related to self-medication and drug interactions.